



HAL
open science

FUI Ecoating. Comprehension of the Scale Formation Mechanism during the Suspension Polymerization of Vinyl Chloride Monomer and Development of a Durable Protective Polymer Coating

Julien Huser

► **To cite this version:**

Julien Huser. FUI Ecoating. Comprehension of the Scale Formation Mechanism during the Suspension Polymerization of Vinyl Chloride Monomer and Development of a Durable Protective Polymer Coating. *Polymers*. Université de Haute Alsace - Mulhouse, 2013. English. NNT : 2013MULH4032 . tel-04416460

HAL Id: tel-04416460

<https://theses.hal.science/tel-04416460>

Submitted on 25 Jan 2024

HAL is a multi-disciplinary open access archive for the deposit and dissemination of scientific research documents, whether they are published or not. The documents may come from teaching and research institutions in France or abroad, or from public or private research centers.

L'archive ouverte pluridisciplinaire **HAL**, est destinée au dépôt et à la diffusion de documents scientifiques de niveau recherche, publiés ou non, émanant des établissements d'enseignement et de recherche français ou étrangers, des laboratoires publics ou privés.

THESE DE DOCTORAT DE L'UNIVERSITE DE HAUTE-ALSACE

Année 2013

N° d'ordre : _____

présentée par
Julien HUSER

pour l'obtention du titre de
Docteur en Chimie des Matériaux

Comprehension of the Scale Formation Mechanism during the Suspension Polymerization of Vinyl Chloride Monomer and Development of a Durable Protective Polymer Coating

Soutenue le 1^{er} octobre 2013 devant la commission d'examen :

Prof. V. NASSIET	Université Toulouse	Rapporteur
Prof. P. LUTZ	Université Strasbourg	Rapporteur
Prof. E. DUGUET	Université Bordeaux 1	Examineur
Prof. C. DELAITE	Université de Haute Alsace	Co-directeur de thèse
Prof. S. BISTAC	Université de Haute Alsace	Co-directeur de thèse
M. T. LASUYE	INEOS ChlorVinyls	Membre invité
M. H. FARGE	Mäder Research	Membre invité

To Elodie
To my family

Acknowledgements

This work was performed in the *Laboratoire de Photochimie et d'Ingénierie Macromoléculaires (LPIM)* in Mulhouse, FRANCE. This Ph.D. was a part of the *Ecoating* project which was supported through a FUI financing.

I wish to express my gratitude to Professor Xavier ALLONAS, director of the LPIM, for welcoming me in the laboratory.

I also want to thank Professor Maurice BROGLY, leadhand of the *Chemistry and Physical-Chemistry of Polymer* in the LPIM, for giving me the opportunity to be a part of his team. I also thank him for the help on the infrared and AFM analyses.

I want to thank Professor Christelle DELAITE, thesis director, for following my work during these three years. Her availability and the great discussions we had were essential for the advancement of the project. Her kindness and the confidence she gave me were much appreciated.

I also thank Professor Sophie BISTAC, thesis co-director, for her presence and generosity during the course of my Ph.D. work. The advice she gave me and the discussions we had were crucial for the achievements of all the results obtained during our research.

I want to express my feelings to Mr. Thierry LASUYE, S-PVC Synthesis&Process Research Manager at INEOS ChlorVinyls and manager of the FUI Ecoating project, for his availability and his enthusiasm throughout the project which were a source of motivation of all the participants.

I want to thank all the partners involved in this project: INEOS ChlorVinyls, Mäder Research, Avenir Group, ESPCI, the P2M-team of the LPIM and all the financial partners. Being part of this ambitious project was deeply gratifying from both a professional and a personal point of view.

I wish to express my gratitude to the people who helped me in some ways during my Ph.D. I express my gratitude to Mr. Bernard STASIK (INEOS ChlorVinyls) for his kindness and for the great discussions during the meetings, Mr. Didier BERLINET (INEOS ChlorVinyls) for the pilot tests he performed during the project, Mr. Hervé FARGE, Dr. Anne-Sophie SCHULLER and Dr. Adrien CRIQUI (Mäder Research) for their enthusiasm throughout the project. I also thank Dr. Didier DENTEL and Dr. Mickael DERIVAZ (IS2M-UHA) for the XPS analyses,

Acknowledgements

Mr. Ludovic JOSIEN (IS2M-UHA) for the SEM-EDX analyses and Mr. Didier LE NOUEN (COB-UHA) for his help with the NMR analyses.

I want to thank all the interns who worked on the project. Elodie, Fabienne, Arlette and Caroline all did a great job and it was a real pleasure working with all of them.

Finally, I want to thank all the Ph.D. students, engineers or interns I met during the course of these three years and especially Elodie who is obviously lots more than a colleague, Julien and Jean-Victor who are the perfect combination of beauty and scientific greatness, Lénaïg and Aurélie, our engineer's dream team, Fanny, my opposite desk neighbor who supported me during this last year, Jérémy W., our couture and fire specialist, Jérémy L., our Justin Bieber doppelganger, Lucie, our self-healing expert and finally Diane and Olivier who have the difficult task to succeed to the leaving Ph.D.s. I also thank our colleagues from the organic chemistry laboratory for all the great moments we had together: Nicolas, Anne-Caroline, Morgan, Cédric, Stéphane, Samir, Arnaud, Virginie, Théophile and Philippe.

Abbreviations

^1H NMR: Proton Nuclear Magnetic Resonance spectroscopy

γ_s : Surface energy

γ_{sp} : Polar component of the surface energy

γ_{sd} : Dispersive component of the surface energy

ν_R : Cross-linking density

AAPS: N-[3-(trimethoxysilyl)propyl]ethylenediamine

AEPA: 1-(2-aminoethyl)piperazine

AFM: Atomic Force Microscopy

AGC: "Acvagen" Graft Copolymer

AHEW: Amine-Hydrogen Equivalent Weight

AISI: American Iron and Steel Institute

APDES: 3-(ethoxydimethylsilyl)propylamine

APTMS: 3-aminopropyl(trimethoxysilane)

BADGE / DGEBA: Bisphenol-A diglycidylether

BuCl: 1-chlorobutan

CMR: Carcinogenic, Mutagenic and / or toxic to Reproduction

DMTA: Dynamic Mechanical Thermal Analysis

DRIFT: Diffuse Reflectance Infrared Fourier Transform

DSC: Differential Scanning Calorimetry

DTMS: Dodecyl-trimethoxysilane

EEW: Epoxy Equivalent Weight

EHP: Di(2-ethylhexyl) peroxydicarbonate

F_{Me} : Metal enrichment factor

G' : Storage modulus

G'' : Loss modulus

GPDES: 3-glycidoxypropyldimethylethoxysilane

GPTMS: (3-glycidyloxypropyl) trimethoxysilane

HD: Hydrolysis Degree

HEDA: Hexaethylenediamine

IPDA: Isophoronediamine

IRRAS: InfraRed Reflection Absorption Spectroscopy

LER: Liquid Epoxy Resin

LPO: Dilauroyl peroxide

Mc: Molecular weight between the crossing points

Mn: Number-average molecular weight

mPDA: m-phenylenediamine

Mw: Weight-average molecular weight

DPn: Polymerization degree

PEHA: Pentaethylenehexamine

PM-IRRAS: Polarization Modulation - InfraRed Reflection Absorption Spectroscopy

PVA: PolyVinyl Alcohol / PolyVinyl Acetate copolymers

PVA I: Primary PVA

PVA II: Secondary PVA

PVC: PolyVinyl Chloride

R_A: Medium roughness

RC-2: Bis[3-(trimethoxysilyl)-1-phenylpropyl] tetrasulfide

S-PVC: PVC obtained by suspension polymerization

SEM-EDX: Scanning Electron Microscopy - Energy Dispersive X-Ray spectroscopy

SER: Solid Epoxy Resin

T-IR: Transmission InfraRed spectroscopy

TEOS: Tetraethoxysilane

TETA: Triethylenetetramine

T_g: Glass transition temperature

TGA: ThermoGravimetric Analysis

TPDTA: N-(3-trimethoxysilylpropyl) diethylenetriamine

Abbreviations

TPSA: 3-(triethoxysilyl)propylsuccinic anhydride

VCM: VinylChloride Monomer

VTES: Vinyltriethoxysilane

WBL: Weak Boundary Layer

XPS: X-Ray Photoelectron Spectroscopy

Table of Contents

Acknowledgements

Abbreviations

Table of Contents

General Introduction.....1

Chapter I: Bibliographical Study

I. Context - Suspension polymerization of VinylChloride Monomer (S-PVC).....	11
I.1. Basics on PolyVinyl Chloride (PVC)	11
I.2. The suspension polymerization process.....	11
I.3. S-PVC production at INEOS ChlorVinyls - Mazingarbe.....	14
I.4. Conclusion.....	15
II. Scale formation during the suspension polymerization of VCM.....	15
II.1. Industrial issues and stakes	15
II.2. Scale formation mechanism described in the literature	17
II.2.a. First step: Formation of a copolymer	17
II.2.b. Second step: Adsorption of the copolymer on the reactor's walls.....	18
II.2.c. Third step: Development of the crust.....	18
II.3. S-PVC anti-scaling solutions.....	19
II.3.a. Solutions used by INEOS ChlorVinyls.....	19
II.3.b. Other patented solutions	22
II.4. Conclusion.....	23
III. AISI 316L stainless steel	24
III.1. General presentation.....	24
III.2. Surface and bulk chemical composition of 316L stainless steel.....	24
III.3. Interactions between stainless steel and suspension polymerization's reactants	26
III.4. Pitting corrosion	27
III.5. Conclusion.....	28
IV. The polymer coatings.....	28
IV.1. General points on coatings	28

IV.2. Coating's specifications.....	29
IV.3. Epoxy resins.....	30
IV.3.a. Presentation of bisphenol-A diglycidylether (BADGE) resins.....	30
IV.3.b. Curing of the BADGE prepolymer / diamine system	32
IV.4. Conclusion.....	33
V. Epoxy coating's adhesion onto stainless steel.....	34
V.1. Basics on adhesion.....	34
V.1.a. Work of adhesion.....	34
V.1.b. Fracture theory	34
V.1.c. Weak boundary layer theory.....	35
V.1.d. Wetting - contact theory.....	35
V.1.e. Diffusion theory.....	35
V.1.f. Chemical adhesion	36
V.1.g. Mechanical adhesion.....	36
V.1.h. Electrostatic adhesion.....	36
V.1.i. Acid-base adhesion	36
V.1.j. Summary of the usual bond types.....	37
V.1.k. Combination of the phenomena	37
V.2. Epoxy / stainless steel adhesion.....	38
V.2.a. Description of the adhesion of epoxy onto stainless steel.....	38
V.2.b. Behavior in an aqueous medium	38
V.3. Optimization of the epoxy / stainless steel interface.....	39
V.3.a. Cleaning / pickling.....	39
V.3.b. Mechanical treatment	41
V.4. Conclusion.....	42
VI. Adhesion promoters / Primers.....	42
VI.1. Phosphonates	42
VI.1.a. Introduction	42
VI.1.b. Phosphonic acid chemistry.....	43
VI.1.c. Adsorption on metallic substrates.....	43
VI.1.d. Bisphosphonates	45
VI.2. Sulfonates	46
VI.3. Trialkoxysilanes.....	47
VI.3.a. Introduction	47
VI.3.b. Behavior of the trialkoxysilanes in aqueous solution.....	48
VI.3.c. Hydrolysis reactions.....	49
VI.3.d. Condensation reactions.....	51
VI.3.e. Factors affecting the hydrolysis / condensation reactions.....	53

VI.3.f.	Composition of the hydrolysis solution	55
VI.3.g.	Grafting of trialkoxysilanes onto inorganic substrates	56
VI.3.h.	Factors affecting the grafting of trialkoxysilanes	58
VI.3.i.	Trialkoxysilanes for the optimization of the epoxy / stainless steel interface	60
VI.3.j.	Conclusion	63
VI.4.	<i>Monoalkoxysilanes</i>	64
VI.4.a.	Introduction	64
VI.4.b.	Hydrolysis	65
VI.4.c.	Grafting	65
VI.4.d.	Conclusion	66
VI.5.	<i>Conclusion</i>	66
VII.	General conclusion	67
References	68

Chapter II: Experimental Part

I. Solvents and products.....	77
I.1. PolyVinyl Alcohols (PVA)	77
I.2. Coupling Agents.....	78
I.3. Epoxy resins.....	79
I.3.a. RenLam CY 219 / Ren HY 5161	79
I.3.b. Araldite DBF CH / Ren HY 956	80
I.3.c. Pure amines.....	80
I.4. Stainless steel.....	80
I.4.a. Cleaning of the stainless steel plates	81
I.4.b. Shot-blasting of the stainless steel plates	81
II. Tests for the determination of the scale's formation mechanism	81
II.1. Simulation tests: Immersion in model systems.....	81
II.1.a. Immersion in a "model" solvent	81
II.1.b. Immersion in water / LPO system.....	82
II.1.c. Immersion in water / PVA systems.....	82
II.1.d. Immersion in BuCl / LPO / PVA systems.....	83
II.1.e. Immersion in water / BuCl emulsions stabilized by PVAs	83
II.2. Pilot tests.....	83
II.2.a. Presentation of the pilot reactor.....	83
II.2.b. Kinetic of the scale formation	85
II.2.c. Influence of the PVA hydrolysis degree on the scale formation.....	85
III. Preparation of the epoxy free films	85
IV. Preparation of the epoxy coatings on stainless steel	86
IV.1. Preparation of the epoxy-coated stainless steel plates	86
IV.2. Application of the sulfonate, phosphonate and bisphosphonate on stainless steel	86
IV.2.a. Preparation of a solution at 10^{-3} M.....	86
IV.2.b. Deposition process	87
IV.3. Application of the alkoxysilanes on the stainless steel plates.....	87
V. Tests of the coated stainless steel plates	87
V.1. Immersion in model solvents.....	87
V.1.a. Immersion in hot BuCl	87
V.1.b. Immersion in hot water	88
V.2. Immersion in pilot reactor.....	88
VI. Analytical techniques.....	88

<i>VI.1. Chemical and surface analyses</i>	88
VI.1.a. InfraRed analyses.....	88
VI.1.b. Nuclear Magnetic Resonance spectroscopy (¹ H NMR)	90
VI.1.c. Scanning Electron Microscopy / Energy Dispersive X-Ray spectroscopy (SEM-EDX)	90
VI.1.d. X-ray Photoelectron Spectroscopy (XPS)	90
VI.1.e. Contact Angle measurements	91
VI.1.f. Optical Microscopy	91
VI.1.g. Atomic Force Microscopy (AFM)	92
<i>VI.2. Thermal and thermo-mechanical analyses</i>	92
VI.2.a. Dynamic Mechanical Thermal Analysis (DMTA)	92
VI.2.b. Differential Scanning Calorimetry (DSC).....	92
VI.2.c. ThermoGravimetric Analysis (TGA).....	93
<i>VI.3. Mechanical tests</i>	93
VI.3.a. Lap-shear tests	93
VI.3.b. Tribology measurements	93
VI.3.c. Pull-off tests	94
<i>VII. Conclusion</i>	94
<i>References</i>	95

Chapter III: Formation of Scale Mechanism

I. Introduction	101
II. Interactions between stainless steel and the reactive medium's components: immersion in model solutions	101
II.1. Immersion of stainless steel plates in model solvents	101
II.2. Immersion of stainless steel plates in water / LPO systems	104
II.3. Immersion of stainless steel plates in water / PVA systems	106
II.4. Immersion of stainless steel plates in BuCl / LPO / PVA systems	109
II.5. Immersion of stainless steel plates in water / BuCl emulsions	112
II.6. Conclusion	114
III. Immersion tests in the pilot reactor	114
III.1. Kinetic of the fouling process	115
III.1.a. Visual observation	115
III.1.b. Chemical analysis of the scale	116
III.1.c. Conclusion	119
III.2. Influence of the hydrolysis degree of the PVAs on the scale formation	120
III.2.a. Visual information	120
III.2.b. Chemical analysis of the scale	121
III.2.c. Conclusion	122
IV. Scale formation mechanism	123
V. Conclusion	125
References	126

Chapter IV: Choice of a Suitable Epoxy Resin

I. Introduction	131
II. Commercial epoxy / amine systems	131
II.1. Characterization of the epoxy free films.....	131
II.1.a. Study and optimization of the curing process.....	132
II.1.b. Properties of the cured epoxy films	138
II.2. Conclusion.....	145
III. Epoxy system based on model polyamines	146
III.1. Presentation	146
III.2. Processing of epoxy free films	147
III.2.a. Determination of the Epoxy Equivalent Weight (EEW)	147
III.2.b. Determination of the Amine-Hydrogen Equivalent Weight (AHEW).....	149
III.2.c. Free films preparation.....	150
III.3. Characterization of the epoxy free films.....	150
III.3.a. Study of the curing processes	151
III.3.b. Properties of the cured epoxy films	153
III.4. Conclusion.....	164
IV. Pilot tests performed on epoxy free films.....	164
IV.1. Free films of the RenLam CY 219 / Ren HY 5161 system	165
IV.2. Free films of the Araldite DBF CH / Ren HY 956 system	166
IV.3. Free films of the RenLam CY 219 / IPDA system.....	167
V. Conclusion.....	168
References.....	169

Chapter V: Adhesion of the Epoxy Coating onto Stainless Steel

I. Introduction	175
II. Non-optimized epoxy / stainless steel interface	175
II.1. Application of the coating	176
II.2. Immersion tests in model solvents	176
II.3. Conclusion	177
III. Cleaning of stainless steel	177
III.1. Presentation of the cleaning methods	177
III.2. Validation of the cleaning process	178
III.3. Immersion tests in model solvents	181
III.4. Conclusion	182
IV. Mechanical treatment	182
IV.1. Presentation of the shot-blasting process	182
IV.2. Characterization of the shot-blasted stainless steel surface	183
IV.3. Immersion test in model solvents	185
IV.4. Conclusion	187
V. Grafting of adhesion promoters onto stainless steel	187
V.1. Grafting of phosphonates, bisphosphonates and sulfonates onto stainless steel	188
V.1.a. Functionalization of stainless steel plates	188
V.1.b. Use of these molecules as coupling agents	189
V.2. Grafting of alkoxysilanes onto stainless steel: Influence of the non-hydrolyzable functional group of an alkoxysilane on its grafting onto stainless steel	189
V.2.a. Influence of the pH	190
V.2.b. Prehydrolysis duration	207
V.3. Influence of the number of hydrolyzable groups of the alkoxysilane on its grafting onto stainless steel	209
V.3.a. Hydrolysis study	210
V.3.b. Grafting of monoalkoxysilanes onto stainless steel	213
V.4. Conclusion	214
VI. Impact of the surface pre-treatments on the adhesion of the epoxy coating onto stainless steel	214
VI.1. Non-optimized epoxy / stainless steel interface	215
VI.2. Impact of the mechanical treatment	217
VI.3. Effect of adhesion promoters	218
VI.3.a. Influence of the non-hydrolyzable functional group	218

VI.3.b. Influence of the prehydrolysis duration.....	220
VI.3.c. Influence of the number of hydrolyzable groups	221
VI.4. <i>Combination of mechanical treatments and adhesion promoters</i>	223
VI.5. <i>Conclusion</i>	224
VII. Validation - pilot tests	224
VII.1. <i>Non-optimized epoxy / stainless steel interface</i>	224
VII.2. <i>Effect of the mechanical treatment</i>	225
VII.3. <i>Effect of adhesion promoters</i>	226
VII.3.a. Influence of the non-hydrolyzable functional group.....	227
VII.3.b. Influence of the number of hydrolyzable groups	228
VII.4. <i>Combination of mechanical treatments and adhesion promoters</i>	229
VII.5. <i>Conclusion – Selection of a system</i>	230
VIII. Conclusion	231
References	232
General Conclusion	237

General Introduction

PolyVinyl Chloride (PVC) is nowadays one of the most used polymers on earth as it can be found in many daily-used devices. There are many polymerization processes that can be used to obtain this material but one of the most widespread is the suspension polymerization. This latter is used at the INEOS ChlorVinyls facility of Mazingarbe and allows an annual production of 255,000 tons for this site. This process is realized thanks to a closed-reactor technology with reactor walls made of stainless steel or enamel. One of the major problems during the production of PVC by suspension polymerization (S-PVC) is the formation of a deposit (called crust or scale) on the reactor walls. The formation of scales leads to numerous sorts of drawbacks like a decrease of the reactors' productivity, the need to clean the reactors after each batch, the exposure of the operators to VinylChloride Monomer (VCM) which is classified CMR, some quality issues...

It is clear that this phenomenon is a major problem for INEOS ChlorVinyls but also for other S-PVC producers. It is in this context that the FUI Ecoating project has been set up. This consortium between industrial and academic partners involves many actors like:

- INEOS ChlorVinyls: S-PVC producer and coordinator of the FUI Ecoating project.
- Mäder: formulation of the coating to achieve the desired properties to enable an easy application.
- Avenir Group: development of a cleaning and application robot for the reactors.
- ESPCI: computer modeling of the stirring profiles in the reactor to better understand the formation of scale.
- LPIM: study of the formation of scale and development of a protective polymer coating.

Actually, INEOS ChlorVinyls and other S-PVC producers apply a non-permanent coating before each batch. For example, in the INEOS ChlorVinyls of Mazingarbe, a formulation is coated 50 times per day in 22 different reactors. This fact involves a large consumption of coatings but also huge money and time issues as these solutions do not provide satisfactory results and are not able to prevent the formation of scale. The development of a permanent coating with good durability and anti-scale properties becomes of major importance as it would give INEOS ChlorVinyls a great advantage over its rivals.

It is in this context that the work presented during this thesis has taken place. The aim of this study was to first understand the formation of scale mechanism in order to develop afterwards a durable polymer coating. This Ph.D. work was divided into two phases. The first part was dedicated to the determination of the scale formation mechanism from a chemical and a physical-chemical point of view. The second part was the development of the coating with first a work on the structure of the coating (presence of diluents, influence of the curing

agent, influence of the curing parameters, and correlation between the intrinsic properties of the coating and the anti-scale properties) and then a study on the adhesion of the coating on the substrate and its optimization. This study must result in the proposal of a durable polymer coating which will be tested at a pilot scale during the following of the Ecoating project.

This manuscript is divided into five chapters that relate the work done during this research.

The first chapter is a bibliographic study which includes interesting information on the formation of scale but also on the development of the polymer coating. The first part is dedicated to general presentations of PVC and the suspension polymerization process. Some information about the formation of scale were gathered in order to check the mechanisms already described in the literature. The next part is dedicated to a presentation of the substrate used during this work, stainless steel, and of polymer coatings, more precisely of epoxy coatings, which were used during this study. Finally, a large part of this bibliographic chapter deals with adhesion mechanisms and the different surface treatments that can be performed in order to strengthen an adhesive / substrate interface. A high focus was made on adhesion promoters like phosphonates or alkoxy silanes.

The second chapter is a presentation of the raw materials, the experimental techniques and the processes used to obtain the samples and the ways of testing them.

The third chapter deals with the study of the scale formation and the determination of this phenomenon's scenario. On one hand, this study was performed by studying model solutions simulating the S-PVC reactive medium in the laboratory. To do so, stainless steel plates were immersed in liquids containing different compounds which are present in the real reactive medium. These plates were then analyzed by microscopy and infrared spectroscopy techniques. On the other hand, some stainless steel plates were immersed in a pilot reactor (standing at the INEOS ChlorVinyls facility in Mazingarbe) that exactly reproduces a real-time S-PVC batch. The variation of different parameters and the analyses of the immersed plates allowed to establish the nature of the responsible chemical species and to have a kinetic approach on this phenomenon.

The fourth chapter was dedicated to the choice of a suitable epoxy system. This choice was made by studying the properties of epoxy free films in terms of curing conditions but also of network properties. These tests were performed on commercial epoxy systems but some experiments were also made by using pure polyamines with a commercial epoxy resin. The goal here was to make a correlation between the structure of the cured network with its main properties mainly in terms of thermal, mechanical and chemical resistances. The system

possessing the best behavior during these tests was selected for immersion tests in the pilot reactor to check its anti-scale properties.

The last chapter is focused on the optimization of the adhesion of the epoxy coating onto stainless steel. The epoxy / stainless steel interface is known to be water-sensitive and it was clear that the adhesion had to be strengthened. To do so, a three-way strategy was set up. The first part deals with the cleaning process. Different cleaning methods were compared and the best one was chosen by performing surface analyses (contact angle measurements and XPS). The second part was about the mechanical treatment of the substrate. The effect of a shot-blasting process was regarded in terms of topographical modification (measurement of the roughness) but also in terms of chemical changes at the surface (SEM-EDX). Finally, a large part of this Ph.D. work was dedicated to the study of adhesion promoters. Many molecules like phosphonates, bisphosphonates, sulfonates or alkoxy silanes were experimented. The behavior of these molecules in aqueous solutions and their grafting onto stainless steel were studied. The effect of these treatments on the epoxy / stainless steel interface was checked by measuring the adhesion force by pull-off tests before and after immersion in hot water. Finally, the most promising formulations were sent to the pilot reactor for final tests.

After all these different steps, an ideal surface preparation process was proposed for the application of a durable and protective polymer coating to prevent the formation of scale during the S-PVC production.

Chapter I

-

Bibliographical Study

CHAPTER I: BIBLIOGRAPHICAL STUDY

I. Context - Suspension polymerization of VinylChloride Monomer (S-PVC).....	11
I.1. Basics on PolyVinyl Chloride (PVC)	11
I.2. The suspension polymerization process.....	11
I.3. S-PVC production at INEOS ChlorVinyls - Mazingarbe.....	14
I.4. Conclusion.....	15
II. Scale formation during the suspension polymerization of VCM.....	15
II.1. Industrial issues and stakes	15
II.2. Scale formation mechanism described in the literature	17
II.2.a. First step: Formation of a copolymer	17
II.2.b. Second step: Adsorption of the copolymer on the reactor's walls.....	18
II.2.c. Third step: Development of the crust.....	18
II.3. S-PVC anti-scaling solutions.....	19
II.3.a. Solutions used by INEOS ChlorVinyls.....	19
II.3.b. Other patented solutions	22
II.4. Conclusion.....	23
III. AISI 316L stainless steel	24
III.1. General presentation.....	24
III.2. Surface and bulk chemical composition of 316L stainless steel.....	24
III.3. Interactions between stainless steel and suspension polymerization's reactants	26
III.4. Pitting corrosion	27
III.5. Conclusion.....	28
IV. The polymer coatings.....	28
IV.1. General points on coatings	28
IV.2. Coating's specifications.....	29
IV.3. Epoxy resins.....	30
IV.3.a. Presentation of bisphenol-A diglycidylether (BADGE) resins.....	30
IV.3.b. Curing of the BADGE prepolymer	32
IV.4. Conclusion.....	33
V. Epoxy coating's adhesion onto stainless steel.....	34
V.1. Basics on adhesion	34
V.1.a. Work of adhesion.....	34
V.1.b. Fracture theory	34
V.1.c. Weak boundary layer theory.....	35

V.1.d.	Wetting - contact theory.....	35
V.1.e.	Diffusion theory.....	35
V.1.f.	Chemical adhesion.....	36
V.1.g.	Mechanical adhesion.....	36
V.1.h.	Electrostatic adhesion.....	36
V.1.i.	Acid-base adhesion.....	36
V.1.j.	Summary of the usual bond types.....	37
V.1.k.	Combination of the phenomena.....	37
V.2.	<i>Epoxy / stainless steel adhesion</i>	38
V.2.a.	Description of the adhesion of epoxy onto stainless steel.....	38
V.2.b.	Behavior in an aqueous medium.....	38
V.3.	<i>Optimization of the epoxy / stainless steel interface</i>	39
V.3.a.	Cleaning / pickling.....	39
V.3.b.	Mechanical treatment.....	41
V.4.	<i>Conclusion</i>	42
VI.	<i>Adhesion promoters / Primers</i>	42
VI.1.	<i>Phosphonates</i>	42
VI.1.a.	Introduction.....	42
VI.1.b.	Phosphonic acid chemistry.....	43
VI.1.c.	Adsorption on metallic substrates.....	43
VI.1.d.	Bisphosphonates.....	45
VI.2.	<i>Sulfonates</i>	46
VI.3.	<i>Trialkoxysilanes</i>	47
VI.3.a.	Introduction.....	47
VI.3.b.	Behavior of the trialkoxysilanes in aqueous solution.....	48
VI.3.c.	Hydrolysis reactions.....	49
VI.3.d.	Condensation reactions.....	51
VI.3.e.	Factors affecting the hydrolysis / condensation reactions.....	53
VI.3.f.	Composition of the hydrolysis solution.....	55
VI.3.g.	Grafting of trialkoxysilanes onto inorganic substrates.....	56
VI.3.h.	Factors affecting the grafting of trialkoxysilanes.....	58
VI.3.i.	Trialkoxysilanes for the optimization of the epoxy / stainless steel interface.....	60
VI.3.j.	Conclusion.....	63
VI.4.	<i>Monoalkoxysilanes</i>	64
VI.4.a.	Introduction.....	64
VI.4.b.	Hydrolysis.....	65
VI.4.c.	Grafting.....	65
VI.4.d.	Conclusion.....	66

VI.5. Conclusion.....	66
VII. General conclusion.....	67
References.....	68

I. Context - Suspension polymerization of VinylChloride Monomer (S-PVC)

I.1. Basics on PolyVinyl Chloride (PVC)

PolyVinyl Chloride (PVC) is nowadays the third-widely used polymer ¹. This material is used in many applications like the construction industry (window frames, flooring, pipes...), clothing, electric cable insulating and is also an alternative for the use of rubber ². This polymer is also found on daily-used devices as for example credit cards, bottles, toys, shoe soles, packaging...

This material is obtained through radical polymerization of VinylChloride Monomer (VCM). The general chemical equation is presented on figure I-1.

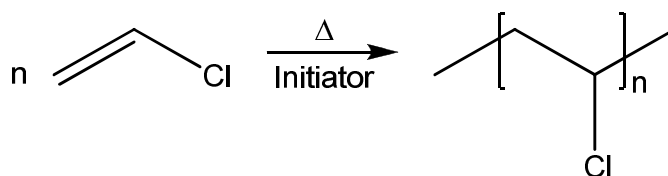


Figure I-1. Polymerization reaction of VCM.

The resulting properties from the chemical structure of PVC are a high hardness, good mechanical properties, poor thermal stability but also flame-retardancy properties and good insulating properties ².

PVC can be obtained by many polymerization processes like mass polymerization, emulsion-based polymerization or suspension polymerization ¹⁻³. This latter is the production process used at the INEOS ChlorVinyls facility in Mazingarbe and will be described in the following of this bibliographical study.

I.2. The suspension polymerization process

The suspension polymerization process is a discontinuous biphasic process in which VCM (organic phase, gaseous at ambient conditions) is dispersed under pressure into water (dispersive medium) ^{3,4}. Stabilization of the monomer is ensured by stirring of the reactive medium and by using a surfactant. In most of the cases, PolyVinyl Alcohol / PolyVinyl Acetate copolymers (PVA / PVAc) are used to both decrease the interfacial tension between

water and VCM and also to protect the formed PVC droplets from coalescing. This process will lead to the formation of VCM droplets of around 10 to 50 μm diameter.

A radical initiator (mainly peroxides) is used to start the polymerization in the monomer droplets. This molecule, soluble in the organic phase, will be decomposed into two radicals, thanks to heating of the reactive medium, leading to the beginning of the formation of PVC chains. Each VCM droplet is, at this point, considered as a little mass polymerization reactor^{3,4}.

The polymerization medium is heated (at around 70 - 80 $^{\circ}\text{C}$) thanks to the double jacket of the reactor with hot water and is submitted to a high pressure (at around 10 bars)⁴. The temperature is a very important factor because it is directly related to the final molecular weight of PVC (known as the K-Wert value)⁵, as this value will decrease by increasing the reactive medium temperature. A precise control of the reactive medium's temperature, adjusted by the double jacket at the reactor's walls, is also a major point to obtain the final polymer with the desired properties.

PVC is almost not soluble in its monomer (around 1 $\text{g}\cdot\text{kg}^{-1}$ at usual polymerization temperature)³ meaning that two steps are occurring during the S-PVC production:

- For conversion rates lower than 0.1 %, the polymerization kinetic is similar to the one observed for an homogeneous polymerization in solution.
- For conversion rates higher than 0.1 %, there will be a biphasic medium with on one hand the polymerization medium and on the other hand the liquid monomer phase (also known as gel) constituted from precipitated and swollen (by VCM) PVC. These two phases will coexist until a conversion rate of 75 % is reached. At this point, the PVC content is high enough to solubilize the remaining VCM and the system becomes again monophasic³.

The formation of PVC grains is a three steps process as described on figure I-2⁶.

Steps	Species	Size	Conversion	
Nucleation	Random macroradical coils		< 1 %	10-20 nm
	Micro-domains		1-2 %	100-300 nm
Growth	Domains		0.6-1.5 μm	
	Primary particles		4-10 %	3-10 μm
Aggregation	Aggregates		> 75 %	20-40 μm
	Porous subgrains			

Figure I-2. PVC grain formation mechanism.

During the very first stages of the process, the radicals formed by decomposition of the initiator will react with VCM molecules resulting in the formation of insoluble PVC macromolecules. The aggregation of these polymer chains will lead to the formation of unstable micro-domains standing at the monomer / water interface and also helping the stabilization of the monomer droplets.

During the growth stage, there is an aggregation of the micro-domains into larger domains (constituted from around 1,000 micro-domains). The primary particles are then formed after growth of the domains and are precipitated in the monomer-rich phase. These particles form a colloidal suspension stabilized by the fact that they carry a negative charge due to the presence of chlorine ions at the VCM / PVC interface ⁷. Unstable micro-domains are absorbed by these primary particles during the first stage of the suspension polymerization.

The last stage is the aggregation step. Flocculation and growth of the primary particles in the monomer droplets continue until a critical conversion rate is reached. At this point, the particles tend to regroup and to form a continuous polymer network called aggregates. At conversion rates higher than 75 %, primary particles and aggregates will merge to form PVC

porous subgrains which correspond to a polymerized VCM solid particle^{3,8}. At the end of the polymerization, 50 to 250 µm-diameter PVC grains, composed at least of one subgrain, are obtained. The final beads are also porous mainly because of the presence of empty spaces between the aggregated subgrains (intercellular porosity).

After the formation of the final polymer beads, PVC is still in the reactor, dispersed in water⁴. The reactor's pressure goes down at a time corresponding to the stop of the polymerization reaction. The remaining unreacted VCM is removed during the degassing step in order to be "recycled". The PVC slurry is then removed and the reactor totally discharged. Slurry from the reactor is blended with other several batches in the slurry tank. A dehydrator is then used to remove water from the slurry and the wet cake is sent to the drier. Coarse particles are removed and the dried PVC powder is stored in silos, controlled in terms of quality and is ready to be shipped⁴.

I.3. S-PVC production at INEOS ChlorVinyls - Mazingarbe

A typical INEOS ChlorVinyls polymerization line is composed of five or six 40 m³ reactors. Two production lines are composed of enamel-type reactors and the other two lines are constituted by stainless steel-made reactors. Each reactor is charged and discharged two times per day enabling the annual production of 255,000 tons for the whole Mazingarbe facility. A typical polymerization line is schemed on figure I-3.

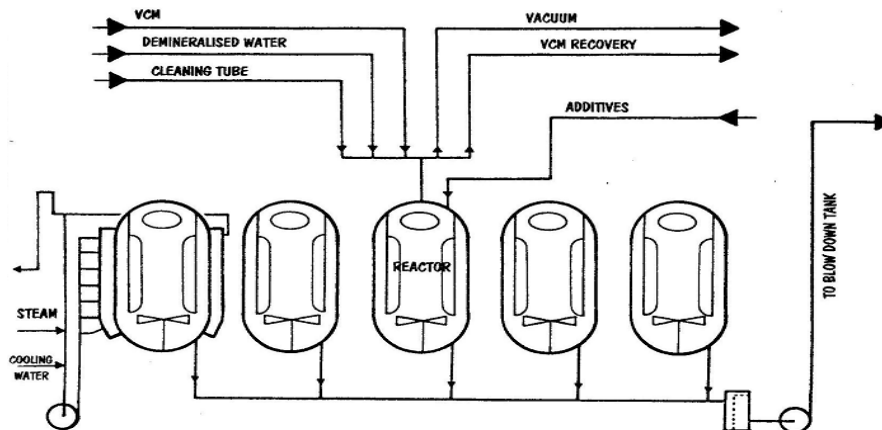


Figure I-3. Typical INEOS ChlorVinyls S-PVC polymerization line.

During one batch, the weight proportions of products used is given in table I-1.

Table I-1. Weight proportions of the raw materials used during a S-PVC polymerization at INEOS ChlorVinyls.

Products	Weight proportions	Weight introduced (kg)
Demineralized water	100	≈ 15,000
VCM	50 - 70	7,500 - 10,500
PVA I / II	0.1 - 0.5	15 - 75
Initiators	0.05 - 0.3	7.5 - 45
Buffer	0 - 0.1	0 - 15
Antifoaming agent	0 - 0.002	0 - 0.3

The R&D section of the INEOS ChlorVinyls facility at Mazingarbe developed a technology enabling to produce PVC without opening the reactor after each batch. This process, leading to a decrease of the released VCM content, is known as the Closed Reactor Technology (CRT).

1.4. Conclusion

The suspension polymerization process, which is basically the most interesting way of synthesizing PVC, from an economical and technical point of view, is still not fully optimized. One of the major issues related to this process is the formation of a scale on the reactor's walls during the production of PVC.

II. Scale formation during the suspension polymerization of VCM

II.1. Industrial issues and stakes

The formation of scale, during the suspension polymerization of vinyl chloride, has always been a major problem for S-PVC producers ⁹. Growth of a hard and strongly adhered polymer crust during successive polymerizations affects the suspension polymerization of VCM in numerous ways:

- The reactor productivity: decrease of the heat transfer at the reactor's walls and blockages during the discharging process.
- The final polymer morphology: change of the stirring profile in the reactor.
- The quality problems: increase of the Fish Eyes (gelified particles) rate.

- The economical issues: shutdowns of the reactors for cleaning and loss of the raw materials stuck in the scale.
- The health hazard: residual CMR (carcinogenic, mutagenic and / or toxic to reproduction) -classified VCM trapped in the PVC scale harmful for the cleaning operators.

This problem is not a recent issue as the Swedish Occupational Health Standard already described this problem in 1979 and mainly the consequences of the exposition of the human body to VCM ¹⁰.

The stakes for INEOS ChlorVinyls to stop the formation of scale during the S-PVC production are huge. As a matter of fact, avoiding scaling of the reactors would give a great lift to Mazingarbe's facility by greatly increasing its production rate and also by decreasing the energetic consumption of the facility. The benefits from the development of an anti-scaling technology are summed up in figure I-4.

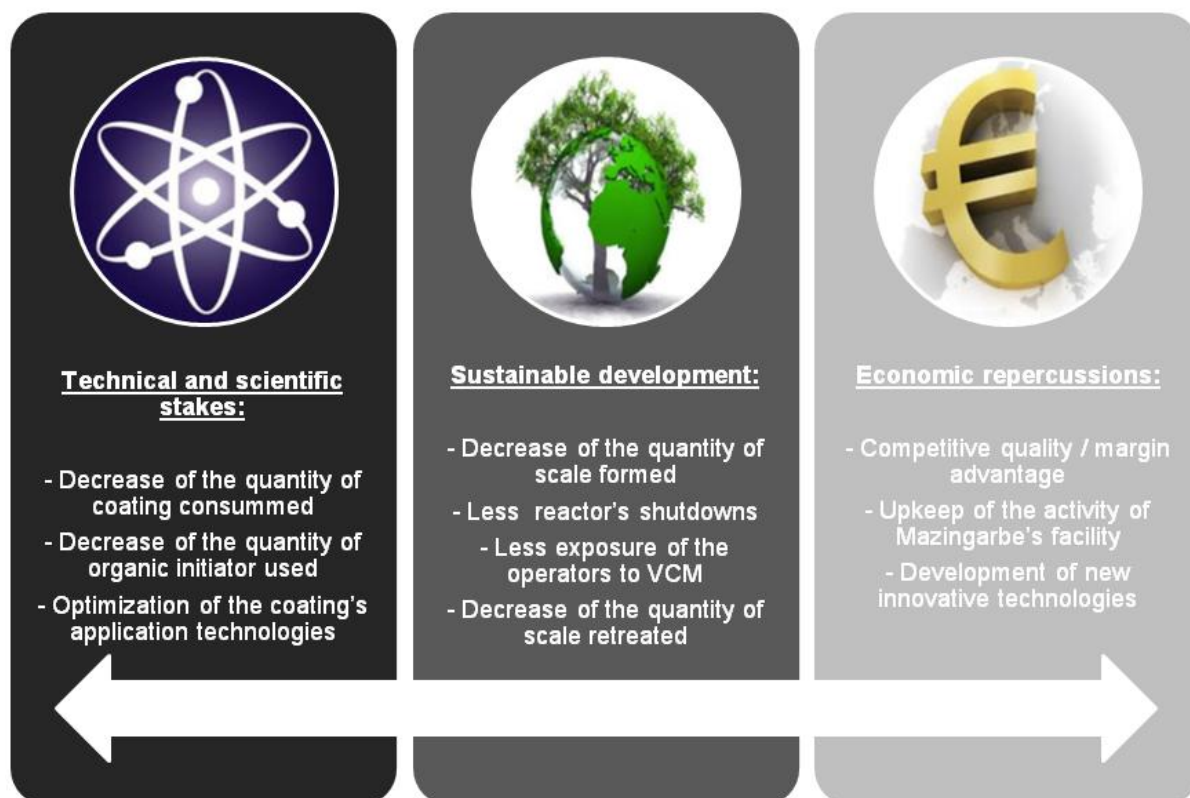


Figure I-4. Recap of the stakes coming from the development of an anti-scale coating.

This problem has not been solved yet and there is no chemical or physical mechanism describing this process. Still, there are a few publications which tried to give an explanation to this phenomenon.

II.2. Scale formation mechanism described in the literature

The first sign of the presence of scale, in the case of suspension polymerization of VCM, is the appearance of a thin layer strongly adhered to the reactor's walls^{9,11}. The crust will then grow from the initial thin skin to thicker sheets. This accumulation of PVC particles is irregularly shaped and harder at the places where the surface of the reactor's walls is discontinuous (agitator, liquid / gas interface...). Although, the formation of this crust is not a continuous process but is due to numerous successive steps. Each of these steps has its own mechanism.

II.2.a. First step: Formation of a copolymer

There is first the formation of a copolymer in the aqueous phase between the VCM and the dispersant or suspending agent (Poly VinylAlcohol, PVA)^{9,11}, probably by a transfer reaction of the PVC macroradicals on PVA. The hypothetical reaction scheme for the formation of the copolymer is presented on figure I-5.

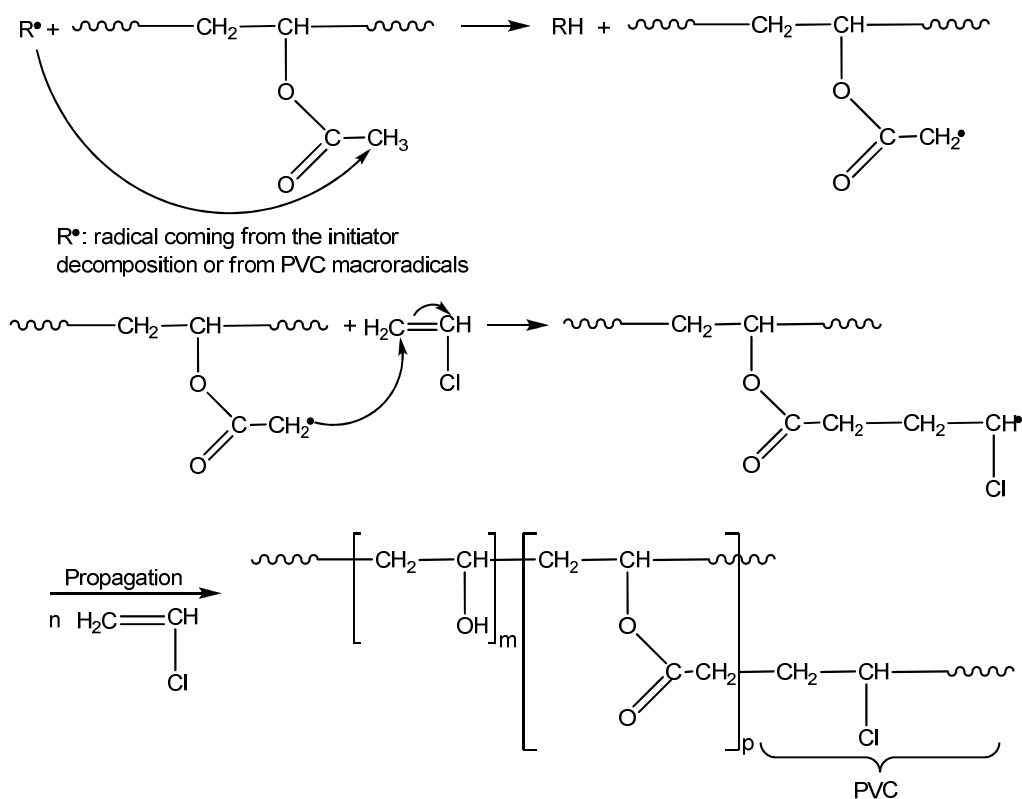


Figure I-5. Formation of a PVA-g-PVC copolymer.

This copolymer (also known as “Acvagen” Graft Copolymer or AGC) has the same structure than the pericellular membrane, which surrounds the polymerization droplets containing the VCM^{9,11}. The formation of this membrane has been described in the literature¹¹. Two phenomena occur at the same time: the polymerization in the monomer droplets dispersed in water and the polymerization of VCM in the aqueous phase (as VCM is 1% by weight soluble in water). The formation of this copolymer mainly occurs in the water phase and is enhanced by the presence of the water-soluble fraction of initiator. The AGC is dispersed in water at this time. Moreover, it is interesting to note that the PVA used contains some double bonds which are useful for the stabilization of the monomer droplets by co-reacting with the growing PVC chains.

The use of ascorbic acid has already been patented to neutralize the water-soluble part of the initiator. Another problem is also faced with this method because this compound disturbs the initial grafting of the suspending agent on the VCM droplets. Moreover, the action of reducing agents is inhibited by the presence of oxygen.

II.2.b. Second step: Adsorption of the copolymer on the reactor's walls

The AGC's particles will then be adsorbed on the monomer droplets (which are 0.2 µm thick) and on the reactor's walls^{9,11}. This adsorption takes place at the immersed parts of the reactor (in the liquid phase and at the liquid/gas interface (presence of foam)). It is also probable that only a part of the AGC particles hitting the surface will be adsorbed on it. The collision efficiency will depend on the energy (that is to say the collision speed) stored by the AGC particles, the place where they are and the irregularities at their surface and at the surface of the walls. The formation of the AGC could also be catalyzed by the presence of transition metals.

II.2.c. Third step: Development of the crust

The first layer adsorbed will act as a nucleation site for the development of the crust^{9,11}. This step can be known as a point of no return: the scale formation process cannot be stopped after this point. These three steps can be diagrammed as follows (figure I-6)¹¹.

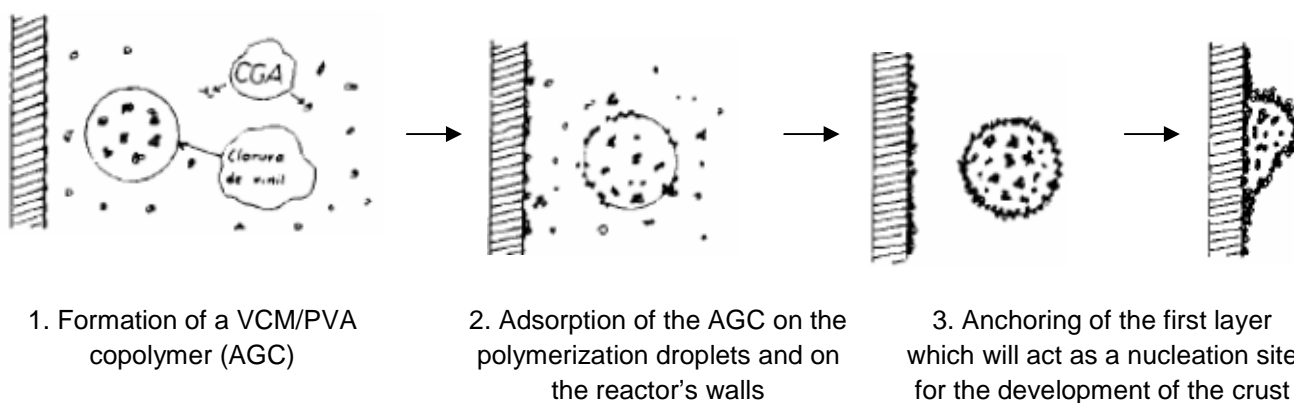


Figure I-6. Development of the crust on the reactor's walls.

According to this mechanism, an effective way to fight against the scale formation is to avoid one of these three steps to happen.

Actually, some solutions have already been developed to prevent this problem and a few are already used by INEOS ChlorVinyls.

II.3. S-PVC anti-scaling solutions

The processes developed to avoid scale can be divided into 3 main methods: the “without additives” solutions, the “anti-scaling” additives and the coatings. The solutions used now by INEOS ChlorVinyls are classified in the third category (coatings) and are presented in the following part.

II.3.a. Solutions used by INEOS ChlorVinyls

II.3.a.i. Coating obtained by condensation of phenol with formaldehyde

This organic coating is obtained by reacting phenol with formaldehyde (figure I-7).

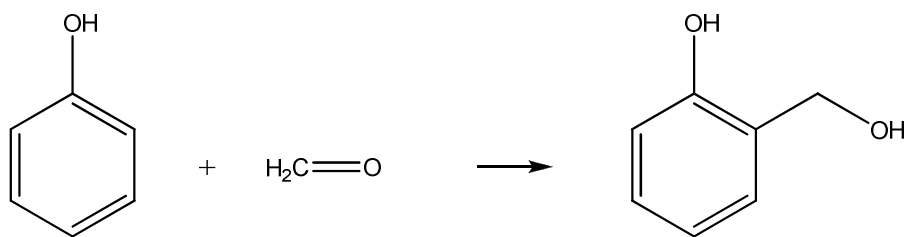


Figure I-7. Chemical reaction of phenol with formaldehyde.

The formation of a phenolic network will be reached by dehydration of the previously obtained molecule (figure I-8) ¹².

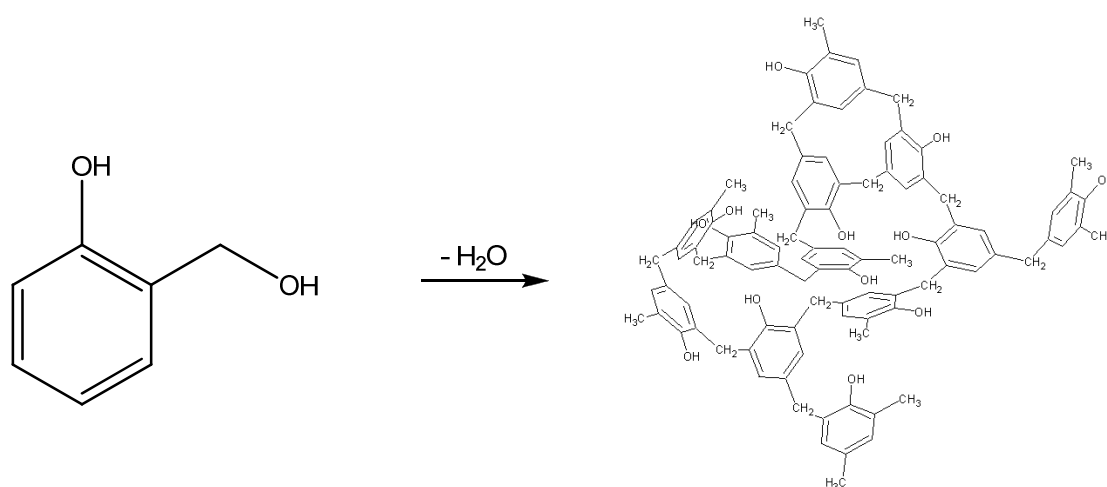


Figure I-8. Formation of a phenol-based coating.

This coating is dispersed in a base-catalyzed solution and is then precipitated on the reactor's walls. Even if it is efficient at pH inferior to 10, this coating has some major drawbacks. First, its extreme oxygen-sensitiveness leads to a color change as the coating becomes dark. Moreover, during the suspension polymerization, some of these dark particles can peel off from the walls and pollute the final polymer (color changes and toxicity). Another problem is the difficulty to control the condensation reaction. Besides, a large amount of coating has to be applied to be efficient causing at the end some economical issues.

However, the mechanism of action of this technology, mainly used by Air Products and Dow Chemicals ¹³, has not been described in the literature.

II.3.a.ii. Coating obtained by condensation of 1-naphtol with formaldehyde

This technology corresponds to an improvement of the previously described coating by replacing phenol by 1-naphtol (figure I-9) ¹⁴.

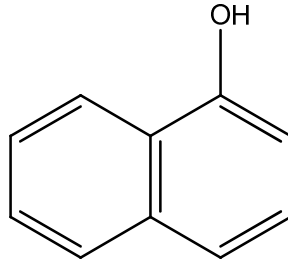


Figure I-9. Chemical formula of 1-naphtol.

The condensation product is synthesized in an aqueous alkaline medium. Better covering of the substrate can be achieved by using surfactants. The coating can be applied by spraying or by manual application (brushing). The simplest way to achieve an optimal covering of the surface is to use an internal equipment to perform deposition of the coating after each batch without opening the reactor.

The main drawback of this solution is that the coating has to be applied after each batch to provide an efficient anti-scaling protection. Again, the mechanism of action of this system has not been extensively studied but some explanations have been proposed as shown on figure I-10 ⁹.

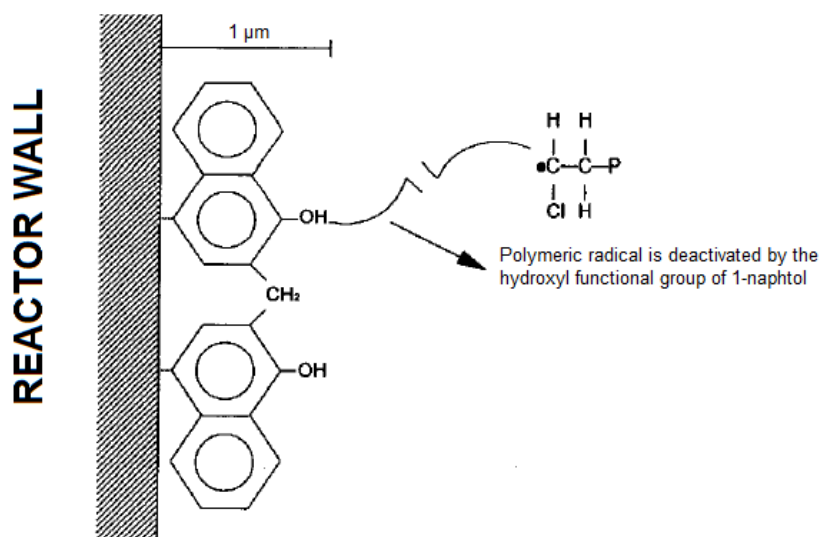


Figure I-10. Mechanism of action of a 1-naphtol-based coating.

The efficiency of this coating could be due to its highly conjugated structure which is used as a chain stopper⁹. As a matter of fact, the polymeric radical is highly stabilized by the aromatic structure (conjugation across the π - system) and further conjugation is obtained through the methylene bridge via the enol structure. In the case of this coating, the reaction with PVC radicals will lead to the formation of a quinone structure¹⁵. Bulky substituents are avoided because such chemical functions prevent the formation of a protective film covering the surface well. Some studies also proved that the aromatic rings in the coating tend to be oriented parallel to reactor walls giving optimal performances of this anti-scaling material¹⁶.

II.3.a.iii. Coating using an amine derivated from benzoic acid and from polyvinyl(alcohol) mixed with a natural polyphenol

Aromatic polyamines were lately used as anti-scaling materials. Even if many drawbacks have been faced (changes of colour and poor efficiency), some solutions were found in order to improve their action like for example the utilization of a polyvinyl(alcohol) mix. These PVAs can be esterified by an amine derivate synthesized from benzoic acid and natural polyphenols^{17,18}. A transparent coating is obtained when applied in a closed oxygen-free reactor. However, this solution is not as durable as expected.

II.3.a.iv. Conclusion

Some of the solutions described above are now used by INEOS ChlorVinyls to prevent the scale formation during the VCM polymerization. However, none of them are durable and satisfactory as the application of the coating is necessary between each batch (leading to economical issues) and also because the synthesized PVC can be polluted by residual coating leaving the reactor walls due to wear in the reactive medium.

II.3.b. Other patented solutions

There are plenty of different solutions that have already been developed and patented to prevent the formation of scale. These methods can be classified into three categories depending on their mode of action.

Some of the methods are just based on process modifications without using additives. Some examples are the modification of the heating periods during the batch ¹⁹, the use of a condenser to reduce the exothermal effect of the reaction ²⁰ or a modification of the reactants' introduction order.

Another category gathers some methods based on the use of "anti-scale" additives. These latter consist in pH regulators (to reduce the corrosion due to chloride ions), in water-soluble oxidizing or reducing additives ²¹ or in the use of inorganic compounds ²² (like magnesium hydroxides).

The last category is based on "anti-scale" coating solutions with mainly the use of organic / polymer coatings ²³ (polyurethanes, phenolic resins...) or inorganic ones ²⁴ (electropolishing, deposition of alloys...).

However, no mention is made in the different patents on the durability and reliability of these methods.

II.4. Conclusion

It is clear that the formation of scale during the suspension polymerization of VCM is a major problem faced by S-PVC producers for a long time. However, the phenomena explaining the formation of this deposit have not been widely described in the literature.

Some methods have already been developed to prevent the scale formation and consist in process solutions, "anti-scale" additives and coatings. INEOS ChlorVinyls is using a coating solution but it is not satisfactory as it has to be applied after each batch.

It is interesting to note that this phenomenon has been observed regardless of the material that constitutes the walls. At INEOS ChlorVinyls, two polymerization lines are enamel made and the two other ones are stainless steel made. It was decided, during this study, to focus on stainless steel for which the low surface reactivity could constitute a problem for the coating's adherence.

III. *AISI 316L stainless steel*

III.1. General presentation

Stainless steel is an alloy of iron and carbon (steel) enriched with chrome to reach resistance against corrosion²⁵⁻²⁷. This metal is widely used due to its mechanical, chemical and thermal resistance properties. Stainless steel can be used in many applications like for cookware, cutlery, household hardware, surgical instruments, major appliances, industrial equipment and as an automotive and aerospace structural alloy and construction material in large buildings.

There is a large variety of stainless steel grades. The one constituting the INEOS ChlorVinyls' reactors is American Iron and Steel Institute (AISI) 316L grade. It is part of the austenitic family (face-cubic centered crystal structure). This grade is the second most used austenitic stainless steel and it can mainly be found in the pharmaceutical, agri-food, chemical and petrochemical industries.

The chemical composition of this material is first presented to better understand the interactions between the suspension polymerization reactive medium and the reactor walls.

III.2. Surface and bulk chemical composition of 316L stainless steel

The chemical composition of the 316L stainless steel bulk is given in table I-2²⁶.

Table I-2. Chemical composition of the 316L stainless steel bulk.

Elements	Fe	C	Cr	Ni	Mo	Mn	Si	P	N	S	Cu
% w/w	69.5	0.02	16.7	10.1	2.12	1.13	0.41	0.032	0.023	0.002	-

The main bulk elements are iron, chromium (resistance against corrosion), nickel (enhancement of the mechanical properties) and molybdenum (enhancement of the thermal properties). However, the chemical composition of the surface is quite close to the one of the bulk and it was underlined that the main elements present at the surface are iron, chromium, nickel and molybdenum. Steel, when exposed to air, is naturally covered by a thin layer composed of oxides (mainly iron and chrome oxides) and hydroxides²⁵. The chromium-rich layer is known as the passivation layer. The formation of this protective layer is responsible of the corrosion resistance properties of stainless steel. The passive film, which is highly

imbricated to the metallic bulk, avoids direct contact between an aggressive medium and stainless steel. The thickness of this layer is, depending on the environment, comprised between 10 Å and 20 nm^{25,28,29}.

Finally, the extreme surface of stainless steel is covered by a last layer which is composed of hydrocarbons and known as a contamination layer (rolling oil, atmospheric pollution...).

A value useful to describe the difference of composition between the bulk and the surface is the enrichment factor (F_{Me}) which is defined as the ratio between the percentage of metal elements present at the surface and the percentage of metal elements present in the bulk^{25,26}. XPS analyses were used to determine the content of the elements at the surface and also the enrichment factor for each of these elements (table I-3)²⁶.

Table I-3. Metallic elements present at the 316L stainless steel's surface and enrichment factor F_{Me} .

Eléments	Fe	Cr	Ni	Mo
% (w/w)	87	11	1	1
F_{Me}	1.2	0.6	0.2	0.5

The F_{Me} values obtained also show that there is an increase of the relative iron content compared to the other elements. It is obvious to say, by viewing the F_{Me} evolution and remembering the presence of the chromium-rich passive layer, that the stainless steel surface is mainly composed of iron and chromium oxides and hydroxides.

It is possible to illustrate 316L stainless steel from a chemical composition point of view (figure I-11).

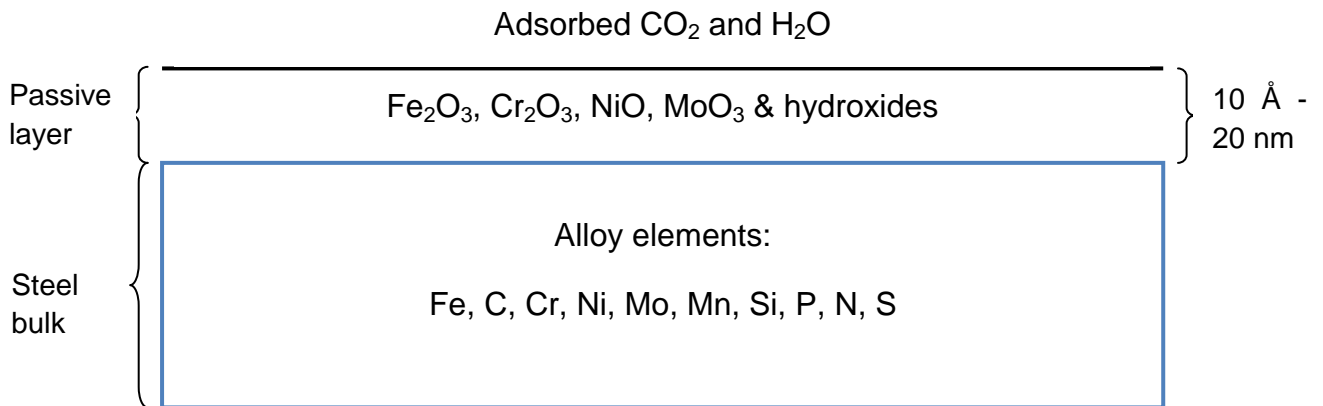


Figure I-11. Representation of the stainless steel's chemical composition.

Despite the fact that stainless steel is stable towards oxidation, it can interact with some compounds of the VCM polymerization medium.

III.3. Interactions between stainless steel and suspension polymerization's reactants

As a reminder, the main reactants present at the beginning of the polymerization are water, peroxides, surfactants and VCM.

The interactions between stainless steel and peroxides have been studied in the literature. Peroxides can be used as pickling agents³⁰ but this effect is not always desired. Wada et al.³¹ worked on the effect of the presence of a failure at the surface of an AISI 304 stainless steel alloy and also to the chemical reactions happening during this process. Even if 304 stainless steel chemical composition is slightly different from the one of 316L, a parallel between both materials can be done in order to understand their interactions with peroxides. Measurement of the corrosion potential during immersion in a peroxide-rich environment allowed to understand the different phenomena happening in presence of such compounds (figure I-12)³¹.

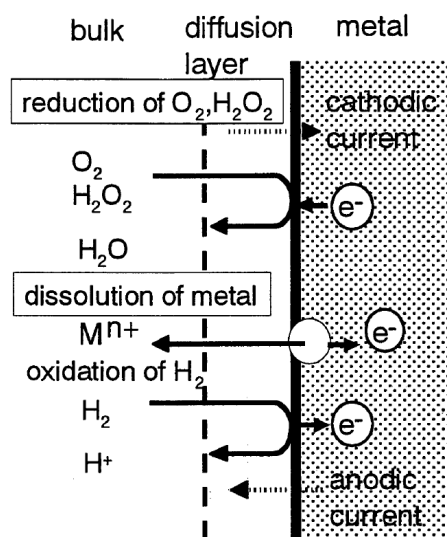
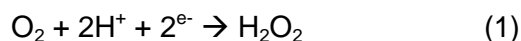
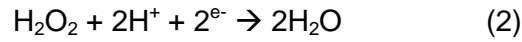


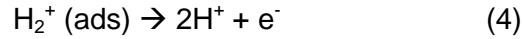
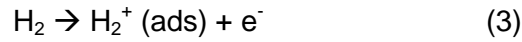
Figure I-12. Electrochemical phenomena at the stainless steel's surface in a hydrogen peroxide-rich medium.

Various electrochemical reactions are occurring at the stainless steel surface. There is first the decomposition of dioxygen and hydrogen peroxide into water:





Oxidations reactions can take place at the metal / H_2O_2 solution interface:



All these reactions induce the formation of an electrochemical current leading to the dissolution of metal (M^{n+}) that is to say corrosion. It is also quite clear that peroxides can have an impact on the degradation of the 316L-made reactors. It will also be necessary during this study to determine the influence of the peroxide on the formation, adsorption and the development of scale during the S-PVC process.

III.4. Pitting corrosion

Another critical factor is the formation of hydrochloric acid (HCl) during the S-PVC process. The presence of this chemical specie can lead in some cases to pitting corrosion²⁹. This phenomenon can happen on a very limited area of the metallic alloy and cause a local failure in the passivation layer of stainless steel. In the worst cases, it can result in the perforation of the material (figure I-13)²⁹.

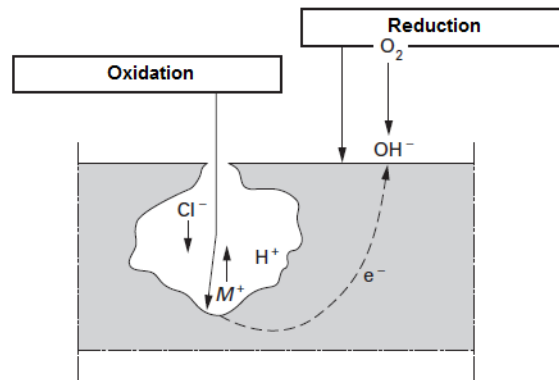


Figure I-13. Propagation of pitting corrosion in a chlorine-rich medium.

It is also interesting to note that high temperature, like during the suspension polymerization of VCM, is an aggravating factor.

In this context, a stainless steel surface which is resistant to uniform corrosion can undergo pitting corrosion²⁹. Many mechanisms, related to the presence of chloride ions (Cl^-) explain this phenomenon. The main steps are the adsorption of chlorine ions on the passivation

layer, the penetration of these species in the passivation film leading to the formation of metallic chlorides (MCl_3) and the acceleration of the anodic dissolution causing the failure of the passivation film.

There are no significant proofs that the corrosion process is responsible of the formation of scale during the suspension polymerization of VCM. However, the formation of HCl during this process has to be taken into account and regarded as a possible way to explain the formation of the deposit.

III.5. Conclusion

Stainless steel is the material used for the manufacturing of the S-PVC reactors used at INEOS ChlorVinyls which was studied during this project. This material has very good anti-corrosion properties thanks to the formation of a stable oxide and hydroxide passivation layer. The reactivity of the extreme surface of this metal is very limited and the polymer coating that will be chosen must have satisfactory adhesive properties.

After studying the formation of scale and the stainless steel composition from a chemical point of view, a great focus will be made in the following of this report on the considered solution: the polymer coatings.

IV. The polymer coatings

IV.1. General points on coatings

Coatings are nowadays a widespread technology^{32,33}. It can mainly be defined by its task as it might be able to provide surface protection, decorative finishes and also other specific properties (corrosion resistance, water-repellency...). There are three main coating families: the inorganic, the metallic and the organic ones.

Inorganic coatings are basically made of fused organic minerals on metallic substrates³⁴. These are mainly composed of porcelain-enamels and ceramic coatings. The first category is used as steel coatings in plumbing and heating equipment... The ceramic coatings are mainly used as electrical insulator. However, these materials will not be used here as they have to be applied at high temperature (from 200 to 500 °C)³⁴.

Metallic coatings are considered as permanent coatings³⁴. The metal used as a substrate must have a higher melting point than the metal used as coating. A large variety of metals can be used like zinc, copper, tin, nickel, gold or chromium and can be applied by hot dipping, electroplating, metalizing... However, the affinity of the PVC scale for stainless steel makes us think that these coatings are not suitable for our purpose.

The organic coatings (or polymer coatings) are nowadays the most used worldwide^{32,33}. A lot of polymer coatings technologies have been developed (acrylic, epoxy, polyurethanes, polyester, amino...). These materials are suitable for many applications due to their large range of properties. Such coatings can be found in the building industry, the automotive industry, daily-life-use products... Their versatility comes from the fact that these coatings can be totally tailored by varying their chemical structures and by using additives (fillers, primers, pigments...).

This is a good point for polymer coatings but it also means that the correct candidate must be chosen to fit with the following specifications needed for our study.

IV.2. Coating's specifications

As a lot of polymer coatings are commercially available on the market, a suitable one had to be chosen by taking a closer look at the specifications needed. The main properties asked for the coating to be efficient are listed below.

First, the polymer coating must offer great adhesion on stainless steel which is known to be a poorly reactive surface. The high adhesion will be one of the greatest challenge due to the severe reactive medium. The coating will be in contact with hot water which is known to be harmful for hydrolysis sensitive interfaces and which can therefore lead to delamination of the coating. In the same time, the coating will have to show no affinity for the reactive medium so that the PVC scale can not be formed on it.

Then, the chemical resistance of the coating must be sufficient. As a matter of fact surfactants, peroxides, VCM, hydrochloric acid formed during the suspension polymerization and hot water again can be dangerous regarding to the intrinsic stability of the thermoset network coated on the reactor walls. Moreover, the swelling of the coating by water will have to be limited in order to avoid the penetration of this liquid between the polymer chains. This phenomenon would be a disaster as it would induce a plasticizing effect, with lower glass transition temperature (T_g) and lower mechanical properties.

The thermal resistance will be a major point too as the coating will have to face multiple temperature changes. In fact, suspension polymerization temperatures can reach 80 °C and the coating will have to sustain rapid heating and cooling while being able to be efficient at 80 °C during 7 hours (approximately the duration of 1 batch). This means that a glass transition temperature close or superior to 80 °C will be preferred so the material can keep its mechanical properties at the S-PVC batch's temperature.

Finally, the mechanical resistance of the coating is of main importance for many reasons. First, there will be, during the process, a lot of pressure changes in the reactor. This causes a double problem as the coating will still have to stay on its substrate and as the high pressure can lead to cracks in the polymer network. Moreover, the coating must exhibit great wear resistance. As a matter of fact, some hard PVC pellets are formed during the suspensions polymerization and this can lead to degradation of the extreme surface of the coating. A deteriorated coating surface means an increase of the surface roughness which can also act as preferential anchoring sites for scale.

All the specifications explained above make the choice of a suitable polymer candidate a difficult task. The final choice has been made on epoxy resins as this type of polymer can fit with the desired properties of the anti-scaling coating.

IV.3. Epoxy resins

The term “epoxy resin” is applied to prepolymers containing reactive epoxy (or oxirane) groups³⁵. These prepolymers allow, after reaction with a curing agent, to obtain a thermoset three-dimensional network. The cured polymer, when applied on a substrate, is known as “epoxy coating”.

Although a lot of chemical structures, based on epoxy functions are available, focus has been made on bisphenol-A diglycidylether (BADGE or DGEBA) resin.

IV.3.a. Presentation of bisphenol-A diglycidylether (BADGE) resins

This epoxy-type resin is the most widely used (worldwide production = 2.3 M tons) and is also known as the “classical epoxy resin”³⁶. This prepolymer is the reaction product of bisphenol A with an excess of epichlorhydrin in an alkaline medium (figure I-14)³⁵.

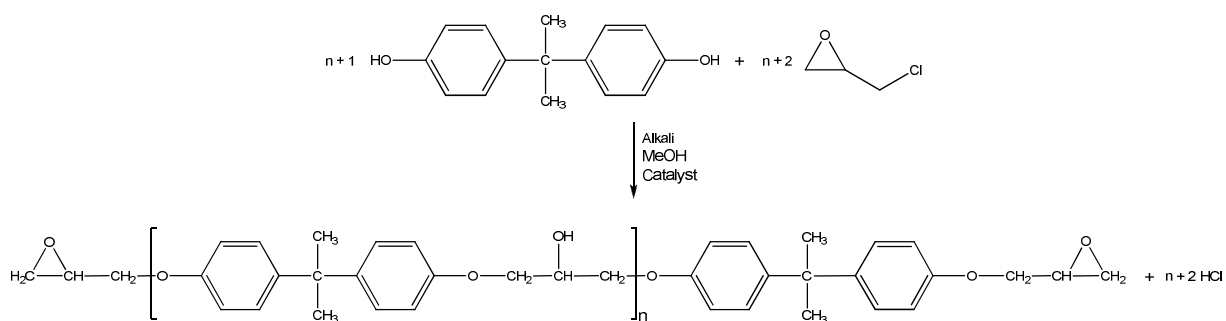


Figure I-14. Formation of a BADGE prepolymer by reaction of bisphenol-A with epichlorhydrin.

The polymerization degree (DP_n) of the BADGE prepolymer is a function of the bisphenol-A / epichlorhydrin ratio. Increasing the molar content of epichlorhydrin will lead to an increase of the polymerization degree.

BADGE prepolymers are often characterized by their Epoxy Equivalent Weight (EEW). This value corresponds to the weight (in grams) of resin containing 1 mole of epoxide group ($\text{g}\cdot\text{mol}^{-1}$). A classification can also be made as a function of the EEW (table I-4) ³⁶.

Table I-4. Classification of the BADGE-type epoxy resins as a function of their EEW.

EEW ($\text{g}\cdot\text{mol}^{-1}$)	DP _n	BADGE type
160 - 225	< 0.3	Liquid Epoxy Resin (LER)
230 - 400	0.3 - 1.5	Semisolids
450 - 4000	> 1.5	Solid Epoxy Resins (SER)

Focus was made during this study on LER which are liquid at room temperature and therefore easier to coat on substrates and will allow to obtain a high network density.

It is clear by looking at the BADGE chemical structure that this material offers a large range of properties: excellent chemical resistance (except against organic acids), good mechanical properties, and high adhesion onto metallic and mineral substrates, thermal resistance and corrosion protection ³⁵. However, these properties are of course achieved when the prepolymer is cured with a crosslinking agent leading to the formation of an epoxy thermoset network.

IV.3.b. Curing of the BADGE prepolymer / diamine system

Two chemical functions (the hydroxyl function and the epoxy rings) standing on the BADGE prepolymer can act as curing sites depending on the crosslinking agent chosen (figure I-15)³⁶.

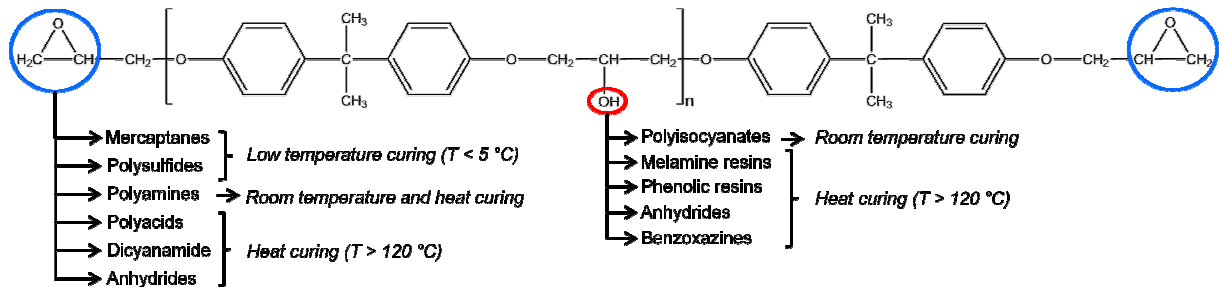


Figure I-15. Curing sites on a BADGE prepolymer.

Curing using the hydroxyl function of the BADGE chain will be preferred for solid resins (DP_n being higher meaning a higher amount of hydroxyl functions per BADGE chain).

In the case of liquid epoxy resins, crosslinking via the epoxy functions will be favored leading to a polymer network with a higher crosslinking density than the ones obtained with SER.

Moreover, a large variety of properties can be reached for these materials not only by playing with the epoxy prepolymer structure (EEW) but also by using different types of curing agents. As a matter of fact, the final properties of the epoxy coating will highly depend on the type of crosslinking agent chosen. In our study, we have focused on polyamines as curing agents.

These compounds are the most commonly used³⁵. Crosslinking can happen at ambient temperature in the case of aliphatic amines but it may be needed to heat the mixture when aromatic amines are used. A typical curing reaction scheme is presented on figure I-16:

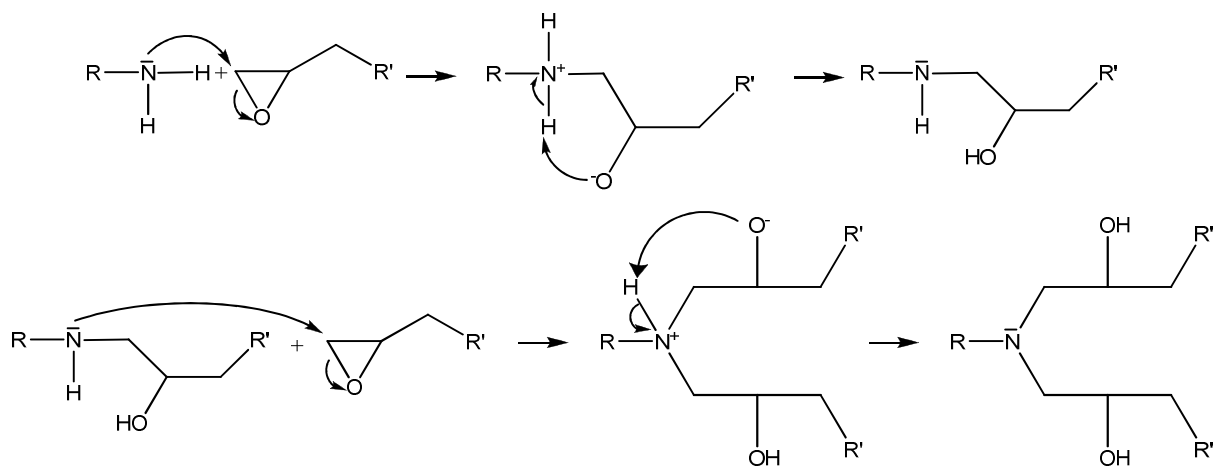


Figure I-16. Addition reaction of an amine on an epoxy group.

There are a lot of amine-based curing agents with various chemical structures: aliphatic polyamines, multifunctional amides, cycloaliphatic and aromatic polyamines are some current examples. The chemical reaction mechanism will still be unchanged but the curing reaction kinetic and the properties of the final polymer network will depend on the amine chemical structure.

IV.4. Conclusion

It is clear that a polymer coating seems to be the solution for the prevention of the scale formation during the S-PVC synthesis. However, the constrain induced by the reactive medium are very severe. As a matter of fact, the selected coating will be submitted to a hot aqueous medium with a lot of stirring and pressure changes. The needed chemical and mechanical resistances make this study a great challenge as well.

This is why epoxy resins were chosen regarding to the specifications asked. This material seems to be the ideal candidate for the obtaining of a durable protective coating if this polymer provides the desired anti-scaling properties. However, some challenges will be faced and the main one is the resistance of the epoxy coating / stainless steel interface in the hot aqueous medium and a part of this Ph. D. work will focus on the optimization of this interface.

V. Epoxy coating's adhesion onto stainless steel

V.1. Basics on adhesion

The efficiency of a coating basically goes through a great adhesion on the substrate as delamination of the coated material corresponds to a total loss of its protective properties³⁷.

Adhesion is basically defined as the attraction between two different bodies and is presented as the sum of multiple physical and chemical phenomena. However, lots of theories have been developed trying to explain the mechanisms involved during adhesion. Some of the main theories are explained below.

V.1.a. Work of adhesion

Bonding between a polymer coating and a metallic substrate is presented as the union of a solid and a liquid phase (which solidifies afterwards)³⁷. The work of adhesion stands for the expression of the reversible separation of the two phases and is expressed by equation I-1³⁷.

$$W_a = \gamma_1 + \gamma_2 - \gamma_{12}$$

Equation I-1. General mathematical expression of the work of adhesion.

where W_a is the work of adhesion, γ_1 and γ_2 are the surface tensions of both materials and γ_{12} the interfacial tension.

However, when theoretical and experimental values are compared, a deviation between the ideal adhesive strength and the practical limit is observed. It is also clear that the work of adhesion is not sufficient to totally describe the interactions between two materials.

V.1.b. Fracture theory

The theory of cohesive fracture was applied to coatings fracture³⁸. According to this theory, delamination propagates from the weakest points leading to a mechanical fracture. The strength of a bond (energy required to induce fracture) is also described as a function of the defect size and the energy dissipated by an irreversible process (equation I-2)³⁷.

$$f = k(EF/d)^{1/2}$$

Equation I-2. Mathematical expression of the bond strength according to the fracture theory.

where f is the fracture stress, $k = (4/\pi)^{1/2}$, E is the elastic modulus of the coating (in Pa), d is the defect length (in m), F is the fracture energy (total work per unit area of fracture surface, in $W.m^{-2}$).

However, this theory also implies that loss of adhesion is due to an interfacial fracture.

V.1.c. Weak boundary layer theory

This theory, widely described^{37,39}, estimates that a weak boundary layer (WBL) is formed near the coating / substrate during adhesive contact of two materials. As true interfacial fracture can occur, it has been proven that, in some cases, cohesively fracture can happen in the WBL. For a strong bond, the boundary layer must be optimized from a rheological and chemical point of view in order to limit its weakness³⁷.

V.1.d. Wetting - contact theory

This theory states that Van der Waals interactions provide satisfactory adhesive strength (perfect molecular "contact") in the case of a good wetting of the surface by the applied coating^{40,41}. This parameter is essential as the lower the contact angle, the more interfacial area of contact meaning an improved adhesion.

In fact, this model does not take the WBL theory, the effects of the defects and the fracture mechanisms into account.

V.1.e. Diffusion theory

This theory is mainly applied for polymer / polymer contact. Diffusion of polymers with one another can occur in time and dramatically improve the adhesion force between the coating and the substrate⁴². As this phenomenon is not likely happening with hard solid systems (like metals), this theory will not be deeper explained.

V.1.f. Chemical adhesion

Covalent bonds are useful when durable stable adhesion is needed. The bond strength brought by these interactions are extremely high ($60 - 700 \text{ kJ.mol}^{-1}$)⁴³. For this purpose, adhesion promoters have been used effectively to enhance adhesion. An important point is the fact that these molecules have to bear a dual reactivity by showing a high affinity for the substrate and for the coating at the same time.

V.1.g. Mechanical adhesion

The important point here is the surface roughness of the substrate as it can provide mechanical interlocking of the coating³⁷. The theory has to be combined with the wetting - contact theory. In fact, roughness of the substrate coupled with a good wetting of the coating will lead to a high increase of adhesion. On the other hand, if wetting is poor, a loss of the adhesive properties will be observed.

Moreover, this kind of treatment can provide interlocked species in the treated surface. In some cases, depending on the chemical nature of the abrasive material, this process can lead to an increase of the surface reactivity. This phenomenon will also be known as mechanical-chemical adhesion⁴⁴.

V.1.h. Electrostatic adhesion

This phenomenon is observed when two similar materials are put in contact³⁷. An electrical double layer will be formed due to a charge transfer between both materials. However, this type of interaction is impossible in the case of polymer / metal contact.

V.1.i. Acid-base adhesion

Adhesion is found to increase when acid-base interactions are involved. The modification of the surface acidity or basicity can lead either to an increase nor to a decrease of the mechanical properties of the coating⁴⁵.

V.1.j. Summary of the usual bond types

As seen before, there are many bond types that can be involved during an adhesion process. The main bonds families and their corresponding energies are listed in table I-5 ⁴⁶.

Table I-5. Summary of the main bond families and their corresponding energies.

Family	Type	Bond energy (kJ.mol ⁻¹)
Donor-acceptor bonds	Brönsted-type	< 1000
	Lewis-type	< 80
Primary bonds	Ionic	600 - 1100
	Covalent	60 - 700
	Metallic	110 - 350
Secondary bonds	Hydrogen bonds	10 - 40
	Van der Waals interactions	0.05 - 40

The importance of having chemical adhesion through covalent bonding is here clearly visible as this type of bonding is known to be stable because of its high energy.

V.1.k. Combination of the phenomena

After description of all these phenomena, it can be established that overall adhesion is a combination of all the interactions described above ³⁷. To conclude, adhesion can be considered as an interfacial interaction in which physical, chemical and mechanical forces operate to form an interface. To better understand the interfacial effects, some factors must be considered:

- The thermodynamics and kinetics of the bond formation
- The forces acting near the coating / substrate interface
- The cohesive forces within the coating layer
- Internal stresses in the coating layer
- The behavior of the coating under stress.

As some works have been done regarding to the behavior of the epoxy / stainless steel interface, a closer look to the interactions occurring with this system is taken in the following of this report.

V.2. Epoxy / stainless steel adhesion

V.2.a. Description of the adhesion of epoxy onto stainless steel

Adhesion of epoxy coatings on stainless steel is a complex process. It is quite sure that adhesion of an epoxy coating onto stainless steel is due to mechanical interlocking and physical adsorption through secondary bonds (Van der Waals interactions, hydrogen bonds, polar interactions)^{47,48}. The presence of covalent bonds might be possible too.

Moreover, some studies performed on BADGE - amine systems pointed out the formation of an interphase⁴⁹ between the coating and the substrate. This phase, having other physical, chemical and mechanical properties than the polymer bulk, is created within the organic layer, on the edge of the metal surface. The formation of this interphase could result from the dissolution of the metallic surface layer. It is also due to chemisorptions of the amine curing agent on the surface and to partial dissolution of the surface oxide metal substrate. This phenomenon can be due to the metal ions diffusion within the liquid monomer mixture leading to a reaction with the amino groups of the hardener. Organometallic complexes are also formed on the metal surface oxide layer which will then diffuse in the liquid monomer mixture. This will also lead to concentration gradients with the interphase which is considered as an amine-rich phase and the polymer bulk which will be the epoxy-rich phase.

Micro-FTIR studies performed on the same systems also showed that the thickness of the interphase is a function of both the amine and the substrate used⁴⁹.

For this study, the main point of interest is the resistance of the epoxy / stainless steel interface regarding to an aqueous medium (which is the case faced during suspension polymerization).

V.2.b. Behavior in an aqueous medium

The epoxy / stainless steel interface is really sensitive to water⁵⁰⁻⁵². As said before, the adhesion of epoxy on steel is mainly due to mechanical anchorage and polar interactions and both are sensitive to water. The delamination of the coating takes place after the penetration of water at the epoxy / steel interface⁵². The formation of bubbling was observed by acoustic microscopy where the epoxy / steel adhesion is weak. This analysis also showed that blisters are formed at places where the adhesion is weaker, proving by this way the existence of a WBL.

The adhesion loss at the epoxy / metal interface is a 3 steps process (figure I-17) ⁵³.

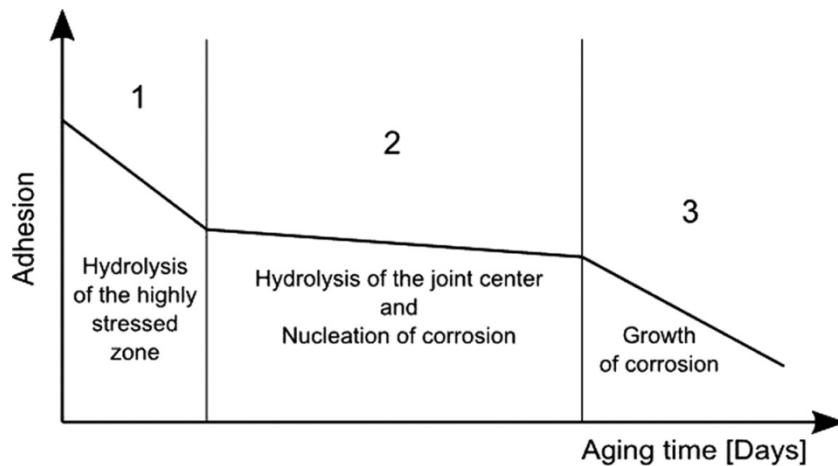


Figure I-17. Adhesion loss at an epoxy / metal interface.

During the first period, there is a hydrolysis of the highly stressed zones due to physical and chemical modifications. Then, a slight loss of adhesion is due to the hydrolysis of the interface and to the beginning of corrosion (which is a very low process for stainless steel). Finally, the growth of corrosion phenomenon will lead to an almost total loss of adhesion. To sum up ⁵⁴, water will enter by transport through the coating / substrate interface and by capillarity action through cracks in the adhesive.

This means that the epoxy / stainless steel interface has to be optimized in order to reach sufficient adhesion in the suspension polymerization reactor.

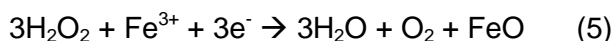
V.3. Optimization of the epoxy / stainless steel interface

V.3.a. *Cleaning / pickling*

As said earlier, the extreme surface of stainless steel is naturally covered by laminating oils (hydrocarbon compounds) used during the industrial production of this material but also by an environmental pollution layer (mainly constituted by water). Removal of these compounds will be important in order to optimize the epoxy / stainless steel adhesion. Many processes have been described to either only remove the pollution layer or to form a new passivation layer with controlled properties.

This latter process is known as chemical pickling. Organic acids (mainly nitric, fluorhydric and citric) are often used ^{27,30,55}. A Shell-patent also described a dip-coating type cleaning by immersing a stainless steel plate in a citric acid bath at a weight concentration of 30 g.L⁻¹. Another well-described solution is the use of a mix of nitric (HNO₃) and fluorhydric (HF) acids ³⁰. A typical solution contains from 10 to 15 % w / w of HNO₃ and from 2 to 4 % w / w of HF. These processes will lead to the formation of a brand new oxide and hydroxide layer which can be totally controlled under certain conditions. The bad point is the high degree of hazard when using such concentrated acids. Moreover, the HNO₃ / HF leads to the formation of nitrogen monoxide and dioxide (respectively NO and NO₂) which are rapidly harmful (from 3 ppm in the air).

Another method has been considered as peroxides can also be used with acids as pickling solution ³⁰. A mix of hydrogen peroxide - fluorhydric acid - sulfuric acid (H₂O₂-HF-H₂SO₄) in water (in the presence of sulfate iron-III (Fe₂(SO₄)₃) can be used as environmentally-friendly pickling agent because of the stripper properties of hydrogen peroxide. A typical solution has a concentration in sulfuric acid of 75 g.L⁻¹, 25 g.L⁻¹ of fluorhydric acid, 30 g.L⁻¹ of hydrogen peroxide and a ferric ion concentration from 0 to 40 g.L⁻¹. The corrosive effect of hydrogen peroxide has been followed by gravimetric titration when a stainless steel plate was immersed in a 5 mL hydrogen peroxide, 5 mL sulfuric acid diluted in 100 mL of distilled water. The loss of peroxide is due to the following reaction:



This type of pickling can be used to efficiently remove the environmental pollution layer but will also remove the oxide layer that has been formed during the successive treatments that stainless steel was subjected to.

A solvent cleaning will be favored in order to remove only the environmental pollution layer and the laminating oils without degrading the passivation layer ⁵⁶. This process may be accomplished by immersion in solvents or spraying on the plates with common organic solvents (acetone, chlorinated hydrocarbons...). Slight heating and agitation can improve the efficiency of the process. Moreover, the use of ultrasonic is the insurance of a deep and performing cleaning. This technique is used to remove contaminants from deep recesses and areas difficult to reach. High-frequency sound leads to a micro-agitation of the solvent meaning that the entire plate is cleaned regardless of its roughness. However, heating of the cleaned stainless steel plate is necessary to remove residual solvents from the surface.

As a complement of this method, mechanical treatment of stainless steel can also provide efficient cleaning and improve other properties of this substrate.

V.3.b. Mechanical treatment

Mechanical treatment of the stainless steel plates can improve the adhesion between the epoxy coating and stainless steel in many ways.

First, this treatment can be considered as a final cleaning of the substrate adapted for the removal of the pollution layer but also of the eventual remaining scale deposited onto stainless steel⁵⁶. The excess of abrasive material used for this purpose must also be removed by chemical cleaning. This means that these two techniques are complementary and chemical cleaning can not simply be replaced by mechanical cleaning.

Finally, the mechanical treatment of stainless steel will be a simple way to improve the roughness of the substrate. The goal of this process is to increase the mechanical anchorage of the epoxy coating that is to say to improve the adhesion. The link between surface roughness and adhesion has been discussed in the past⁵⁷. From this point of view, the adhesion can be divided into two components: the specific component concerning all the concepts described above (V.1) and the mechanical component for porous and rough surface⁵⁸. To be fully understood, the influence of the mechanical treatment on the adhesion must be looked from a surface energy point of view.

Two surfaces put in contact can not be considered as two distinct materials with no interactions⁵⁷. Some asymmetry in the intermolecular forces will occur as an interface will be formed between the two materials. The excess of energy produced at the interface is known as surface energy. This concept is directly related to the adhesion because it is associated to the formation of the adhesive bonds between the liquid polymer and the solid substrate. The affinity of both materials for one another will be crucial for the mechanical treatment to be efficient. A good wetting of the substrate by the liquid polymer system will allow penetration of the adhesive in the created surface roughness. The increase of the specific surface area, the formation of a new passivation layer and the increase of the mechanical anchorage of the coating (due to an increase of the work of adhesion) will all lead to a highly improved adhesion of the coating.

The material used for shot-blasting must have a high hardness and a controlled particles size. For this purpose, corundum is often used for stainless steel⁵⁹. This material is a nearly pure aluminum oxide (Al_2O_3) with traces of iron, chromium and titanium⁶⁰. Its relatively low cost, availability and extreme hardness (9 on the Mohs scale compared to a value of around 6 for stainless steel) make it a very efficient material for surface mechanical treatment of stainless steel.

V.4. Conclusion

The optimization of the epoxy / stainless steel interface goes through an increase of the interactions between the metallic substrate and the organic coating. Cleaning will allow to access efficiently to the surface's oxides and hydroxides. The use of a shot-blasting treatment will be an efficient way to increase the mechanical anchorage of the coating. One final way to improve the epoxy coating / stainless steel interface is to use adhesion promoters which will be described in the following of this report.

VI. *Adhesion promoters / Primers*

Adhesion promoters are molecules able to act as coupling agents at an organic - inorganic interface ⁶¹. As described earlier, the compatibility between organic and inorganic materials is not always optimal and such molecules are supposed to make a strong and stable covalent link between the coating and the substrate. The main goal from the use of these molecules is to provide stability of the epoxy / metal interface in hot aqueous medium.

The structure of these adhesion promoters consists in a dual functionality molecule ⁶¹. The first part of the molecule will be able to chemically react with the inorganic substrate. Many possibilities are discussed in the literature like the use of organophosphorous material or the use of molecules with a central metallic atom bearing hydrolysable functions (like alkoxy, chlorine functions...). At the other end, an organofunctional group will be able to react with the polymer coating. The final result is the formation of covalent bonds between two dissimilar materials.

Some possible adhesion promoters, able to react with the stainless steel surface, are presented in the following of this report.

VI.1. Phosphonates

VI.1.a. *Introduction*

Organophosphorous-based compounds are nowadays more and more used as adhesion promoters on inorganic surfaces ⁶²⁻⁶⁵ and on stainless steel as well ⁶⁶. These molecules,

thanks to the properties of the phosphorus atom, present some advantages when adhesion promoting is needed. In fact, these molecules have a great affinity for inorganic and metallic substrates and mainly on metallic oxides like chromium and iron present at the extreme surface of stainless steel.

The molecules used are organophosphoric acids like phosphoric, phosphonic or phosphinic acids and their derivatives. The general formula is $R_xP(O)(OX)_{3-x}$ (with $x = 1$ or 2 and $X =$ organofunctional group). The general chemical formula of the phosphonic acids is presented on figure I-18.

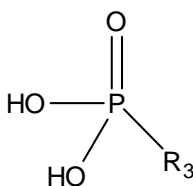


Figure I-18. General chemical formula of a phosphonic acid.

Nowadays, phosphonic acids with a lot of possibilities for the R_3 organofunctional group are available⁶⁷.

VI.1.b. Phosphonic acid chemistry

The use of these molecules offers many advantages from a chemical point of view. Compared for example to trialkoxysilanes, these compounds will not undergo self-condensation. This comes from the fact that the phosphorus atom is less sensitive to nucleophilic substitution than the silicon atom. The consequence of this property is that the resulting P-O-C is quite stable regarding to hydrolysis and condensation. As a matter of fact, P-O-P bonds are only formed under high temperature⁶⁷.

VI.1.c. Adsorption on metallic substrates

Phosphonic acids will be able to bond with oxide or hydroxide composed surfaces^{65,66,68}. As a matter of fact, these molecules will form stable complexes with the metallic atoms and covalent bonding will also be possible with the surface's oxides. The formation of a complex can be made from a mono-, bi- or tridentate manner (figure I-19).

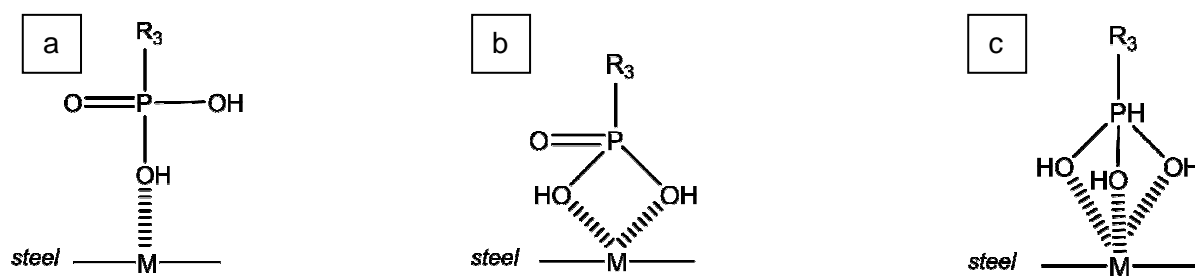


Figure I-19. Formation of a complex at a metallic surface from a: a. mono-, b. bi-, c. tridentate manner.

The formation of a multidentate complex seems to be the most likely happening and is the sign of a highly stabilized phosphonate at the substrate's surface.

The adsorption of such molecules have been described for AISI 316L stainless steel⁶⁶. The 316L stainless steel plates were first polished and immersed in the phosphonic acid solutions for dip coating. The molecules tested are octylphosphonic acid (OPA) and octadecylphosphonic acid (ODPA) at a 1 mM concentration in THF.

Acid phosphonic self-assembled monolayers (SAMs) were formed by simple deposition at ambient temperature. FT-IR and XPS analyses showed that the molecules tested were covalently linked to stainless steel from a bidentate manner. The phosphonate vibration modes are $\nu(\text{P-O}) = 1050 \text{ cm}^{-1}$ and $\nu(\text{P=O}) = 1160 \text{ cm}^{-1}$. By coupling this result with disappearance of the $\nu(\text{P-OH})$ peak at 920 cm^{-1} , it has been concluded that OPA and ODPA are bonded in a bidentate manner (figure I-20).

Complete covering of the substrate was proven by contact angle measurements and Atomic Force Microscopy (AFM)⁶⁶.

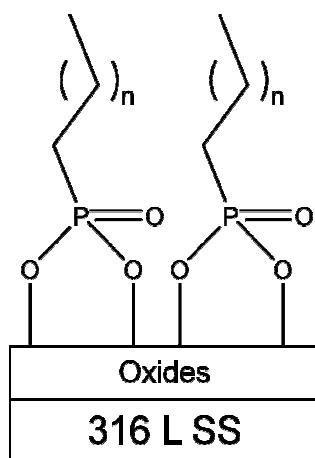


Figure I-20. Bidendate-type grafting of a phosphonate at the 316L stainless steel surface.

All phosphonic acids are not able to form SAMs. In fact, the minimal chain length to obtain such conformation is a C₈ linear chain⁶⁶. Moreover, a good point is that this surface modification is not dependant on the amount of water adsorbed at the surface and can easily be done in water depending on the compound solubility.

Even if condensation reactions and formation of P-O-P bonds can not occur, it has been reported that, depending on the processing conditions and the stability of the metallic oxide surface to dissolution in the solvent, a dissolution - precipitation process can compete with the earlier described monolayer adsorption. This phenomenon is illustrated on figure I-21⁶⁹.

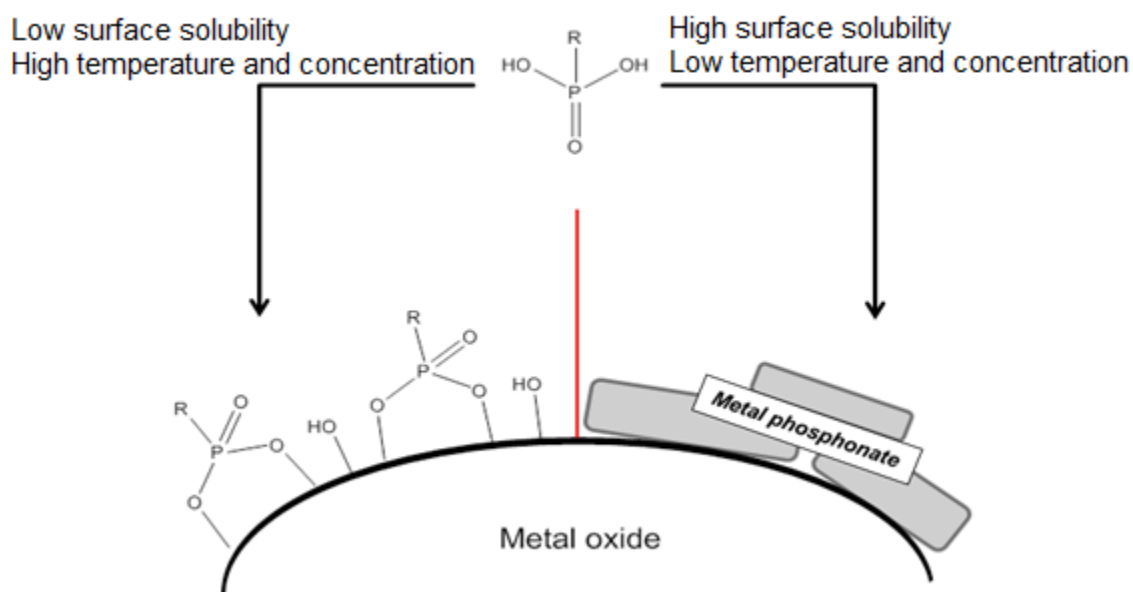


Figure I-21. Difference between the grafting of a phosphonate from a poorly-soluble or a highly-soluble solution.

VI.1.d. Bisphosphonates

Bisphosphonates are quite similar to the phosphonates described above except from the fact that these molecules contain two phosphorous atoms (figure I-22)^{65,70,71}.

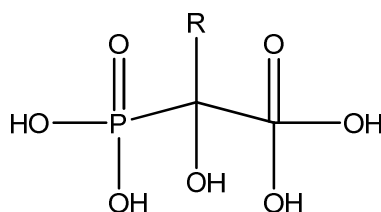


Figure I-22. General formula of a bisphosphonate.

The behavior of these molecules is quite similar to the one of classical phosphonates. In fact, the bisphosphonic group increases the affinity for the oxide surface^{68,70} and the polarity of the molecule (figure I-23).

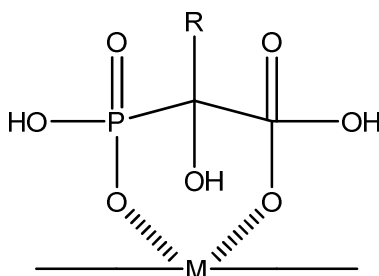


Figure I-23. Grafting of a bisphosphonate on a metal surface.

Most of the time, bisphosphonates allow an easy aqueous deposition of monolayers on various substrates compared to monophosphonates and the resulting grafted layer is more stable.

VI.2. Sulfonates

These molecules are less used as coupling agents due to their weaker stability at metal surfaces^{70,72}. These molecules are poorly documented and their grafting mechanism is not really known. Their general chemical formula is presented on figure I-24.

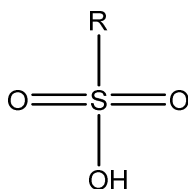


Figure I-24. General chemical formula of a sulfonate.

It has also been proven that their stability on oxidized substrates, compared to the one of phosphonates and bisphosphonates in the same condition, is lower⁷⁰.

VI.3. Trialkoxysilanes

VI.3.a. Introduction

Silanes and mainly trialkoxysilanes are often used when increasing the compatibility between an inorganic / metallic and an organic material is needed⁷³⁻⁷⁷. The use of these adhesion promoters will greatly improve the adhesion between a polymer (coating, adhesive...) and a substrate⁷⁸⁻⁸¹. A lot of substrates can be functionalized by these molecules like iron oxide^{78,82}, glass^{80,83,84}, aluminum^{85,86}, silica⁸⁷⁻⁸⁹ and stainless steel^{50,90}... The general chemical formula of a trialkoxysilane is presented on figure I-25.

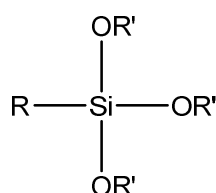


Figure I-25. General chemical formula of a trialkoxysilane.

On this general chemical formula, OR' stands for easily hydrolyzable functions (mainly methoxy or ethoxy) that will be able, after hydrolysis, to form highly reactive silanols. On the other end, R is a non-hydrolyzable organic moiety. This chemical function must be chosen to be reactive toward the organic material it will be linked with. This dual reactivity is essential as it will allow to form a bridge between the substrate and the organic / polymer matrix (figure I-26).

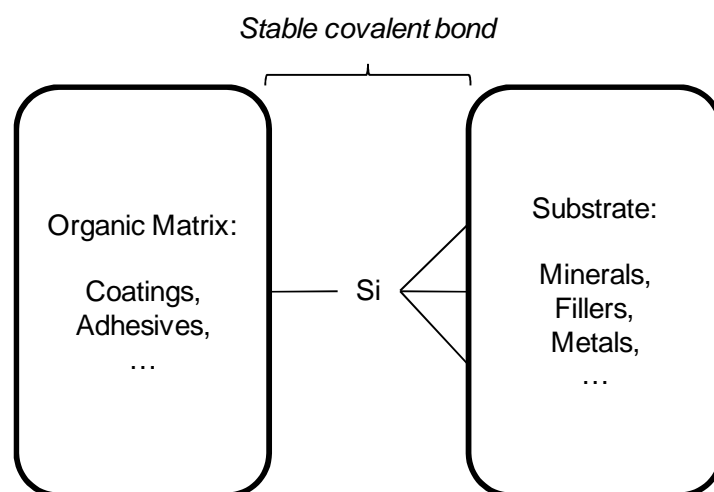


Figure I-26. Formation of a covalent bond between a substrate and an organic matrix.

However, the chemical behavior of these molecules is quite particular and will be presented in the following of this report.

VI.3.b. Behavior of the trialkoxysilanes in aqueous solution

The reactivity of the trialkoxysilanes in aqueous solution has been widely described in the literature^{73,75,81,83,91-94}. When a trialkoxysilane is added in an aqueous medium, the first reaction is an hydrolysis of the alkoxy groups into silanols (Si-OH). From this moment, depending on the experimental conditions, homocondensation of these compounds can occur leading to the formation of oligomers which stands for the birth of a siloxane network. The homocondensation reaction includes the reaction between two trialkoxysilanes molecules. Siloxane bonds can come from the reaction of two silanols together (oxolation) with loss of water or between one silanol and one non-hydrolyzed alkoxy silane (alkoxolation) with loss of the corresponding alcohol. It is interesting to note that the hydrolysis reaction also leads to a loss of an alcohol molecule. The basic hydrolysis / condensation reactions are presented on figure I-27.

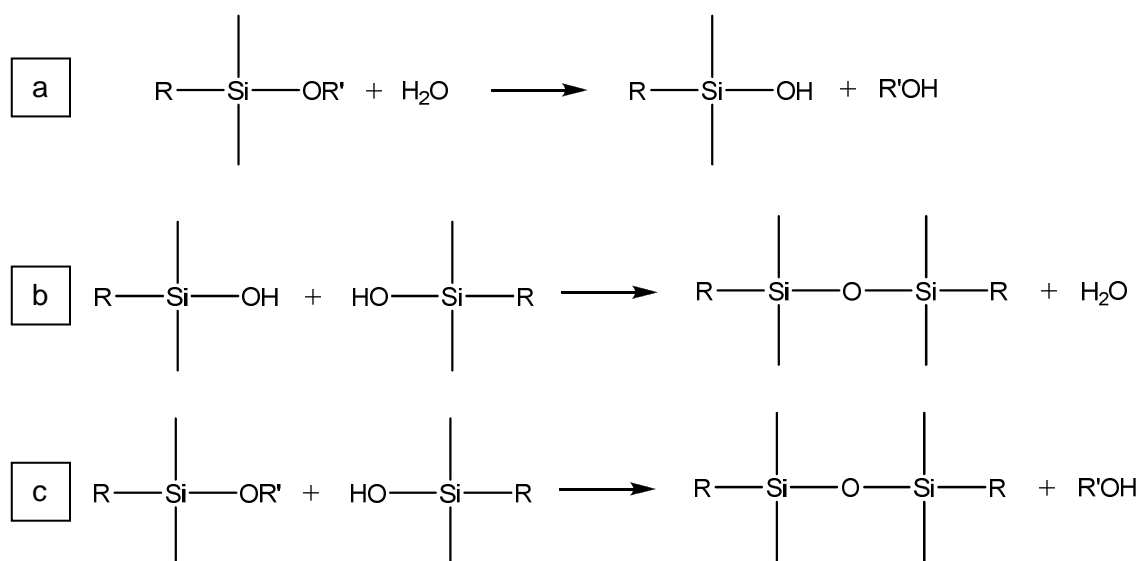


Figure I-27. Typical hydrolysis / condensation reactions for a trialkoxysilane: a. hydrolysis, b. condensation (oxolation), c. condensation (alkoxolation).

The optimal grafting of these molecules goes through a total control of the hydrolysis / condensation reactions.

VI.3.c. Hydrolysis reactions

Hydrolysis is the reaction leading to the formation of highly reactive silanols. Its complete mechanism is described on figure I-28.

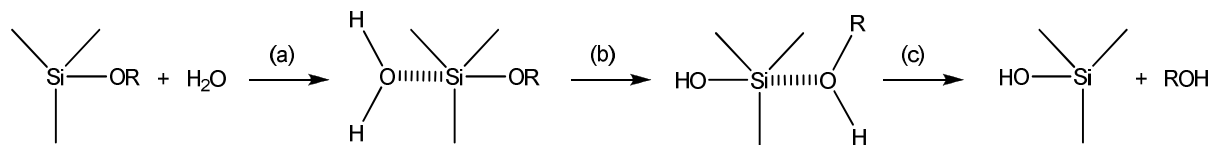


Figure I-28. Hydrolysis reaction of a trialkoxysilane.

This reaction goes through a type-2 nucleophilic substitution (S_N2) with first a nucleophilic addition of a water molecule on the trialkoxysilane molecule (a), then a proton transfer from the water molecule to the silane (b) and finally the elimination of an alcohol molecule (c).

This mechanism can be acid- or base-catalyzed. However, the hydrolysis reaction is favored in an acid medium. In more basic medium, the hydrolysis reaction will be in competition with the condensation reaction (figure I-29) ⁹⁶.

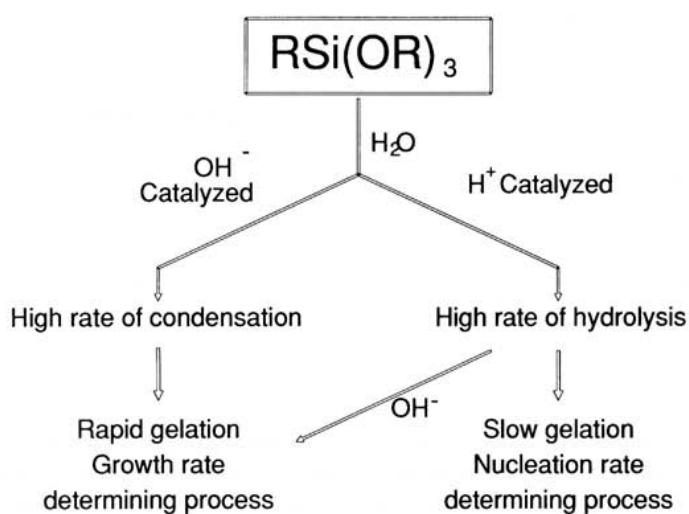


Figure I-29. Behavior of a trialkoxysilane in an acidic or a basic solution.

Both acid- and base-catalyzed hydrolysis will be discussed in the following of this report.

VI.3.c.i. Acid-catalyzed hydrolysis

The acid-catalyzed hydrolysis reaction goes through a rapid equilibrium protonation of the leaving group followed by a S_N2-type displacement by water (figure I-30)⁷⁵.

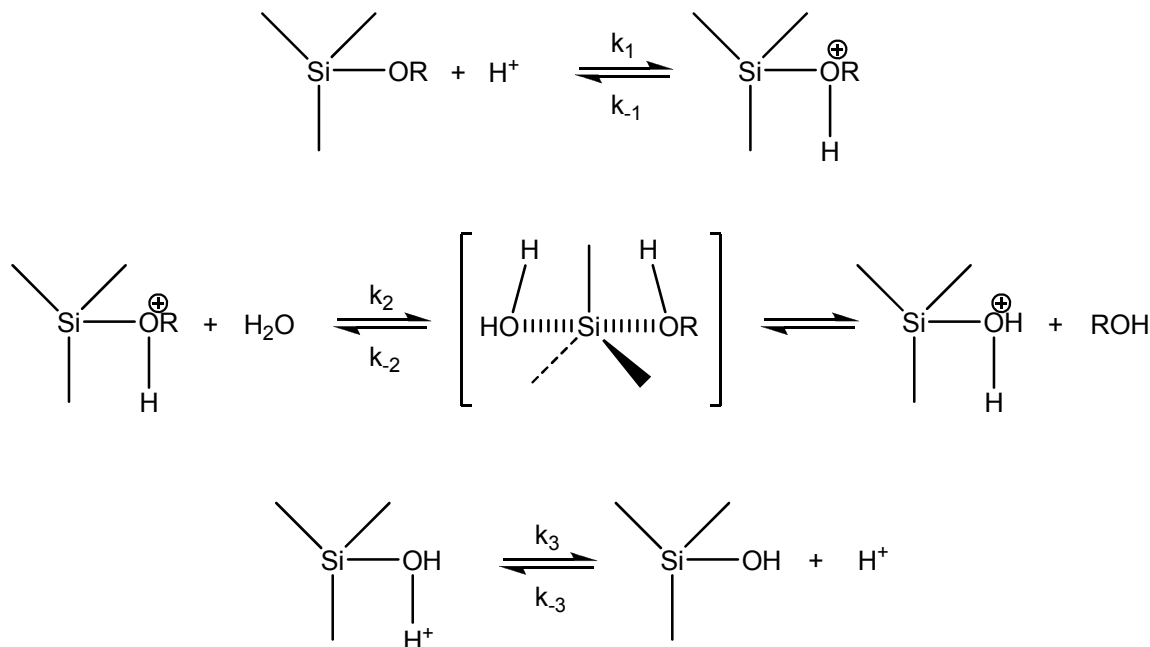


Figure I-30. Acid-catalyzed hydrolysis of a trialkoxysilane.

There are many factors affecting the hydrolysis kinetic and the main one is the length of the alkoxy functions. It has been proven that its rate of hydrolysis is generally related to their steric bulk^{73,96}. A methoxysilane, for example, will be hydrolyzed from 6 to 10 times faster compare to an ethoxysilane.

VI.3.c.ii. Base-catalyzed hydrolysis

The base-catalyzed reaction goes through a bimolecular nucleophilic mechanism with a pentacoordinate intermediate (figure I-31)⁷⁵.

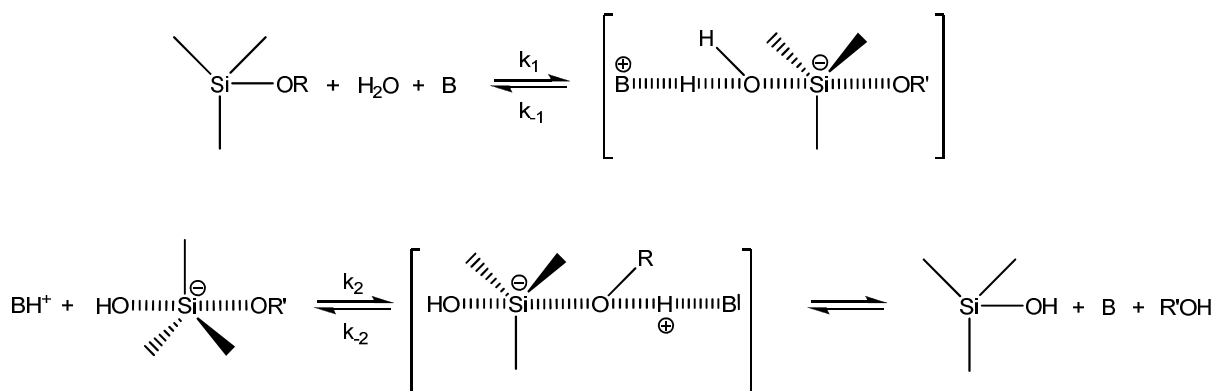


Figure I-31. Base-catalyzed hydrolysis of a trialkoxysilane.

This mechanism involves an important negative charge on the silicon atom during the transition state. Contrary to the acid catalysis, every chemical function stabilizing this negative charge will accelerate the hydrolysis reaction ⁷⁵.

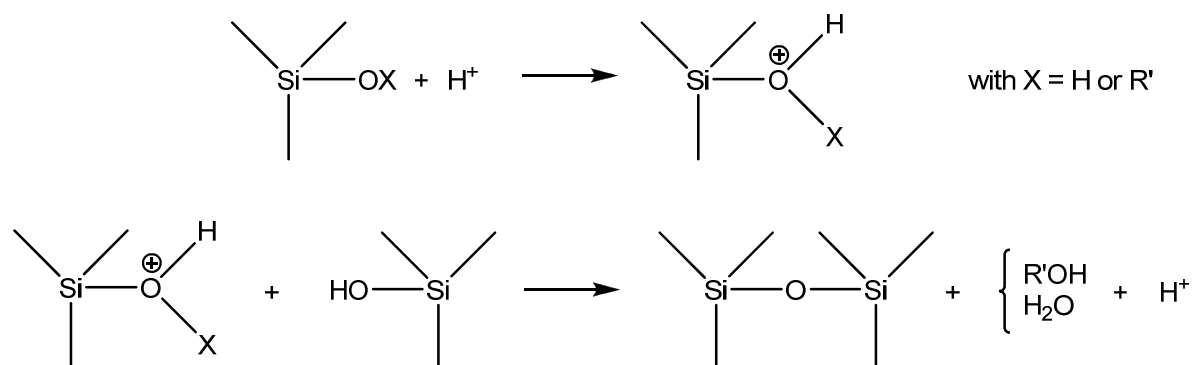
Like for the acid-catalyzed hydrolysis, the length of the alkoxy chain will have an effect on the silanols' formation kinetics. In fact, the differential between a methoxy and an ethoxy function will be greater in terms of hydrolysis rate.

VI.3.d. Condensation reactions

The formation of silanols during the hydrolysis of the trialkoxysilanes leads to homocondensation reactions which stand for the growth of a siloxane network (Si-O-Si). As described earlier (figure I-27 b and c) two different reactions can occur: the oxolation with the loss of a water molecule and the alkoxolation with a loss of an alcohol molecule. The structure of the alcohol released corresponds to the nature of the alkoxy function beared by the trialkoxysilane. For example, an ethoxysilane will release, during alkoxolation, an ethanol molecule.

These reactions involve nucleophilic substitutions similar to those observed during hydrolysis. Again, this reaction can be acid- or base-catalyzed and is highly pH-dependent (figure I-32) ⁹⁵.

a *Acid-catalyzed condensation*



b *Base-catalyzed condensation*

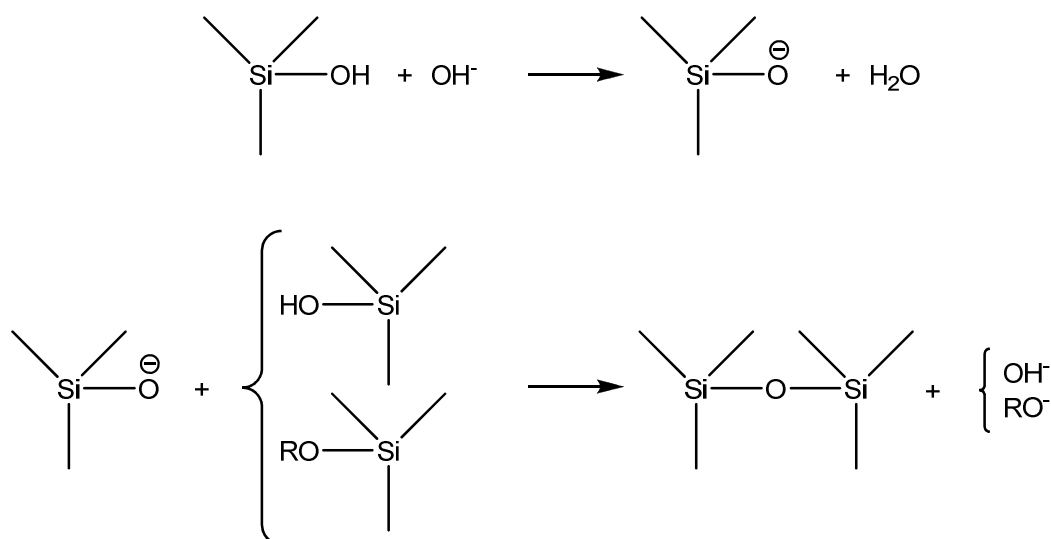


Figure I-32. Homocondensation of a trialkoxysilane: a. acid catalysis, b. base catalysis.

As for the hydrolysis reaction, nucleophilic substitutions are involved in this reaction. This means that the charge of the silicon atom will again have a major impact on the condensation reaction.

Even if it is impossible to totally avoid formation of siloxane networks, some experimental conditions can affect the hydrolysis / condensation ratio.

VI.3.e. Factors affecting the hydrolysis / condensation reactions

As described earlier, hydrolysis of an alkoxy silane happens in an aqueous medium. In these conditions, both hydrolysis and condensation are inseparable. However, there are several experimental parameters which can favor one reaction or the other. These factors are for example the solution's pH, the silane's concentration, the prehydrolysis duration...

VI.3.e.i. Solution's pH

As described earlier, the pH plays a major role during the hydrolysis / condensation process as the reaction mechanisms involved are different depending on the solution's pH^{75,96,97}. In fact, both reaction rates are influenced by changing pH levels. Moreover, an optimum pH for hydrolysis is not necessarily optimal for condensation. It is also crucial to find the best balance between hydrolysis and condensation in terms of pH in order to successfully use these molecules for a specific application. An example of the best balance that can be found, based on both hydrolysis and condensation rates, are presented for (3-glycidyoxypropyl) trimethoxysilane on figure I-33⁹⁷.

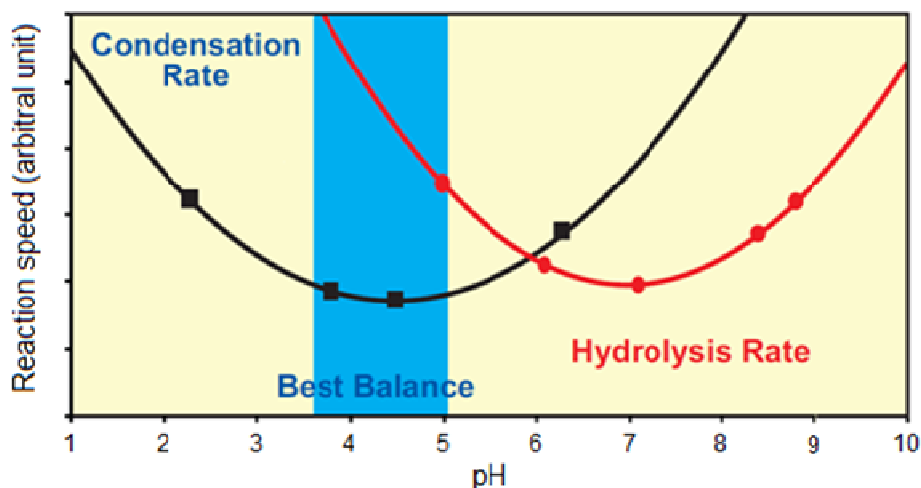


Figure I-33. Hydrolysis and condensation rate of (3-glycidyoxypropyl) trimethoxysilane as a function of the hydrolysis pH.

The best balance, when grafting of these molecules is needed, stands at the point where the hydrolysis rate / condensation rate ratio is at the highest point. It usually happens when the condensation rate is at its lower value. At this typical pH, the amount of silanols formed will be satisfactory and their stability regarding to self-condensation will be at its higher point.

Some studies were also made on 3-(2-aminoethylamino)propyl trimethoxysilane as a function of the pH and showed that the relative amount of silanols formed is a function of the medium pH⁹³. This fact also clearly shows the protective role of an acidic medium regarding to homocondensation. However, the optimal hydrolysis / condensation balance is a function of many parameters like the nature of the organofunctional group on the trialkoxysilane molecule.

VI.3.e.ii. Influence of the organofunctional group on the prehydrolysis duration

As explained earlier, the main point during the hydrolysis / condensation reactions is the force of the negative charge carried by the silicon atom. ²⁹Si NMR studies performed on numerous trialkoxysilanes bearing different chemical functions have shown the influence of this organofunctional group on the hydrolysis / condensation rates⁹⁴. Hydrolysis / condensation reaction of trialkoxysilanes bearing amine, phenyl amino, imidazole, alcane, alkene, vinyl, mercapto, phenyl, methacryloxy and cyano functions were compared. The majority of them were trimethoxysilane meaning that the nature of the alkoxy group had no influence on the different hydrolysis / condensation rates.

In a slightly acidic medium, the influence of the nature of the organofunctional group has clearly been proven as both the maximal amount of silanols formed and the hydrolysis / condensation kinetics varied⁹⁴. In the case of aminosilanes, the maximal amount of silanols formed is not so important (between 33 and 65 % mol) compared to other functions (98 % mol reached for the trialkoxysilane bearing a mercapto function). However, the kinetic is way faster for aminosilanes as the maximum amount of silanols formed is reached after less than 1 hour for all of them. This means that the condensation reaction must be controlled. As a matter of fact, a fast hydrolysis leads to a fast condensation as a lot of dimers and trimers are formed after less than 1 hour. For the other trialkoxysilanes, both hydrolysis and condensation reactions are slower. This means that the prehydrolysis duration will have to be chosen cleverly for each trialkoxysilane studied in order to obtain the better grafting efficiency possible.

These results point out the particular behavior of aminosilanes. In fact, these molecules are the rare trialkoxysilanes that can efficiently be grafted by using a base-catalyzed deposition⁹⁶. It has been proven that primary, secondary or tertiary amines can catalyze base-medium hydrolysis likely due to the basic property of the amine function which increases the nucleophilic character of the silicon atom^{75,98}. A mechanism for the catalysis of

condensation by primary and secondary amines was described for dialkylsilanediols (figure I-34)⁷⁵.

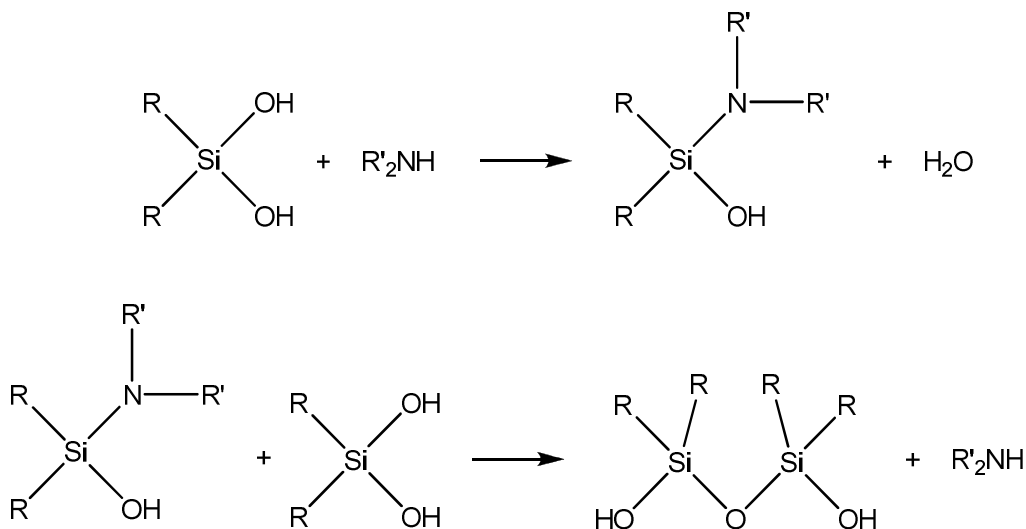


Figure I-34. Condensation reaction catalyzed by amines.

Moreover, for high concentrated aminosilane solution, the molecule will form a ring structure with the formation of hydrogen bonds between the silanol and the primary amine function (figure I-35)^{80,99}.

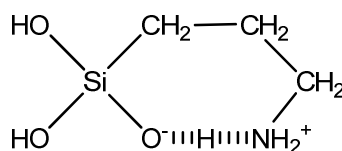


Figure I-35. Structure of an aminosilane in an aqueous solution.

VI.3.f. Composition of the hydrolysis solution

As explained earlier, the hydrolysis / condensation process takes place in an aqueous medium. In fact, a mix of a volatile solvent with water is often used when deposition on a substrate is needed. Evaporation of the solvent during the curing phase of the trialkoxysilane deposition will be facilitated and better covering of the substrate will be reached. To this purpose, alcohols (and mainly ethanol) are widely used^{87,88,100}. Moreover, some studies were made by varying the ethanol / water ratio and studying the influence of this parameter on the hydrolysis / condensation ratio¹⁰⁰.

Again, the optimal ratio is a function of the nature of the organofunctional group. For example, a 100 % water solution seems to be the best fit for aminosilanes. From a general point of view, the hydrolysis in a pure water medium seems to be more adapted in terms of quantity and stability of silanols formed. However, an ethanol / water mix still enables the obtaining of a satisfactory amount of silanols and such mix of solvents will be preferred for the deposition issues explained above.

VI.3.g. Grafting of trialkoxysilanes onto inorganic substrates

The hydrolysis process described earlier will have a direct effect on the grafting of trialkoxysilanes.

The understanding of the grafting of these molecules will be of major importance in order to obtain a high surface density of grafted molecules. Normally, the use of a trialkoxysilane will lead to the formation of a surface siloxane network assembled in a multi-layer way ⁷³.

The grafting mechanism of these molecules has been described for many oxidized surfaces. This process will be developed in the following of this report.

The classical mechanism for trialkoxysilane deposition has been described in the literature as a 4 steps process (figure I-36) ^{73,76,99}.

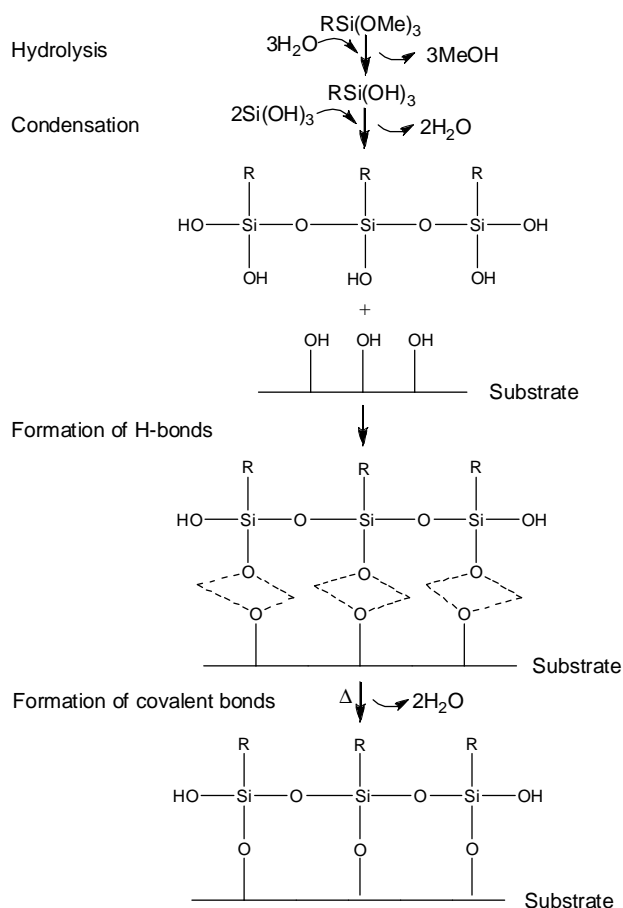


Figure I-36. 4-steps deposition of a trialkoxysilane on a substrate.

The first step is the hydrolysis of the alkoxy groups into silanols. These molecules can undergo condensation and / or simultaneously form hydrogen bonds with the substrate's surface. During the last step and thanks to heating, covalent bonds will be formed between the oxidized surface and the silane molecule.

However, this representation is kind of the ideal one and does not consider the fact that polyfunctional silanes can induce more complex reactions. For example, horizontal polymerization can happen and will lead to an unstructured three dimensional grafted network. The main interest from the use of these molecules is the formation of covalent bonds with a substrate but the greatest problem from using trialkoxysilanes is the many possibilities in terms of intermolecular interactions. This means that the grafting of these molecules must be done under total control to perform efficient surface covering.

VI.3.h. Factors affecting the grafting of trialkoxysilanes

As for the hydrolysis / condensation step, some factors can affect the grafting efficiency like the nature of the organofunctional group or the presence of a catalyst.

VI.3.h.i. Nature of the organofunctional group on the grafting of trialkoxysilanes

The grafting density can be a function of the chemical structure of the silane used. First, the link between this parameter and the grafting efficiency is directly related to the hydrolysis / condensation issues explained earlier. One can admit that the higher the number of silanols formed, the more efficient the grafting.

Then, some organofunctional groups can themselves interact with an oxidized surface and favor grafting. Some well-known examples are amino, thiol and malonic acid functions^{82,101-104}. The case of aminosilanes has already been described in the literature for grafting onto silica^{101,105} and iron oxide⁸². The process, known as the “flip mechanism”, has been demonstrated for the grafting of aminosilanes from anhydrous solvents (dimethylformamide, toluene). It can be divided into three steps (figure I-37)¹⁰¹: first, the formation of hydrogen bonds (a) between the amine function of the alkoxy silane and the hydroxyl groups of the surface. Second, a coordination / condensation reaction (b) will happen with another aminosilane molecule which, third, will lead to the formation of a covalent bond (c) between the silanol group of the aminosilane and a hydroxyl group (with loss of water) at the surface.

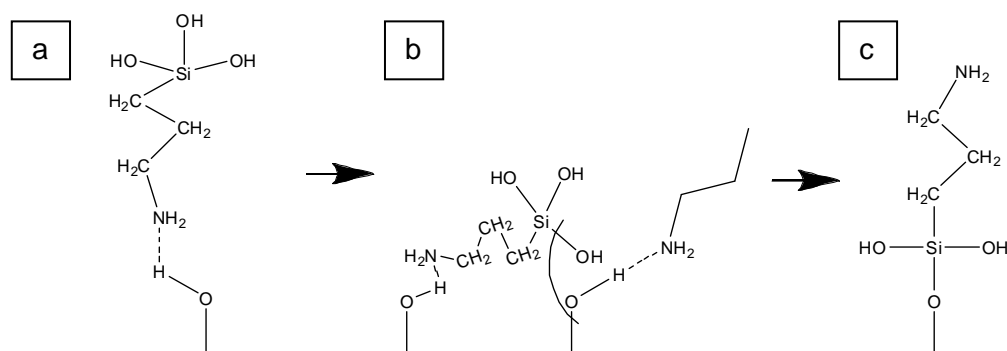


Figure I-37. Flip mechanism between an aminosilane and a hydroxylated surface.

When taking a look at the interactions that an aminosilane can make with an oxidized substrate, 3 types of conformations have been reported (figure I-38)^{101,106}.

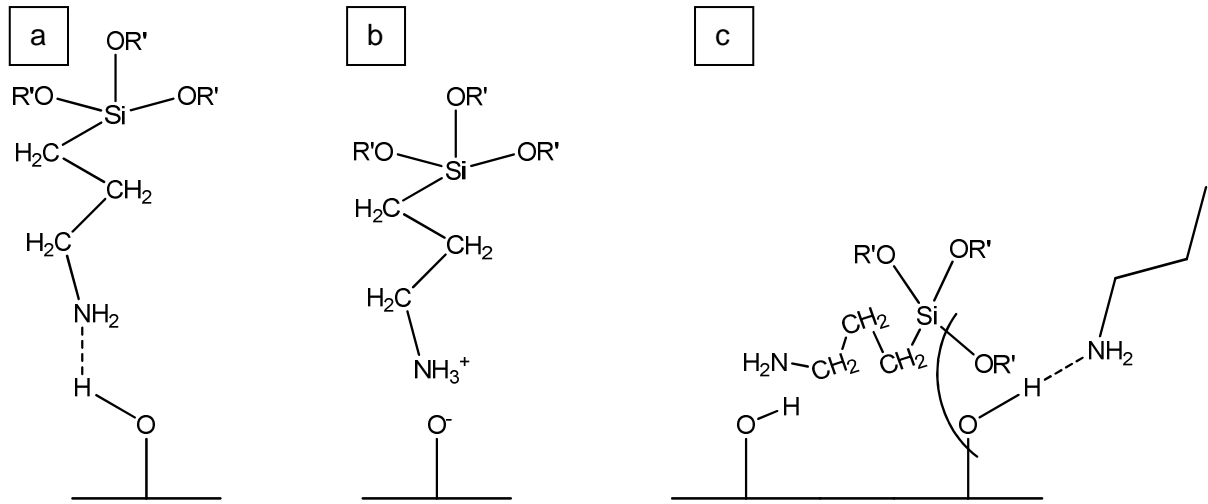


Figure I-38. Possible conformations for an aminosilane at the surface of a substrate: a. hydrogen bonding, b. proton transfer, c. condensation.

Still based on the strong amine / oxidized surface interactions, an amine-based catalyst can be used to improve grafting of silanes.

VI.3.h.ii. Use of a catalyst

The use of catalysts has been described to enhance the grafting efficiency of trialkoxysilanes onto silica (figure I-39) ⁹⁸.

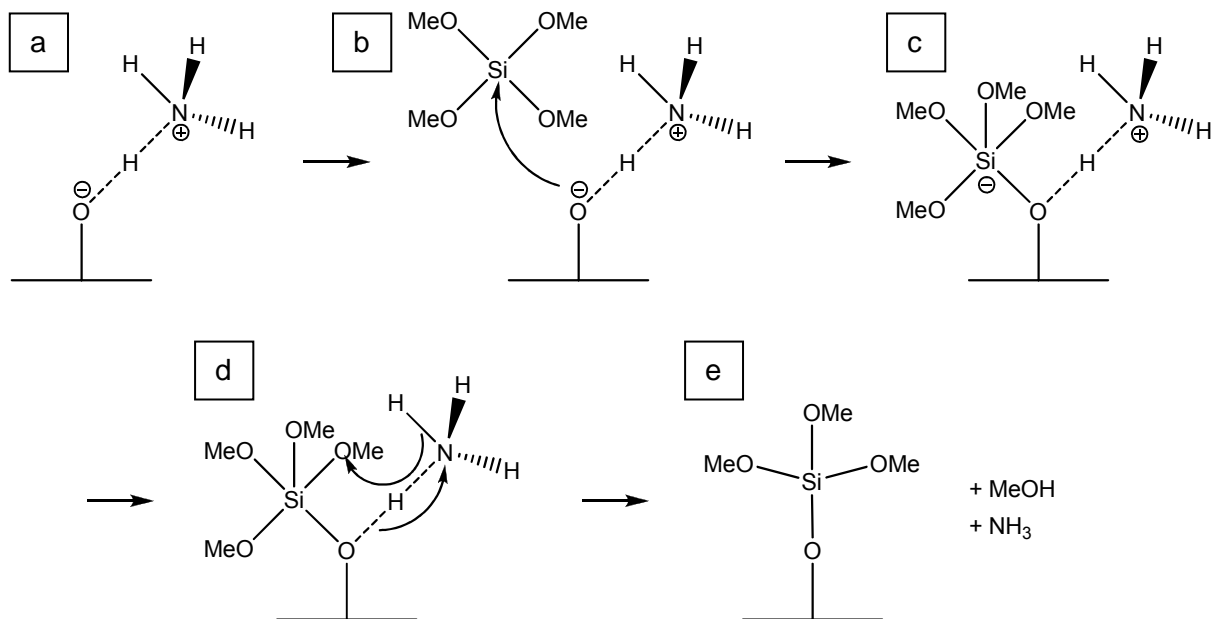


Figure I-39. Grafting of a trialkoxysilane catalyzed by a pre-grafted amine.

First, ammonia was adsorbed onto the surface's reactive sites (a). By doing so, the functionalized site becomes highly nucleophilic. The next step consists in the adsorption of the organosilane (here tetramethoxysilane) on the surface's nucleophilic site (b) resulting during the next step in a pentacoordinate intermediate (c). The leaving methoxy group will interact with one of the ammonia proton producing a methanol molecule (d). Ammonia is then regenerated and an organosilane-modified surface is obtained (e).

VI.3.i. Trialkoxysilanes for the optimization of the epoxy / stainless steel interface

In the case of grafting onto stainless steel, infrared analyses exhibit the formation of Si-O-Si bonds coming from the hydrolysis and the condensation of Si-O-R bonds⁹⁰. The siloxane network obtained is a good barrier against corrosion. The silanol functions (Si-OH) obtained by the hydrolysis of the silane will react with the iron hydroxides (Fe-OH) at the surface of steel to form Fe-O-Si bonds very stable to water. Siloxane bonds are formed by self condensation of silanol functions. All of these bonds avoid the penetration of water at the epoxy / steel interface. It is then necessary to choose a R' function which is reactive with an epoxy resin. Two main solutions are conceivable:

- An amine function: able to react with the epoxy functions of the resin
- An epoxy function: able to react with the amine functions of the curing agent

Alkoxysilanes with different R' functions have been studied in the literature⁹⁰: the N-[3-(trimethoxysilyl)propyl]ethylenediamine (AAPS, figure I-40), the (3-glycidyloxypropyl) trimethoxysilane (GPTMS, figure I-41) and the bis[3-(trimethoxysilyl)-1-phenylpropyl] tetrasulfide (RC-2, figure I-42).

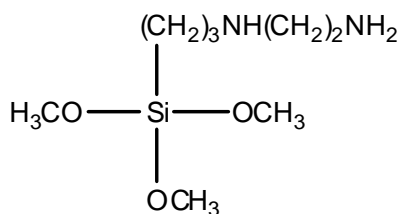


Figure I-40. Chemical formula of N-[3-(trimethoxysilyl)propyl]ethylenediamine (AAPS)

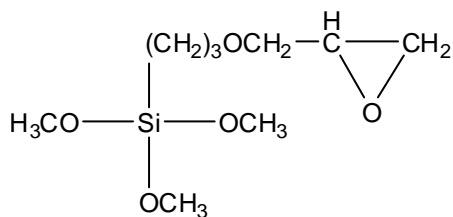


Figure I-41. Chemical formula of (3-glycidyloxypropyl) trimethoxysilane (GPTMS)

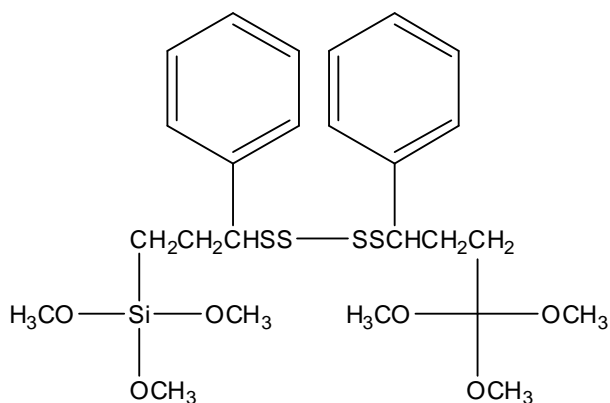


Figure I-42. Chemical formula of bis[3-(trimethoxysilyl)-1-phenylpropyl] tetrasulfide (RC-2).

The AAPS and the GPTMS are selected because their end groups (respectively an amine and an epoxy function) are capable to react with an epoxy system⁹⁰. The RC-2 has been chosen by the authors because the sulfur atom is known to have a great reactivity with metals but its capacity to react with an epoxy resin is unknown⁹⁰. Infrared reflection absorption spectroscopy (IRRAS) has been used to analyse the chemical bonds that will be formed at the extreme surface (at a depth from 1 nm to 1 μ m) of steel. The epoxy resin used is a BADGE and the curing agent is diethyltriamine. The stainless steel plates studied have first been cleaned with n-hexane, ethanol, hydrochloric acid and acetone and then polished with chromium V oxide. The silanes have been tested at different ratios (molar silane / epoxy ratios of 0-10 ; 2-8 ; 4-6 ; 6-4 ; 8-2 ; 10-0)⁹⁰.

Adhesion tests conducted on epoxy coatings without the use of a primer showed the extreme sensitivity of epoxy / stainless steel interface regarding to hydrolysis. This result shows the absolute necessity to use a silane as a coupling agent.

Different surface treatments based on epoxy / silane mixtures were also tested. From a general point of view, there is always the formation of a Si-O-Si network at the surface due to the hydrolysis / condensation reaction during the thermal treatment of the silanes. Silanols, obtained by the hydrolysis of Si-O-CH₃, will react with iron hydroxides too. There will also be

the formation of Fe-O-Si bonds which are stable in regards to hydrolysis. However, all the silanes presented by Jang & al.⁹⁰ do not behave in the same manner because of their different chemical structures. AAPS will form a denser network than GPTMS. For AAPS, the amine functions will act as a catalyst for the hydrolysis. Most of the siloxanes will be hydrolyzed to form a network. GPTMS does not have amine functions to catalyze this reaction and will form a less dense network. On the same basis, the result is the same for RC-2. Moreover, the network formed will be less dense because of the steric hindrance of the benzene groups in the RC-2 molecule.

The best results, in terms of stability in an aqueous medium, are obtained for an AAPS / epoxy system (with a molar ratio of 6 / 4). The corrosion for a stainless steel sheet coated with this system has almost disappeared under drastic conditions.

Other trialkoxysilanes have been used but they were not used as primers¹⁰⁷. The compounds were first mixed with the resin before being coated on steel. GPTMS, dodecyl-trimethoxysilane (DTMS, figure I-43), tetraethoxysilane (TEOS, figure I-44) and vinyltriethoxysilane (VTEOS, figure I-45) were tested in the literature for this purpose.

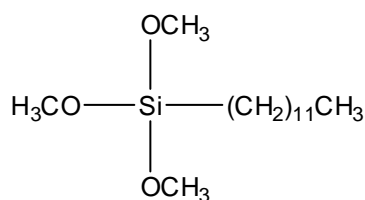


Figure I-43. Chemical formula of dodecyl-trimethoxysilane (DTMS).

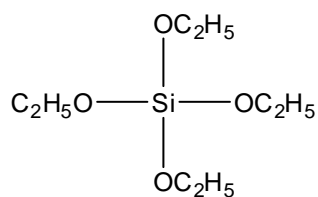


Figure I-44. Chemical formula of tetraethoxysilane (TEOS).

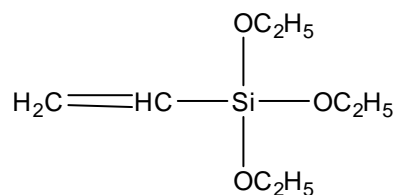


Figure I-45. Chemical formula of vinyltriethoxysilane (VTEOS).

This system is obtained by mixing the epoxy resin diluted in xylene with a certain amount of these silanes (the hydroxides molar ratio of the epoxy / silane is equal to 1)¹⁰⁷. The reaction is presented on figure I-46¹⁰⁷:

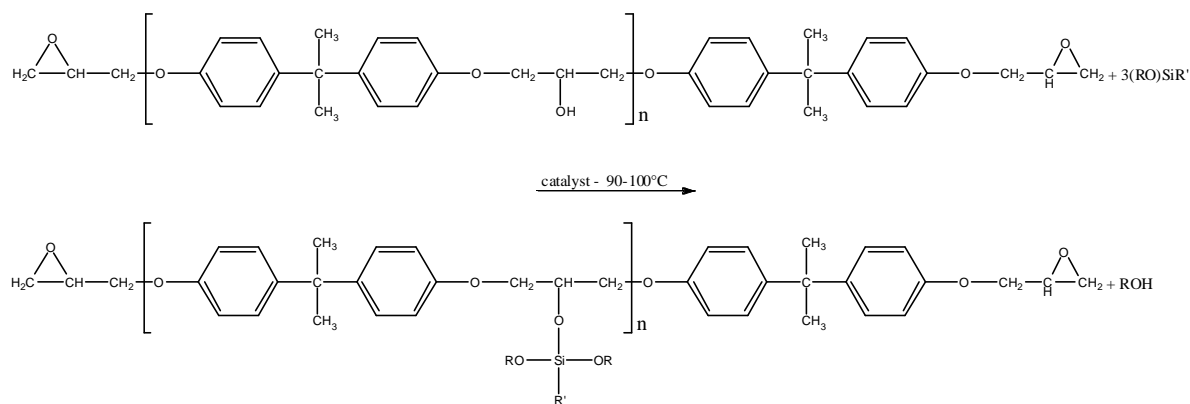


Figure I-46. Trialkoxysilane-modified epoxy prepolymer.

As we can see, methanol and ethanol can be formed during this reaction. It is so necessary to put this system under vacuum to remove all traces of alcohol.

Regarding the anti-corrosive properties, the addition of a silane increases the resistance of the epoxy resin. In this case, GPTMS offered the best results. However, TEOS has offered good performances too.

VI.3.j. Conclusion

The trialkoxysilane chemistry is very complex as a great number of parameters have to be taken into account during the functionalization of a substrate. A complete optimization and control of the deposition conditions will be needed in order to achieve a maximum adhesion between the epoxy coating and stainless steel and a great part of this study will be done on the optimization of these molecules as adhesion promoters. Finally, a last type of adhesion promoters, the monoalkoxysilanes, was tested during this study.

VI.4. Monoalkoxysilanes

VI.4.a. Introduction

The action mode of monoalkoxysilanes is based on the same basis than trialkoxysilanes. The main difference comes from their chemical structure as trialkoxysilanes are composed of 3 alkoxy functions compared to monoalkoxysilanes which are bearing 1 alkoxy function and 2 non-hydrolysable methyl functions (figure I-47).

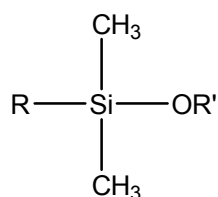


Figure I-47. General chemical formula of a monoalkoxysilane.

Again, OR' stands for easily hydrolyzable functions (mainly methoxy or ethoxy) that will be able, after hydrolysis, to form highly reactive silanols. On the other end, R is a non-hydrolysable organic moiety.

The behavior of these molecules is quite similar to the one of trialkoxysilanes except that homocondensation only leads to the formation of a dimer which can not cause the formation of a 3D siloxane network. The fact that there is only 1 hydrolysable alkoxy function means that there will be only 1 silanol formed after hydrolysis. This means that homocondensation can only lead to the formation of a non-reactive dimer (figure I-48).

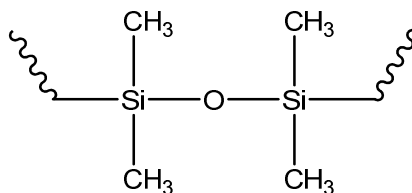


Figure I-48. Chemical formula of a non-reactive monoalkoxysilane dimer.

These molecules are poorly documented in the literature because of their limited utilization compared to trialkoxysilanes. However, some examples are found in publications ¹⁰⁸⁻¹¹².

These molecules were, for example, immobilized for biophase separation purposes ¹⁰⁸. During this study, 3-aminopropyldimethylethoxysilane (monoalkoxysilane with a primary amine function) was immobilized on the surface of a mesoporous molecular sieve (MCM-48). Vapor-phase deposition of this molecule allowed the obtaining of a monolayer due to the formation of covalent Si-O-substrate bonds and hydrogen bonds between the substrate and the primary amine of the molecule.

VI.4.b. Hydrolysis

Compared to trialkoxysilanes, the hydrolysis process of monoalkoxysilanes is not well-documented. In fact, the case of organofunctional monoalkoxysilane has not been described. However, few studies were made on methylmethoxysilanes by varying the methyl / methoxy ratio and measuring the effect on the hydrolysis kinetic ¹⁰⁹. These experiments were made in water and the chemical structures are too far from the ones used during our study to rely on these results. The hydrolysis of the monoalkoxysilanes compatible with the epoxy system will have to be totally studied during this work.

VI.4.c. Grafting

Grafting of amine- and epoxy-functionalized monoalkoxysilanes was performed on glass ¹¹² and on silica ¹¹⁰⁻¹¹². Long-time vapor-phase deposition of 3-aminopropyldimethylethoxysilane (with a primary amine) and (3-glycidoxy)propyldimethylethoxysilane (with an epoxy function) allowed the obtaining of a grafted monolayer at the surface of silica ¹¹⁰. Ellipsometry measurements also proved that an immobilized monolayer was obtained for each molecules (film thickness of around 10 Å).

Again, some techniques were developed to improve the grafting of these molecules at a surface. Amine molecules like triethylamine ¹¹¹ and ethylenediamine ¹¹² were first immobilized and the monoalkoxysilanes were then applied on the surface. The example with triethylamine is presented on figure I-49 ¹¹¹.

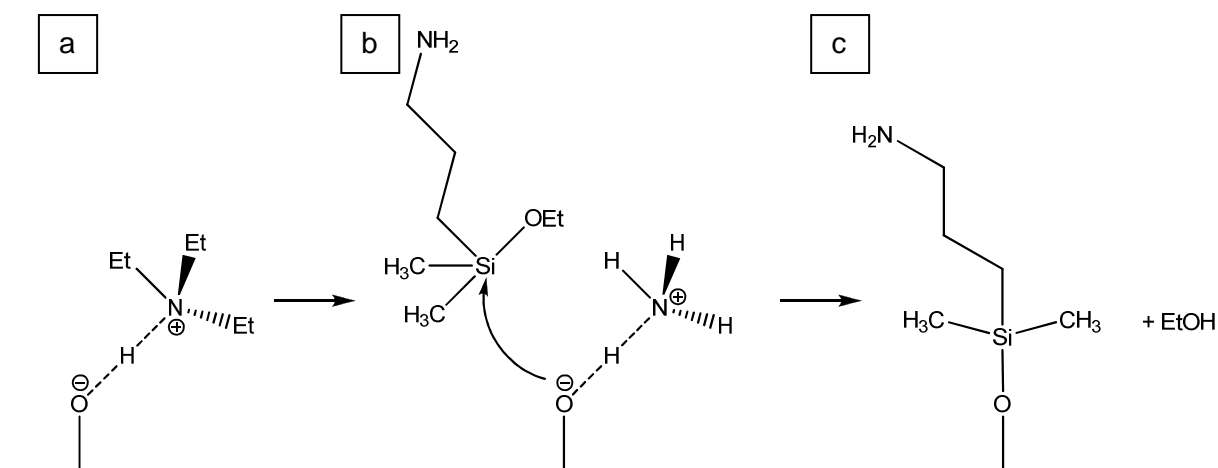


Figure I-49. Grafting of a monoalkoxysilane catalyzed by a pre-grafted amine.

However, grafting of these molecules has not been described on stainless steel and will have to be optimized.

VI.4.d. Conclusion

Monoalkoxysilanes have not been extensively used as adhesion promoters. However, their chemical structure, allowing the obtaining of a highly stable monolayer is interesting. As a matter of fact, it would allow to obtain the formation of covalent bonds between the substrate and the polymer coating without covering the surface roughness which is important to reach the maximum adhesion.

VI.5. Conclusion

The overview performed on the molecules that are suitable candidates showed that some solutions are available to efficiently improve adhesion of epoxy onto stainless steel. A special focus was made on alkoxy silanes with the widely used trialkoxy silanes but also with the monoalkoxy silanes which are less used but offer many advantages. The fact that these molecules are grafted on a surface in a monolayer way will allow to form stable covalent bonds without covering the substrate's roughness.

A quick look will also be given at phosphonate and sulfonate molecules.

VII. General conclusion

This chapter gave an overview on the state of the art about the Ecoating research project.

Eventhough it has not been well described in the literature, the formation of scale during the suspension polymerization of VCM is a real issue for S-PVC producers. Some explanations were given but these were only based on practical and process hypothesis. During this study, it was decided to establish the scale formation mechanism by the help of experimental analyses. Variation of some process parameters and analysis of the crust composition as a function of the batch duration will allow to more precisely describe this phenomenon.

This step is crucial because the understanding of the formation of scale will be the basis of the development of a durable anti-scale coating. However, some major difficulties will be faced during the progression of the coating's formulation. Regarding to the very restrictive specifications, epoxy systems were selected as a suitable solution. The behavior of this material will have to be tested in the extremely constraining S-PVC reactive medium. The first problem will be the resistance of the formed thermoset network but a major focus will have to be made on the highly water-sensitive epoxy / stainless steel interface.

References

- (1) Allsopp, M. W.; Vianello, G. *Ullmann's Encyclopedia of Industrial Chemistry*, A21; Wiley-VCH Verlag GmbH & Co. KGaA: New-York, **1992**, 717–742.
- (2) Titow, W. V. *Pvc Technology*; Springer: London, **1984**, 1–78.
- (3) Bodart, V. *Chimie et procédés de polymérisation : Initiation à la science des polymères*; GFP, **2010**, 18, 121–163.
- (4) Saeki, Y.; Emura, T. *Prog. Polym. Sci.* **2002**, 27, 2055–2131.
- (5) Hruska, Z.; Guesnet, P.; Salin, C.; Chouchoud, J. J. *Tech. Ingénieur, AM3325*, **2007**, 5.
- (6) Allsopp, M. W. *Pure Appl. Chem.* **1981**, 53, 449–465.
- (7) Rance, D. G. *Polymer colloids*; Elsevier Applied Science Publishers: London, **1985**, 289–316.
- (8) Burgess, R. H. *Manufacture and Processing of PVC*; Taylor & Francis, New-York, **2003**, 1–27.
- (9) Visentini, A. *IOM Communications: Brighton, Proceedings*; **2002**, 317–321.
- (10) Holmberg, B.; Westli, A. *Ann. N. Y. Acad. Sci.* **1979**, 329, 201–206.
- (11) Glück, P.; Pătrașcu, M.; Oșanu, P. *Mater. Plast.* **1980**, 17, 160–165.
- (12) Poljansek, I.; Krajnc, M. *Acta Chim. Slov.* **2005**, 52, 238–244.
- (13) CIRS SPA (IT). Anti-Scaling Agent for Coating of Polymerization Reactors and Preparation Process Thereof. Carlin, F.; Sattin, M. WO9635723 (A1), November 14, **1996**.
- (14) CIRS SPA (IT). Anti-Scaling Agent for Coating of Polymerization Reactors. Carlin, F.; Sattin, M. WO9635724 (A1), November 14, **1996**.
- (15) Adams, G. E.; Michael, B. D. *Trans. Faraday Soc.* **1967**, 63, 1171–1180.
- (16) Soriaga, M. P.; Hubbard, A. T. *J. Am. Chem. Soc.* **1982**, 104, 2742–2747.
- (17) CIRS COMPAGNIA ITALIANA RIC (IT). An Anti-Crust Decolorized Material for the Polymerization of the Chlorinated Olefinic Monomers. Carlin, F. WO9213897 (A1), August 20, **1992**.
- (18) CIRS CO IT RICERCA SVILUP (IT). Anti-Fouling Agent for the Polymerization of Olefinic Chloride Monomers. Polacco, F. WO8805055 (A1), July 14, **1988**.
- (19) BASF AG (GE). Procédé de polymérisation en suspension du chlorure de vinyle. FR2176735 (A1), November 2, **1973**.
- (20) SHINETSU CHEMICAL COMPANY (JP). Procédé perfectionné pour la polymérisation en suspension du chlorure de vinyle. FR2091147 (A5), January 14, **1972**.

- (21) THE GOODYEAR TIRE & RUBBER COMPANY (US). Reduction of reactor fouling and improvement in the thermal stability of pvc using nitrites. Mowdood, S. K. US3926910 (A), December 16, **1975**.
- (22) ANIC S.P.A (IT). Procédé de polymérisation en suspension de chlorure de vinyle. Claudio, F. FR2294189 (A1), July 9, **1976**.
- (23) CONTINENTAL OIL COMPANY (US). Procédé pour empêcher une accumulation de poly-chlorure de vinyle dans des réacteurs de polymérisation. FR2355890 (A1), January 20, **1978**.
- (24) BASF AG (GE). Colorants azoïques, leur préparation et leurs utilisations. FR2405978 (A1), May 11, **1979**.
- (25) Haïdopoulos, M.; Turgeon, S.; Laroche, G.; Mantovani, D. *Surf Coat Technol* **2005**, *197*, 278–287.
- (26) He, W.; Knudsen, O. Ø.; Diplas, S. *Corros Sci* **2009**, *51*, 2811–2819.
- (28) Crookes, R. *Le Décapage et la Passivation de l'Acier Inoxydable*; The European Stainless Steel Development Association, **2007**, 1–16.
- (28) Landolt, D. *Corrosion et chimie des surfaces des métaux*; PPUR presses polytechniques, **1997**, 468-470.
- (29) Cunat, P. J. Aciers inoxydables - Propriétés, Résistance à la corrosion. *Tech. Ingénieur M4554*, **2000**, 9-11.
- (30) Narváez, L.; Cano, E.; Bastidas, J. M. *Mater. Corros.* **2003**, *54*, 84–87.
- (31) Wada, Y.; Watanabe, A.; Tachibana, M.; Uetake, N.; Uchida, S.; Ishigure, K. *J. Nucl. Sci. Technol.* **2000**, *37*, 901–912.
- (32) Goldschmidt, A. J.; Streitberger, H. J. *BASF Handbook on Basics of Coating Technology*; William Andrew, **2003**, 15-25.
- (33) Wicks Jr, Z. W.; Jones, F. N.; Pappas, S. P.; Wicks, D. A. *Organic Coatings: Science and Technology*; John Wiley & Sons, **2007**, 1–7.
- (34) Kaushish, J. P. *Fundamental Principles of Manufacturing Process*; Industrial Press Inc., **1994**, 541–556.
- (35) Ellis, B. *Chemistry and technology of epoxy resins*; Blackie Academic & Professional, **1993**, 1–60.
- (36) Gerlitz, M. *Fundamentals of epoxy coatings*; Pre-congress tutorial - European Coatings Show, **2013**.
- (37) Koleske, J. V. *Paint and Coating Testing Manual*; ASTM International, **1995**.
- (38) Good R. J. *Recent advances in adhesion: proceedings*; Gordon and Breach Science Publishers, **1973**, 357-380.
- (39) Bikerman, J. J. *Ind. Eng. Chem.* **1967**, *59*, 40–44.
- (40) Barbarisi, M. J. *Nature* **1967**, *215*, 383–384.

- (41) Boucher, E. A. *Nature* **1967**, 215, 1054–1071.
- (42) Voyutskii, S. S. *J. Adhes.* **1971**, 3, 69–76.
- (43) Ahagon, A.; Gent, A. N. *J. Polym. Sci. Polym. Phys. Ed.* **1975**, 13, 1285–1300.
- (44) Basin, V. E. *Prog. Org. Coatings* **1984**, 12, 213–250.
- (45) Fowkes, F. M. *J. Adhes. Sci. Technol.* **1987**, 1, 7–27.
- (46) Kinloch, A. J. *Adhesion and Adhesives: Science and Technology*; Springer, **1987**, 79.
- (47) Semoto, T.; Tsuji, Y.; Yoshizawa, K. *J. Phys. Chem. C* **2011**, 115, 11701–11708.
- (48) Zhai, L. L.; Ling, G. P.; Wang, Y. W. *Int. J. Adhes. Adhes.* **2008**, 28, 23–28.
- (49) Possart, W. *Adhesion*; John Wiley & Sons, **2006**.
- (50) Legghe, E.; Aragon, E.; Bélec, L.; Margailan, A.; Melot, D. *Prog. Org. Coat.* **2009**, 66, 276–280.
- (51) Rouw, A. . *Prog. Org. Coatings* **1997**, 34, 181–192.
- (52) Galliano, F.; Landolt, D. *Prog. Org. Coatings* **2002**, 44, 217–225.
- (53) Calvez, P.; Bistac, S.; Brogly, M.; Richard, J.; Verchère, D. *J. Adhes.* **2012**, 88, 145–170.
- (54) Al-Harhi, M.; Loughlin, K.; Kahraman, R. *Adsorption* **2007**, 13, 115–120.
- (55) SHELL OIL COMPANY (US). Process for improving steel-epoxy adhesion. Bell, J. P.; De Nicola Jr, A. J. US4448847 A, May 15, **1984**.
- (56) Kopecki, E. S. *Cleaning Stainless Steel: A Symposium*; ASTM International, American Society for Testing and Materials **1973**, 6–13.
- (57) Thouless, M. D.; Yang Q. D. *Surfaces, chemistry and applications*; Elsevier: London, **2002**, 193–236.
- (58) McBain, J. W.; Hopkins, D. G. *J. Phys. Chem.* **1924**, 29, 188–204.
- (59) Tavakoli, S. M. *The Automotive Industry: Core Research from TWI*; Woodhead Publishing, **2000**, 53.
- (60) Anthony, J. W. *Handbook of Mineralogy: Halides, hydroxides, oxides*; Mineral Data Pub., **1997**.
- (61) Ebnesajjad, S. *Handbook of Adhesives and Surface Preparation: Technology, Applications and Manufacturing*; William Andrew: New-York, **2010**, 369–384.
- (62) Zenobi, M. C.; Luengo, C. V.; Avena, M. J.; Rueda, E. H. *Spectrochim. Acta. A. Mol. Biomol. Spectrosc.* **2010**, 75, 1283–1288.
- (63) Guerrero, G.; Mutin, P. H.; Vioux, A. *Chem. Mater.* **2001**, 13, 4367–4373.
- (64) Adolphi, B.; Jähne, E.; Busch, G.; Cai, X. *Anal. Bioanal. Chem.* **2004**, 379, 646–652.
- (65) Lecollinet, G.; Delorme, N.; Edely, M.; Gibaud, A.; Bardeau, J.-F.; Hindré, F.; Boury, F.; Portet, D. *Langmuir* **2009**, 25, 7828–7835.
- (66) Raman, A.; Dubey, M.; Gouzman, I.; Gawalt, E. S. *Langmuir* **2006**, 22, 6469–6472.
- (67) Mutin, P. H.; Guerrero, G.; Vioux, A. *J. Mater. Chem.* **2005**, 15, 3761–3768.

- (68) Denizot, B.; Tanguy, G.; Hindre, F.; Rump, E.; Jacques Le Jeune, J.; Jallet, P. *J. Colloid Interface Sci.* **1999**, *209*, 66–71.
- (69) Mutin, P. H.; Guerrero, G.; Vioux, A. *Comptes Rendus Chim.* **2003**, *6*, 1153–1164.
- (70) Portet, D.; Denizot, B.; Rump, E.; Lejeune, J.-J.; Jallet, P. *J. Colloid Interface Sci.* **2001**, *238*, 37–42.
- (71) SURFACTIS TECHNOLOGIES (FR). Procédé de Recouvrement de Surfaces Métalliques ou Minérales par des Couches de Composés Gem-Bisphosphonates et leur Utilisations. Benjanin, S.; Chappard, D.; Denizot, B.; Hindre, F.; Lecollinet, G.; Portet, D. WO0758320 (A1), August 10, **2007**.
- (72) Poussard, L.; Ouédraogo, C. P.; Pavon-Djavid, G.; Migonney, V. *Pathol. Biol.* **2012**, *60*, 84–90.
- (73) Plueddemann, E. P. *Silane coupling agents*; Plenum Press: New York, **1982**, 4–5.
- (74) Mittal, K. L.; Plueddemann, E. P. *Silanes and other coupling agents*; VSP: Utrecht, **1992**, VII–IX.
- (75) Osterholtz, F. D.; Pohl, E. R. *J Adhes Sci Technol* **1992**, *6*, 127–149.
- (76) Witucki, G. L. *JCT, Journal of coatings technology*; Federation of Societies for Coatings Technology **2006**, *65*, 57–60.
- (77) Sathyanarayana, M. N.; Yaseen, M. *Prog. Org. Coatings* **1995**, *26*, 275–313.
- (78) Quinton, J. S.; Dastoor, P. C. *Surf. Interface Anal.* **2000**, *30*, 21–24.
- (79) Quinton, J. S.; Dastoor, P. C. *Surf. Interface Anal.* **1999**, *28*, 12–15.
- (80) Chiang, C. H.; Ishida, H.; Koenig, J. L. *J. Colloid Interface Sci.* **1980**, *74*, 396–404.
- (81) Chiang, C. H.; Liu, N. I.; Koenig, J. L. *J. Colloid Interface Sci.* **1982**, *86*, 26–34.
- (82) Flesch, C.; Joubert, M.; Bourgeat-Lami, E.; Mornet, S.; Duguet, E.; Delaite, C.; Dumas, P. *Colloids Surf.* **2005**, *262*, 150–157.
- (83) Naviroj, S.; Culler, S.; Koenig, J.; Ishida, H. *J Colloid Interface Sci* **1984**, *97*, 308–317.
- (84) Kim, J. K.; Sham, M. L.; Sohn, M. S.; Hamada, H. *Polymer* **2001**, *42*, 7455–7460.
- (85) Underhill, P. R.; Goring, G.; DuQuesnay, D. L. *Int. J. Adhes. Adhes.* **1998**, *18*, 313–317.
- (86) Qiu, J.; Sakai, E.; Lei, L.; Takarada, Y.; Murakami, S. *J. Mater. Process Technol.* **2012**, *212*, 2406–2412.
- (87) Nishiyama, N.; Komatsu, K.; Fukai, K.; Nemoto, K.; Kumagai, M. *Composites* **1995**, *26*, 309–313.
- (88) Nishiyama, N.; Horie, K.; Asakura, T. *J. Colloid Interface Sci.* **1989**, *129*, 113–119.
- (89) Nishiyama, N.; Shick, R.; Ishida, H. *J. Colloid Interface Sci.* **1991**, *143*, 146–156.
- (90) Jang, J.; Kim, E. K. *J. Appl. Polym. Sci.* **1999**, *71*, 585–593.
- (91) Brochier Salon, M.-C.; Bayle, P.-A.; Abdelmouleh, M.; Boufi, S.; Belgacem, M. N. *Colloids Surf. Physicochem. Eng. Asp.* **2008**, *312*, 83–91.

- (92) Riegel, B.; Blittersdorf, S.; Kiefer, W.; Hofacker, S.; Müller, M.; Schottner, G. *J. Non-Cryst. Solids* **1998**, 226, 76–84.
- (93) Paquet, O.; Brochier Salon, M. C.; Zeno, E.; Belgacem, M. N. *Mater. Sci. Eng. C* **2012**, 32, 487–493.
- (94) Brochier Salon, M.-C.; Belgacem, M. N. *Phosphorus Sulfur Silicon Relat. Elem.* **2011**, 186, 240–254.
- (95) Brinker, C. J.; Scherer, G. W. *Sol-gel Science: The Physics and Chemistry of Sol-gel Processing*; Gulf Professional Publishing, **1990**.
- (96) Arkles, B.; Steinmetz, J. R.; Zazyczny, J.; Mehta, P. *J. Adhes. Sci. Technol.* **1992**, 6, 193–206.
- (97) Materne, T.; de Buyl, F.; Witucki, G. L. *Dow Corning Rev.* **2006**.
- (98) Blitz, J. .; Shreedhara Murthy, R. .; Leyden, D. J. *Colloid Interface Sci.* **1988**, 126, 387–392.
- (99) Xie, Y.; Hill, C. A. S.; Xiao, Z.; Miltz, H.; Mai, C. *Compos. Part A: Appl. Sci. Manuf.* **2010**, 41, 806–819.
- (100) Brochier Salon, M.-C.; Belgacem, M. N. *Colloids Surfaces Physicochem. Eng. Asp.* **2010**, 366, 147–154.
- (101) Vrancken, K. .; Possemiers, K.; Van Der Voort, P.; Vansant, E. *Colloids Surf* **1995**, 98, 235–241.
- (102) Okabayashi, H.; Shimizu, I.; Nishio, E.; Connor, C. J. O. *Colloid Polym. Sci.* **1997**, 275, 744–753.
- (103) Hüsing, N.; Schubert, U. *Mrs Online Proc. Libr.* **1999**, 576.
- (104) Yee, J. K.; Parry, D. B.; Caldwell, K. D.; Harris, J. M. *Langmuir* **1991**, 7, 307–313.
- (105) Trens, P.; Denoyel, R. *Langmuir* **1996**, 12, 2781–2784.
- (106) Caravajal, G. S.; Leyden, D. E.; Quinting, G. R.; Maciel, G. E. *Anal. Chem.* **1988**, 60, 1776–1786.
- (107) Ji, W. G.; Hu, J. M.; Liu, L.; Zhang, J. Q.; Cao, C. N. *Surf. Coat. Technol.* **2007**, 201, 4789–4795.
- (108) Daehler, A.; Boskovic, S.; Gee, M. L.; Separovic, F.; Stevens, G. W.; O'Connor, A. J. *J. Phys. Chem. B* **2005**, 109, 16263–16271.
- (109) Bennett, M. D.; Wolters, C. J.; Brandstadt, K. F.; Tecklenburg, M. M. J. *J. Mol. Struct.* **2012**, 1023, 204–211.
- (110) Dorvel, B.; Reddy, B.; Block, I.; Mathias, P.; Clare, S. E.; Cunningham, B.; Bergstrom, D. E.; Bashir, R. *Adv. Funct. Mater.* **2010**, 20, 87–95.
- (111) White, L. D.; Tripp, C. P. *J. Colloid Interface Sci.* **2000**, 232, 400–407.
- (112) Kanan, S. M.; Tze, W. T. Y.; Tripp, C. P. *Langmuir* **2002**, 18, 6623–6627.

Chapter II

-

Experimental Part

CHAPTER II: EXPERIMENTAL PART

I. Solvents and products	77
I.1. PolyVinyl Alcohols (PVA).....	77
I.2. Coupling Agents.....	78
I.3. Epoxy resins.....	79
I.3.a. RenLam CY 219 / Ren HY 5161.....	79
I.3.b. Araldite DBF CH / Ren HY 956.....	80
I.3.c. Pure amines.....	80
I.4. Stainless steel.....	80
I.4.a. Cleaning of the stainless steel plates.....	81
I.4.b. Shot-blasting of the stainless steel plates.....	81
II. Tests for the determination of the scale's formation mechanism	81
II.1. Simulation tests: Immersion in model systems.....	81
II.1.a. Immersion in a "model" solvent.....	81
II.1.b. Immersion in water / LPO system.....	82
II.1.c. Immersion in water / PVA systems.....	82
II.1.d. Immersion in BuCl / LPO / PVA systems.....	83
II.1.e. Immersion in water / BuCl emulsions stabilized by PVAs.....	83
II.2. Pilot tests.....	83
II.2.a. Presentation of the pilot reactor.....	83
II.2.b. Kinetic of the scale formation.....	85
II.2.c. Influence of the PVA hydrolysis degree on the scale formation.....	85
III. Preparation of the epoxy free films	85
IV. Preparation of the epoxy coatings on stainless steel	86
IV.1. Preparation of the epoxy-coated stainless steel plates.....	86
IV.2. Application of the sulfonate, phosphonate and bisphosphonate on stainless steel.....	86
IV.2.a. Preparation of a solution at 10^{-3} M.....	86
IV.2.b. Deposition process.....	87
IV.3. Application of the alkoxysilanes on the stainless steel plates.....	87
V. Tests of the coated stainless steel plates	87
V.1. Immersion in model solvents.....	87
V.1.a. Immersion in hot BuCl.....	87
V.1.b. Immersion in hot water.....	88
V.2. Immersion in pilot reactor.....	88

VI. Analytical techniques	88
VI.1. Chemical and surface analyses.....	88
VI.1.a. InfraRed analyses.....	88
VI.1.b. Nuclear Magnetic Resonance spectroscopy (¹ H NMR).....	90
VI.1.c. Scanning Electron Microscopy / Energy Dispersive X-Ray spectroscopy (SEM-EDX)....	90
VI.1.d. X-ray Photoelectron Spectroscopy (XPS).....	90
VI.1.e. Contact Angle measurements.....	91
VI.1.f. Optical Microscopy.....	91
VI.1.g. Atomic Force Microscopy (AFM).....	92
VI.2. Thermal and thermo-mechanical analyses.....	92
VI.2.a. Dynamic Mechanical Thermal Analysis (DMTA).....	92
VI.2.b. Differential Scanning Calorimetry (DSC).....	92
VI.2.c. ThermoGravimetric Analysis (TGA).....	93
VI.3. Mechanical tests.....	93
VI.3.a. Lap-shear tests.....	93
VI.3.b. Tribology measurements.....	93
VI.3.c. Pull-off tests.....	94
VII. Conclusion	94
References	95

I. Solvents and products

Distilled water was obtained by purification of common water by a Millipore Direct-Q 3 purifier. Ethanol was supplied by VWR (96 %, ref. 20824.365), acetic acid by Fisher Scientific (> 99 %, ref. A/0360/PB15) and caustic soda by Riedel-de-Haën (99-100 %, ref. 06203). Acetone was supplied by Biosolve (99.5%, ref. CP) and dichloromethane (100 %, ref. 25631.362) by VWR.

Dilauroyl Peroxide (LPO) was supplied by Sigma-Aldrich (ref. 290785), di(2-ethylhexyl) peroxydicarbonate (EHP) by AkzoNobel (60 % emulsion in water and methanol, Trigonox EHP-W60) and 1-chlorobutan (BuCl) by Alfa Aesar (> 99 %, ref. A11494). LPO chemical formula used during the tests in model solutions is presented on figure II-1.

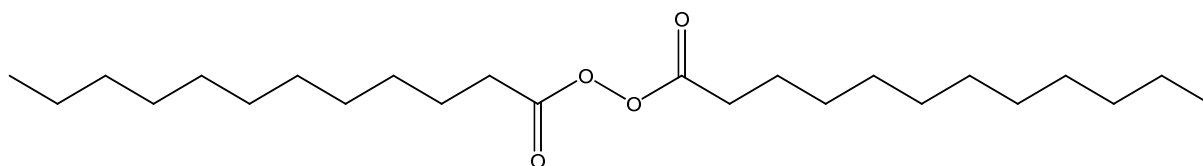


Figure II-1. General chemical formula of dilauroyl peroxide (LPO).

I.1. PolyVinyl Alcohols (PVA)

PVAs are polyvinyl alcohol / polyvinyl acetate block copolymers which are used on the different production sites of INEOS ChlorVinyls as surfactants. Their general chemical formula is presented on figure II-2.

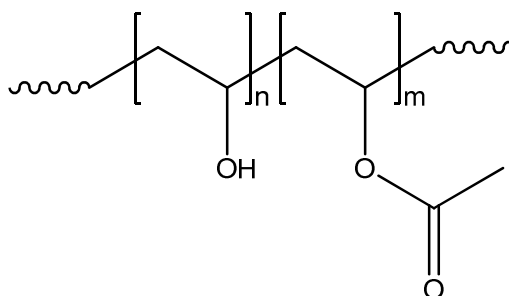


Figure II-2. General chemical formula of a polyvinyl alcohol / polyvinyl acetate copolymer (PVA).

Four PVA were tested during this study and their main characteristics given by their producers are reported in table II-1.

Table II-1. Presentation of the PVAs used during the study (supplier's datas).

	PVA	Abbreviation	Supplier	HD (% mol)*	Mw (g.mol ⁻¹)**	Solvent
PVA I	KP08R	1-H72M40	Nippon Gohsei	72.5	40,000	-
	B72	1-H72M36	Synthomer	72.5	36,000	-
PVA II	A45	2-H45M15	CIRS	45	15,000	EtOH/AcOEt
	A432P	2-H43M15	Synthomer	43	15,000	MeOH/AcOMe

* Hydrolysis degree: molar ratio of the polyvinyl alcohol part over the polyvinyl acetate part

** Supplier's data

These compounds are classified into two categories: primary (PVA I) and secondary (PVA II). A PVA is considered as a primary one when its hydrolysis degree (HD) is superior to 60% (molar) contrary to a secondary PVA (with a HD inferior to 60%).

A simple annotation was used in this thesis to identify the different PVA by using the following model. The KP08R is known as the 1-H72M40 where 1 stands for the type of PVA (2 if the concerned PVA is a PVA II), the number following the letter "H" corresponds to the HD and the one following "M" stands for an abbreviation of the Mw value.

1.2. Coupling Agents

3-aminopropyl(trimethoxysilane) (APTMS, 97 %, Sigma-Aldrich ref. 281778), N-[3-(trimethoxysilyl)propyl]ethylenediamine (AAPS, 97 %, Sigma-Aldrich ref. 104884), N-(3-trimethoxysilylpropyl) diethylenetriamine (TPDTA, 95 %, Sigma-Aldrich ref. 413348), (3-glycidyloxypropyl) trimethoxysilane (GPTMS, 98 %, Sigma-Aldrich ref. 440167), 3-(triethoxysilyl)propylsuccinic anhydride (TPSA, 94 %, ABCR ref. AB128800), 3-(ethoxydimethylsilyl)propylamine (APDES, 97 %, Sigma-Aldrich ref. 588857), 3-glycidoxypropyldimethylethoxysilane (GPDES, 97 %, Sigma-Aldrich ref. 539260), taurine (\geq 99 %, Sigma Aldrich ref. T0625), 3-aminopropylphosphonic acid (98 %, Sigma Aldrich ref. 268615) and 3-aminopropylbisphosphonic acid (pure, Surfactis ref. 01-102) were used as received.

1.3. Epoxy resins

The epoxy resins (RenLam CY 219 and Araldite DBF CH) and their respective curing agents (Ren HY 5161 and Ren HY 956) were supplied by Huntsman.

1.3.a. *RenLam CY 219 / Ren HY 5161*

The main properties of this resin and its curing agent are listed in table II-2.

Table II-2. Main properties of the CY219 / HY5161 system (supplier's datas).

Properties	Unit	CY219	HY5161	CY219 + HY516 (100/50pp)
Aspect	-	Orange liquid	Yellow liquid	Yellow liquid
Viscosity (at 25°C)	mPa.s	10,000 - 12,000	30 - 70	1,000 - 1,200
Density	-	1.1	1	1.1
Curing conditions		5 - 7 hours at 80°C (non-optimized)		

The composition of the curing agent Ren HY5161 is given in table II-3.

Table II-3. Chemical composition of the HY5161 commercial curing system (supplier's data).

Compound	Proportions (w / w)	Chemical formula
Polyoxypropylenediamine (Jeffamine)	30-42 %	
Benzyl alcohol	25-32 %	
Isophorone diamine	22-30 %	
Trimethylhexamethylenediamine	4-10 %	
Bisphenol-A	1-5 %	

I.3.b. Araldite DBF CH / Ren HY 956

The main properties of this resin and its curing agent are listed in table II-4.

Table II-4. Main properties of the Araldite DBF CH/HY956 system (supplier's datas).

Properties	Unit	Araldite DBF	HY956	Ar DBF + HY956 (100/20pp)
Aspect	-	Orange liquid	Yellow liquid	Yellow liquid
Viscosity (at 25°C)	mPa.s	1,350 - 2,000	370 - 470	1,000 - 1,200
Density	-	1.1 - 1.2	1 - 1.05	1.1
Curing conditions		5 - 7 hours at 80°C (non-optimized)		

This epoxy resin contains around 20 % (w/w) of diethyl phthalate as a non-reactive diluent in order to decrease the viscosity of the epoxy prepolymer. The chemical composition of the curing agent Ren HY 956 is not given by the supplier.

I.3.c. Pure amines

Some pure amines were tested as crosslinking agents for the epoxy resin RenLam CY 219. Hexamethylenediamine (ref. H11696), pentaethylenehexamine (ref. 292753), triethylenetetramine (ref. 132098), isophoronediamine (ref. 118184), 1-(2-aminoethyl)piperazine (ref. A55209) and m-phenylenediamine (ref. P23954) were all provided by Sigma-Aldrich and used as received.

I.4. Stainless steel

American Iron and Steel Institute (AISI) 316L stainless steel was supplied by AcerInox. Dimensions of the plates used for the tests are 100 * 60 * 1.5 mm.

The exact composition of the stainless steel used was given by its authenticity certificate provided by AcerInox (table II-5).

Table II-5. Bulk chemical composition of AISI 316L stainless steel .

Alloy element	Fe	C	Cr	Ni	Mo	Mn	Si	N	P	S
% (w/w)	69.041	0.018	16.930	10.097	2.032	1.326	0.475	0.048	0.029	0.004

1.4.a. Cleaning of the stainless steel plates

The stainless steel plates were each times previously cleaned using a wet tissue of acetone and a 5 minutes dichloromethane ultrasonic bath. The stainless steel plates were then dried at 110 °C during 5 minutes.

1.4.b. Shot-blasting of the stainless steel plates

This surface treatment was performed by Mäder. The stainless steel plates were subjected to a high-pressure flow of corundum (Al₂O₃) particles. Particles diameters of 40, 120 and 220 mesh were used to obtain a large range of surface roughness.

II. Tests for the determination of the scale's formation mechanism

II.1. Simulation tests: Immersion in model systems

II.1.a. Immersion in a "model" solvent

1-chlorobutan was chosen as a model solvent due to its main physical and chemical properties which are relatively similar to the ones of VCM.

The main properties of 1-chlorobutan (BuCl) and VCM are summed up in table II-6 ¹.

Table II-6. Comparison between the main physical and chemical properties of BuCl and VCM.

	BuCl	VCM
Boiling Temperature (°C)	78	-13.4
Total Solubility Parameter (J.cm⁻³)^{1/2}	17	17.4
Density (20°C)	0.886	0.911
Molar Mass (g.mol⁻¹)	93.6	62.5
Refractive Index (20°C)	1.402	1.37
Viscosity (mPa.s)	0.51 (at 20°C)	0.23 (0°C)
Solubility in water (mg.kg⁻¹)	-	1100
Interfacial Tension/H₂O (mN.m⁻¹)	38.7	32

Cleaned 316L stainless steel plates have been immersed during 7h in BuCl at various temperatures (room temperature and 70°C).

II.1.b. Immersion in water / LPO system

0.145 g of LPO was added in 200 g of water (725 ppm of LPO in water) at room temperature under magnetic stirring. A 316L plate was directly immersed in this suspension. The solution containing the plate was heated at 70 °C during 7h. The plate was then dried and analyzed by optical microscopy and IRRAS.

II.1.c. Immersion in water / PVA systems

2 g of the PVA tested were added to 200 g of water (1 % w / w). This solution was heated at around 50 °C under magnetic stirring in order to to tally solubilize the PVA. The solution was then either heated at 70 °C or cooled down to get back at room temperature. 316L stainless steel plates were then placed in the solution.

II.1.d. Immersion in BuCl / LPO / PVA systems

The preparations were made in a 250 mL round-bottomed flask. 150 mL of BuCl, 2.658 g of LPO (2% w/w) and 1.329 g of the PVA chosen (1% w/w) were added and heated at 70 °C under magnetic stirring. 316L stainless steel plates were immersed afterwards.

II.1.e. Immersion in water / BuCl emulsions stabilized by PVAs

The preparation of these samples was done in two parts.

First, 0.75 g of the chosen PVA were weighed and added to 74.25 g of water. This solution was stirred during 5 minutes with an ultraturrax (7500 rpm).

Then, 2 g of LPO were added to 25 g of BuCl. This solution was magnetically stirred until the complete dissolution of LPO. Finally, the second solution was added to the first one and the entire mix was stirred during 5 minutes with an ultraturrax (7500 rpm).

The whole emulsion was then put into a 250 mL round-bottomed flask and heated at 70 °C. The studied substrate was immersed just before the heating period and during 7 h.

This led to a water / BuCl emulsion (3:1) with 2% of LPO and 0.75% of PVA.

II.2. Pilot tests

A pilot reactor installed at the INEOS ChlorVinyls France production site in Mazingarbe, permits the study of the encrusting process in a real-time polymerization. The structure of this reactor allows modifying certain parameters (rotation speed, quantity of products, temperature...) and allows stopping the polymerization at a given time.

II.2.a. Presentation of the pilot reactor

The pilot reactor's inner surface is enamel recovered and stainless steel plates can be immersed in the reactive medium by the help of a crown. The capacity of the reactor is

100 L, its inner diameter is 500 mm and its maximal pressure is 15 bars. Pictures of the pilot reactor used at INEOS ChlorVinyls for the pilot tests are presented on figure II-3.

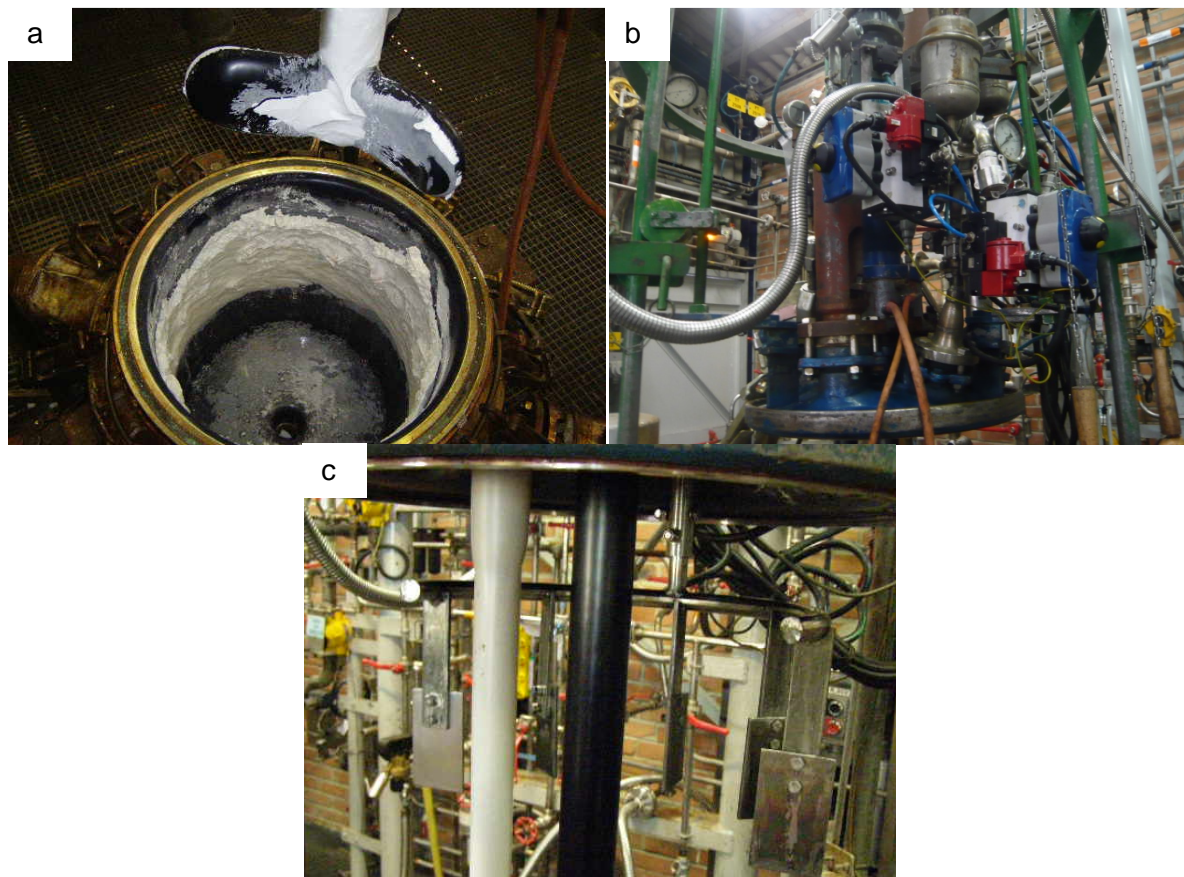


Figure II-3. Pictures of: a. the inside of the scale-recovered pilot reactor; b. the upper part of the pilot reactor and c. ready-to-be-immersed stainless steel plates.

For a typical polymerization, the reactor is first filled with 43.6 kg of water. The reactor is then degassed in order to remove the maximum oxygen of the reactive medium during around 30 minutes at an agitating speed of 200 rpm. The other additives (460.1 g of 1-H72M40, 36.4 g of 2-H45M15, 8.5 g of EHP, 32.7 g of LPO) are then introduced. Vacuum (at around 100 mm Hg) is made in the reactor and the pressure is then stabilized at 200 mm Hg. Finally, 29.1 kg of VCM are introduced. The reactor is then pre-agitated during 20 minutes and heated to reach a temperature of 69.5 °C. 10.9 g of ammoniac are added as a buffer to obtain a pH value between 6.5 and 7. A stopper (chemical product which stops the polymerization) is added when the desired polymerization time is reached.

II.2.b. Kinetic of the scale formation

The kinetic of the scale formation has first been studied. These tests were made during a classical VCM polymerization using a PVAs pair of 800 ppm of 1-H72M40 and of 500 ppm of 2-H45M15.

Numerous stainless steel plates were immersed in the pilot reactor and polymerizations were stopped after different times: 5, 10, 15, 30 and 60 minutes. The aim of these tests was to determine the beginning of the fouling process and to identify the compounds which are firstly adsorbed. The plates are then analyzed by optical microscopy and by IRRAS.

II.2.c. Influence of the PVA hydrolysis degree on the scale formation

VCM polymerizations were made during 15 minutes using different PVA I / PVA II couples at a total concentration of respectively 800 ppm and 500 ppm.

The aim of these tests is to determine the influence of the PVA I and II structures (mainly their double bonds content) on the scale formation. The plates are then analyzed by optical microscopy and by IRRAS.

III. Preparation of the epoxy free films

Free films were prepared by mixing the epoxy with its corresponding curing agent (using the supplier's ratios). This solution is manually mixed to obtain a homogeneous blend and vacuum is then applied during 5 minutes in order to remove air from the sample.

3 g of this mixture were then poured into silicon molds. Two curing conditions were experimented for the commercial systems: 150 °C during 1 h for both systems and 80 °C during 3 h only for the RenLam CY 219 system. The main information about the systems used are summed up in table II-7.

Table II-7. Main information on the two commercial epoxy resins used.

Epoxy resin	Curing agent	Epoxy parts	Curing agent parts
RenLam CY 219	Ren HY 5161	100	50
Araldite DBF CH	Ren HY 956	100	20

The dimensions of the free films obtained after curing are: L = 70 mm / l = 30 mm / h = 1 – 2 mm.

For the tests performed on pure polyamines, the curing conditions for each molecule are presented in Chapter IV., part. III, 2, c.

IV. Preparation of the epoxy coatings on stainless steel

IV.1. Preparation of the epoxy-coated stainless steel plates

The films were prepared by mixing the epoxy with its curing agent (in the ratios recommended by the epoxy supplier). This solution was manually mixed to obtain a homogeneous blend. The coating was finally applied by using a painting brush (obtaining a thickness of 200 μm). The final step was the curing of the coated plate during 1 hour at 150 $^{\circ}\text{C}$.

IV.2. Application of the sulfonate, phosphonate and bisphosphonate on stainless steel

IV.2.a. Preparation of a solution at 10^{-3} M

0,1 mmol of the reactive molecule were weighted in 100 mL of water and the pH of the solution was stabilized at 7 with NaOH. It was necessary to cool the solution to avoid any excessive increase of temperature. The solution was stirred until complete dissolution of the reactive molecule.

IV.2.b. Deposition process

The cleaned stainless steel plate was immersed in the solution during 10 min and was then rinsed into a water ultrasonic bath (during 30 s). This first step was repeated twice and the functionalized plate was dried at 80 °C during 30 min.

IV.3. Application of the alkoxysilanes on the stainless steel plates

Alkoxysilane (2% w / w) hydrolysis took place in a 95 / 5^{2,3} (w / w) ethanol / water mixture at a controlled pH (acetic acid for acidic medium and caustic soda for basic medium). The alkoxysilane was then poured into this solution during a given time (between 90 seconds and 1 hour) to allow the hydrolysis.

The stainless steel plates were immersed in the alkoxysilane solution during a given time (between 2 and 30 minutes). The functionalized plates were then rapidly poured into an ethanol bath to remove the physically adsorbed species. The plates were then dried during 30 minutes at 110 °C in order to allow the grafting of the alkoxysilane layer.

The epoxy coating was then applied as described above (IV.1).

V. Tests of the coated stainless steel plates

V.1. Immersion in model solvents

The two solvents used for these tests were water which was the dispersive medium for the suspension polymerization of Vinyl Chloride Monomer (VCM) and BuCl to simulate VCM.

V.1.a. Immersion in hot BuCl

The first immersion tests were performed in hot BuCl (75 °C) in order to evaluate the effect of the solvent on the epoxy / stainless steel interface.

The coated steel plates were put in BuCl during at least two days and their aspects were looked after drying under ambient air.

V.1.b. Immersion in hot water

The immersion tests performed in hot water (80 °C) were critical in order to evaluate the effect of the solvent on the epoxy / stainless steel interface.

The coated steel plates were put in water during at least two days and their aspects were looked after drying under ambient air.

V.2. Immersion in pilot reactor

The coated stainless steel plates were immersed in the pilot reactor and were subjected to classical polymerizations (described in II.2.a). All the samples were examined after each batch and were either reintroduced if the coating was efficient or either removed if degradation of the coating was observed.

VI. Analytical techniques

VI.1. Chemical and surface analyses

VI.1.a. InfraRed analyses

InfraRed spectra were recorded using a Bruker Vertex 70 spectrometer run by OPUS 3.5. Different moduli were used to analyse samples with different infrared modes.

VI.1.a.i. Transmission mode (T-IR)

The sample was deposited on a pellet made of a material which does not absorb the infrared beam in the desired spectral range. The incident beam passing through the sample was

recorded by the detector and the spectrum was finally obtained after an inverse Fourier transform. These analyses were made using silver bromide (supplied by Alfa Aesar) pellets, by an accumulation of 50 scans in a spectral range from 400 to 4000 cm^{-1} and a resolution of 4 cm^{-1} . Silver bromide (AgBr) pellets were prepared using a press at a pressure of 10 tons.

VI.1.a.ii. Infrared reflection absorption spectroscopy (IRRAS)

IRRAS is an established analytical technique for the characterization of adsorbed matter and thin layers (from 0.1 to 100 μm) on metal surfaces. The sample is investigated in reflection geometry under grazing incidence (typically 75-90°). The IRRAS spectra were obtained using a resolution of 4 cm^{-1} in a range going from 400 to 4000 cm^{-1} . The number of scans for the reference was 500 and was made on a 316L stainless steel plate in order to free ourselves from the potential peaks coming from the substrate. The number of scans for the measure was 500 too. For each measure, a delay time of 10 minutes was used to remove the intense peaks coming from carbon dioxide and water. The aperture of the diaphragm was 6 mm and the angle of incidence used was 75°.

VI.1.a.iii. Polarization Modulation - InfraRed Reflection Absorption Spectroscopy (PM-IRRAS)

PM-IRRAS enhances the performances obtained by IRRAS by eliminating the disturbance caused by atmosphere water and CO_2 . It also takes advantage on the difference of adsorption between p- and s-polarized components of the infrared beam allowing to obtain some information on the structure of the grafted molecules. The PM-IRRAS spectra were obtained using a Brucker Vertex 70 spectrometer associated to a PMA 50 modulus. Both are driven by the software OPUS 6.5. The resolution used was 4 cm^{-1} in a range going from 600 to 4000 cm^{-1} . The aperture of the diaphragm was 2.5 mm and the angle of incidence used was 80°^{4,5}. A ZnSe photoelastic modulator provided by HINDS Instruments was used at a modulation frequency of 100 kHz. The lock-in amplifier used for signal demodulation and treatment was provided by Stanford Research Systems.

VI.1.a.iv. Diffuse Reflectance Infrared Fourier Transform (DRIFT)

DRIFT is an infrared technique normally used to analyze powders or rough surfaces but it was used here to analyze the grafted molecules on stainless steel. This modulus is used like IRRAS but it allows to obtain a greater amount of information as the spot size obtained in DRIFT is bigger than the one of IRRAS.

VI.1.b. Nuclear Magnetic Resonance spectroscopy (^1H NMR)

This technique is used for the chemical analysis of molecules with a non-null nuclear spin when placed under a magnetic field. The atomic nucleus, when submitted to an electromagnetic beam, will absorb its energy and release it during a relaxation process giving access to the molecule spectrum. The NMR spectra were obtained using 10 % by weight solutions in deuterated-chloroform (CDCl_3). The apparatus used was a Bruker 300 Ultrashield spectrometer at 300 MHz driven by the XWIN-NMR V. 3.5 software.

VI.1.c. Scanning Electron Microscopy / Energy Dispersive X-Ray spectroscopy (SEM-EDX)

The samples, during the SEM analysis, are scanned by a focalized electron beam. The incident beam interacts with the electrons of the sample and the signal produced gives some information on the surface's topography. Moreover, an X-ray beam is generated from the entire scan area of the SEM analysis and is collected in order to give some details on the chemical composition of the sample thanks to the EDX modulus. The apparatus used was a Philips XL30 FEG equipped with a field effect canon at an acceleration voltage of 7 kV. The EDX modulus was composed of a Si(Li) detector and spectrum were made until a tension of 20 keV in order to analyse all elemental elements from carbon to uranium.

VI.1.d. X-ray Photoelectron Spectroscopy (XPS)

XPS is a quantitative spectroscopic technique used to analyze the chemical composition of a crude substrate or of a material after surface treatment based on the photoelectric effect. X-rays are focalized on the analyzed substrate, penetrate the sample at a 1 μm depth and

transfer their energy while hurting the electrons of the studied surface. When the energy of the photons is sufficient, the electrons of the sample are ejected and will be collected by a detector. It is at this point possible, by knowing the wavelength of the incident photons and the kinetic energy of the emitted photoelectron, to calculate the binding energy (BE) of a detected electron. BE is a characteristic value for each core and orbital levels of a given atom giving after analysis the chemical composition of the analyzed surface.

XPS, during this study, was used to characterize and visualize the different steel's surface treatments when infrared spectroscopy was not sensitive enough to obtain some information on grafted molecules.

XPS was performed using a conventional MgK α ($h\nu = 1253.6$ eV) and AlK α ($h\nu = 1486.6$ eV) photon source (Omicron DAR 400) and a 7-channels hemispherical spectrometer (Omicron EA 125). The binding energies indicated in the spectra refer to Fermi level E_f . The electron acceptance angle is about $\pm 8^\circ$ and the analysis area does not exceed 1.5 mm. XPS survey spectra are recorded with a 100 eV pass energy while the chemical species core levels are analyzed with a 20 eV pass energy. Core level spectra were fitted to mixed Gaussian-Lorentzian components using CasaXPS software version 2.3.15⁶.

VI.1.e. Contact Angle measurements

Contact angle measurement is a technique used to measure the wettability of a material. It is also possible to determine the surface energy of a sample by measuring the contact angle with a polar solvent (water) and a non-polar solvent (diiodomethane). The apparatus used was a Kruss DSA 100 with the software Drop Shape Analysis. The deposited volume was 0.2 μ L with a 0.53 mm diameter syringe. The contact angle θ was determined using the tangent method.

VI.1.f. Optical Microscopy

Optical microscopy snapshots were obtained from an Olympus BX51 piloted by the software cell^A. The images were taken in a reflecting mode at enlargements of 100 and 500 ($\times 10$ for the eyepiece and $\times 10$ and $\times 50$ for the two lenses used). Pictures obtained were optimized in term of contrasts in order to get well-defined photos.

VI.1.g. Atomic Force Microscopy (AFM)

The AFM was a Bruker Dimension Edge driven by the software NanoDrive v8.01. The tip was supplied by Veeco, the model is TAP150 and is a Phosphorous (n) doped Si tip. Its spring constant is equal to 5 N.m^{-1} and its resonance frequency is near 154 kHz. The target tapping signal is 4 V and a 20x gain is used to obtain a clear image. The surface analyzed is a $20 \mu\text{m} \times 20 \mu\text{m}$ square.

VI.2. Thermal and thermo-mechanical analyses

VI.2.a. Dynamic Mechanical Thermal Analysis (DMTA)

DMTA is used in torsion mode on crosslinked epoxy films to determine the viscoelastic properties of polymers (given by their complex modulus) as a function of the temperature. A given strain is applied to the sample under a fixed frequency and the storage modulus (G') and the loss modulus (G'') are measured during a temperature ramp. The analysis will give some information on the T_g of the samples but also on their molecular weight between the crossing points (M_c)^{7,8}. The apparatus used was an Anton Paar MCR 302 driven by the software RheoPlus. The tests were made on epoxy free films samples ($35 * 10 * 2 \text{ mm}$) performing a temperature ramp from 20 to 250 °C on a torsion-shear mode. The shear strain was fixed at 0.01 % at a frequency of 1 Hz.

VI.2.b. Differential Scanning Calorimetry (DSC)

This analysis allows to determine the typical thermal transitions of a polymer (melting, crystallization, glass transition, heat of reaction...). The apparatus used was a TA Instrument TGA Q200 driven by the software TA Explorer.

All the analyses were performed under a nitrogen flow. For typical T_g measurement, 2 successive temperature ramps from -80 to 200 °C at a heating rate of 10 °C.min^{-1} were performed.

For the epoxy network curing speed measurement directly made in the DSC pans, an isothermal analysis was performed at the desired temperature. This step was followed by a

30 °C cooling and by a heating (10 °C.min⁻¹) to 250 °C to check the presence of an eventual residual exothermal peak.

For the curing rate measurements on free epoxy films, a simple temperature ramp from 25 to 250 °C at a heating rate of 10 °C.min⁻¹ was performed to check the conversion speed as a function of time.

VI.2.c. ThermoGravimetric Analysis (TGA)

The TGA technique consists in the measurement of the mass variations of a sample as a function of the temperature (determination of the different thermal degradations, of the volatile rates...).

The apparatus used was a TA Instrument TGA Q500 driven by the software TA Explorer. The tests consisted in a 10 °C.min⁻¹ temperature ramp from 30 to 900 °C under a nitrogen flow.

VI.3. Mechanical tests

VI.3.a. Lap-shear tests

Lap-shear determines the shear strength of adhesives for bonding materials when tested on a single-lap-joint specimen. The test was used for determining adhesive strength and durability of a stainless steel / epoxy / stainless steel joint after immersion in hot water (80 °C). For this purpose, two stainless steel plates were bonded together with the epoxy coating and cured as specified. The test specimens were then placed in the grips of a Testometric M500-30AT tensile-testing machine and pulled at 1 mm.min⁻¹.

VI.3.b. Tribology measurements

Tribology tests were performed in order to determine the resistance of the coating to friction. The friction coefficient μ , which is the ratio between the tangential force (F_T) required to produce sliding divided by the normal force between the surfaces (F_N), and its evolution as a

function of time, will give some information on the resistance of the coating regarding to wear and abrasion. Measurements were made at ambient temperature by rubbing the sample with a steel ball (10 mm diameter). A CSN tribometer was used (software TriboX, the friction force was 2 N, the rotation speed was 2 cm.s⁻¹ and the number of rotations was 500.

Measurements were also made at 80 °C in order to simulate the abrasion at the reactor's temperature. These were made using a CSM High Temperature Pin-on-Disk tribometer driven by the software TriboX 2.5. The friction force, rotation speed and number of rotations are the same than the ones used for ambient temperature.

VI.3.c. Pull-off tests

The pull-off tests were made to quantify the adhesion of a coating to a substrate. This analysis is useful to compare the different systems with each other and to establish a ranking of the best ones. During this test, a steel disc was stuck to the coating with a 2K-component epoxy resin (supplied by Sader). After 24 h of drying, the disc was pulled off at a rate of 10 mm.min⁻¹. The apparatus was a TCM 201 supplied by Lloyd Instrument with a DFIS 100 dynamometer.

VII. Conclusion

During this second chapter, all the materials, experimental techniques and parameters used during this research project have been presented.

The results obtained during this Ph.D. will be presented in the following of this report and the next chapter will be focused on the determination of the scale formation mechanism.

References

- (1) Hong, S. *Modélisation de Dispersions Eau-Vcm-Pvc En Présence de Tensio-Actifs Macromoléculaires À Base de Pva*, Thesis n° 029FR2005MULH0784, **2005**, Université de Haute-Alsace, France.
- (2) Plueddemann, E. P. *Silane coupling agents*; Plenum Press: New York, 1982.
- (3) Mittal, K. L.; Plueddemann, E. P. *Silanes and other coupling agents*; VSP: Utrecht, 1992.
- (4) Elzein, T.; Brogly, M.; Schultz, J. *Polymer* **2003**, *44*, 3649–3660.
- (5) Elzein, T.; Brogly, M.; Castelein, G.; Schultz, J. *J. Polym. Sci. Part B Polym. Phys.* **2002**, *40*, 1464–1476.
- (6) Fearly, N. CasaXPS Software <http://www.casaxps.com/> (accessed Apr 16, 2013).
- (7) Nielsen, L. E. *J. Macromol. Sci. Part C Polym. Rev.* **1969**, *3*, 69–103.
- (8) Bussu, G.; Lazzeri, A. *J. Mater. Sci.* **2006**, *41*, 6072–6076.

Chapter III

-

Scale Formation Mechanism

CHAPTER III: SCALE FORMATION MECHANISM

I. Introduction	101
II. Interactions between stainless steel and the reactive medium's components: immersion in model solutions	101
II.1. Immersion of stainless steel plates in model solvents	101
II.2. Immersion of stainless steel plates in water / LPO systems	104
II.3. Immersion of stainless steel plates in water / PVA systems	106
II.4. Immersion of stainless steel plates in BuCl / LPO / PVA systems	109
II.5. Immersion of stainless steel plates in water / BuCl emulsions	112
II.6. Conclusion	114
III. Immersion tests in the pilot reactor	114
III.1. Kinetic of the fouling process	115
III.1.a. Visual observation	115
III.1.b. Chemical analysis of the scale	116
III.1.c. Conclusion	119
III.2. Influence of the hydrolysis degree of the PVAs on the scale formation	120
III.2.a. Visual information	120
III.2.b. Chemical analysis of the scale	121
III.2.c. Conclusion	122
IV. Scale formation mechanism	123
V. Conclusion	125
References	126

I. Introduction

The formation of scale is a major issue for S-PVC producers. The formation of a thick and hard PVC deposit on the reactor walls causes a lot of damages in terms of productivity, final product quality and quantity of raw materials used. However, this phenomenon has remained unexplained even if some hypotheses have been made¹⁻³. The aim of this third chapter is to establish a complete scenario explaining the scale formation.

For that, immersion tests were made in model solvents. Water and 1-chlorobutan (BuCl) were selected as models to simulate respectively the aqueous dispersive medium during the suspension polymerization process and to simulate VCM which is a gas at ambient conditions. Tests were also made in water containing polyvinylalcohols (PVA) and dilauroyl peroxide (LPO) which are used during the S-PVC production as these products are supposed to play a major role in the formation of scale.

On the other hand, some tests were made in a pilot reactor reproducing exactly the industrial reactors. These experiments allowed to study the kinetic of the scale formation but also to evaluate the influence of some parameters.

All these analyses led to the establishment of a formation of scale mechanism that will be helpful for the development of a durable “anti-scale” polymer coating.

II. Interactions between stainless steel and the reactive medium’s components: immersion in model solutions

II.1. Immersion of stainless steel plates in model solvents

Non-cleaned 316L stainless steel plates have been immersed during 7h in the two selected solvents: water which is the dispersive medium during the suspension polymerization of VCM and BuCl used to simulate VCM at various temperatures (room temperature and polymerization temperature: 70°C).

Table III-1 is a recap of the different tests.

Table III-1. Recap of the samples for the immersion of 316L stainless steel plates in model solvents.

Solvent	Temperature (°C)
Water	20-25 (room)
Water	70
BuCl	20-25 (room)
BuCl	70

Microscopy pictures have been taken to check the effect of the immersion of the plates in these solvents from a macroscopic point of view. They were taken after the plates were dried at room temperature (figure III-1).

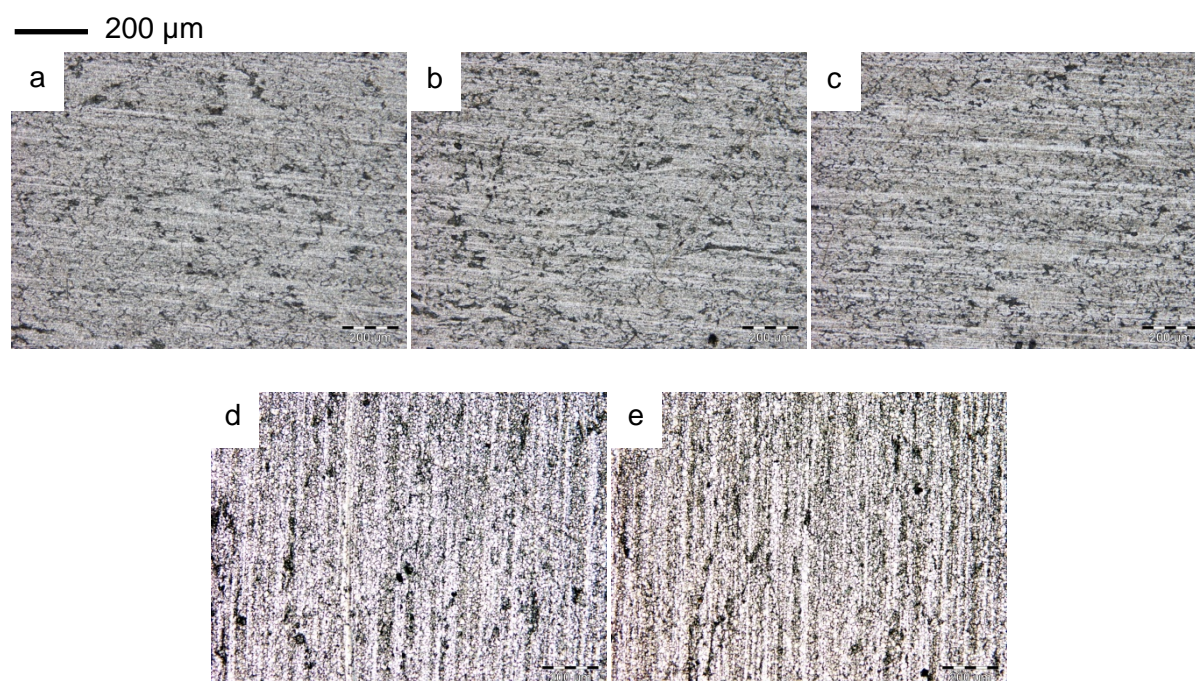


Figure III-1. Optical microscopy snapshots (*100) of stainless steel plates: a. before immersion; b. after immersion in water (20 °C); c. after immersion in water (70 °C); d. after immersion in BuCl (20 °C); e. after immersion in BuCl (70 °C).

The picture of a raw 316L stainless steel plate (figure III-1, a) exhibits the heterogeneity of steel surface with micro-domains of various sizes and shapes. The steel surface is very rough at a nanoscale and has a typical microstructure of a laminated surface with deep scratches and fractures⁴.

The five pictures look quite similar. As a matter of fact, it was predictable that these liquids would not have a huge effect on the surface appearance of 316L stainless steel. However,

contact angle measurements were made on substrates after immersion and drying in order to determine the water contact angle values.

The analyses were made at room temperature, the results shown are averages made on 10 values. Figure III-2 shows the results obtained for these samples.

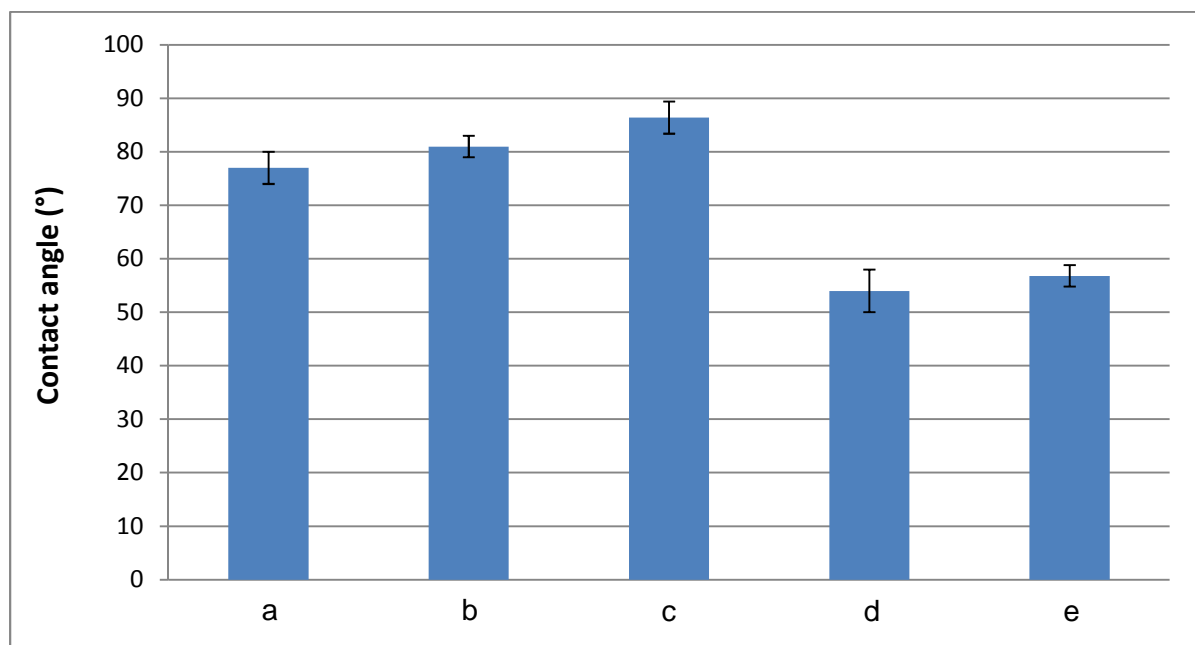


Figure III-2. Contact angles of water deposited on stainless steel plates : a. before immersion; b. after immersion in water (20 °C); c. after immersion in water (70 °C); d. after immersion in BuCl (20 °C) ; e. after immersion in BuCl (70 °C).

The raw sample exhibits a contact angle with water of 77 °. This value might be surprising because it is well known that a classic stainless steel surface is mainly composed of metallic and hydroxyl groups which are highly hydrophilic. However, commercial steels are classically covered by some oils. These products consist in some aliphatic carbon chains which increase the hydrophobic character of steel.

A slight increase of the contact angle is observed when a 316L plate is immersed in water (not depending on the temperature). However, this increase does not seem to be significant because the observed values are comprised in the standard deviation of the raw sample.

The immersion of 316L plates in BuCl leads to a sharper decrease of the contact angle. Actually, BuCl seems to be a great solvent of the oils which are coating the 316L surface. The dissolution of these oils allows the water drop to be in contact with more hydroxyl groups and leads to a value of $\Theta = 54$ °.

On the following of this chapter, some systems were tested to simulate the S-PVC reactive medium.

II.2. Immersion of stainless steel plates in water / LPO systems

This system allows to study the behavior of a non-cleaned 316L plate immersed in water containing 725 ppm of peroxide (during 7 h at 70 °C) which might be incriminated in the formation of scale as this compound is used as an initiator during the S-PVC synthesis.

The optical microscopy pictures are shown on figure III-3.

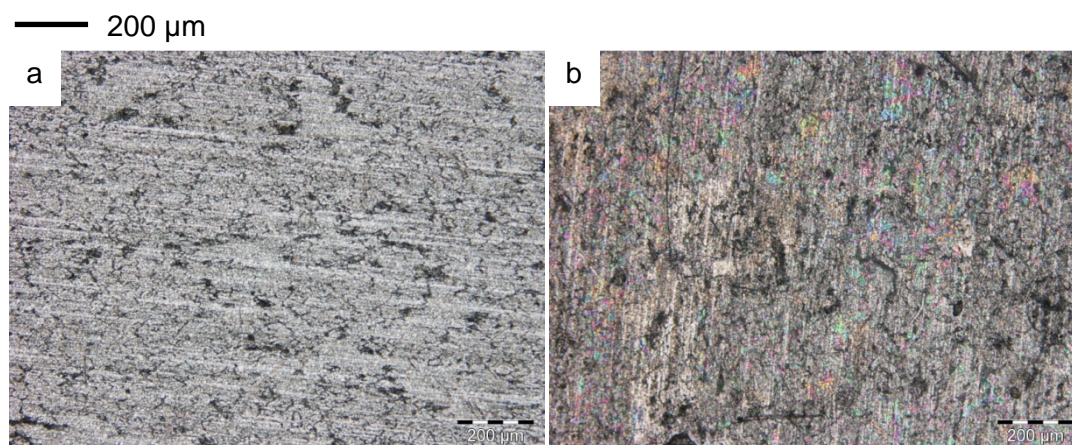


Figure III-3. Optical microscopy snapshots (*100) of stainless steel plates: a. before immersion; b. after immersion in the water / LPO system (70 °C).

No real differences are visible between both samples. Even if LPO must have been decomposed during this experiment, the steel surface does not seem to be modified.

Chemical analyses, made by IRRAS, may allow to determine if there is adsorption or chemical surface modification of stainless steel after immersion in an aqueous LPO dispersion. The comparison between pure LPO and a stainless steel plate immersed in a LPO dispersion is shown on figure III-4.

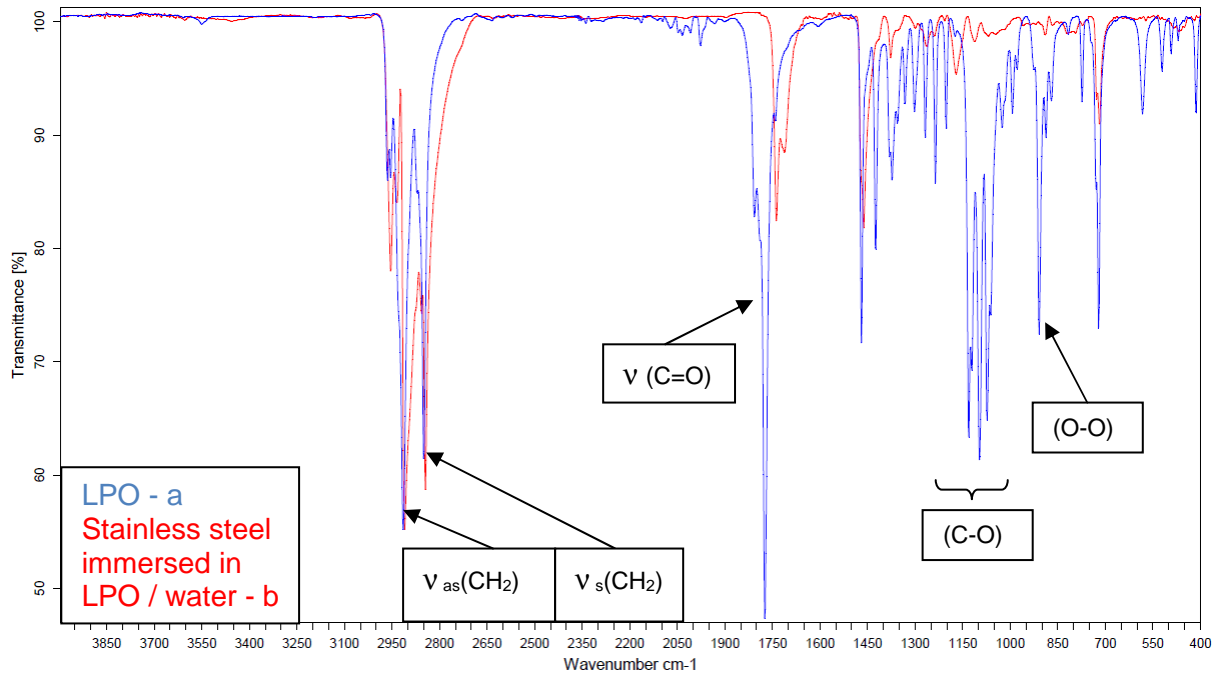


Figure III-4. Comparison of an ATR-IR spectrum of pure LPO (a) and an IRRAS spectrum of a stainless steel plate after immersion in the water / LPO system (b).

The spectrum of pure stainless steel is not presented during this study as the IRRAS analysis of this substrate does not provide any information on the sample. This is due to the fact that stainless steel has a reflective surface which does not allow penetration of the infrared incident beam. This means that the spectra presented during this study only correspond to chemical species adsorbed on this substrate. Moreover, the fact that a raw stainless steel plate is used as reference removes any possible contribution from the substrate.

Some of the LPO main peaks are present on the 316L surface. These peaks are the C=O peak ($1700\text{--}1750\text{ cm}^{-1}$), the C-O peaks (around $1050\text{--}1200\text{ cm}^{-1}$) and the O-O peak (700 cm^{-1}). Even if these peaks are less intense than in the case of LPO alone, it seems that LPO is standing at the steel surface. However, the adsorbed LPO is completely removed after rinsing with water, indicating a reversible physical adsorption.

The immersion of 316L plates in LPO solutions finally gave two information. The surface of steel does not seem to be modified or deteriorated by the presence of LPO even after immersion during a long time and at a temperature above its decomposition temperature. However, IRRAS showed that LPO is physically adsorbed at the steel's surface because this adsorbed layer disappears after rinsing in water. This can imply that some radicals, able to

act as initiators for the development of the crust, might be present at the steel surface during the VCM polymerization.

II.3. Immersion of stainless steel plates in water / PVA systems

According to the mechanism found in the literature concerning the fouling process, the PVAs used as suspending agents might be responsible of the appearance and development of the crust. These compounds are widely used as protective colloids in the field of suspension polymerization of VCM⁵⁻⁸. To get the closest possible to the real polymerization systems, the PVAs tested are the ones usually used in the INEOS ChlorVinyls facilities.

Simple tests consist in immersing non-cleaned 316L plates in a 1% PVA I (with an hydrolysis degree superior to 60 % molar) solution in order to study the behavior of this substrate regarding to the properties of the PVAs studied.

The 316L plates have also been immersed in 1% w / w solutions of PVA I dispersed in water for 7h. Experiments have been run at room temperature and at 70°C.

A recap of the samples analyzed during this study is presented in table III-2. A little reminder about the PVA annotations: the KP08R is known as the 1-H72M40 where 1 stands for the type of PVA (2 if the concerned PVA is a PVA II), the number following the letter “H” corresponds to the HD and the one following “M” stands for an abbreviation of the Mw value.

Table III-2. Recap of the samples for the immersion of 316L stainless steel plates in water / PVA systems.

PVA (1% w / w) in water	T (°C)	HD (% mol)*	Mw (g.mol⁻¹)**
1-H72M40	20-25 (room)	72.5	40,000
1-H72M36	20-25 (room)	72.5	36,000
1-H72M40	70	72.5	40,000
1-H72M36	70	72.5	36,000

* Hydrolysis degree: molar ratio of the polyvinyl alcohol part over the polyvinyl acetate part

** Supplier's data

From a macroscopic point of view, it is clearly visible that adsorption of some species is happening (figure III-5).

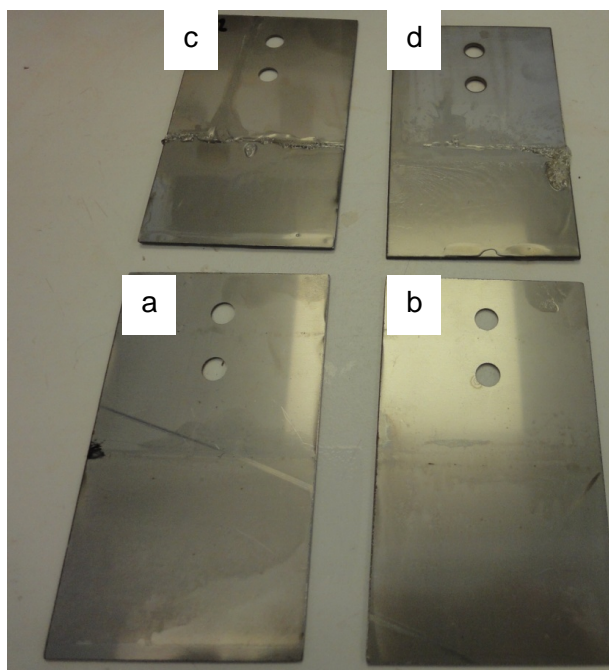


Figure III-5. Pictures of stainless steel plates: a. after immersion in water / 1-H72M40 (20 °C); b. after immersion in water / 1-H72M36 (20 °C); c. after immersion in water / 1-H72M40 (70 °C); d. after immersion in water / 1-H72M36 (70 °C).

The samples immersed in solutions at 70 °C (on the upper side of figure III-5) exhibit a much more important deposit than the plates immersed in a room temperature solution. However, a deposit is visible on the samples whatever the immersion temperature.

At a constant temperature, the type of PVA used does not seem to have an impact on the quantity of PVA deposited on a 316L plate. As a matter of fact, the chemical structure differences are not so significant to explain the little variation in the results. The effect of the structure of the PVA (HD, DPn...) on the formation of this deposit will be discussed later, during the tests made in the pilot reactor.

Optical microscopy was also performed in order to better observe the formation of this deposit (figure III-6).

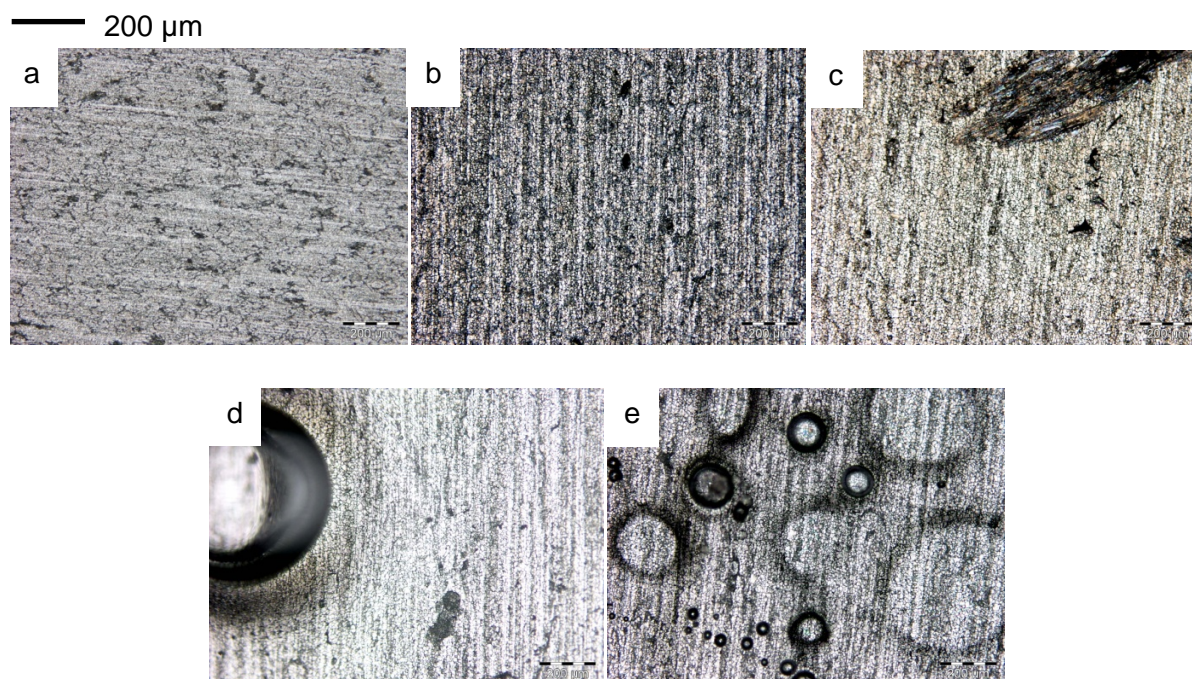


Figure III-6. Optical microscopy snapshots (*100) of stainless steel plates: a. before immersion; b. after immersion in water / 1-H72M40 (20 °C); c. after immersion in water / 1-H72M36 (20 °C); d. after immersion in water / 1-H72M40 (70 °C); e. after immersion in water / 1-H72M36 (70 °C).

The previous observations are here confirmed as the only samples showing an important deposit are the ones immersed at 70°C. A large amount of adsorbed PVA is visible for these samples and some blisters are formed during the drying of the samples due to the evaporation of water which is trapped inside the PVA layer.

Concerning the samples immersed at room temperature, it is difficult to conclude from the visual tests and chemical analyses were therefore performed in order to determine if adsorption of some species at room temperature is occurring. Some IRRAS analyses were made for this purpose and are presented on figure III-7.

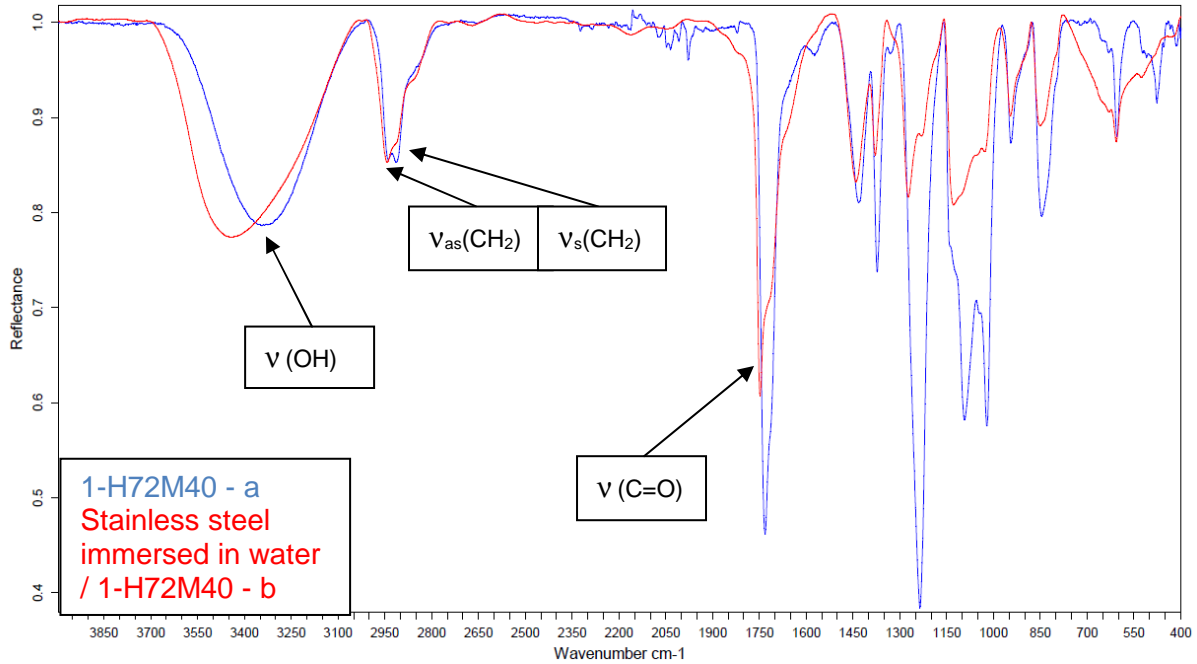


Figure III-7. Comparison of an ATR-IR spectrum of pure 1-H72M40 (a) and an IRRAS spectrum of a stainless steel plate after immersion in the water / 1-H72M40 system at 70 °C (b).

The spectra presented here are a comparison between an IRRAS spectrum of a stainless steel plate after immersion in water / 1-H72M40 and pure 1-H72M40 by T-IR. The spectra obtained for the samples immersed at ambient temperature conditions are not presented here as they were very noisy. A very slight signal was observed meaning that a very few PVA species were adsorbed. Moreover, PVA was removed after rinsing for these samples.

The first assessment is that the appearance of a PVA deposit on a stainless steel plate is dependent on the temperature and not on the properties of the PVA used (keeping in mind that the two PVA studied are relatively similar to one another). As a matter of fact, the immersion of a stainless steel plate in a 1 % w / w PVA solution at 70 °C leads to the formation of a thick deposit on the substrate. This can be considered as the first step for the explanation of the scale formation mechanism.

The next tests were made on more complex solutions combining BuCl, LPO and PVAs.

II.4. Immersion of stainless steel plates in BuCl / LPO / PVA systems

The tests are performed here with solutions containing either a primary (1-H72M40 or 1-H72M36) or a secondary (2-H45M15 or 2-H43M15) PVA. Stainless steel plates were immersed in these systems to simulate a reactive medium containing peroxide, surfactants

and VCM. For this purpose, 150 mL of BuCl, 2.658 g of LPO (2% w / w) and 1.329 g of the PVA chosen (1% w / w) were added and heated at 70 °C under magnetic stirring. All the experiments made are presented in table III-3.

Table III-3. Recap of the samples for the immersion in BuCl / LPO / PVA systems.

PVA	HD (% mol)*	Mw (g.mol ⁻¹)**	Solvent
1-H72M40	72.5	40,000	-
1-H72M36	72.5	36,000	-
2-H45M15	45	15,000	EtOH / AcOEt
2-H43M15	43	15,000	MeOH / AcOMe

* Hydrolysis degree: molar ratio of the polyvinyl alcohol part over the polyvinyl acetate part

** Supplier's data

It is interesting to note that, contrary to PVA I, PVA II are insoluble into water. These molecules are so solubilized into a mix of solvents (an alcohol and acetate) in order to increase its solubility into water and to enhance the quality of the dispersion of PVA II into water. The immersion time for each sample is 7 h which corresponds to the duration of 1 industrial batch. The pictures of these samples are shown on figure III-8.

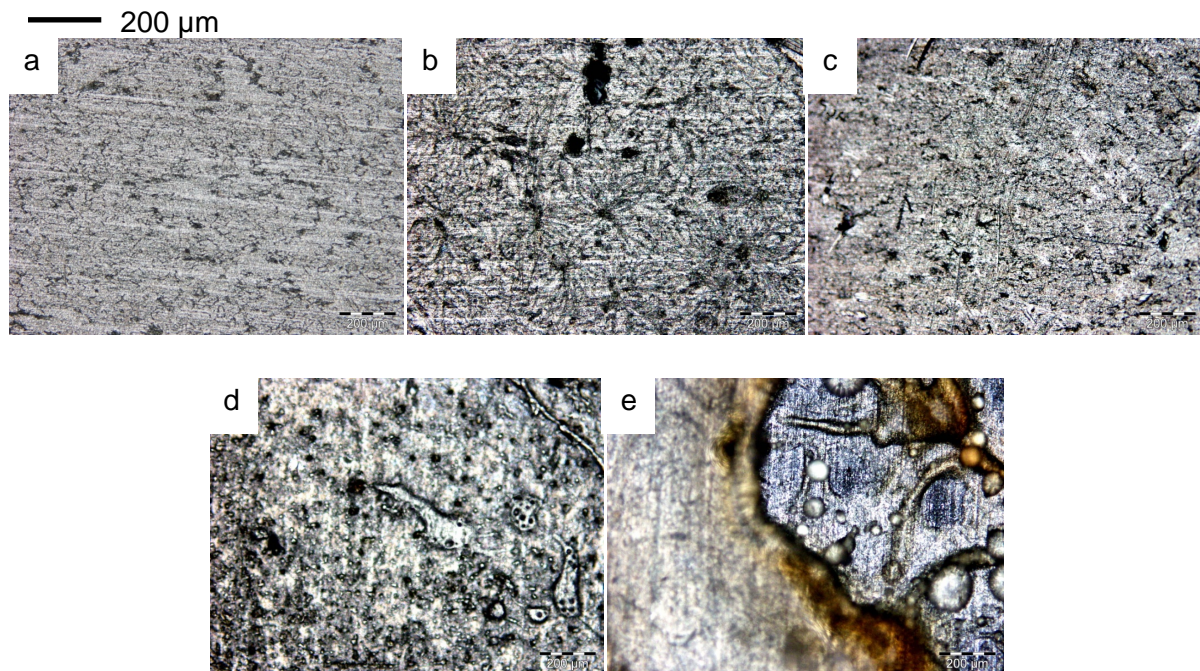


Figure III-8. Optical microscopy snapshots of stainless steel plates before (a) and after immersion in BuCl / LPO systems at 70 °C containing different PVA: b. 1- H72M40; c. 1-H72M36; d. 2-H45M15; e. 2-H45M15.

From a general point of view, a light deposit is visible on each sample. However, this phenomenon is more visible and important when a PVA II is used. This fact could be related to the viscosity of the PVA II which makes it more tacky and sticky. This property of the PVA will make it adsorb on the surface and will then be hard to remove from the steel's surface due to the affinity between stainless steel and PVA. For example, rinsing with water does not allow complete removal of the adsorbed PVA.

These plates were also analyzed by IRRAS to identify the chemical nature of the species adsorbed at the stainless steel surface.

The results are presented on figure III-9.

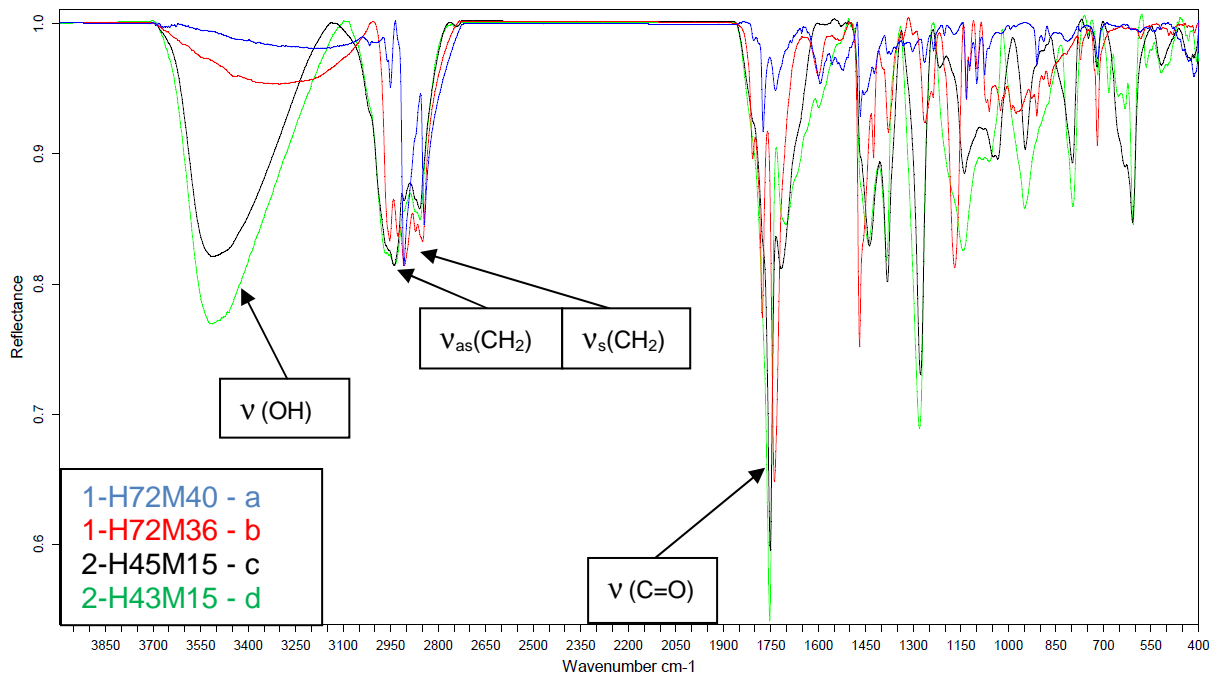


Figure III-9. IRRAS spectra of stainless steel plates after immersion in BuCl / LPO systems with different PVA: a. 1-H72M40; b. 1-H72M36; c. 2-H45M15; d. 2-H43M15.

Typical peaks of PVAs are visible regardless to the PVA used. Normalization and scaling were performed relative to the $v_{as}(\text{CH}_2)$ vibration mode at 2939 cm^{-1} . The intensities of the different spectra can not be compared with one another as the amount of CH_2 groups is different for each molecules (differences in the Mw values of each PVA). These tests tend to prove that the presence of PVA in the reactive medium is still critical regarding to the formation of a deposit on stainless steel.

All the immersion tests performed yet were made in either an aqueous solution with additives or in BuCl with additives. A final experiment was made by mixing both systems to get a little bit closer to the real S-PVC reactive medium.

II.5. Immersion of stainless steel plates in water / BuCl emulsions

The best way to simulate the suspension polymerization of VCM is to create a water / BuCl emulsion stabilized by a PVA. To do so, a water / BuCl emulsion (3:1) with 2% of LPO and 0.75% of PVA was prepared. Again, 316L plates were immersed in these emulsions at 70 °C. This test was performed with all the PVA studied: 1-H72M40, 1-H72M36, 2-H45M15 and 2-H43M15.

The pictures taken after 7 h of immersion at 70 °C are shown on figure III-10.

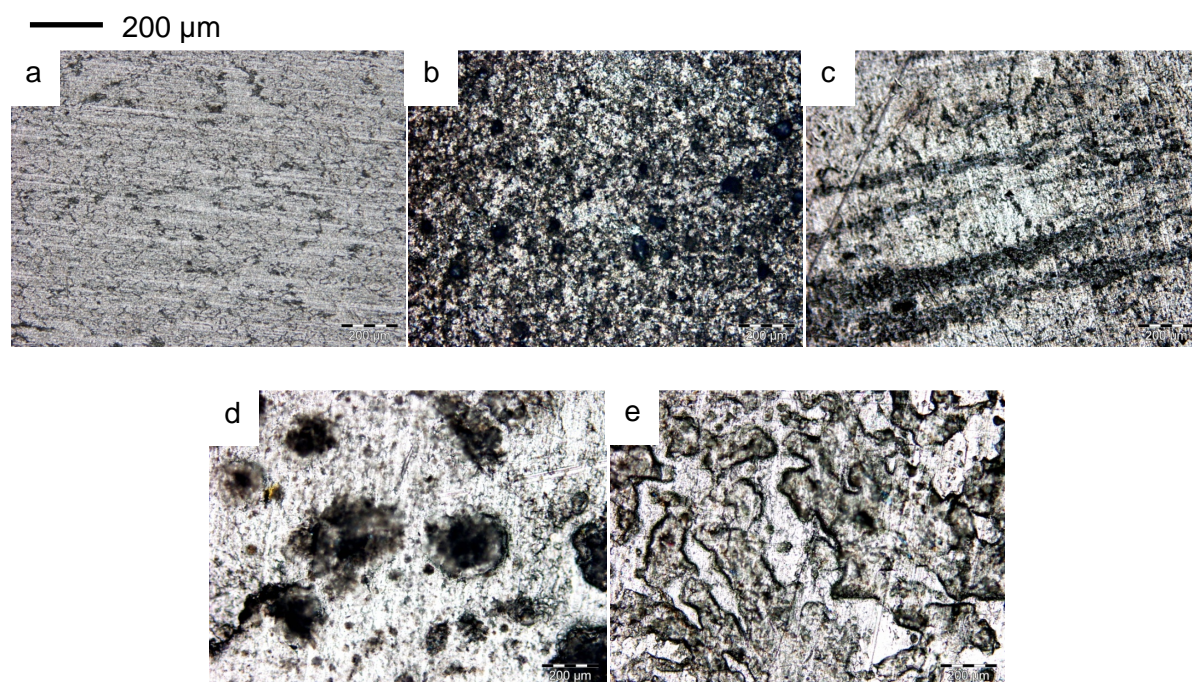


Figure III-10. Optical microscopy snapshots of stainless steel plates before (a) and after immersion in water / BuCl emulsions with different PVA: b. 1-H72M40; c. 1-H72M36; d. 2-H45M15; e. 2-H43M15.

Again, two types of deposits are observed. In presence of PVA II (2-H45M15 and 2-H43M15), the species adsorbed at the surface are thicker and stickier. This might again come from the fact that the PVAs II are tackier than the PVAs I (1-H72M40 and 1-H72M36).

However, the aspect of the deposit in the presence of PVA I is really interesting. As we will see later, the look of the surface is quite similar to a surface that has been exposed at a short time of polymerization. It is here not possible to measure any particle size for the deposit but the opacification of the surface looks pretty identical.

IRRAS analyses made on these samples are presented on figure III-11.

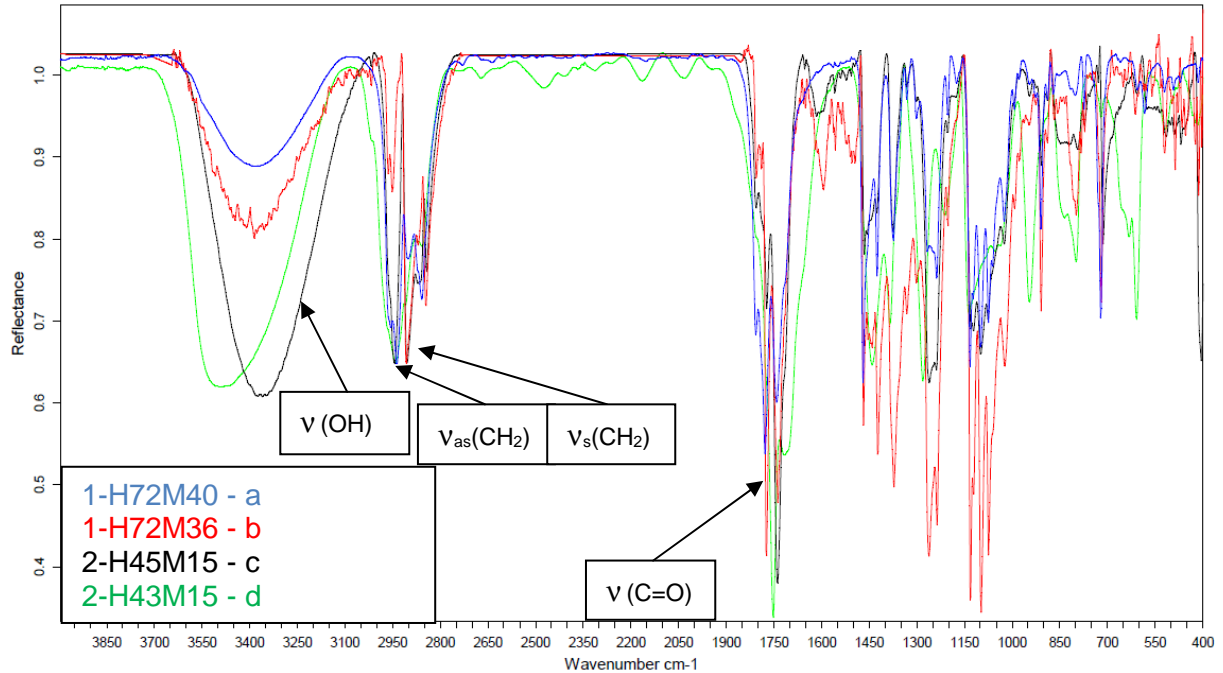


Figure III-11. IRRAS spectra of stainless steel plates after immersion in water / BuCl emulsions with different PVA: a. 1-H72M40; b. 1-H72M36; c. 2-H45M15; d. 2-H43M15.

From a general point of view, a PVA deposit is visible for each sample.

The IRRAS spectra of the samples containing PVA I are not well defined (a lot of noise) because the upper layer is very thin and it is difficult to obtain a spectrum with less noise. However, some characteristic peaks of a PVA / PVAc copolymer are visible such as the OH peaks ($3100\text{--}3700\text{ cm}^{-1}$; 600 cm^{-1}), the CH peaks (mainly at $2800\text{--}3000\text{ cm}^{-1}$) and the C=O peak at 1750 cm^{-1} .

For the samples containing a PVA II, the spectra obtained are typical of a PVA / PVAc copolymer too and the typical peaks observed are more intense.

IRRAS gives the confirmation that PVA is adsorbed when a 316L plate is immersed in a water / BuCl emulsion containing LPO and PVA.

II.6. Conclusion

The immersion of 316L stainless steel plates in a water / BuCl emulsion with LPO and PVA seems to be the better way to simulate the industrial reactive medium for suspension polymerization of VCM.

Actually, there is the appearance of a thin deposit which looks quite similar to the one obtained when 316L plates are immersed in the industrial reactive medium.

As seen before, the deposit is thicker in presence of a PVA II than in presence of a PVA I. This might be due to the tacky aspect of the PVA II which might stick harder to the surface than the PVAs I.

IRRAS showed the presence of a deposit at the surface. The peaks observed completely corresponded to the peaks of a PVA / PVAc copolymer.

All the tests done in this part of the study tend to show that PVA-PVAc copolymers in solutions have an affinity with 316L stainless steel and these results were checked by running some experiments in the INEOS pilot reactor.

III. *Immersion tests in the pilot reactor*

The pilot reactor, a device installed at the INEOS facility, allows to put up to five 316L stainless steel plates in a reactor in order to closely simulate a real S-PVC batch. This device permitted to study the encrusting process in a real-time polymerization. The structure of this reactor allows to modify some parameters (rotation speed, quantity of products, temperature...) and allows to stop the polymerization at a given time. The first goal was to determine at which time the encrusting process becomes critical and which parameters are discriminating for the fouling mechanism.

The first step was also to determine a kinetic of the crust formation to choose a polymerization time for the further tests.

III.1. Kinetic of the fouling process

Stainless steel plates were immersed in the pilot reactor and polymerizations were stopped after different times: 5, 10, 15, 30 and 60 minutes. The goal of these tests was to establish a complete kinetic of the formation of the scale by determining which compounds are deposited on stainless steel at a given time. The plates were then analyzed by optical microscopy and by IRRAS.

III.1.a. Visual observation

The plates immersed after different polymerization times were observed by optical microscopy in order to study the development of the crust as a function of time. The pictures taken are shown on figure III-12.

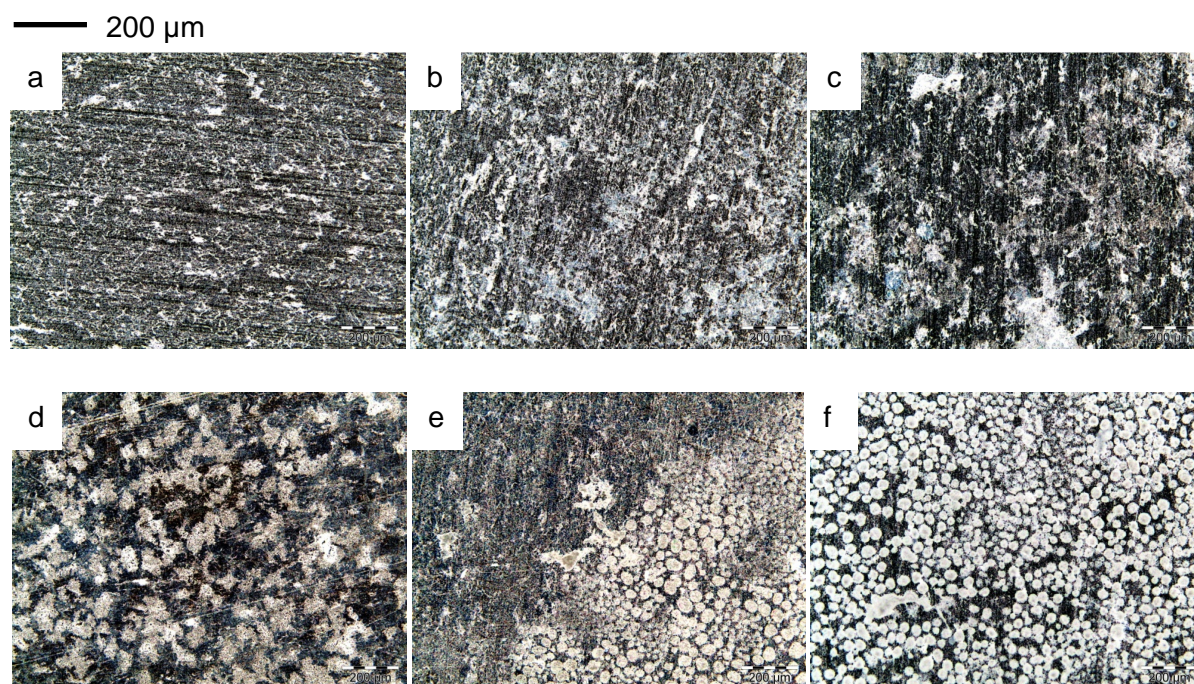


Figure III-12. Optical microscopy snapshots (*100) of stainless steel plates immersed in the reactive medium for different polymerization times: a. before polymerization; b. 5 min; c. 10 min; d. 15 min; e. 30 min; f. 60 min.

The same pictures were taken with a bigger enlargement (figure III-13).

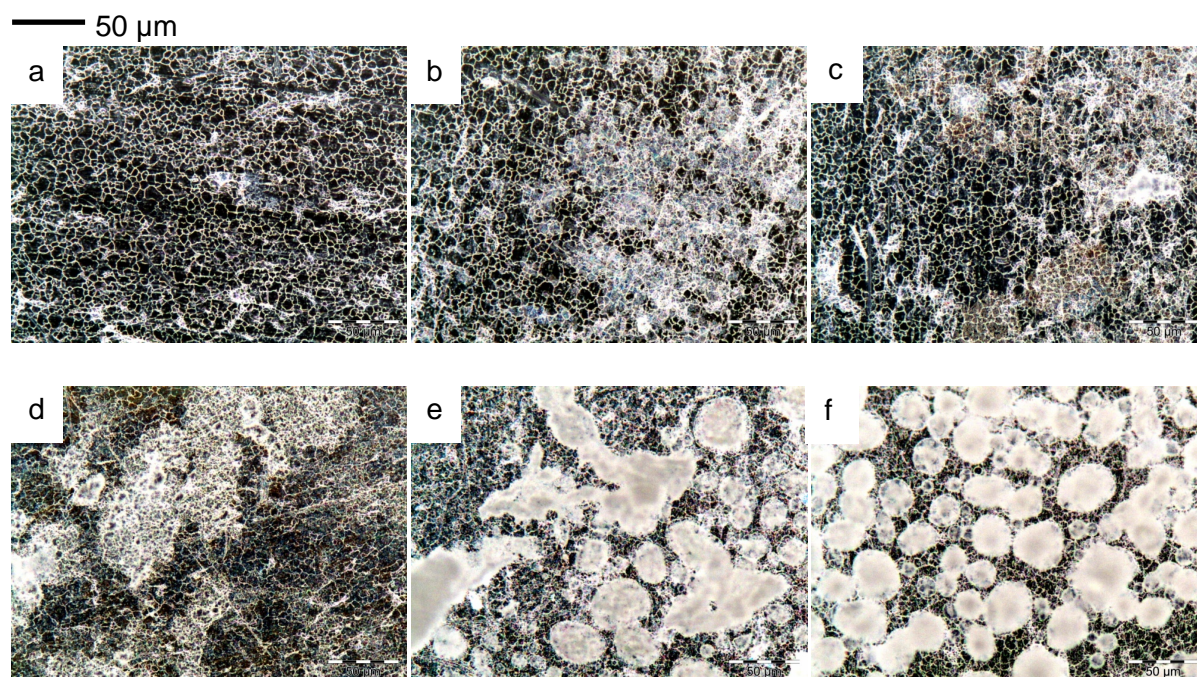


Figure III-13. Optical microscopy snapshots (*500) of stainless steel plates immersed in the reactive medium for different polymerization times: a. before polymerization; b. 5 min; c. 10 min; d. 15 min; e. 30 min; f. 60 min.

These pictures show that there is the appearance of a slight deposit directly at the beginning of the polymerization. Actually, a thin layer is observed after 5 minutes. Even if this deposit is not homogeneous, it shows that the fouling process is really fast and happens at the first stages of the polymerization. This first layer will then cover more and more surface as the polymerization goes on. After 15 minutes, the appearance of a heterogeneous layer covering a large area of the stainless steel plate is observed. The adsorption of 30 μm large particles is obtained after 30 minutes of polymerization leading to an even more scaled stainless steel surface. The formation of scale is then a continuous process with a deposit which keeps on growing leading to a covering of the entire surface. This process can be considered as the beginning of the formation of scale. It was then interesting to determine the chemical nature of the deposited species as a function of time. IRRAS analyses allowed to obtain this information.

III.1.b. Chemical analysis of the scale

IRRAS analysis, directly performed on steel plates after immersion in the reactor, was used to study the evolution of the scale composition on the plates as a function of time. The results are shown on figure III-14.

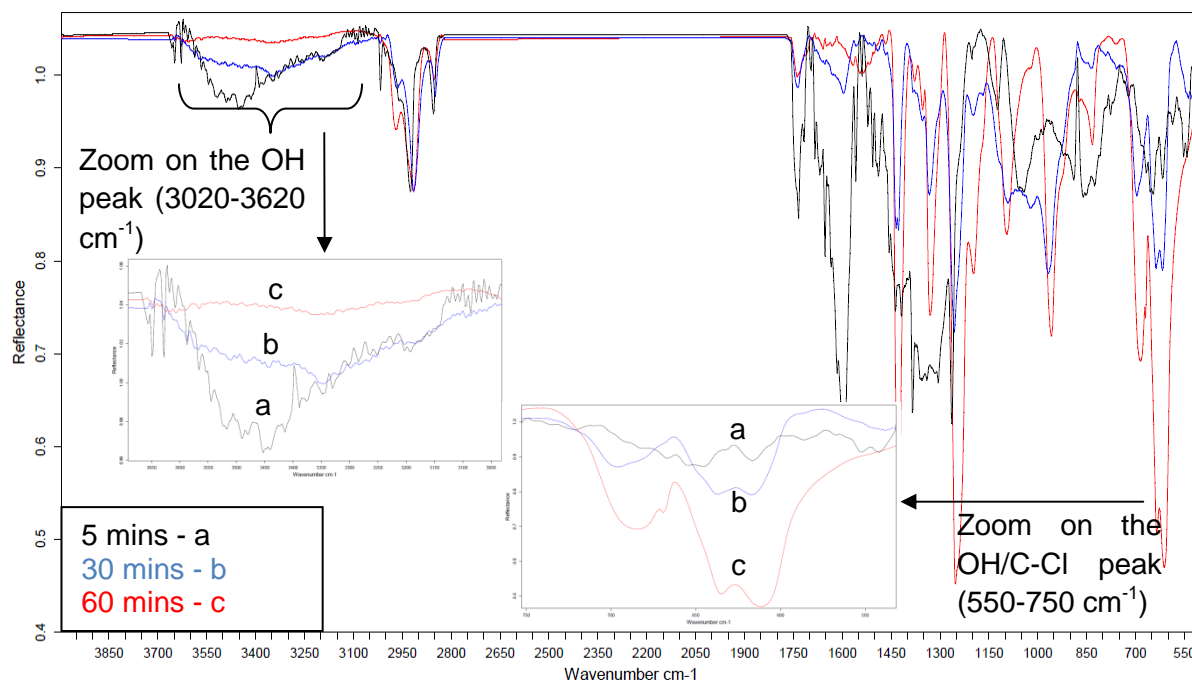


Figure III-14. IRRAS spectra of stainless steel plates immersed in the reactive medium during different times of polymerization: a. 5 min; b. 30 min; c. 60 min.

The presence of a crust is confirmed by IRRAS analysis and these results were related to the visual information obtained by optical microscopy. The thin heterogeneous deposit observed after 5 minutes of polymerization is mainly composed of PVA (at least during the 15 first minutes of reaction). However, after 15 minutes, the appearance of typical PVC peaks is observed (wide C-Cl vibration mode at 600-650 cm⁻¹) and their intensities greatly increases with time. This tends to prove that the first step of the fouling process is the adsorption of PVA followed by the development of a PVC-rich crust. This phenomenon is probably due to a transfer reaction of the growing PVC chains on the methyl group of the PVAc part⁹ or to copolymerization of VCM with the double bonds of the PVA.

A zoom in the range of 3020-3620 cm⁻¹ was made to better observe the evolution of the composition of the deposit. The evolution of the characteristic ν (OH) vibration mode is here clearly visible. This peak, which is really visible after 5 minutes of polymerization, has its intensity decreasing with time. A real drop of this -OH contribution is observed after, for the 30 minutes sample. However, for the 60 minutes sample, this ν (OH) vibration mode has almost disappeared. This result proves that the deposit is mainly composed of PVA which is adsorbed at the early first stage of the polymerization but that its composition will change over time to finally be mainly composed of PVC after 60 minutes of polymerization. This observation is strengthened by the zoom made in the 750-500 cm⁻¹ region which is characteristic of a C-Cl vibration mode as its intensity is very low for the 5 minutes sample

(small intensity in this range which is typical of an OH group). The intensity of this peak will also grow with time to become a typical vibration mode of a C-Cl group.

To verify this hypothesis, the spectrum of the 5 minutes sample was compared with the spectrum of pure PVA (figure III-15) and the 60 minutes was compared to pure PVC (figure III-16).

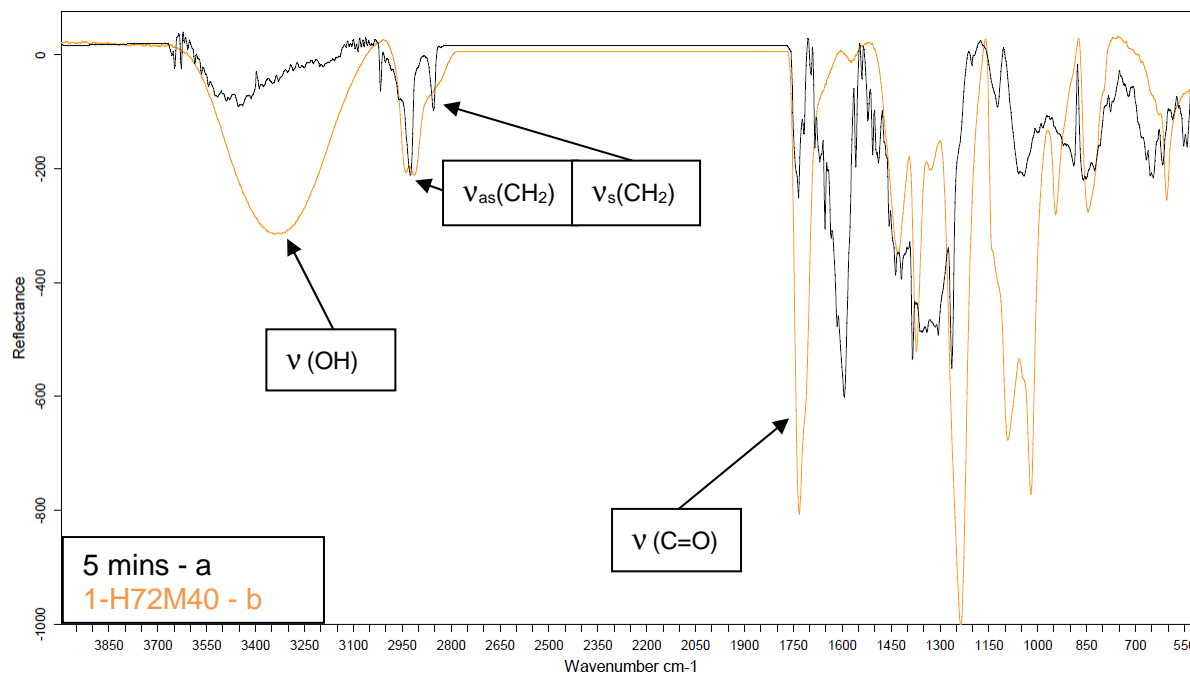


Figure III-15. Comparison of the (a) IRRAS spectrum of the 5 minutes sample with the (b) ATR-IR spectrum of 1-H72M40 PVA.

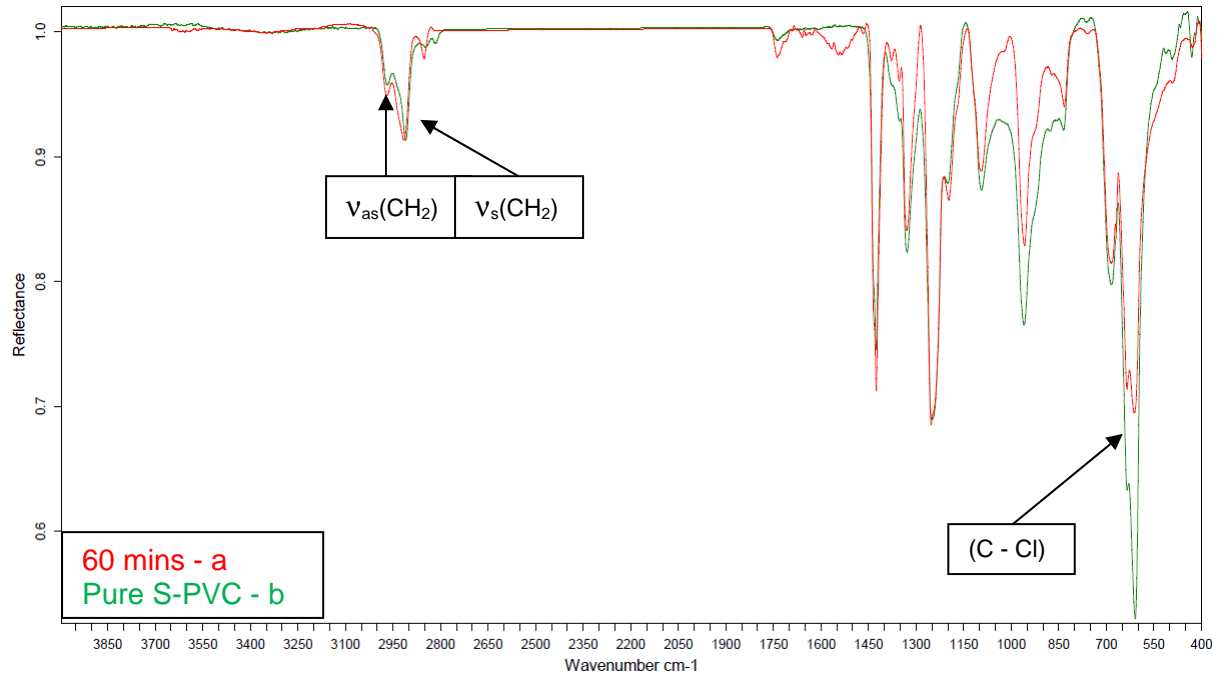


Figure III-16. Comparison of the (a) IRRAS spectrum of the 60 minutes sample with the (b) ATR-IR spectrum of pure S-PVC.

Both comparisons confirm the previously proposed hypothesis. As a matter of fact, some of the major PVA vibration modes are visible on the 5 minutes sample analyzed by IRRAS. The composition of the deposit will then evolve and tend from a relatively pure PVA (5 minutes) to relatively pure S-PVC (60 minutes). This is also visible when the IRRAS spectrum of the 60 minutes sample is compared to a pure S-PVC. Typical peaks of S-PVC are present and allow us to confirm our hypothesis.

This first study showed the importance and the major role of PVA in the fouling process.

III.1.c. Conclusion

Optical microscopy and IRRAS analyses showed that the fouling mechanism is a multi-steps process. The first 15 minutes are dedicated to the adsorption of a first layer composed of PVA. After 15 minutes, the beginning of the development of the crust is visible. After this limit, the expansion of the PVC-rich part of the crust takes place leading to the formation of a thick and hard crust.

As the main part of the study is devoted to the adsorption of the crust on 316L stainless steel, the duration chosen for the further study was 15 minutes. As the time of immersion is

now selected, another part of the study was focused on the study of the influence of the PVA nature on the formation of scale.

III.2. Influence of the hydrolysis degree of the PVAs on the scale formation

IRRAS analyses indicate the formation of a slight PVA deposit at the straight beginning of the polymerization. The influence of the PVA nature on the formation of the crust was also studied. The two primary PVAs tested have quite similar properties except their double bond content. The unsaturations, which play a major role in the stabilization of the VCM droplets, might have an impact on the fouling process. This fact is similar in the case of the two secondary PVAs tested. The double bonds content for each couple of PVA (800 ppm of primary PVA and 500 ppm of a secondary) are summed up in table III-4.

Table III-4. Presentation of the double bonds contents for each PVA studied.

	Name	HD (% mol) [*]	Mw (g.mol ⁻¹) ^{**}	Solvent	Double bond content ^{***}
PVA I	1-H72M40	72.5	40,000	-	+
	1-H72M36	72.5	36,000	-	++
PVA II	2-H45M15	45	15,000	EtOH/AcOEt	++
	2-H43M15	43	15,000	MeOH/AcOMe	+

^{*} Hydrolysis degree: molar ratio of the polyvinyl alcohol part over the polyvinyl acetate part

^{**} Supplier's data

^{***} Determined by UV-visible spectroscopy¹⁰

316L stainless steel plates were placed in the pilot reactor for 15 minutes (appearance of a thin layer of scale) of polymerization using these different PVA mixtures. Five 316L plates were immersed to study reproducibility.

III.2.a. Visual information

Snapshots were taken on the different stainless steel plates by optical microscopy in order to study the influence of the nature of the PVA on the scale process after 15 minutes of polymerization. The pictures taken with an enlargement of x100 are shown on figure III-17.

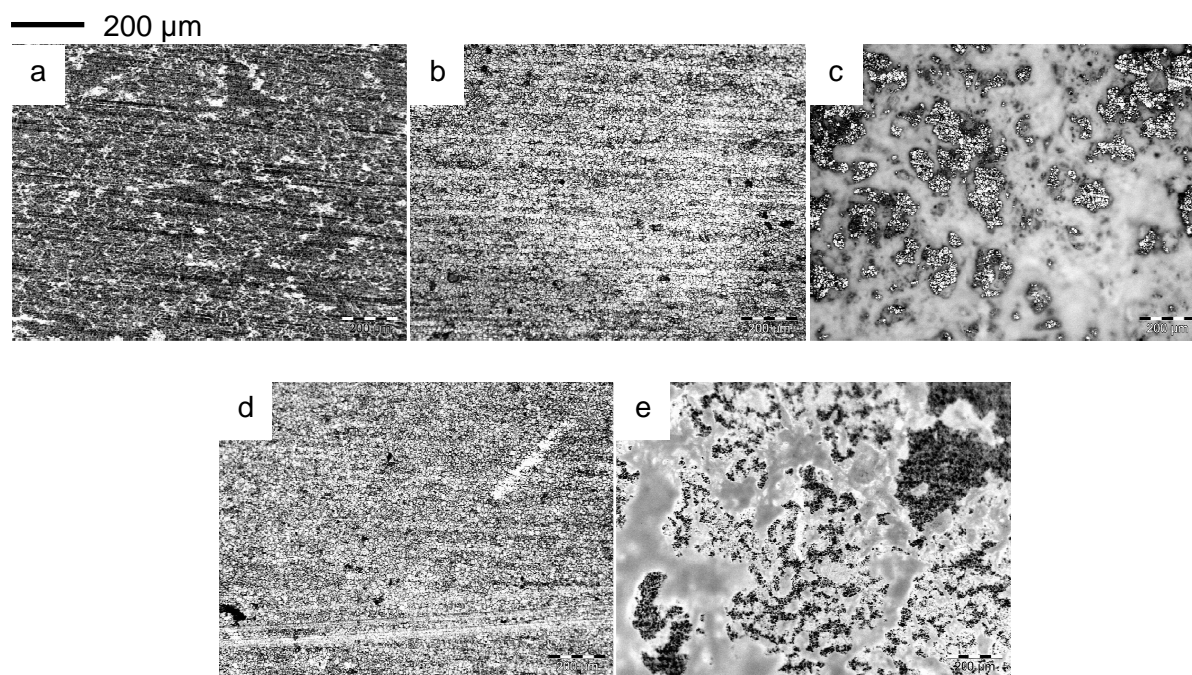


Figure III-17. Pictures (x100) of 316L stainless steel plates immersed for 15 minutes of polymerization in reactive medium containing different PVA couples: a. before polymerization; b. 1-H72M36 / 2-H45M15; c. 1-H72M36 / 2-H43M15; d. 1-H72M40 / 2-H45M15; e. 1-H72M40.

These pictures show significant differences as a function of the PVA couple used for the polymerization. The plates immersed in the reactive medium containing 2-H43M15 as secondary PVA (figure III-17, c and e) indicate signs of advanced encrusting after only 15 minutes of immersion. The two other samples do not exhibit the same kind of behavior. Actually, the plates immersed in a reactive medium containing 2-H45M15 as a secondary PVA (figure III-17, b and d) do not present any signs of scale after 15 minutes of polymerization. The reproducibility of these tests is quite good as the five plates immersed in the same reactive medium exhibit the same kind of scale formation.

IRRAS analyses were also realized in order to check the chemical composition of the crust present at the surface of the samples.

III.2.b. Chemical analysis of the scale

IRRAS spectra of the different samples were realized and the results are presented on figure III-18.

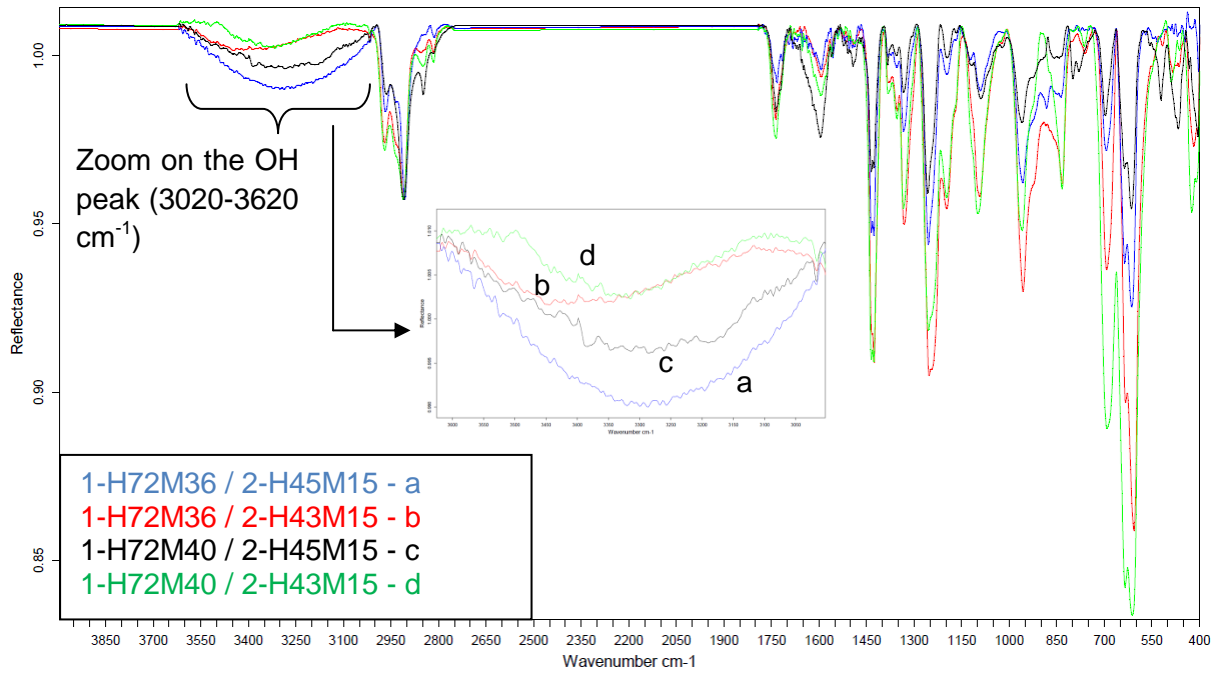


Figure III-18. IRRAS spectra of 316L stainless steel plates immersed for 15 minutes of polymerization in a reactive medium containing different PVA couples: a. 1-H72M36 / 2-H45M15; b. 1-H72M36 / 2-H43M15; c. 1-H72M40 / 2-H45M15; d. 1-H72M40 / 2-H43M15 .

The spectra obtained for each samples look quite similar and are characteristic of a PVA. Typical peaks of PVC (wide C-Cl band at $600\text{-}650\text{ cm}^{-1}$) are more intense in the case of plates immersed in a reactive medium containing 2-H43M15.

As a matter of fact, samples containing 2-H45M15 do not seem to have crust adsorbed according to microscopy pictures but IRRAS showed the presence of PVA proving the adsorption of PVA at an early stage of the fouling mechanism. Samples containing 2-H43M15 present a visible crust and IRRAS proved that it is mainly composed of PVC. Fouling happens regardless to the PVA used but it seems to be accelerated in the presence of 2-H43M15 which has an HD just a bit smaller than 2-H45M15 but which contains less double bonds.

III.2.c. Conclusion

The nature of the PVA has a great impact on the scale formation (table III-5) on the basis of the results obtained. The “+” is an arbitrary scale corresponding to the amount of double bonds or quantity scale formed with “+++” being the maximum and “+” being the minimum.

Table III-5. Recap of the scale formation regarding to the PVA couple used.

PVA Mixture	Primary PVA's HD / Mw (g.mol ⁻¹)	Secondary PVA's HD / Mw (g.mol ⁻¹)	Double Bonds ratio*	Scale formation
1-H72M36 / 2-H45M15	72 / 36,000	45 / 15,000	+++	+
1-H72M36 / 2-H43M15	72 / 36,000	43 / 15,000	++	+++
1-H72M40 / 2-H45M15	72 / 40,000	45 / 15,000	++	+
1-H72M40 / 2-H43M15	72 / 40,000	43 / 15,000	+	+++

* determined by UV-visible spectroscopy¹⁰

The plates immersed in a reactive medium containing 2-H43M15 show the formation of scale at an advanced stage compared to plates immersed in media containing 2-H45M15. The formation of scale is not influenced by the primary PVA. Each sample exhibiting an advanced scale formation is composed of a different primary PVA. The nature of the secondary PVA seems to be more critical regarding to the formation of scale. Actually, the secondary PVA having less double bonds looks to favor the scale process. This might be due to the fact that the double bonds in the surfactant's skeleton are useful in order to stabilize the growing PVC droplets. Having less double bonds can be critical regarding to the stabilization of the droplets and might favor the development of a crust. The formation of the crust is not a continuous process but the chaining of different steps. Each of these steps has its own mechanism.

IV. Scale formation mechanism

The tests made during this study exhibited the fact that the scale formation mechanism is complex. The first deposit is mainly composed of PVA and PVC only appears after this first adsorption. The deposition of PVC takes place at the first stage of the polymerization. Tests realized in 1% PVA solutions (in water) showed that adsorption of PVA on steel happens very quickly and leads to the formation of a thin deposit. This phenomenon might happen in the case of the VCM polymerization.

The depositing of a thin PVA film is then followed by the adsorption of PVC (formation of a copolymer ¹¹ or simple adsorption of PVC on the PVA layer). This will then lead to the appearance of greater beads mainly composed of PVC and then the development of the crust which is mainly composed of PVC too. The mechanism in accordance with our results is presented on figure III-19 ¹².

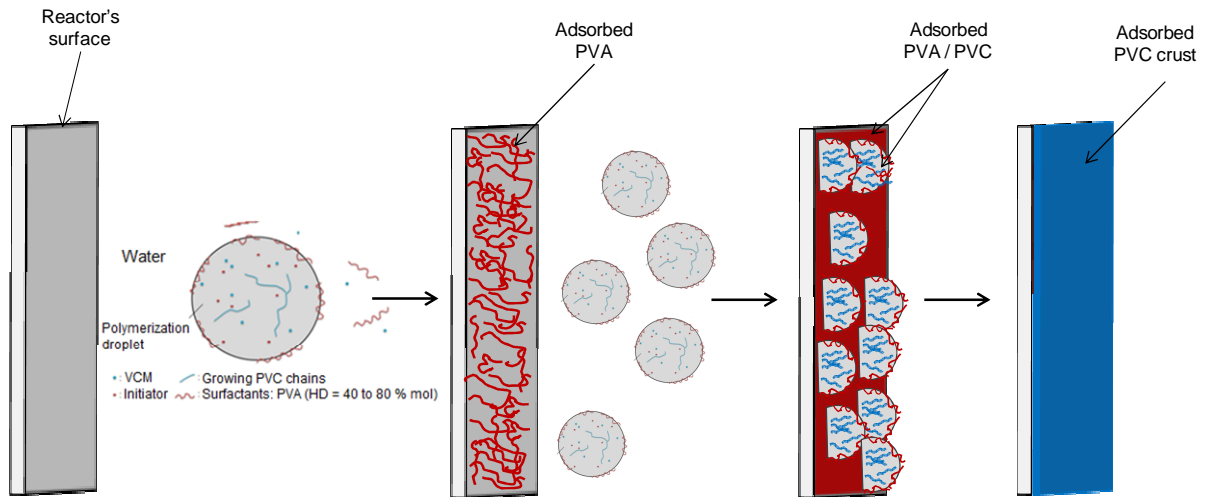


Figure III-19. Development of the crust on the reactor's walls: adsorption of the PVA first and depositing of PVC in a second step.

These observations have to be confronted to the information found in the literature ^{1,11}. The main mechanism found described the fouling process as a three-step course.

According to Glück ¹¹, the first step corresponds to the formation of a copolymer (AGC) in the aqueous phase between VCM and the suspending agent (PVA) ^{1,11} (due to a transfer reaction of the PVC macroradicals on the methyl group of the vinyl acetate residual function or by copolymerization with the double bonds of the PVA). The AGC's particles formed will then adsorb, during the second step, on the monomer droplets and on the reactor's walls. This adsorption takes place at the immersed parts of the reactors (in the liquid phase and at the liquid / gas interface). The first layer adsorbed will then act as a nucleation site for the development of the crust during the following polymerizations (third and last step).

Our study allowed us to propose a new overview on the mechanism of fouling during the suspension polymerization of VCM. It is now clear that the PVAs used as surfactant play a major role in this process by adsorbing first on the reactor's walls and acting as an initiation site for the adsorption of PVC leading to the development of the crust.

V. Conclusion

The immersion tests performed in model solvents and in the pilot reactor allowed to establish a complete scenario for the scale formation during the S-PVC synthesis.

During the first part of this study performed in model systems, it was clear that PVA plays an essential role in the formation of scale mechanism. As a matter of fact, a deposit was observed for all the systems containing a PVA. The immersion of 316L stainless steel plates in a water / BuCl emulsion with LPO and PVA, the model system tested which was the closest to the industrial reactive medium for suspension polymerization of VCM, confirmed this result as typical vibration modes of PVA were visible regardless of the chemical nature of the PVA used.

The most interesting results were obtained in the pilot reactor. The immersion of crude stainless steel plates during short polymerization times allowed to determine a complete scenario for the first stages of the scale formation. This study showed that the deposit is visible at the very first stage of the polymerization as only PVA is visible by IRRAS. The PVA layer will then evolve as a PVC-rich phase will be formed after 30 minutes of polymerization. According to this mechanism, it is again PVA which is incriminated in the formation of scale.

Moreover, it was determined that the chemical structure of the PVA (mainly the double bond content of the PVA II) plays a role on the formation of scale as well. In fact, decreasing the number of unsaturations of the PVA II leads to an increase of the scale formed.

The next part of the project was dedicated to the development of a coating preventing the phenomenon described during this last chapter.

References

- (1) Visentini, A. *IOM Communications: Brighton, Proceedings*; **2002**, 317–321.
- (2) Bilgiç, T.; Savaşçı, Ö. T. *Polym.-Plast. Technol. Eng.* **1994**, 33, 381–390.
- (3) Ravey, M. *J. Appl. Polym. Sci.* **1977**, 21, 839–840.
- (4) Haïdopoulos, M.; Turgeon, S.; Laroche, G.; Mantovani, D. *Surf Coat Technol* **2005**, 197, 278–287.
- (5) Hong, S.; Albu, R.; Labbe, C.; Lasuye, T.; Stasik, B.; Riess, G. *Polym. Int.* **2006**, 55, 1426–1434.
- (6) Vivaldo-Lima, E.; Wood, P. E.; Hamielec, A. E.; Penlidis, A. *Ind. Eng. Chem. Res.* **1997**, 36, 939–965.
- (7) Nilsson, H.; Norviit, T.; Silvegren, C.; Törnelli, B. *J. Vinyl Technol.* **1985**, 7, 119–122.
- (8) Chatzi, E. G.; Kiparissides, C. *Chem. Eng. Sci.* **1994**, 49, 5039–5052.
- (9) Endo, K. *Prog. Polym. Sci.* **2002**, 27, 2021–2054.
- (10) Hong, S. *Modélisation de Dispersions Eau-Vcm-Pvc En Présence de Tensio-Actifs Macromoléculaires À Base de Pva*, Thesis n°029FR2005MULH0784, **2005**, Université de Haute-Alsace, France.
- (11) Glück, P.; Pătraşcu, M.; Oşanu, P. *Mater. Plast.* **1980**, 17, 160–165.
- (12) Huser, J.; Bistac, S.; Delaite, C.; Lasuye, T.; Stasik, B. *Polym.-Plast. Technol. Eng.* **2012**, 51, 932–939.

Chapter IV

-

Choice of a Suitable Epoxy Resin

CHAPTER IV: CHOICE OF A SUITABLE EPOXY RESIN

I. Introduction	131
II. Commercial epoxy / amine systems	131
II.1. Characterization of the epoxy free films.....	131
II.1.a. Study and optimization of the curing process.....	132
II.1.b. Properties of the cured epoxy films	138
II.2. Conclusion.....	145
III. Epoxy system based on model polyamines	146
III.1. Presentation	146
III.2. Processing of epoxy free films	147
III.2.a. Determination of the Epoxy Equivalent Weight (EEW)	147
III.2.b. Determination of the Amine-Hydrogen Equivalent Weight (AHEW).....	149
III.2.c. Free films preparation.....	150
III.3. Characterization of the epoxy free films.....	150
III.3.a. Study of the curing processes	151
III.3.b. Properties of the cured epoxy films	153
III.4. Conclusion.....	164
IV. Pilot tests performed on epoxy free films.....	164
IV.1. Free films of the RenLam CY 219 / Ren HY 5161 system	165
IV.2. Free films of the Araldite DBF CH / Ren HY 956 system	166
IV.3. Free films of the RenLam CY 219 / IPDA system.....	167
V. Conclusion.....	168
References.....	169

I. Introduction

Epoxy coatings were chosen as suitable candidates regarding to the coating's specifications for the Ecoating project. Epoxy prepolymers allow, after reaction with a curing agent, to obtain a thermoset three-dimensional network. The structure of the final film obtained is highly dependent on both the epoxy prepolymer structures and the curing agent chosen. A large range of different coatings with various properties can so be obtained.

For this purpose, two commercial epoxy / curing agent systems were tested. The epoxy resin exhibiting the best performances was then selected to be cured with pure polyamines. For all these systems, the curing conditions (temperature and time) were first set and the curing rates and conversions were checked.

Afterwards, some of the main film properties were evaluated. Thermal and mechanical properties were determined as well as wettability and swelling experiments. This work was done to select three systems that were immersed in the pilot reactor in order to check their anti-scale properties. This last experiment is considered as critical because the epoxy system used as a coating was chosen thanks to this test.

II. Commercial epoxy / amine systems

Two bisphenol-A epoxy resins with amines as curing agents (supplied by Huntsman) were tested in the laboratory and in the pilot reactor. These two systems are the RenLam CY 219 epoxy resin with its curing agent Ren HY 5161 containing Jeffamine, benzylic alcohol, isophoronediamine, trimethylhexamethylenediamine and bisphenol-A (epoxy / curing agent ratio: 100 / 50 w / w) and the Araldite DBF with Ren HY 956 (epoxy / curing agent ratio: 100 / 20 w / w) as a curing agent. The main information on both systems are presented in Chapter II, part I, 4. The process for the epoxy free films preparation using the commercial system was described earlier too (Chapter II, part III.).

II.1. Characterization of the epoxy free films

The commercial systems studied were first characterized. The first point was to determine the curing kinetic of both systems in order to check the necessary time to obtain a fully cured system. Afterwards, the resulting properties of the cured epoxy free films were studied to

make a link between the physical and the chemical properties of the obtained thermoset network and to check their behavior in the pilot reactor.

II.1.a. Study and optimization of the curing process

The first step was to follow the curing reaction of the epoxy systems. The curing conditions for both systems were set to 150 °C during 1 h. However, it was decided to study a 80 °C curing for the RenLam CY 219 / Ren HY 5161 system. This last temperature was tested because it corresponds to the temperature which can be reached by heating the double jacket of the reactor. The idea here was to determine the time necessary to obtain a fully cured coating if the reactor wall is pre-heated at 80 °C.

Differential Scanning Calorimetry (DSC) was used by performing either in-situ measurements or free films measurements. The curing reaction was directly performed in the DSC pans or followed by measuring the residual exothermal peak of epoxy free films after different curing times.

II.1.a.i. In-situ following of the curing reaction

Curing is here directly followed in the hermetic DSC pans during an isothermal measurement at a given temperature. The curing kinetic and rate are obtained thanks to part-by-part integration of the area under the exothermal peak. The exact curing rate at any given time is equal to the ratio between the integration values at this time on the total exothermal peak under-the-curve area (ΔH_t). A general example of a DSC curve obtained with this type of measurement is shown on figure IV-1.

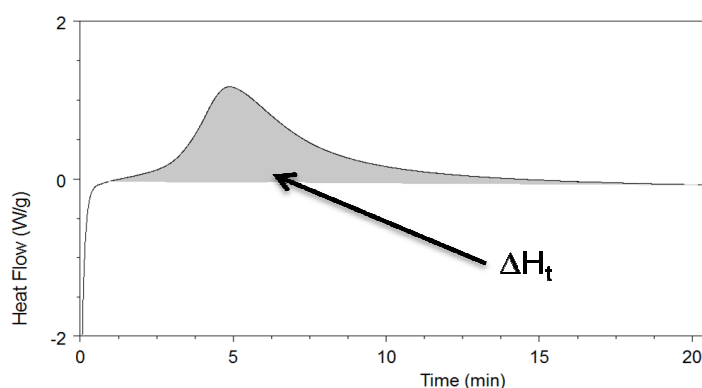


Figure IV-1. General DSC curve obtained with an isothermal pan measurement.

The main advantage is that this analysis is performed without interruption of the analysis but the major drawback is that the experiment is realized with a very small amount of material (10 mg) which is not representative of a coating's curing. It is possible to determine the conversion rate as a function of time during an isothermal curing through equation IV-1¹⁻³.

$$\alpha_t = \frac{1}{H_t} \int_0^t \Delta H . dt$$

Equation IV-1. Determination of the conversion rate during pan measurements by DSC.

Where α_t is the conversion rate at a given time, H_t is the total heat flow measured for the curing of the material during a temperature ramp. $\int_0^t \Delta H$ represents the integration of the under-the-curve area of the exothermal peak at a given time.

To check if curing is complete under the studied conditions, the isothermal measurement was followed by a temperature ramp. This is made to check the presence of an eventual residual peak which would mean that the curing reaction is not complete at 150 °C.

An example of the curves obtained for the RenLam CY 219 / Ren HY 5161 system is presented on figure IV-2.

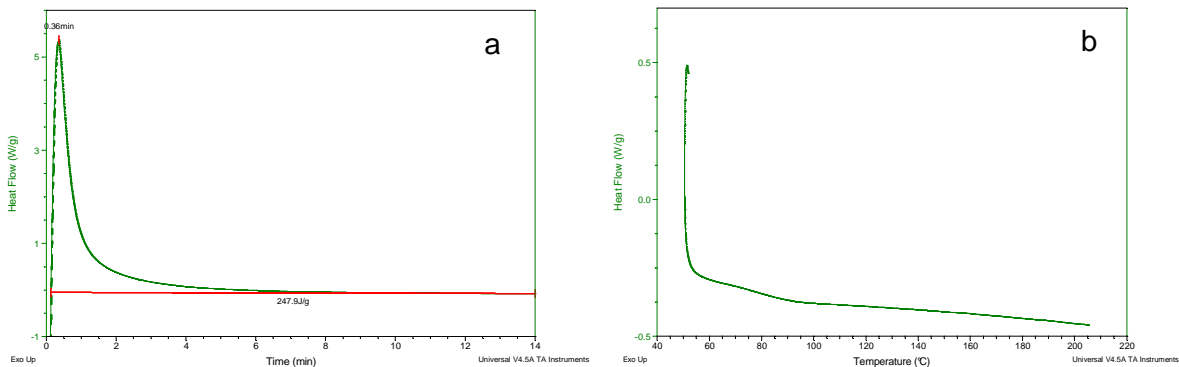


Figure IV-2. DSC thermogram during the curing reaction for the RenLam CY 219 / Ren HY 5161 system at 150 °C: a. 150 °C isotherm during 30 minutes b. ramp from 130 to 200 °C at a rate of 10 °C.min⁻¹.

The exothermal peak due to the curing reaction is clearly visible and shows that the curing reaction at 150 °C starts very quickly. Complete curing is obtained after around 15 minutes. Moreover, the reaction is total because no residual exothermal peak is observed during the temperature ramp which goes until 200 °C. This result is obtained for all the systems at all the curing temperatures studied.

The evolution of the conversion rate was obtained by performing a part by part integration. It is also possible to determine the curing rates of each system as a function of time. The

results obtained for the Araldite DBF CH / Ren HY 956 system at 150 °C and the RenLam CY 219 / Ren HY 5161 system at 80 and 150 °C are shown on figure IV-3.

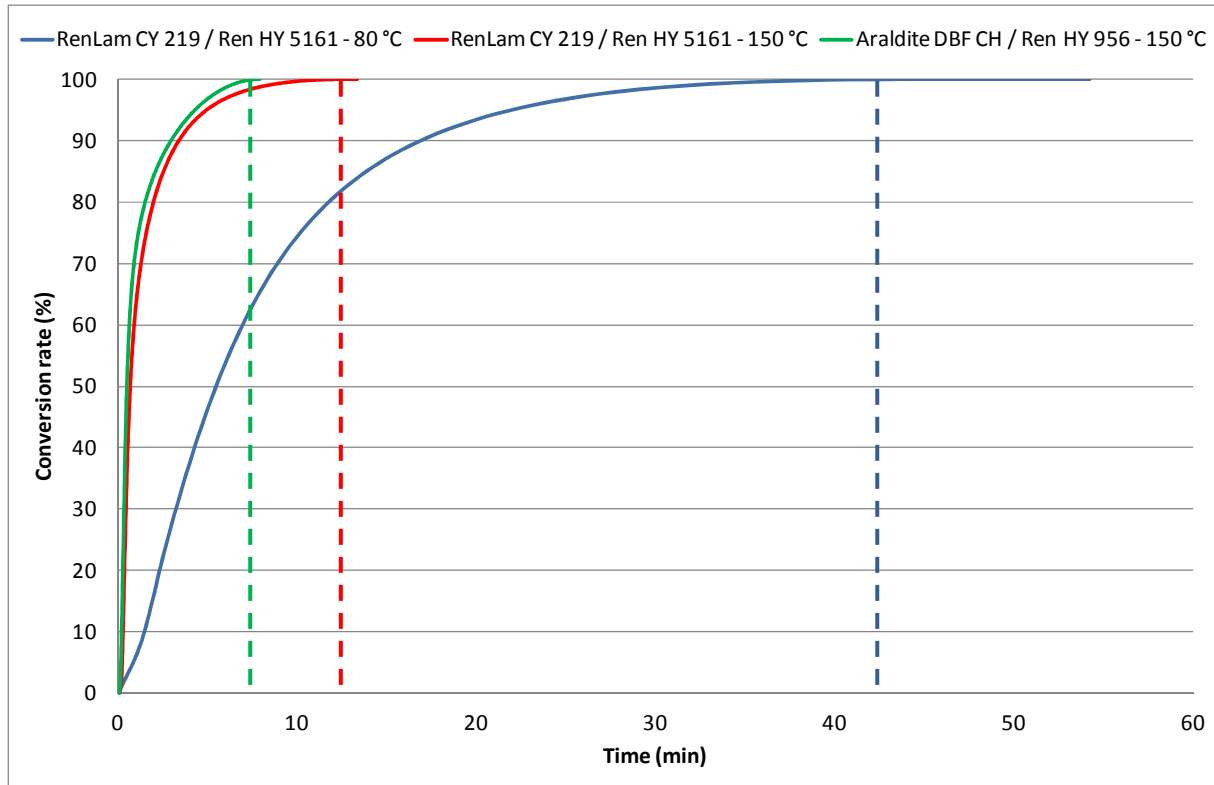


Figure IV-3. Curing rate of the RenLam CY 219 / Ren HY 5161 system at 80 °C (blue) and at 150 °C (red) and for the Araldite DBF CH / Ren HY 956 system at 150 °C (green) during DSC in-situ measurements.

First of all, it is interesting to note that a total conversion is obtained for the RenLam CY 219 / Ren HY 5161 system at both temperatures and also for the Araldite DBF CH / Ren HY 956 system cured at 150 °C. This means that the epoxy network is totally formed after a curing at the temperatures chosen.

The curing rate (corresponding to the slope of the curve) obtained for a 80 °C curing is slower as the total conversion is obtained after 40 minutes of curing compared to the 150 °C curing which gives a total conversion time of 13 minutes for the RenLam CY 219 / Ren HY 5161 system. Total conversion is reached for the Araldite DBF CH / Ren HY 956 system after 8 minutes at 150 °C.

However, as said before, this technique is not totally representative of a real coating's curing. To get closer to reality, the curing rate was also determined by DSC measurements performed on epoxy free films.

II.1.a.ii. Measurements on epoxy free films

Curing of epoxy free films (thickness $\approx 500 \mu\text{m}$) was made at a given temperature in an oven (following the procedure described in Chapter II, part III.) and then stopped at different times. Afterwards, each film was analyzed by DSC during a temperature ramp in order to determine the exothermal residual peak. This value was compared to the total exothermal peak obtained with the same temperature ramp performed on a system that has not undergone any previous curing reaction. A general example of a DSC curve obtained with this type of measurement is shown on figure IV-4.

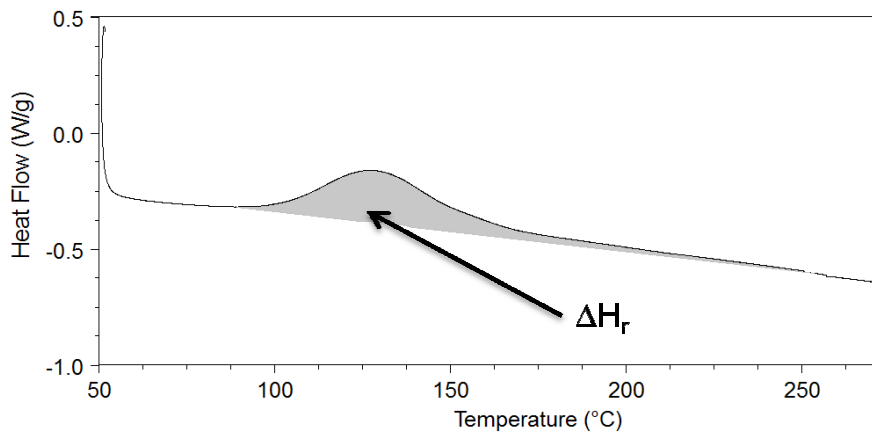


Figure IV-4. General DSC curve obtained when following a curing reaction of an epoxy free film during a temperature ramp.

The main advantage is that this experiment is more representative of a coating but the major drawback is that the system has to be efficiently cooled off to totally stop the curing reaction. Some examples of the DSC curves obtained for the RenLam CY 219 / Ren HY 5161 system before curing (figure IV-5, a) and after 35 minutes of curing at 150 °C (figure IV-5, b) are presented below.

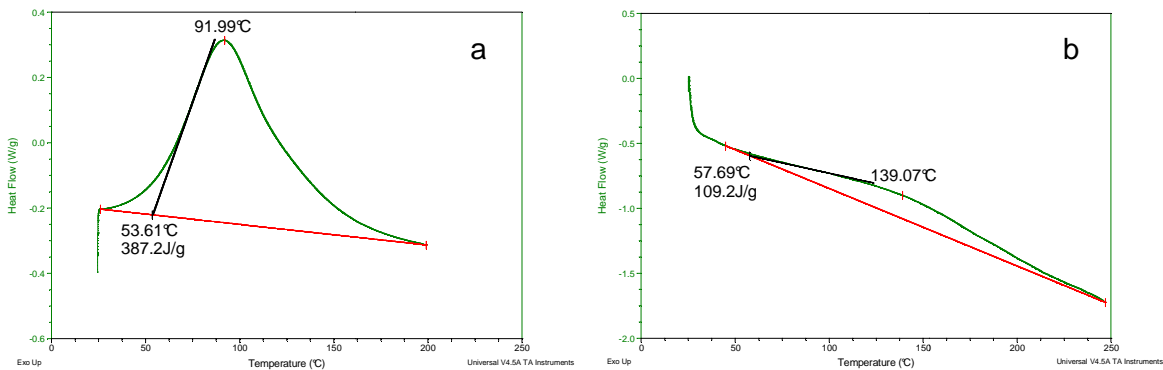


Figure IV-5. DSC curves obtained during a temperature ramp for the RenLam CY 219 / Ren HY 5161 system a. before curing and b. after 35 minutes of curing at 150 °C.

Again, a numerical approach, given by equation IV-2 on the DSC measurements is possible to determine the conversion rate as a function of time during an isothermal curing.

$$\alpha = 100 - \frac{\Delta H_t}{\Delta H_T} * 100$$

Equation IV-2. Determination of the conversion rate during free films measurements by DSC.

Where α is the conversion rate, ΔH_t is the heat flow measured at a given time ΔH_T is the total exothermal peak measured for the studied system.

In this case, the total exothermal peak for the RenLam CY 219 / Ren HY 5161 system is equal to 387 J.g⁻¹. The residual exothermal peak obtained after 35 minutes of curing at 150 °C is equal to 109 J.g⁻¹ meaning that, at this time, the conversion of the epoxy film is equal to 72 %.

The other results, obtained on the same basis, are collected on the graph below (figure IV-6).

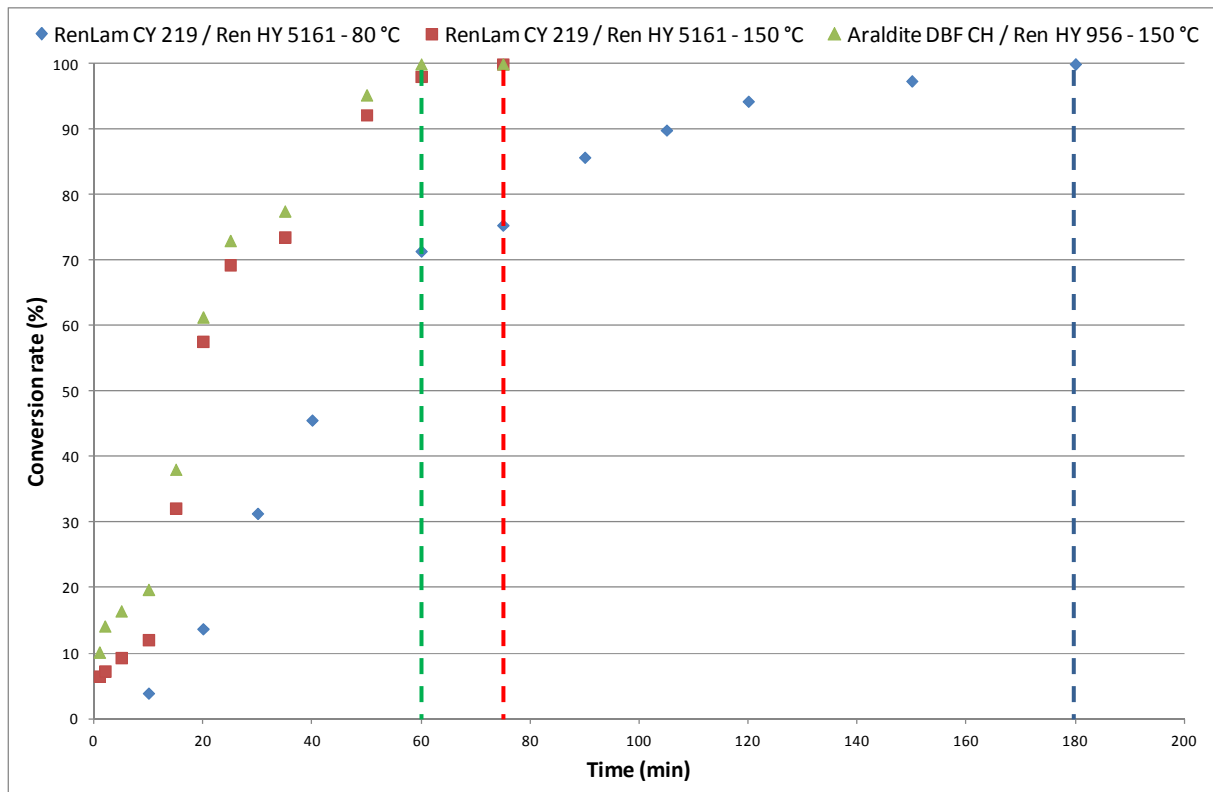


Figure IV-6. Curing rate of the RenLam CY219/ Ren HY5161 system at 80 °C (blue) and at 150 °C (red) and for the Araldite DBF CH / Ren HY 956 system at 150 °C (green) during DSC measurements on epoxy free films.

The curing rates obtained here are slower than the ones measured during the in-situ measurements due to the higher thickness of the samples (the dotted lines corresponding to

the total conversion time). For an 80 °C curing, the total conversion is obtained after 180 minutes compared to the 150 °C curing which gives a total conversion time of 75 minutes for the RenLam CY 219 / Ren HY 5161 system. For the Araldite DBF CH / Ren HY 956 mix cured at 150 °C, a total conversion is obtained after 60 minutes during the same experiment.

After these two DSC tests, the different curing times were set for each system at their corresponding temperatures. The coating's dried thickness was set at 200 µm which is a value that is comprised between the quantity used during the pan measurements (that is very low) and the dried film thickness of the samples used during the epoxy free films measurements (around 500 µm). The curing durations selected, which are in between values of the total conversion times obtained during in-situ and free films measurements, are listed in table IV-1.

Table IV-1. Curing conditions tested with the different epoxy / curing agent systems.

System	Curing temperature (°C)	Total conversion time (in-situ)	Total conversion time (free films)	Curing duration for the coating
RenLam CY 219 / Ren HY 5161	80	40 min	180 min	180 min
RenLam CY 219 / Ren HY 5161	150	13 min	75 min	60 min
Araldite DBF CH / Ren HY 956	150	8 min	60 min	60 min

The properties of the cured epoxy films determined in the next part of this report were made on samples prepared by using the curing conditions described above.

Another way to check the curing of an epoxy based system is the infrared analysis.

II.1.a.iii. Study of the curing reaction by infrared analysis

Transmission-infrared analysis (T-IR) was used to follow the curing of the epoxy resin. For this purpose, a droplet of the epoxy / curing agent system was deposited after mixing on a

KBr pellet and was analyzed before and after curing at the selected conditions. The example for the RenLam CY 219 / Ren HY 5161 is presented on figure IV-7.

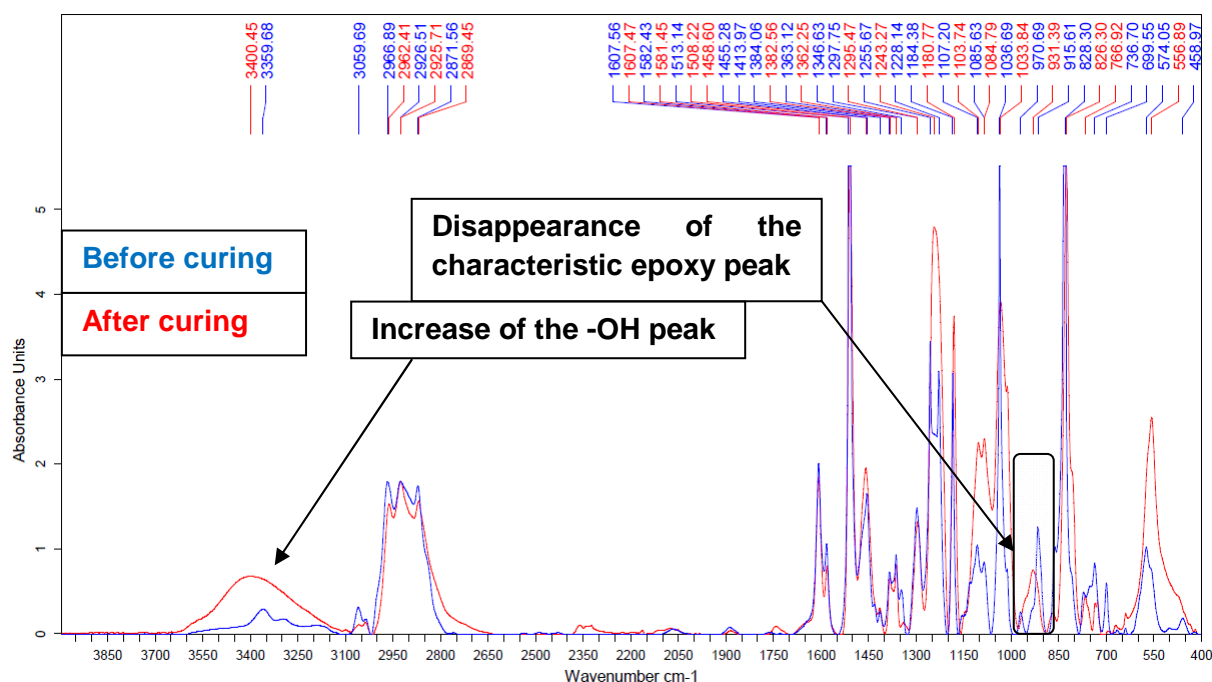


Figure IV-7. T-IR spectra of the RenLam CY 219 / Ren HY 5161 system before curing (blue) and after curing with its commercial curing agent (red).

Two characteristic epoxy peaks are observed at 917 and 970 cm^{-1} before curing. These peaks will disappear after curing giving birth to a unique peak at 934 cm^{-1} . Besides the appearance of a peak at 934 cm^{-1} , a slight increase of the -OH peak is observed after curing due to the reaction of the epoxy functions with the amines which leads to the formation of hydroxyl groups.

It is now essential to analyze the effect of the curing conditions on the epoxy film properties.

II.1.b. Properties of the cured epoxy films

The main properties of the obtained epoxy networks were studied to determine the factors which are important to obtain a durable coating. To do so, the thermal properties were determined as well as wettability and swelling experiments.

II.1.b.i. Thermal properties

It is of major importance to determine the thermal properties of the epoxy systems used because it is directly related to their resistance and to the behavior of the coating in the reactor. The glass transition temperatures of the films were first determined. As a matter of fact, the coating will be at a glassy state in the reactor if its T_g is higher than 80 °C but will be at a more rubbery state if its T_g is inferior to this value. On one hand, a too high T_g would lead to a brittle coating but on the other hand, a too low T_g will lead to a complete loss of the mechanical properties and the tacky rubbery epoxy coating could act as an anchoring site for the development of the crust as well.

DSC was used to determine the T_g of both epoxy systems. Two ramps were performed from -80 °C to 200 °C at a speed of 10 °C.min⁻¹ on the cured systems. The thermograms obtained for the RenLam CY 219 / Ren HY 5161 system cured at 150 °C during 1 h are shown on figure IV-8.

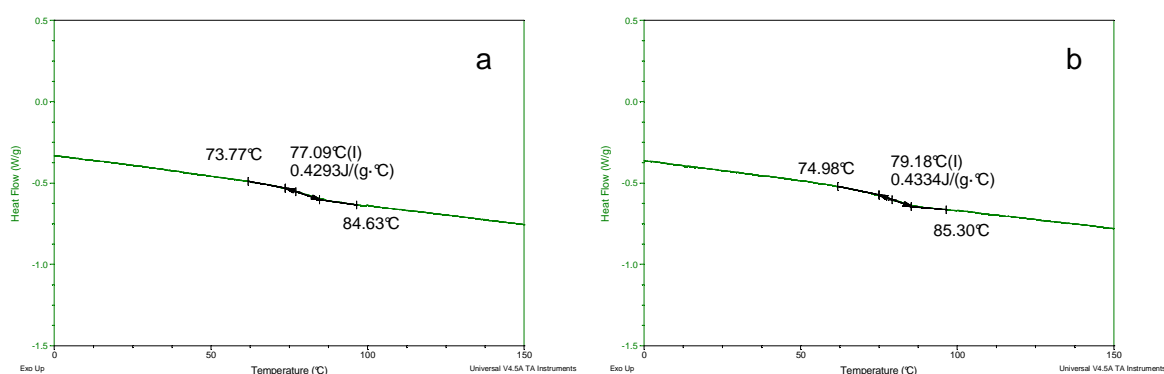


Figure IV-8. DSC thermograms (-80 to 200 °C at 10 °C.min⁻¹) of the cured (at 150 °C) RenLam CY 219 / Ren HY 5161 system: a. 1st ramp, b. 2nd ramp.

The results obtained for all the systems are listed in table IV-2.

Table IV-2. T_g of the different epoxy / curing agent systems as a function of their curing temperatures.

System	Curing temperature (°C)	T_g - 1 st ramp (°C)	T_g - 2 nd ramp (°C)
RenLam CY 219 / Ren HY 5161	80 (3 h)	60 ± 2	64 ± 2
RenLam CY 219 / Ren HY 5161	150 (1 h)	77 ± 2	79 ± 2
Araldite DBF CH / Ren HY 956	150 (1 h)	64 ± 2	67 ± 2

The T_g obtained here for the cured RenLam CY 219 / Ren HY 5161 system after a 150 °C curing is 77 °C during the first ramp and 79 °C during the second. That means that a coating based on this system would be at a slightly rubbery state in the S-PVC polymerization reactor. This is satisfactory as the desired T_g was around 80 °C in order to obtain a good stability with time.

A decrease of the curing temperature leads, for the same system, to a decrease of the T_g of the obtained epoxy films (around 60 °C). This difference might be due to a slower curing rate at a lower curing temperature which leads to the formation of a less dense network. The resulting material's T_g would also be lower in this case. This value is a bit low and is not considered as sufficient in order to obtain a durable coating. The differences observed between the two curing temperatures can be due to numerous effects. First, a curing at a higher temperature can lead to a bigger loss of volatile compounds (like benzylic alcohol) or to an evaporation of volatile amines. The second possibility is the differences of reactivity of the amines which compose the Ren HY 5161 system. One can guess that some amines are more reactive at 150 °C than at 80 °C. The more reactive amines will react first and lead to the gelation of the system. The remaining non-reacted species will finally participate to the formation of the network and finish the curing reaction (as no residual exothermal peak is observed during the temperature ramp meaning that the curing reaction is complete). This fact causes a modification of the structure of the epoxy network depending on the curing temperature and this is why a 150 °C curing would also be preferred for this system.

The T_g measured for the Araldite DBF CH / Ren HY 956 is around 65 °C which is not sufficient for our purpose. A coating at a rubbery state will lead to a softening of the polymer on the reactor walls.

TGA analyses were made as well to evaluate the volatile content and the thermal resistance of the cured epoxy systems tested. The thermal degradations of these resins were evaluated with a temperature ramp from 30 to 900 °C at a speed of 10 °C.min⁻¹. Results for both resins are presented on figure IV-9.

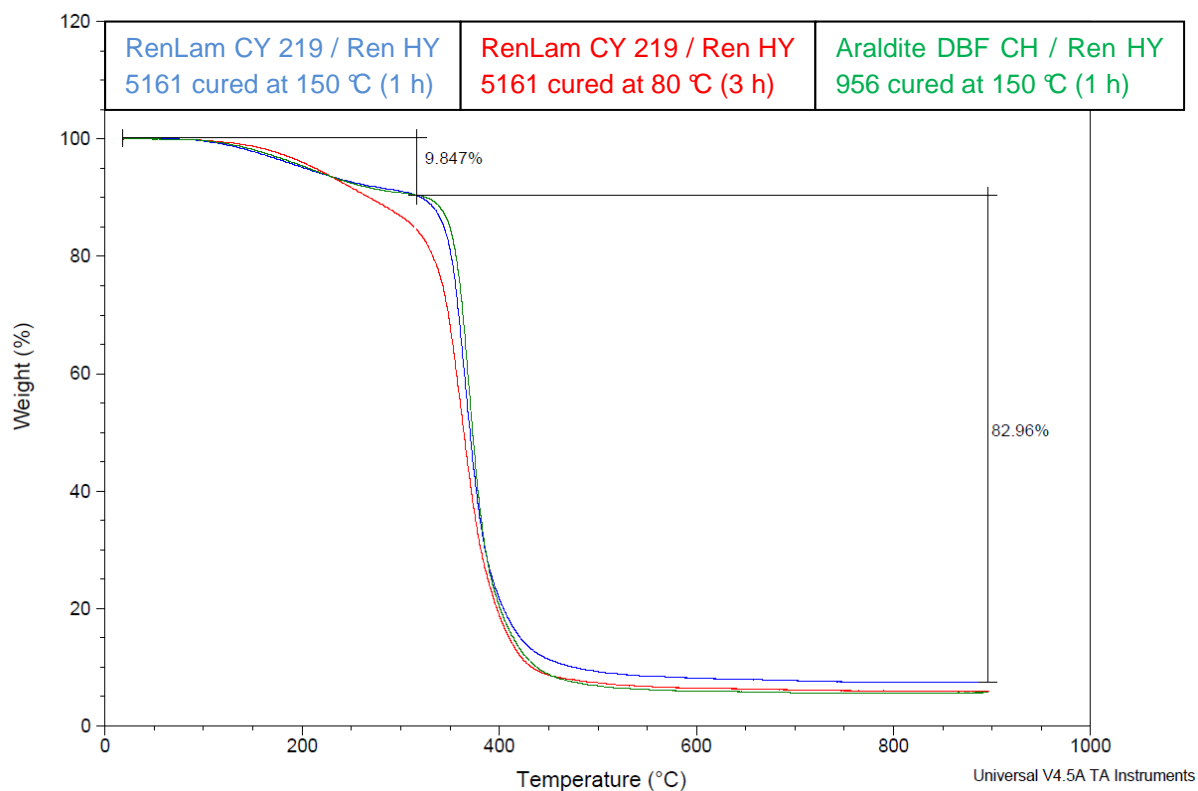


Figure IV-9. TGA thermograms (30 to 900 °C at 10 °C.min⁻¹) of the cured commercial epoxy systems.

The beginning of the weight loss happens at around 100 °C and might be due to evaporation of residual monomers or curing agent. The loss of weight for the system containing the Araldite DBF CH resin is a bit higher due to the presence of the non-reactive diluent (diethyl phthalate; Chapter 2, part I, 4, a.) which is highly volatile. The thermal degradation of the polymer happens around 350 °C and leads to an ash content of 7 % for the RenLam CY 219 / Ren HY 5161 system cured at 150 °C, 6 % for the same system cured at 80 °C and 6 % for the Araldite DBF CH / Ren HY 956 system.

However, the main issue during this study is the stability of the coating at 80 °C (the temperature reached in the S-PVC polymerization's reactor). An 80 °C isotherm was performed during 7h to check the behavior of both cured resins in a dried 80 °C nitrogen-rich atmosphere. The stability of both systems is correct. As a matter of fact, a slight loss of weight (around 1 % for all systems) is observed at the beginning of the heating period but this mass decrease is stabilized after 2 h of analysis. No degradation occurs meaning that the resins are resistant enough to be put on the reactor's walls without declining with time.

The thermal properties obtained are mainly satisfactory for the RenLam CY 219 / Ren HY 5161 system cured at 150 °C. However, some other properties of the tested epoxy resins /

curing agents combinations must be determined such as the surface properties of the obtained free films.

II.1.b.ii. Surface energy

The surface energy is a good way to predict the interactions of a material with its environment ^{4,5}. A low surface energy would be required for the surface because this type of material (PolyTetraFluoroEthylene for example) does not favor the anchorage of any species ⁶. However, the adhesion with stainless steel has to be high.

To determine the surface energy of a material, some contact angle measurements have to be performed with a polar solvent (water) and with an apolar solvent (diiodomethan). These values will respectively give the polar and dispersive components of the surface energy. By adding both of these values, the surface energy of the studied material is obtained.

The surface energy determined for the systems previously tested are compared to the values obtained for stainless steel (after cleaning) which is the material composing the reactor's walls. These values are presented on table IV-3.

Table IV-3. Surface energy values obtained for the different commercial epoxy systems and for stainless steel.

Sample	$\theta_{\text{eau}}^{(^\circ)}$	$\theta_{\text{diiodo}}^{(^\circ)}$	$\gamma_s \text{ (mJ.m}^{-2}\text{)}$	$\gamma_{\text{sp}} \text{ (mJ.m}^{-2}\text{)}$	$\gamma_{\text{sd}} \text{ (mJ.m}^{-2}\text{)}$
Cleaned stainless steel	46 ± 3	44 ± 3	59 ± 1	22	37
RenLam CY 219 / Ren HY 5161 - 80 °C	80 ± 4	50 ± 2	39 ± 2	5	34
RenLam CY 219 / Ren HY 5161 - 150 °C	82 ± 5	47 ± 5	40 ± 1	4	36
Araldite DBF CH / Ren HY 956 - 150 °C	69 ± 4	36 ± 2	50 ± 2	8	42

The difference between contact angles obtained with diiodomethan is not significant as all the values are quite close. These results do not allow making any notable difference between stainless steel and the RenLam CY 219 resin film before and after immersion in solvents.

The contact angle of cleaned stainless steel with water is around 46°. This confirms the fact that its surface is mainly composed of polar groups. RenLam CY 219 / Ren HY 5161 films are more hydrophobic as the contact angle obtained with water is 82°. This might come from the fact that a cured epoxy film has only a few numbers of hydrophilic functions at its surface. This fact also leads to an increase of the surface energy meaning that this coating is less able to make interactions with its surrounding medium than stainless steel. This is a good point because it would mean that the tendency for the scale to adsorb on the coating is lower than on stainless steel.

Finally, a focus was made on the properties of the networks obtained with the systems described earlier and mainly their resistance in two model solvents: water and 1-chlorobutan.

II.1.b.iii. Network properties

Hygrothermal aging of epoxy films could induce a modification of the material's chemical, physical or mechanical properties. Two main hypotheses were set to explain the absorption of water by an epoxy network. First, in the free volume approach, the absorbed water occupies the polymer network's free volume ⁷. But since some polymers with high free volumes ⁸ do not absorb a large amount of water, this first theory has to be coupled with the second approach which takes into account the interactions between the water molecules and the epoxy's polar groups ⁹. Swelling tests were used to check the behavior of the epoxy coating when it is immersed in a solvent ¹⁰. As a matter of fact, this phenomenon can be accompanied by a dimensional growth of the thermoset network which leads to a damaging of the polymer ¹¹. Water, the solvent used as the dispersive medium during the suspension polymerization, will be used as testing solvent and 1-chlorobutan will be the solvent used in order to simulate vinyl chloride monomer ¹². Swelling of free films will also be a key factor in the choice of the resin for the following of our study. In the case of water, swelling can be due to a rupture of the inner chains hydrogen bonds by water molecules ¹¹. It is also interesting to note that, for low mass swelling values (<3 % w/w), the water molecules standing in the polymer network free volume are not involved in a volume swelling phenomenon.

Swelling values (S) were obtained by measuring the weight uptakes of the epoxy films (equation IV-3).

$$S(\%) = \frac{m_1 - m_0}{m_0} * 100$$

Equation IV-3. Mathematical calculation for the determination of the swelling values.

Where m_0 is the mass of the free film before immersion and m_1 is the mass of the film after immersion.

The results for both solvents are shown on figure IV-10.

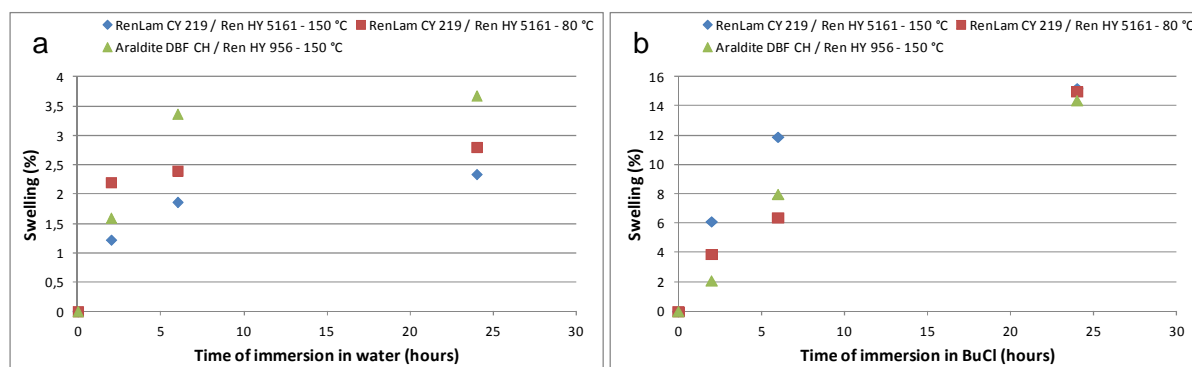


Figure IV-10. Evolution of the swelling of the cured commercial epoxy systems as a function of the immersion time in: a. BuCl (75 °C), b. water (80 °C).

The values obtained after immersion of the films in 1-chlorobutan (BuCl) are much higher than those achieved in water and almost equal for both resins. That means that 1-chlorobutan is a better solvent of the epoxy resins than water. The absorption of BuCl is faster for the RenLam CY 219 / Ren HY 5161 system cured at 150 °C (6 % after 3h of immersion) than for the Araldite DBF CH system (2 % after 3h of immersion). However, the values obtained in this non-polar solvent are relatively low (almost 16 %) and acceptable for our study.

The tests made in water are more significant because this liquid is the dispersive medium used in the suspension polymerization of VCM. Moreover, the results obtained for both resins are not equal. Araldite DBF CH system's swelling value stabilizes at around 4 % after a 24h immersion in water contrary to the RenLam CY 219 system which stabilizes at around 2.5 %. That means that the Araldite DBF CH system absorbs two times more water than the other one.

The swelling values can be correlated with the evolution of the T_g as a function of the immersion time. DSC was used in order to determine the T_g of the free films after swelling in both liquids. Two ramps (from -80 to 200 °C at 10 °C.min⁻¹) were performed for each film. The T_g determined during the first ramp will give an information on the plastifying effect observed in these solvents whereas the second ramp permits to check the reversibility of the liquid uptake (after drying). The T_g during the first ramp (T_{g1}) and the second ramp (T_{g2}) were measured (figure IV-11).

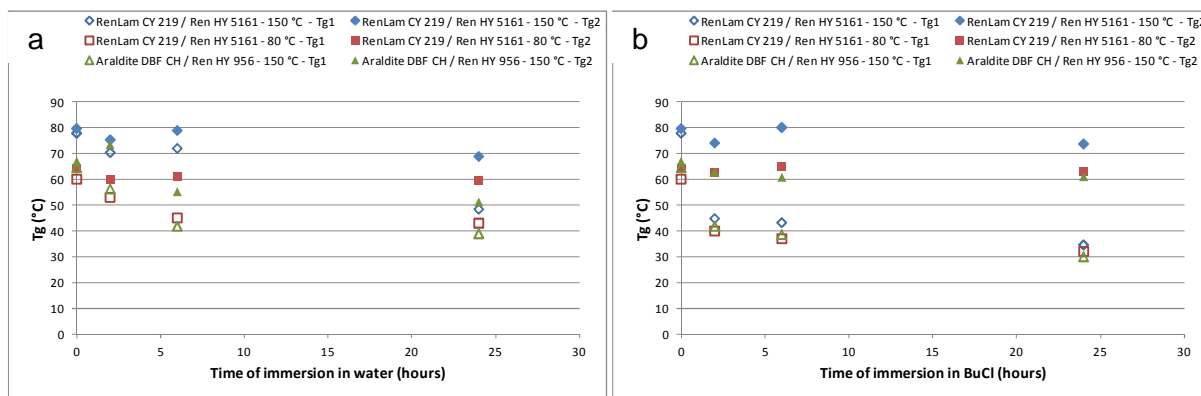


Figure IV-11. Evolution of the T_g of the cured commercial epoxy systems as a function of the immersion time in: a. BuCl (75 °C), b. water (80 °C).

In BuCl, there is a decrease of T_{g1} values with the immersion time. In fact, T_{g1} for these free films are around 40 °C after 3h of immersion and 30 °C after 24h of immersion. However, T_{g2} shows that there is a complete recovery of the T_g after one ramp. This means that the plastifying of the epoxy films by BuCl is a reversible process.

In water, the decrease of the T_g is less important but the recovery of the T_g is not complete for the Araldite DBF CH system. The results obtained after a 24h immersion for T_{g1} is 40 °C and 50 °C for T_{g2} (T_g before immersion is 65 °C). The decrease of T_g can be explained by the swelling of the films by the solvents. Moreover, the difference between T_{g1} and T_{g2} might be due to a loss of the non-reactive diluent of the Araldite DBF CH system or a chemical degradation of the epoxy network. The results are quite similar for the other systems but the recovery of the T_g is almost complete.

II.2. Conclusion

All the analyses performed on free films showed that the RenLam CY 219 / Ren HY 5161 system cured at 150 °C is more adapted for our purpose. The swelling values in water and the T_g of this epoxy film makes it totally suitable as a coating for S-PVC reactors. This formulation will be kept for the following tests as a coating on stainless steel.

A study was made in parallel using model polyamines as curing agents. The properties of the epoxy resins as free films were studied in the following of this report.

III. Epoxy system based on model polyamines

III.1. Presentation

Different polyamines were tested as curing agents for the RenLam CY 219 epoxy resin. These compounds were chosen based on the molecules used in commercial preparations and on various molecules used in literature¹³⁻¹⁷. All the molecules tested are listed below (figure IV-12).

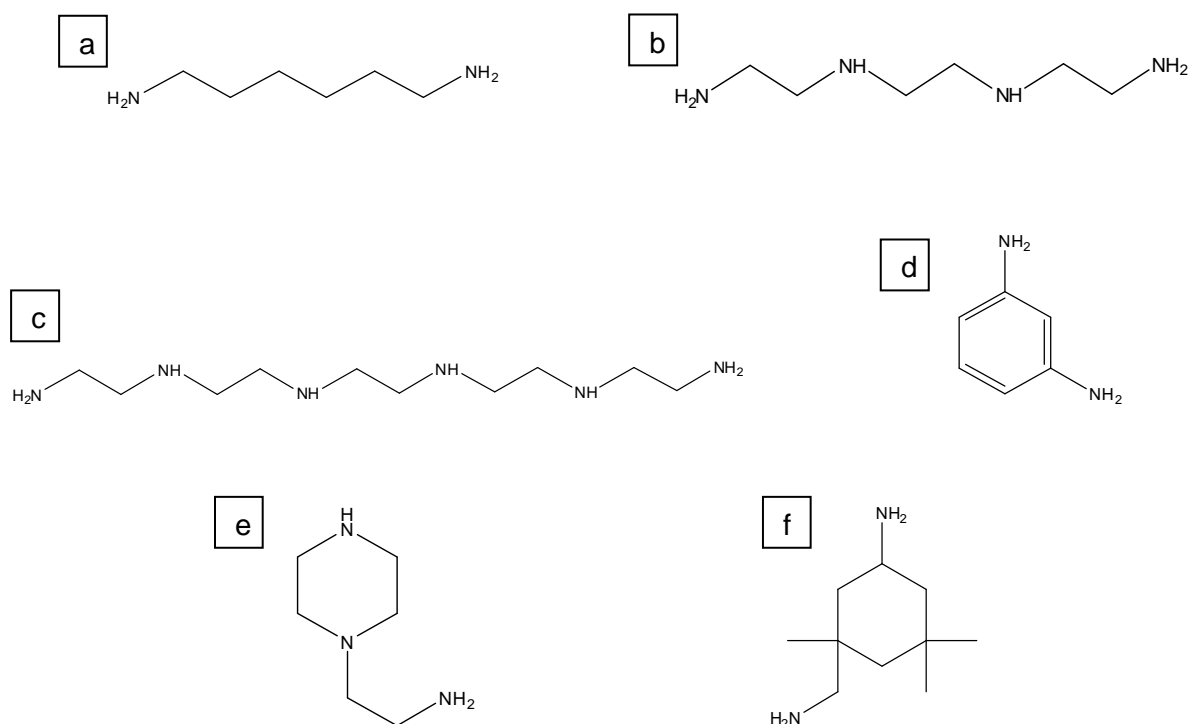


Figure IV-12. Chemical formula of: a. hexaethylenediamine (HEDA), b. triethylenetetramine (TETA), c. pentaethylenehexamine (PEHA), d. m-phenylenediamine (mPDA), e. 1-(2-aminoethyl)piperazine (AEPA), f. isophoronediamine (IPDA).

The same tests than the ones made for the commercial systems were made to evaluate if one of these systems would be more efficient as anti-scale coatings than those tested earlier.

The preparation of free films, compared to the ones obtained with the commercial curing systems, goes through the determination of two important parameters: the Epoxy Equivalent Weight (EEW) of the RenLam CY 219 resin and the Amine-Hydrogen Equivalent Weight (AHEW) of each pure polyamine used.

III.2. Processing of epoxy free films

III.2.a. Determination of the Epoxy Equivalent Weight (EEW)

^1H NMR analyses were performed in order to determine the exact equivalent epoxy weight (EEW) and number average molecular weight (M_n) of the BADGE resin ¹⁸. A NMR spectrum was performed in deuterated chloroform and the result obtained is presented on figure IV-13.

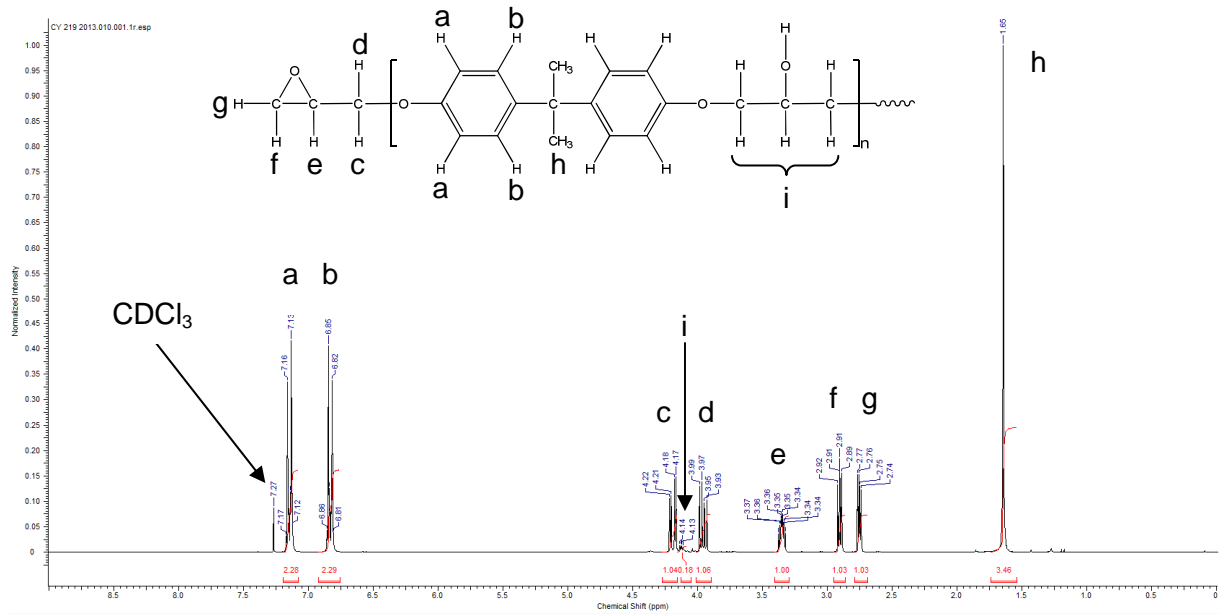


Figure IV-13. ^1H NMR spectrum of the RenLam CY 219 prepolymer (CDCl_3).

The proton relation R_p can be calculated according to equation IV-4 ¹⁸:

$$R_p = \frac{I_{(a+b)}}{I_{(e+f+g)}}$$

Equation IV-4. Mathematical formula for the calculation of the proton relation R_p .

This equation leads to the determination of the polymerization degree (DPn). The ratio R_p is compared to the theoretical value R_t (for a polymerization degree DPn=0) according to equation IV-5 and equation IV-6 ¹⁸:

$$R_t = \frac{I_{(a+b)}}{I_{(e+f+g)}} = \frac{8}{6} = 1.33$$

Equation IV-5. Mathematical formula for the calculation of the theoretical proton relation R_t .

$$DPn = \frac{R_p - R_t}{R_t} = \frac{R_p - 1.33}{1.33}$$

Equation IV-6. Calculation of n thanks to R_p and R_t .

Knowing the DPn value, it is possible to determine the EEW (equation IV-7) ¹⁸:

$$EEW = 142 * DPn + 170$$

Equation IV-7. Calculation of the EEW value of an epoxy resin thanks to DPn.

Where 170 corresponds to the EEW of the oligomer with DPn = 0 and 142 to the EEW of the repetitive BADGE unit.

Finally, Mn can be calculated using equation IV-8 ¹⁸:

$$Mn = 284 * DPn + 340$$

Equation IV-8. Calculation of the Number-average molecular weight (Mn) of an epoxy resin thanks to DPn.

Where 340 corresponds to the molecular weight of the oligomer with DPn = 0 and 284 to the molecular weight of the repetitive BADGE unit.

All results are listed in table IV-4.

Table IV-4. Main molecular properties of the RenLam CY 219 prepolymer determined by ¹H NMR.

RenLam CY 219	
R_p	1.5
DPn	0.128
EEW (g.eq⁻¹)	188
Mn (g.mol⁻¹)	376

The NMR results are consistent with the results given by the supplier (EEW comprised between 167 and 200 g.eq⁻¹). The RenLam CY 219 resin has a very low molecular weight which can explain its relatively low viscosity. Moreover, the EEW will be useful later when tests will be made with pure amines as curing agents. This value will allow us to calculate the quantity of pure amine that must be used in order to respect a stoichiometric ratio between the epoxy resin and the curing agent.

III.2.b. Determination of the Amine-Hydrogen Equivalent Weight (AHEW)

This value has to be calculated for each polyamine in order to know the quantity to introduce with the epoxy. It is essential to know the Equivalent Epoxy Weight (EEW) of the RenLam CY 219 resin (determined by ^1H NMR). The EEW stands for the number of epoxy functions available in a non-cured epoxy for 1 g of resin. The AHEW is also the number of amine groups that can be involved in a classical curing reaction ¹³.

Isophorone diamine (IPDA) is taken as an example. AHEW is calculated using equation IV-9:

$$AHEW = \frac{M(IPDA)}{x_{NH}} = \frac{170}{4} = 42.5 \text{ g.eq}^{-1}$$

Equation IV-9. Calculation of the AHEW for an amine molecule.

Where x_{NH} is the number of hydrogen attached to a nitrogen atom that can react with an epoxy function, M is the molar mass of the polyamine (g.mol^{-1}).

The mass of IPDA to add is calculated using equation IV-10 (based on 1 g of RenLam CY 219 epoxy prepolymer):

$$m(IPDA) = \frac{m(\text{resin})}{EEW(\text{resin})} * AHEW(IPDA) = \frac{1}{188} * 42.5 = 0.23 \text{ g}$$

Equation IV-10. Calculation of the IPDA mass to add for 1 g of RenLam CY 219 resin.

Equation IV-10 shows that 0.33 g of IPDA must be added to 1g of RenLam CY 219 resin in order to be in the stoichiometric ratio. The whole values for each amines tested are listed in table IV-5.

Table IV-5. AHEW values for pure polyamines.

Amines	M (g.mol^{-1})	x_{NH}	AHEW (g.eq^{-1})	Mass for 1 g of resin (g)
HEDA	116	4	29	0.15
PEHA	146	6	24.3	0.13
TETA	232	8	29	0.15
IPDA	170	4	42.5	0.23
AEPA	129	4	32.25	0.17
mPDA	108	3	36	0.19

The case of mPDA is a bit more particular because it contains a tertiary amine function. This type of amine does not have any hydrogen bonded but it participates by catalyzing the curing reaction based on the formation of a tertiary amine / epoxy zwitterions ¹⁹.

The first tests performed were the measurements of the free films properties.

III.2.c. Free films preparation

The films were prepared by mixing the epoxy prepolymer with one polyamine (in the ratios given in table IV-5). This solution is manually mixed to obtain a homogeneous blend and vacuum is then applied during 5 minutes in order to remove air from the sample and to obtain smooth films. Around 3 g of this mixture are then poured into silicon molds. The curing conditions for each polyamines were selected ¹³⁻¹⁷ and the aspect of the films obtained (presence of cracks, roughness, non-homogeneity of the surface...) by using these conditions are listed below (table IV-6).

Table IV-6. Curing conditions selected for the curing of RenLam CY 219 with pure polyamines.

Amines	Curing temperature (°C)	Curing duration (h)	Aspect of the films
HEDA	120	1	Very poor
PEHA	120	1	Irregular
TETA	130	1	Good
IPDA	150	1	Good
AEPA	120	1	Good
mPDA	180	1	Irregular

The aspect of the films obtained by using HEDA is very poor (cracks and shrinkage) and not homogeneous enough to perform further tests. This polyamine was cancelled and the main properties of the films obtained with the other polyamines were determined

III.3. Characterization of the epoxy free films

Again, the model systems studied were characterized. The first point was to study the curing kinetic of all systems in order to check if the curing conditions selected allowed to obtain a fully cured epoxy network. Afterwards, the properties of the resulting cured epoxy free films were studied to make a link between the physical and the chemical properties of the

thermoset network obtained and its behavior in the pilot reactor. At the end of this study, one of the pure polyamines presented above will be chosen to undergo one batch in the pilot reactor.

III.3.a. Study of the curing processes

III.3.a.i. Comparison of the curing kinetics

The first step was to follow the formation of the epoxy network at the selected curing conditions. The curing reaction was followed by performing the measurements directly in the DSC pans. The epoxy / curing agent mixtures (before curing) were poured into a DSC cell and were then heated at their corresponding curing temperatures. A temperature ramp was then performed to check the presence of an eventual residual exothermal peak (example of IPDA on figure IV-14).

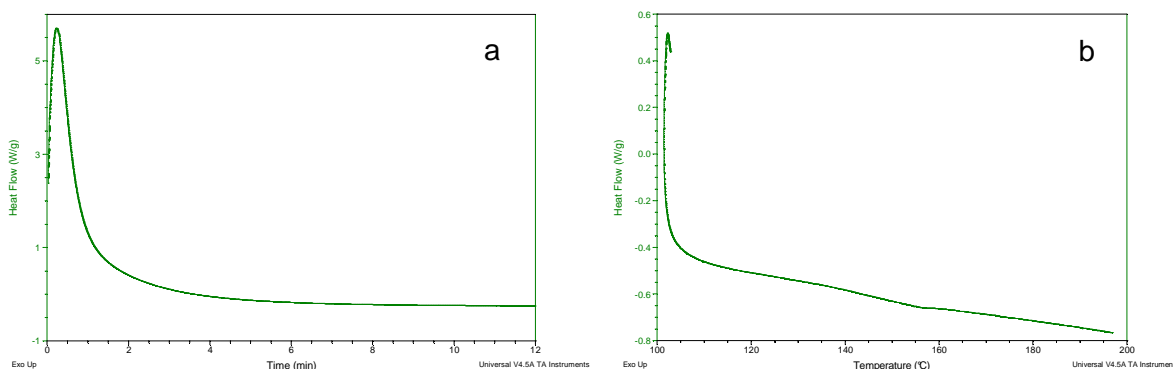


Figure IV-14. DSC thermograms during the curing reaction for an IPDA-cured RenLam CY 219 at 150 °C: a. 150 °C isotherm during 60 minutes, b. ramp from 80 to 200 °C at a speed of 10 °C.min⁻¹.

For a curing with IPDA, the exothermal peak due to the curing reaction (figure IV-14, a) is clearly visible and shows that the curing reaction at 150 °C starts very quickly and complete curing is obtained after only 10 minutes. As a matter of fact, the reaction begins so quickly that the integration of the peak's under-the-curve area is impossible. The reaction is total because no residual exothermal peak is observed during the temperature ramp which goes until 200 °C. This result was obtained for all the polyamines tested at their respective curing temperatures.

It was complicated to measure the evolution of the conversion rate because of the quick start of the curing reaction for all systems. However, another way to compare the curing kinetics is

to evaluate the time necessary to achieve a 100 % conversion for each polyamines (table IV-7).

Table IV-7. Comparison of the times necessary to reach total conversion during DSC pan measurements for each polyamines.

Amines	Curing temperature (°C)	Total conversion time (min)
Ren HY 5161	150	18
PEHA	120	9
TETA	130	7
IPDA	150	12
AEPA	120	8
mPDA	180	10

The commercial system Ren HY 5161 is the slowest to get to a total conversion. This is mainly due to the fact that this formulation is mainly composed of Jeffamine which induces a slower curing speed.

For the pure polyamines, it is interesting to note that complete conversion is obtained after around 10 minutes for each molecule. This value is obtained at a lower curing temperature for PEHA and TETA. This comes from the fact that these polyamines are linear and this type of amines is known to exhibit high curing speeds²⁰. The other compound showing a higher curing rate is AEPA. This cyclic compound should propose a slower curing rate than PEHA and TETA. However, this molecule contains a tertiary amine in its structure which is well-known to catalyze the curing of epoxy resins²⁰.

However, the important thing here is to be sure that complete curing is obtained within the curing conditions selected.

III.3.a.i. Observation of the curing reaction by infrared analysis

As made previously for the commercial systems, some infrared analyses were performed to check if the curing reaction is complete or not. For this purpose, a droplet of the epoxy / curing agent system was deposited after mixing on a KBr pellet and was analyzed by transmission infrared spectroscopy before and after curing at the selected conditions. The results obtained for the RenLam CY 219 / IPDA system are presented on figure IV-15.

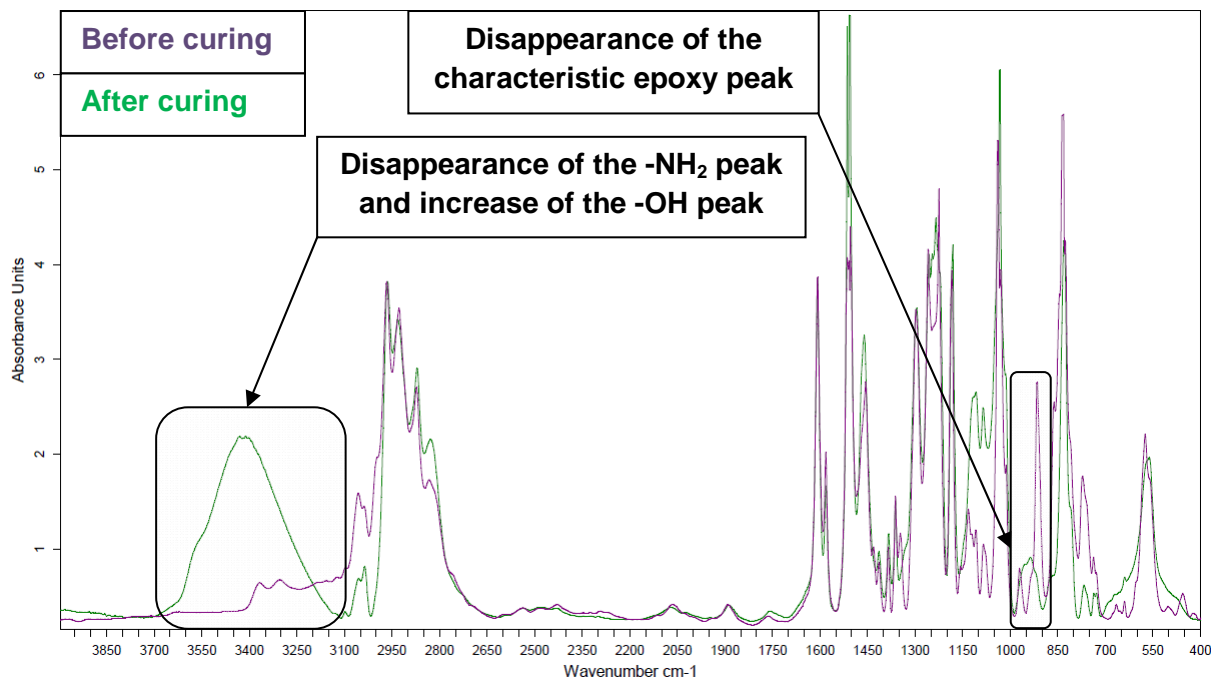


Figure IV-15. T-IR spectra of the RenLam CY 219 resin with TETA before (blue) and after (red) curing at 130 °C during 1h.

The two characteristic epoxy peaks are again observed at 917 and 970 cm^{-1} before curing. These peaks will disappear after curing giving birth to a unique peak at 934 cm^{-1} which can be combined with a slight increases of the -OH peak vibration mode after curing. This result evidences the fact that curing is complete.

Same results have been obtained for the other RenLam CY 219 / polyamine systems. The main properties of the cured films were then determined in order to choose the most efficient system for a pilot test.

III.3.b. Properties of the cured epoxy films

As it was previously done, the main properties of the obtained epoxy films were tested and compared between each other for all pure polyamines and compared with the results obtained for the selected commercial system (RenLam CY 219 / Ren HY 5161 cured at 150 °C).

III.3.b.i. Thermal properties

The tests made on the selected commercial system permitted to get a T_g of around 80 °C. This value is satisfactory but it is quite interesting to investigate the range of T_g which can be obtained by using the RenLam CY 219 resin cured with pure polyamines.

DSC has also been used to determine the T_g of this epoxy resin cured by the different polyamines. Two ramps were performed from -80 °C to 200 °C at a speed of 10 °C.min⁻¹. The thermograms obtained for the RenLam CY 219 / IPDA cured at 150 °C during 1 h are shown on figure IV-16.

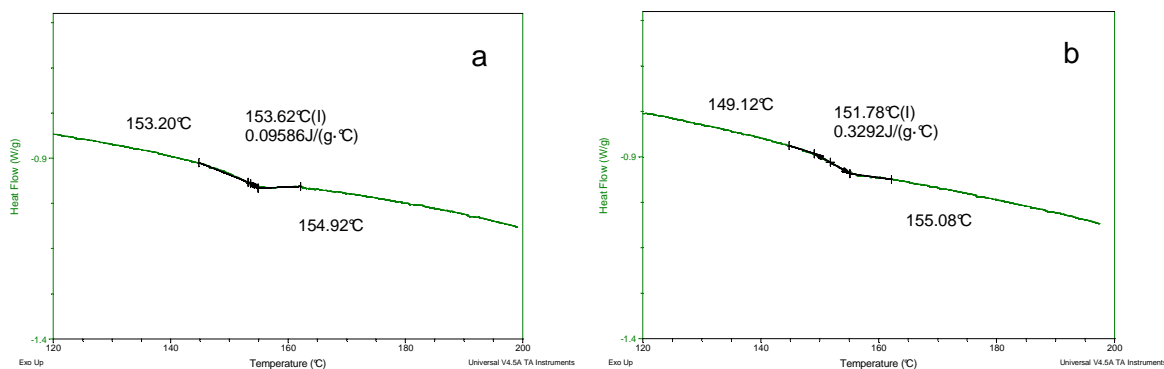


Figure IV-16. DSC thermograms (-80 to 200 °C at 10 °C.min⁻¹) of an IPDA-cured RenLam CY 219 resin: a. 1st ramp, b. 2nd ramp.

The T_g obtained here for the IPDA-cured RenLam CY 219 resin is 153 °C for the two ramps. This value is way higher than the T_g needed. The IPDA-cured epoxy coating will also be at a straight glassy state when immersed in the S-PVC medium improving its mechanical resistance but also leading to a more brittle coating.

The T_g measured for each polyamines used as curing agents are listed in table IV-8.

Table IV-8. T_g obtained for the RenLam CY 219 resin cured with pure amines.

Curing agent	T_g - 1 st ramp (°C)	T_g - 2 nd ramp (°C)
Ren HY 5161	77 ± 2	79 ± 2
PEHA	130 ± 2	128 ± 2
TETA	123 ± 2	123 ± 2
IPDA	154 ± 2	152 ± 2
AEPA	113 ± 2	113 ± 2
mPDA	150 ± 2	149 ± 2

These results are interesting because using pure polyamines permit to increase the T_g of the final material. As all the obtained films have a T_g higher or close to 80 °C, all the amines tested above are still corresponding to the targeted application. All the T_g obtained with pure polyamines are higher than the one obtained with the commercial curing agent. This might come from the fact that Ren HY 5161 contains a large amount of benzyl alcohol and bisphenol-A. These compounds are used in curing agent formulations as catalysts but play the role of plasticizers as well ²¹ as they are incorporated in the network during the curing reaction. Moreover, the low T_g obtained with the Ren HY 5161 system comes from the fact that it is mainly composed of Jeffamine (30 - 42 % w / w). The flexible character of this molecule leads to a decrease of the thermoset material's T_g ^{22,23}. The combination of these two factors leads to a T_g that is way lower than the ones obtained with pure polyamines.

When comparing the values obtained with the model polyamines, it can be seen that the higher T_g were obtained with the cyclic amines: IPDA (154 °C) and mPDA (150 °C). These values are very high but are suitable as well. All the films obtained during this study are satisfactory in terms of glass transition temperature.

The trends observed during this study and the relationship between the chemical structure of the polyamines and the resulting epoxy network T_g will be discussed later.

The thermal stability of the cured films was studied by TGA too and was found to be equivalent to the one obtained for the commercial systems tested. Again, the surface properties had to be determined to evaluate the interactions that the cured epoxy systems can have with their surrounding medium.

III.3.b.ii. Surface energy

The evolution of the surface energy was studied to evaluate the surface properties of the epoxy film as a function of the polyamine used. The results for the RenLam CY 219 resin are listed in table IV-9.

Table IV-9. Surface energy for the RenLam CY 219 resin cured with different pure amines.

Curing agent	θ_{eau} (°)	$\theta_{\text{diiodomethane}}$ (°)	γ_s (mJ.m ⁻²)	γ_{sp} (mJ.m ⁻²)	γ_{sd} (mJ.m ⁻²)
Ren HY 5161	82 ± 5	47 ± 5	40 ± 2	4 ± 1	36 ± 1
PEHA	115 ± 5	44 ± 3	39 ± 2	1 ± 1	38 ± 1
TETA	71 ± 4	36 ± 5	48 ± 2	7 ± 1	41 ± 1
IPDA	82 ± 3	46 ± 2	40 ± 2	4 ± 1	36 ± 1
AEPA	84 ± 12	44 ± 4	40 ± 2	3 ± 1	37 ± 1
mPDA	82 ± 2	44 ± 3	41 ± 2	3 ± 1	37 ± 1

The differences between the contact angles determined with diiodomethan for the different systems are not really significant as all values are comprised between 36 and 47 °.

The contact angles measured with water for IPDA, AEPA and mPDA are quite similar to the ones obtained with the Ren HY 5161 curing agent. This comes from the fact that IPDA is a major part of this commercial curing system. Moreover, the chemical structures of AEPA and mPDA are equivalent to the one of IPDA with a six-carbon ring and two primary or secondary amine functions. The structures of the final cured films obtained are so quite similar to one other explaining the values.

The contact angle values with water obtained for PEHA and TETA are really different giving access to really disparate values. An epoxy network obtained with PEHA may be more cross-linked and this can lead to a more hydrophobic material.

All the results shown above are correct regarding to our study as the films cured are not too highly hydrophilic and should provide great resistance to scale formation. However, these results have to be correlated with a study of the network properties performed by Dynamical Mechanical Thermal Analysis (DMTA) and swelling measurements.

III.3.b.iii. Network properties

DMTA analyses were used in order to characterize the thermomechanical properties of the polymer networks obtained by using different curing agents in order to access to the cross-linking density. Curing of an epoxy resin involves the formation of a 3D-thermoset network with its particular properties.

The cross-linking density (ν_R) and the molecular weight between the crossing points (M_C) were determined by measuring the storage modulus (G') at the rubbery state^{24,25}. The ν_R value will be calculated using equation IV-11.

$$\nu_R = \frac{G'}{RT}$$

Equation IV-11. Calculation of the crosslinking density of a thermoset network.

Where G' is the storage modulus at the rubbery state, R is the gas constant ($R = 8.314 \text{ J.mol}^{-1}.\text{K}^{-1}$), T is the temperature of the plateau (K).

The molecular weight between the crossing points (M_C) is related to the cross-linking density (ν_R) with equation IV-12.

$$M_C = \frac{\rho}{\nu_R}$$

Equation IV-12. Calculation of the molecular weight between the crossing point of a thermoset network.

Where ρ is the density of the cured epoxy resin.

The tests were made performing a temperature ramp from 20 to 250 °C. The shear strain was fixed at 0.01 % at a frequency of 1 Hz.

An example of the curve obtained for the RenLam CY 219 resin cured by IPDA is shown on figure IV-17.

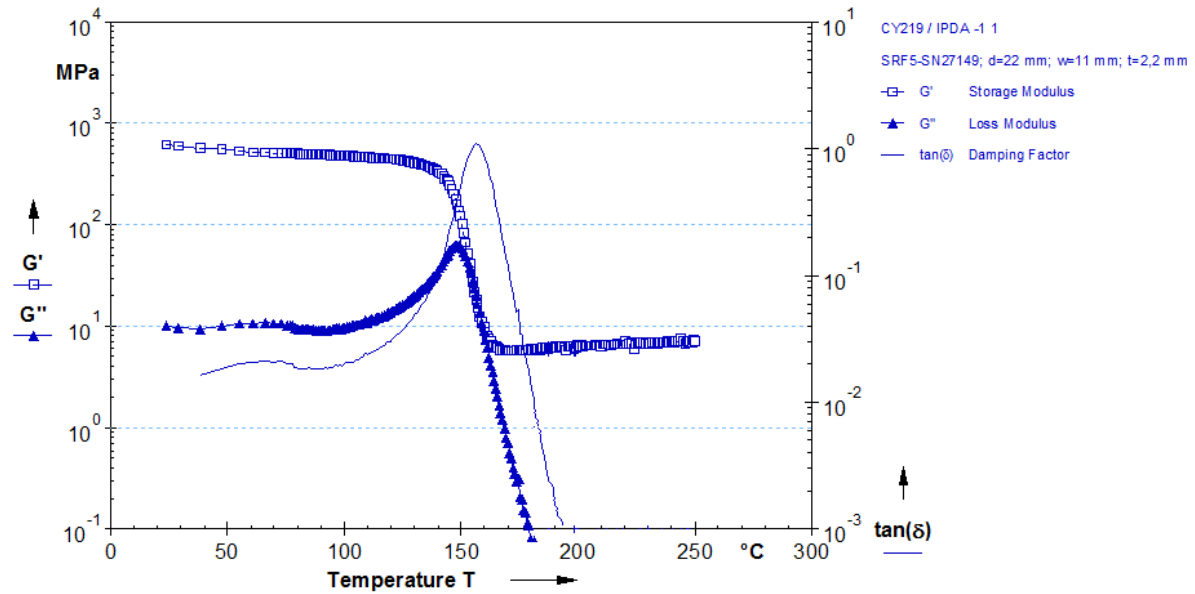
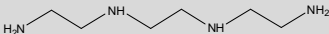
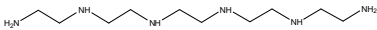
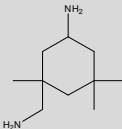
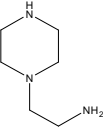
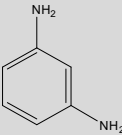


Figure IV-17. DMTA curve for the RenLam CY 219 / IPDA system.

The evolution of the RenLam CY 219 - IPDA network mechanical behavior as a function of the temperature can be observed during this DMTA analysis. The T_g of the material is obtained at the $\tan \delta$ maximum peak. Before this value, the polymer is at a glassy state. The $\tan \delta$ peak is due to a slight increase of G'' (then followed by a sharp decrease) and to an important decrease of G' . The G' value used to calculate the cross-linking density will be taken after the $\tan \delta$ peak, at the beginning of the rubbery plateau (at 170 °C for the example of figure IV-17). All the values obtained for the DMTA tests are presented in table IV-10.

Table IV-10. Cured networks properties for the RenLam CY 219 resin cured with different pure amines.

Curing agent	G' (MPa)	ρ	$v_R (*10^{-3})$	Mc (g.mol ⁻¹)	T _g (°C)*
Ren HY 5161 - 80 °C	7	1.3	2.35	543	73
Ren HY 5161 - 150 °C	7	1.1	2.23	483	79
PEHA 	24	1.2	6.96	207	119
TETA 	10	1.1	3.00	362	134
IPDA 	11	1.0	2.95	423	157
AEPA 	9	1.2	2.59	475	115
mPDA 	5	1.2	1.36	647	137

*: determined by DMTA

First, we can see that the network obtained using the commercial curing system is the less dense. This is due to the fact that a mix of amine is used and this can lead to a network which is less ordered with a broader distribution of the Mc values. Again, the lower T_g value obtained for this system can be explained by the presence of benzyl alcohol and bisphenol-A in the Ren HY 5161 formulation ²¹ but also by the presence of Jeffamine as its main compound ²². This latter effect of this solvent leads to a decrease of the T_g.

When comparing the Ren HY 5161 curing agent cured at 80 °C or 150 °C, it is interesting to compare the difference in the density of the cured system as ρ is quite higher when cured at 80 °C. This is due to the fact that the two catalyts ²⁶ (benzyl alcohol and bisphenol-A) are highly volatile. At 150 °C, these compounds evaporate very rapidly and before gelation of the epoxy network. At 80 °C, the loss of these compounds is not as important and this causes the formation of a more swollen network (higher Mc) with a lower T_g.

For the samples using pure polyamines, the results obtained are in accordance with the ones found in the literature ^{13,17}. Concerning the linear polyamines, it can be seen that a higher T_g

is reached when using TETA instead of PEHA. As a matter of fact, the increase of the glass transition temperature is due to an increase of the polyamine functionality¹³ (number of amine functions able to react with an epoxy ring: 6 for PEHA and 8 for TETA). These two compounds are also the ones that allow to obtain the higher cross-linking densities. This result is consistent with the literature as ethyleneamines are known to be very reactive²⁰. Moreover, their polyfunctional nature and the short distances between the reactive sites lead to an increase of the V_R value. This fact can also explain the fact that the M_c (207 g.mol⁻¹ with PEHA and 362 g.mol⁻¹ with TETA) values obtained for the epoxy films cured with these polyamines are lower than the M_w value of the epoxy resin (376 g.mol⁻¹).

The M_c values obtained with the cyclic polyamines (IPDA, AEPA and mPDA) are quite higher. This is due to the steric hindrance provided by the bulky cyclic structure leading to a looser network. For AEPA, the lower T_g can be explained by the presence of a small linear pendant group which gives finally a greater flexibility of the polymer chains and a lower T_g ¹³ while keeping a quite high M_c value. The values obtained for mPDA are consistent with the literature²⁰ as this compound leads to the obtaining of the lowest cross-linking density.

Again, swelling tests were performed to make a correlation between the structure of the networks obtained and the resistance regarding to the two model solvents tested: water and 1-chlorobutan.

These tests were performed as explained earlier (II.1.b.iii) by using equation IV-3¹⁰. The results obtained for each pure polyamine look similar to the ones obtained for both resins cured by their respective commercial curing systems. The results presented in table IV-11 correspond to the values obtained for all systems after a 24 h immersion in both solvents. This duration was chosen because it corresponds to the point where the swelling value is stabilized and does not evolve anymore.

Table IV-11. Swelling values obtained in BuCl (75 °C) and water (80 °C) for the RenLam CY 219 resin cured with different pure amines.

Curing agent	Swelling after 24h in water (80 °C) (%)	Swelling after 24h in BuCl (75 °C) (%)
Ren HY 5161	2.5	16
PEHA	7	1.5
TETA	7	2
IPDA	6	6
AEPA	12	10
mPDA	6	2

In BuCl, the swelling values for pure amines are lower than the values determined with the commercial systems. This might come from the fact that the commercial curing system is composed of non reactive diluents such as benzyl alcohol and 4,4'-isopropylidenephenol which can lead to a less cross-linked network. This latter can have a greater affinity with a non-polar solvent such as BuCl.

However, the most important results are the swelling values in water. All the epoxy networks cured with pure polyamines have a greater swelling value than the epoxy network cured with the commercial system. This latter seems also to be more adapted to our study because none of the results obtained for pure amines are close to 2.5%.

The mechanical resistances of the films were studied in order to evaluate the behavior of the epoxy films regarding to wear and abrasion.

III.3.b.iv. Tribological properties

Tribology tests were performed in order to determine the resistance of the coating to friction. Abrasion in the reactive medium can come from the PVC pellets formed during the suspension polymerization. This test is so a rapid way to predict the resistance of the epoxy coating to this phenomenon ²⁷.

Epoxy films were immersed in water (80 °C) during one day and the friction coefficients (μ) were taken after different times of immersion. These films were then dried and rubbed by a steel ball (10 mm diameter). A CSN tribometer was used, the friction force was 2 N, the rotation speed was 2 cm.s⁻¹ and the number of rotations was 400. The results for the commercial curing system (cured at 150 °C) are shown on figure IV-18.

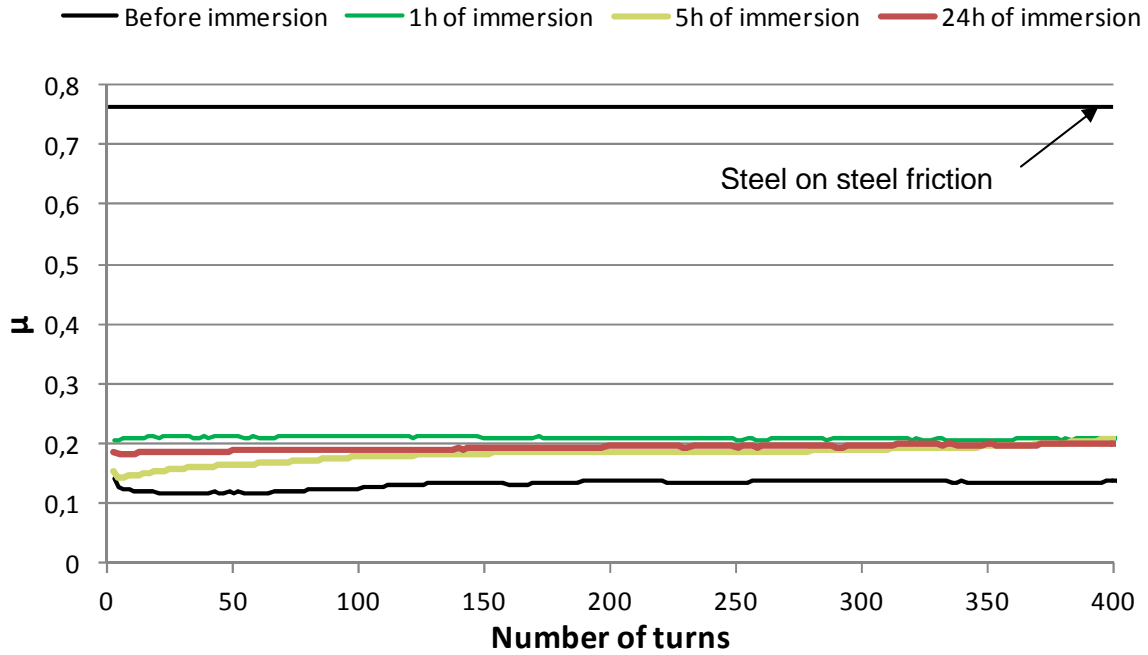


Figure IV-18. Evolution of the friction coefficient (μ) of the RenLam CY 219 / Ren HY 5161 system cured at 150 °C as a function of the immersion time in water (80 °C).

The friction coefficient of pure stainless steel ($\mu = 0.76$) was measured under the same conditions. This value will be used as the limit value obtained in the case of a complete degradation of the coating.

The μ value for the epoxy resin cured with the commercial system is equal to 0.14 before immersion. A slight increase of μ is observed even after a short immersion time but its value is still way under the value of stainless steel. In fact, the μ of a RenLam CY 219 based coating is 0.20 even after a 24 h immersion in water (80 °C). This slight increase of μ is due to the plastifying effect of water which softens the material. However, no delamination of the coating was observed.

A comparison between the Ren HY 5161 system and the other polyamines was made on samples before immersion and after 24 h of immersion. The values presented in table IV-12 correspond to the values after 400 turns, when the friction coefficient is stabilized.

Table IV-12. Evolution of the friction coefficient (μ) of the RenLam CY 219 resin cured with different polyamines before and after immersion in water.

Curing agent	μ (before immersion)	μ (after a 24 h-immersion)
Ren HY 5161	0.14 ± 0.03	0.20 ± 0.05
PEHA	0.60 ± 0.08	0.60 ± 0.07
TETA	0.18 ± 0.05	0.18 ± 0.03
IPDA	0.20 ± 0.04	0.25 ± 0.05
AEPA	0.20 ± 0.03	0.30 ± 0.06
mPDA	0.20 ± 0.02	0.22 ± 0.03

The values obtained for the pure polyamines are a little bit higher than the ones obtained for the Ren HY 5161 system but are still in a suitable range except for PEHA. This compound did not give sufficient wear resistance to the cured epoxy matrix because a great increase of the friction coefficient, caused by a degradation of the film, is rapidly observed. This might be due to the fact that PEHA allowed to obtain a film with a high cross-linking density which might be more brittle than the others.

The abrasion of the coating can also be evaluated by performing optical microscopy on the coatings after tribology tests. The snapshots taken for the RenLam CY 219 / Ren HY 5161 samples are presented on figure IV-19.

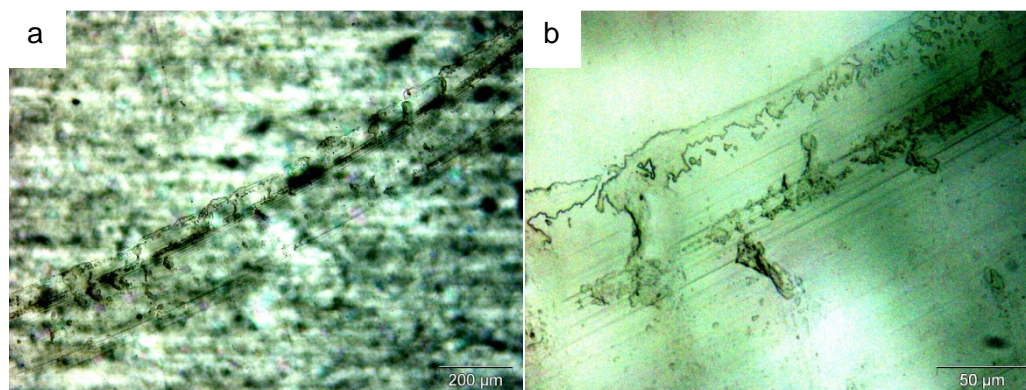


Figure IV-19. Optical microscopy snapshots of RenLam CY 219 / Ren HY 5161 resin samples after tribology tests at enlargements: a. * 100 and b. * 500.

The damages due to the passage of the stainless steel ball are clearly visible. Wrenching of the coating is visible after 400 turns but this process seems to be finished as the friction coefficient is stabilized until 400 turns. That means that wrenching happens rapidly but is not destroying irreversibly the epoxy coating.

Except for PEHA, the RenLam CY 219 resin cured with the tested curing agents has an enough abrasion resistant in order to be durable in a S-PVC reactor.

III.4. Conclusion

The results obtained for pure amines are quite interesting. As a matter of fact, these compounds permit to obtain fully cured RenLam CY 219 resin films with higher T_g than the commercial system. However, the aspects of the free films obtained may sometimes be poor notably for HEDA, PEHA and mPDA. These amines were cancelled. AEPA was cancelled as well because of its poor results regarding to swelling in the modeling solvents. IPDA was finally kept for tests as a curing agent for the RenLam CY 219-based epoxy coating.

All the analyses done previously allowed to select the systems that seem more suitable in terms of properties of the final film. To sum up, three systems were selected to undergo tests in the pilot reactor:

- The RenLam CY 219 / Ren HY 5161 system cured at 150 °C.
- The Araldite DBF CH / Ren HY 956 system cured at 150 °C.
- The RenLam CY 219 / IPDA system cured at 150 °C.

IV. Pilot tests performed on epoxy free films

The experiments in the pilot reactor were made to evaluate the behavior of the tested epoxy systems as free films in the reactive medium. To do so, epoxy free films were immersed in the pilot reactor and classical S-PVC batches were run. The samples were removed after 1 or 2 batches and were then analyzed by simply visual evaluation and by optical microscopy. Three samples were selected to undergo this test: the two commercial systems and the RenLam CY 219 / IPDA system which was the one exhibiting the best results for the model polyamines.

IV.1. Free films of the RenLam CY 219 / Ren HY 5161 system

Three free films were introduced in the pilot reactor for reproducibility purposes. These three free films were a bit thicker ($L = 70 \text{ mm} / l = 30 \text{ mm} / e = 20 \text{ mm}$) than the one classically used for the other characterization tests but the method for preparing these samples was similar to the one used above (Ch II, III.).

These films were immersed in the pilot reactor in order to check the resistance of the RenLam CY 219 / Ren HY 5161 epoxy free films regarding to encrusting. Two polymerizations were made on these samples. Pictures and microscopy snapshots of the samples before and after immersion are shown on figure IV-20.

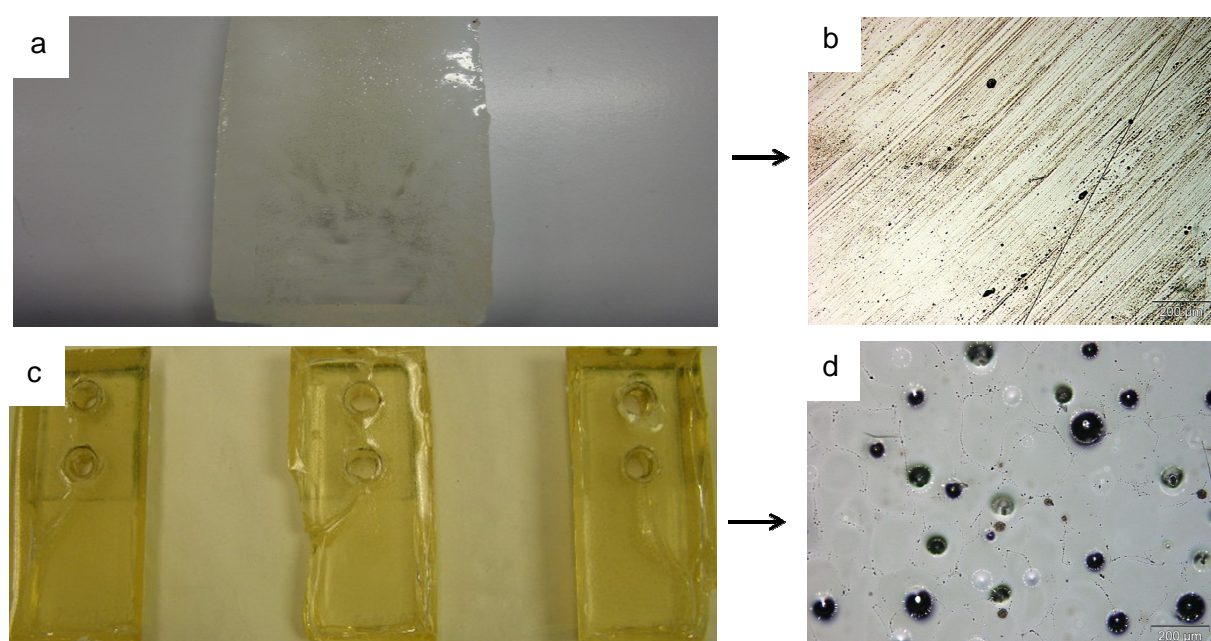


Figure IV-20. Pictures and microscopy snapshots of the RenLam CY 219 / Ren HY 5161 system before (a and b) and after (c and d) two polymerizations.

The general aspect of the films before immersion is good. It is well cured and the upper skin of the film is smooth. That means that mechanical anchorage of the crust would not likely happen on this type of surface.

After immersion in the pilot reactor for two polymerizations, no crust is visible. Some impacts (maybe made by PVC solid particles) and craters are visible but the aspect of the film's surface is good in general. The same results were obtained for the three samples which means that reproducibility is satisfactory. The behavior of this system's free films is really satisfactory as no encrusting has been noted. It is now necessary to check the adhesion of the RenLam CY 219 system onto stainless steel.

IV.2. Free films of the Araldite DBF CH / Ren HY 956 system

As for the previous system, these free films were a bit thicker ($L = 70 \text{ mm} / l = 30 \text{ mm} / e = 20 \text{ mm}$) but the method for preparing these samples was similar to the one used above (Ch II, III.).

These films were immersed in the pilot reactor in order to check the resistance of the Araldite DBF CH / Ren HY 956 epoxy free films regarding to encrusting. Two polymerizations were made on these samples. Pictures and microscopy snapshots of the samples before and after immersion are shown on figure IV-21.

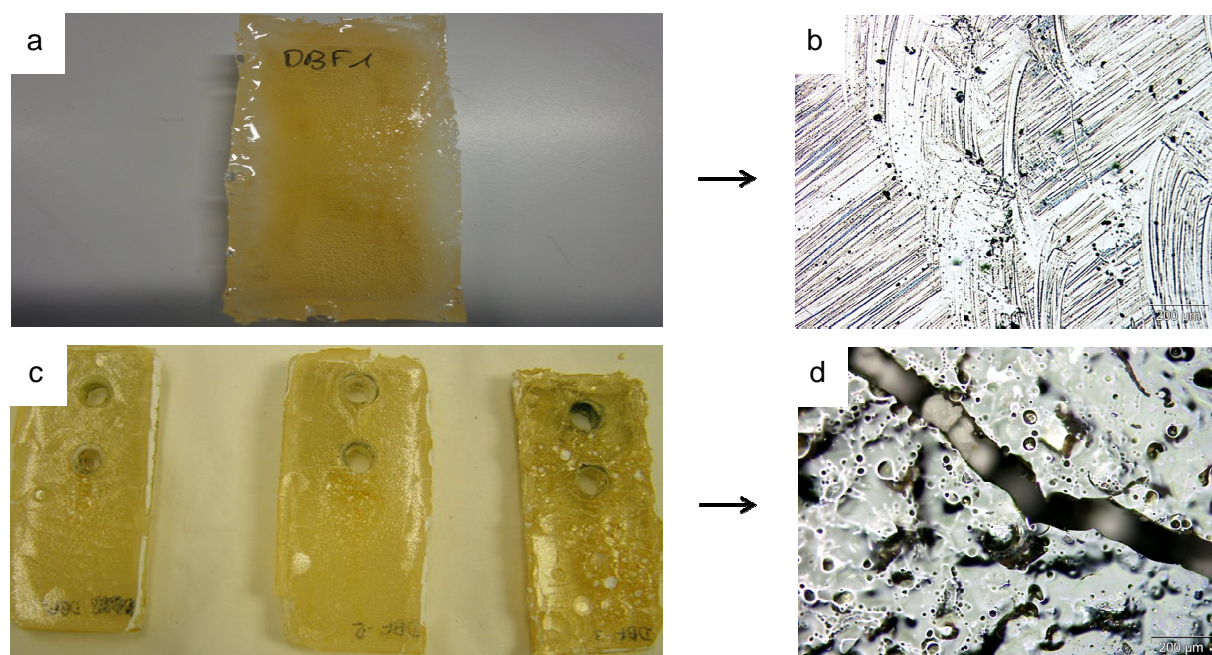


Figure IV-21. Pictures and microscopy snapshots of the Araldite DBF CH / Ren HY 956 before (a and b) and after (c and d) two polymerizations.

The general aspect of the films before immersion is good. It is well cured and the upper skin of the film is smooth. That means that mechanical anchorage of the crust would not likely happening on this type of surface.

After immersion in the pilot reactor for two polymerizations, the aspect of the film has been degraded. Some deep cracks are visible and little PVC pellets are adsorbed at the surface. This is considered as the beginning of the encrusting process so the behavior of this system's free films is not adapted to our study.

IV.3. Free films of the RenLam CY 219 / IPDA system

These samples were prepared by using the curing conditions presented earlier (Chapter IV, III. 2. b.). These films were immersed in the pilot reactor in order to check the resistance of the IPDA-cured RenLam CY 219 epoxy free films regarding to encrusting. One polymerization was made on these samples. Pictures of the samples after immersion are shown on figure IV-22.

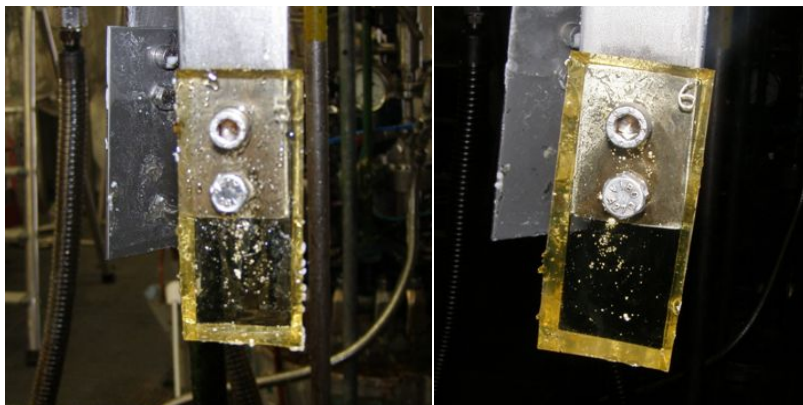


Figure IV-22. Pictures of IPDA-cured RenLam CY 219 free films after one polymerization.

The aspect after immersion is good as no significant encrusting is observed. However, a slight deposit is observed at certain points on the epoxy films. This mainly comes from the fact that the film aspect is not as smooth as the ones obtained with the Ren HY 5161 system. As a matter of fact, IPDA is one of the major components of the commercial curing system of the RenLam CY 219 resin. The properties of the film regarding to swelling in modeling solvents and encrusting resistance are quite similar. The difference is that the commercial formulation exhibits a better wetting of stainless steel during the application. That means that the coating obtained has a better aspect.

The epoxy resin used for the following of this study was chosen based on these pilot reactor results. Based on these experiments, the RenLam CY 219 / Ren HY 5161 system was chosen because of its great resistance versus the polymerization medium and the absence of scale at its surface after 2 straight batches.

V. Conclusion

All the tests performed previously showed that an epoxy coating can be a suitable solution as a protective coating against encrusting of the S-PVC reactors.

Two commercial epoxy / curing agent systems were tested under different curing conditions. After validation of the curing conditions, the properties of the obtained films have been evaluated. The best commercial system tested was the RenLam CY 219 / Ren HY 5161 cured at 150 °C.

Tests were also made using the RenLam CY 219 resin with model polyamines as curing agents. The properties of the films synthesized with these molecules were compared with one another and IPDA was chosen as the best solution when pure polyamines are used.

Three samples were so selected to undergo one or two S-PVC batches: the RenLam CY 219 / Ren HY 5161 cured at 150 °C, the Araldite DBF CH / Ren HY 956 cured at 150 °C and the RenLam CY 219 / Ren HY 5161 cured at 150 °C.

All the results tend to show that the RenLam CY 219 / Ren HY 5161 system is the more adapted to our application thanks to low swelling values in water, to a T_g standing in the suitable range, correct resistance against wear and most of all good anti-scale properties. The optimization of the epoxy coating / stainless steel interface, in the following of this report, was done by using this system.

References

- (1) Han, C. D.; Lee, D. *J. Appl. Polym. Sci.* **1987**, *33*, 2859–2876.
- (2) Fan, J. D.; Marinelli, J. M.; Lee, L. J. *Polym. Compos.* **1986**, *7*, 239–249.
- (3) Turi, E. *Therm. Charact. Polym. Mater.*, Elsevier **1981**, 534.
- (4) Raman, A.; Dubey, M.; Gouzman, I.; Gawalt, E. S. *Langmuir* **2006**, *22*, 6469–6472.
- (5) Wu, S.; Brandrup, J.; Immergut, E. H.; Grulke, E. A. *Polymer Handbook, 4th Ed.*; Wiley-Interscience Publishers: New-York **2003**, VI – 521–535.
- (6) Malloy, R. A. *Plast. Part Des. Inject. Molding Introd.*, Hanser Verlag: Munich, **1994**, 439.
- (7) Apicella, A.; Nicolais, L.; Mikols, W. J.; Seferis, J. C. *Interrelat. Process. Struct. Prop. Polym. Mater. Proc. Iupac Int. Symp. Interrelat. Process. Struct. Prop. Polym. Mater.* Elsevier **1984**, 629.
- (8) Tcharkhtchi, A.; Bronnec, P. Y.; Verdu, J. *Polymer* **2000**, *41*, 5777–5785.
- (9) Pethrick, R. A.; Hollins, E. A.; McEwan, L.; Pollock, A.; Hayward, D.; Johncock, P. *Polym. Int.* **1996**, *39*, 275–288.
- (10) Perrin, F. X.; Hanh Nguyen, M.; Vernet, J. L. *Eur. Polym. J.* **2009**, *45*, 1524–1534.
- (11) Adamson, M. J. *J. Mater. Sci.* **1980**, *15*, 1736–1745.
- (12) Hong, S. *Modélisation de Dispersions Eau-Vcm-Pvc En Présence de Tensio-Actifs Macromoléculaires À Base de Pva*, Thesis n°029FR2005MULH0784, **2005**, Université de Haute-Alsace, France.
- (13) Garcia, F. G.; Soares, B. G.; Pita, V. J. R. R.; Sánchez, R.; Rieumont, J. *J. Appl. Polym. Sci.* **2007**, *106*, 2047–2055.
- (14) Vanlandingham, M. R.; Eduljee, R. F.; Gillespie Jr., J. W. *J. Appl. Polym. Sci.* **1999**, *71*, 699–712.
- (15) Wang, H.; Wang, H.; Zhou, G. *Polym. Int.* **2011**, *60*, 557–563.
- (16) Su, W.; Huang, H.; Pan, W. *Thermochim. Acta* **2002**, *392-393*, 391–394.
- (17) Lou, C.; Xianzhi, K.; Jianxin, W.; Liqun, M. *J. Appl. Polym. Sci.* **2012**, *125*, 578–583.
- (18) Garcia, F. G.; Soares, B. G. *Polym. Test.* **2003**, *22*, 51–56.
- (19) Shalati, M. D.; McBee, J. H.; DeGooyer, W. J.; Thys, F.; van der Ven, L.; Leijzer, R. T. *Prog. Org. Coatings* **2003**, *48*, 236–250.
- (20) Ellis, B. *Chemistry and technology of epoxy resins*; Blackie Academic & Professional: London, **1993**, 1-60.
- (21) Gerlitz, M. *Fundamentals of epoxy coatings*; Pre-congress tutorial - European Coatings Show, **2013**.

- (22) Nguyen, T. M. H. *Systèmes Époxy-Amine Incluant Un Catal. Externe Phénolique Cinétique Réticulation-Vieil. Hydrolytique*, Thesis, **2007**, Université du Sud Toulon Var, France.
- (23) Liu, Z.; Zhang, G.; Liu, Z.; Sun, H.; Zhao, C.; Wang, S.; Li, G.; Na, H. *Polym. Degrad. Stab.* **2012**, *97*, 691–697.
- (24) Nielsen, L. E. *J. Macromol. Sci. Part C Polym. Rev.* **1969**, *3*, 69–103.
- (25) Bussu, G.; Lazzeri, A. *J. Mater. Sci.* **2006**, *41*, 6072–6076.
- (26) Bieleman, J. *Additives for Coatings*; John Wiley & Sons: New-York, **2008**, 250.
- (27) Larsen, T. Ø.; Andersen, T. L.; Thorning, B.; Horsewell, A.; Vigild, M. E. *Wear* **2007**, *262*, 1013–1020.

Chapter V

-

*Adhesion of the Epoxy Coating
onto Stainless Steel*

CHAPTER V: ADHESION OF THE EPOXY COATING ONTO STAINLESS STEEL

I. Introduction	175
II. Non-optimized epoxy / stainless steel interface	175
II.1. Application of the coating	176
II.2. Immersion tests in model solvents	176
II.3. Conclusion.....	177
III. Cleaning of stainless steel.....	177
III.1. Presentation of the cleaning methods.....	177
III.2. Validation of the cleaning process	178
III.3. Immersion tests in model solvents.....	181
III.4. Conclusion.....	182
IV. Mechanical treatment.....	182
IV.1. Presentation of the shot-blasting process.....	182
IV.2. Characterization of the shot-blasted stainless steel surface.....	183
IV.3. Immersion test in model solvents.....	185
IV.4. Conclusion.....	187
V. Grafting of adhesion promoters onto stainless steel	187
V.1. Grafting of phosphonates, bisphosphonates and sulfonates onto stainless steel.....	188
V.1.a. Functionalization of stainless steel plates	188
V.1.b. Use of these molecules as coupling agents	189
V.2. Grafting of alkoxysilanes onto stainless steel: Influence of the non-hydrolyzable functional group of an alkoxysilane on its grafting onto stainless steel	189
V.2.a. Influence of the pH.....	190
V.2.b. Prehydrolysis duration	207
V.3. Influence of the number of hydrolyzable groups of the alkoxysilane on its grafting onto stainless steel	209
V.3.a. Hydrolysis study.....	210
V.3.b. Grafting of monoalkoxysilanes onto stainless steel.....	213
V.4. Conclusion.....	214
VI. Impact of the surface pre-treatments on the adhesion of the epoxy coating onto stainless steel.....	214
VI.1. Non-optimized epoxy / stainless steel interface.....	215
VI.2. Impact of the mechanical treatment.....	217

VI.3. Effect of adhesion promoters	218
VI.3.a. Influence of the non-hydrolyzable functional group	218
VI.3.b. Influence of the prehydrolysis duration	220
VI.3.c. Influence of the number of hydrolyzable groups	221
VI.4. Combination of mechanical treatments and adhesion promoters.....	223
VI.5. Conclusion.....	224
VII. Validation - pilot tests.....	224
VII.1. Non-optimized epoxy / stainless steel interface.....	224
VII.2. Effect of the mechanical treatment	225
VII.3. Effect of adhesion promoters	226
VII.3.a. Influence of the non-hydrolyzable functional group	227
VII.3.b. Influence of the number of hydrolyzable groups	228
VII.4. Combination of mechanical treatments and adhesion promoters.....	229
VII.5. Conclusion – Selection of a system	230
VIII. Conclusion	231
References.....	232

I. Introduction

A suitable epoxy coating has been chosen in the previous chapter in terms of bulk and surface resistance regarding to the scale formation. This system is the RenLam CY 219 / Ren HY 5161 system cured at 150 °C during 1h.

The next step is now to obtain a satisfactory adhesion of the coating on the stainless steel substrate. The establishment of stable and strong interactions between stainless steel and the coating is essential to obtain a durable anti-scale coating. The adhesion of epoxy coatings onto stainless steel is usually very strong under ambient air conditions. However, this same interface can be very sensitive regarding to hydrolysis in an aqueous medium (which is the case during the S-PVC synthesis). Penetration of water happens at the epoxy / stainless steel interface causing the formation of blisters which can lead to a delamination of the coating¹⁻⁵.

This chapter is dedicated to the optimization of the epoxy / stainless steel interface in order to reach the higher adhesion forces and to obtain a durable anti-scale polymer coating. To do so, a three-step strategy was used:

- A cleaning of the stainless steel plates in order to remove the contamination layer.
- A mechanical treatment to improve the mechanical anchorage of the epoxy coating.
- The use of coupling agents to form strong covalent bonds between the coating and the substrate.

The influence of each of these three treatments is discussed regarding to their consequences on the stainless steel surface but also in terms of benefits on the adhesion before and after immersion in hot water. Finally, tests in pilot reactor were made on the best systems to determine their resistance in the real VCM polymerization medium and to choose the most performing one.

II. Non-optimized epoxy / stainless steel interface

These first tests were performed on stainless steel plates that were used as received in order to check the evolution of the adhesion improvement for each step of the optimization strategy used.

II.1. Application of the coating

The coatings were prepared by mixing the RenLam CY 219 epoxy resin with the Ren HY 5161 curing agent (in the respectively 2 / 1 w / w ratio recommended by the supplier). This solution is manually stirred to obtain a homogeneous blend. The coating is finally applied by using a painting brush (obtaining of a dried-film-thickness of 200 μm). The final step is the curing of the coated plate during 1 hour at 150 $^{\circ}\text{C}$.

After application of the epoxy system, the coated stainless steel plates were immersed in model solutions in order to evaluate the adhesion of the coating at a laboratory scale. Again, the solvents used are water and 1-chlorobutan (BuCl).

II.2. Immersion tests in model solvents

The immersion tests were performed in hot BuCl (75 $^{\circ}\text{C}$) which is modeling vinyl chloride monomer and also in hot water (80 $^{\circ}\text{C}$), which is the dispersive liquid for the suspension polymerization of VCM.

The coated stainless steel samples were let in these solvents during seven days and their aspects were looked after drying in ambient air. Pictures of epoxy-coated stainless steel plates before and after immersion in BuCl and in water are presented on figure V-1.

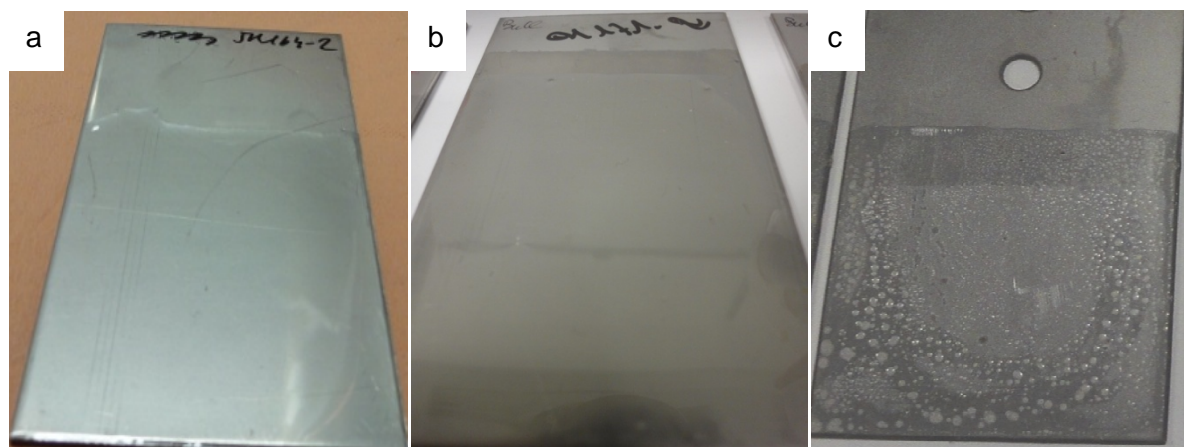


Figure V-1. Picture of a non-cleaned stainless steel plate coated with the RenLam CY 219 / Ren HY 5161 system: a. before immersion, b. after immersion in BuCl (75 $^{\circ}\text{C}$), c. after immersion in water (80 $^{\circ}\text{C}$).

First, it is interesting to note that the aspect of the coating before immersion is uniform. This means that the selected epoxy system provides a good wetting of the substrate even without

previous cleaning. This point is of major importance as the obtaining of a well coated substrate is the first step towards a performing polymer coating.

Secondly, the result obtained after immersion in BuCl is satisfactory as no deterioration of the epoxy / stainless steel surface is observed. This fact was expected as the organic solvents are not so critical regarding to this interface even if swelling tests proved that the epoxy thermoset network is swollen by BuCl. This phenomenon does not seem to influence the adhesion of the coating. In fact, immersion tests performed in BuCl were cancelled at this point because this experiment does not allow to differentiate the samples exhibiting poor or satisfactory adhesion.

The immersion in water is more problematic as the formation of blisters is observed. However, this treatment does not lead to a spontaneous delamination of the coating under these conditions. The blisters always start from a weakness point of the epoxy / stainless steel interface and then propagate to the entire immersed coating. This is mainly due to the diffusion of water at the interface because of the weak interactions (mechanical anchorage and polar interactions) between epoxy and stainless steel. It is at this point clear that such a non-optimized coating would not be durable for our application. However, this system was tested in the pilot reactor as a reference (Ch.5, VII., 1.).

II.3. Conclusion

The immersion tests of stainless steel plates coated with the RenLam CY 219 / Ren HY 5161 system showed that reinforcement of the epoxy / stainless steel interface is necessary. The immersion tests performed in model liquids showed that the immersion in water is more severe than the tests performed in BuCl. As a matter of fact, experiments performed in water led to the rapid formation of blisters at the epoxy / substrate interface meaning that it must be optimized in order to sustain in the S-PVC reactors.

III. Cleaning of stainless steel

III.1. Presentation of the cleaning methods

Cleaning of stainless steel plates before the coating application is necessary in order to remove the undesired contamination layer (mainly composed of hydrocarbonated

compounds) at the surface of this material. This pollution film does not allow a good wetting of the coating and the access to the reactive functions at the surface of steel which will be useful in order to obtain chemical bonding. Several surface treatments are available but the focus was made on simple methods.

Different approaches were tested:

Method A: wet tissue of acetone.

Method B: wet tissue of acetone and a dichloromethane ultrasonic bath.

Method C: wet tissue of acetone and a citric acid ultrasonic bath.

Method D: wet tissue of acetone and a caustic soda ultrasonic bath.

All the plates were then dried at 110 °C during 5 minutes. Contact angle measurements were performed in order to determine the most efficient method.

III.2. Validation of the cleaning process

Water was used as a polar liquid for contact angle measurements. The cleaning method kept will be the one with the lowest contact angle (corresponding to an increase of the hydrophilic character of the surface) because it means that the contamination layer at the surface of stainless steel is removed. The results, presented in table V-1, are averages on 8 values.

Table V-1. Water contact angles for stainless steel plates cleaned by different methods.

Method	θ_{eau} (°)
No cleaning	69 ± 3
A	56 ± 7
B	46 ± 3
C	67 ± 12
D	66 ± 5

Values obtained for methods C and D are quite similar to the one obtained without any cleaning. The values obtained are quite astonishing as the first step, cleaning with an acetone wet tissue, should lead to a contact angle value similar to the one obtained with method A. This latter is an easy and rapid way to decrease the contact angle of the surface with water but the best results are observed with method B. The decrease of the contact

angle with water shows that the polar groups at the steel's surface are more available for the anchorage of a coating. The lower the contact angle value with water, the higher the polarity of the surface and the higher the wetting of the surface by the coating. The values obtained for method B are quite similar to values obtained in the literature for 316L stainless steel ⁶. Method B will be retained as the cleaning method for the following of this study.

This method was validated by X-Ray Photoelectron Spectroscopy (XPS). A general scan was made to identify the elements of the cleaned stainless steel surface. The Al-K α radiation source was used to realize the spectrum presented on figure V-2.

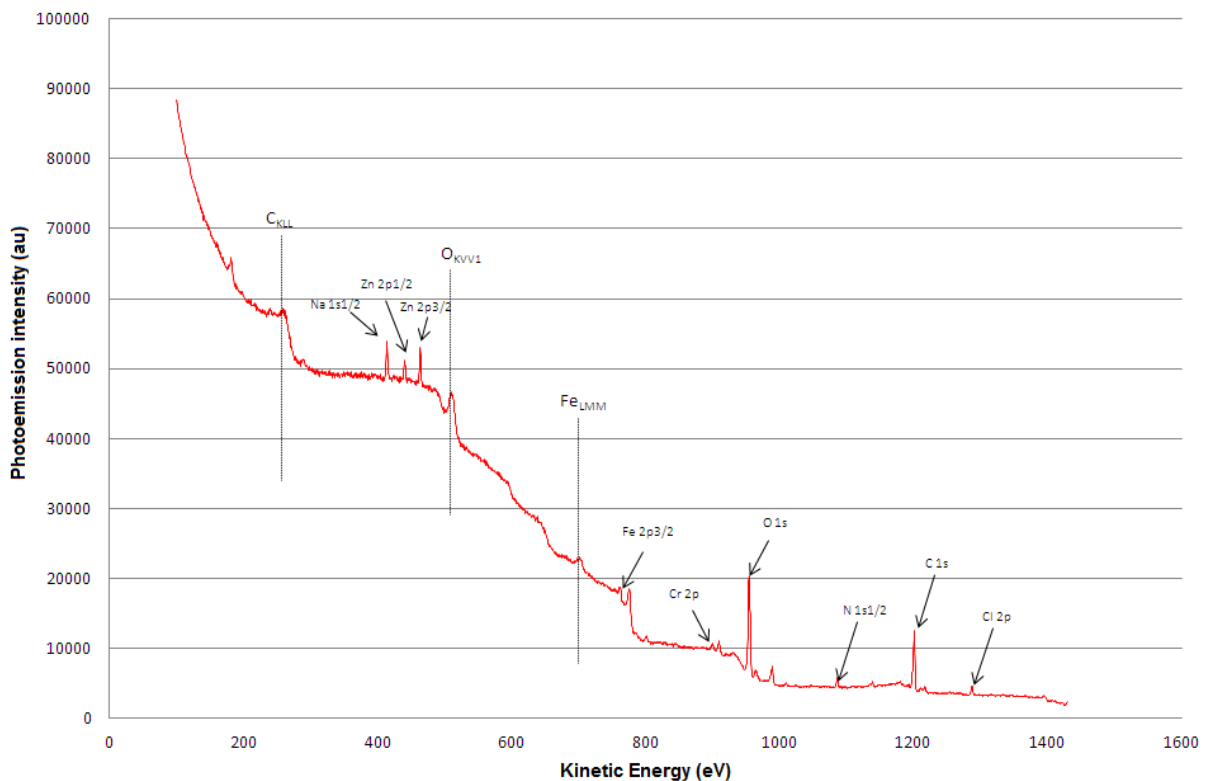


Figure V-2. XPS spectrum of cleaned stainless steel.

The presence of core level peaks from the Fe, Cr, O and C is consistent with the elements present in the stainless steel ^{7,8}. These peaks are visible because these elements are present in the upper oxide layer covering stainless steel. The two peaks with the highest intensity are the O 1s and the C 1s. These peaks are visible because the XPS analysis only concerns the upper oxide layer or passivation layer covering the stainless steel. As the two main metallic elements composing the oxide layers are known to be iron and chromium, spectral decomposition has been performed for the Fe 2p_{3/2} peak (figure V-3, a) and for the Cr 2p peak (figure V-3, b).

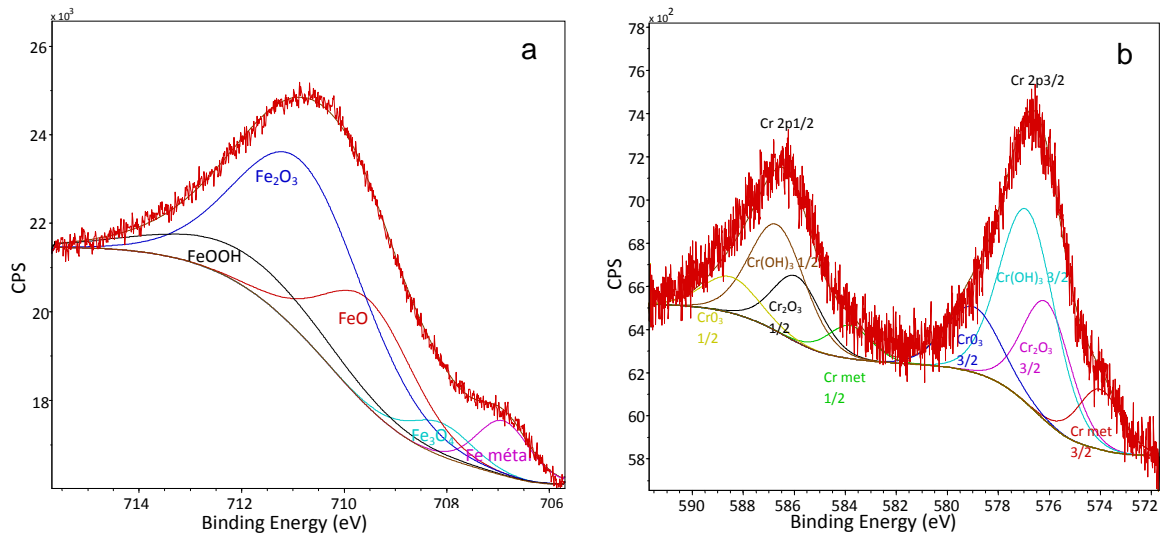


Figure V-3. XPS spectra zoom on the Fe 2p_{3/2} peak (a) and the Cr 2p peak (b).

The different components obtained from the spectral decompositions for both peaks are listed in table V-2.

Table V-2. Spectral decomposition for the Fe 2p_{3/2} and Cr 2p peaks.

Element	Component	Position (eV)	Reference
Fe	Fe metal	706.8	9
	Fe ₃ O ₄	708.1	10
	FeO	709.6	11
	Fe ₂ O ₃	710.8	10
	FeOOH	711.8	12
Cr	Cr metal	574.1	13
	Cr ₂ O ₃	576.1	13
	Cr(OH) ₃	576.8	13
	CrO ₃	578.9	13
	The gap between the peaks is 9.8 eV		

The Fe 2p_{3/2} peak contains numerous iron oxide components (Fe₃O₄, FeO, Fe₂O₃, FeOOH) and also the metallic contribution. This result confirms the presence of a high amount of iron oxides on the surface, with iron being at different oxidation states.

The Cr doublet, presented on figure V-3, b (with both Cr 2p_{1/2} and 3/2 contributions), shows that chromium is visible at the stainless steel surface, as iron, under its metallic form but mainly under oxidized forms like Cr₂O₃, CrO₃ and Cr(OH)₃. This result is consistent with

the supposed oxide-rich composition of the passivation layer, responsible of the anti-oxidizing properties of this material.

Both contact angle measurements and XPS proved that the cleaning method used is efficient and allows the access to the surface reactive functions (iron and chromium oxides). Cleaned stainless steel plates were then coated with the RenLam CY 219 / Ren HY 5161 system to check the effect of cleaning on the adhesion of the coating.

III.3. Immersion tests in model solvents

Cleaning of stainless steel stands for the removal of the laminating oils present at this substrate's surface. Removing this pollution enables greater interactions between the coating and stainless steel leading to a more efficient adhesion. Immersion tests were performed in water in order to check if the cleaning is sufficient to provide good adhesion of the coating. Samples before and after immersion in water are shown on figure V-4.

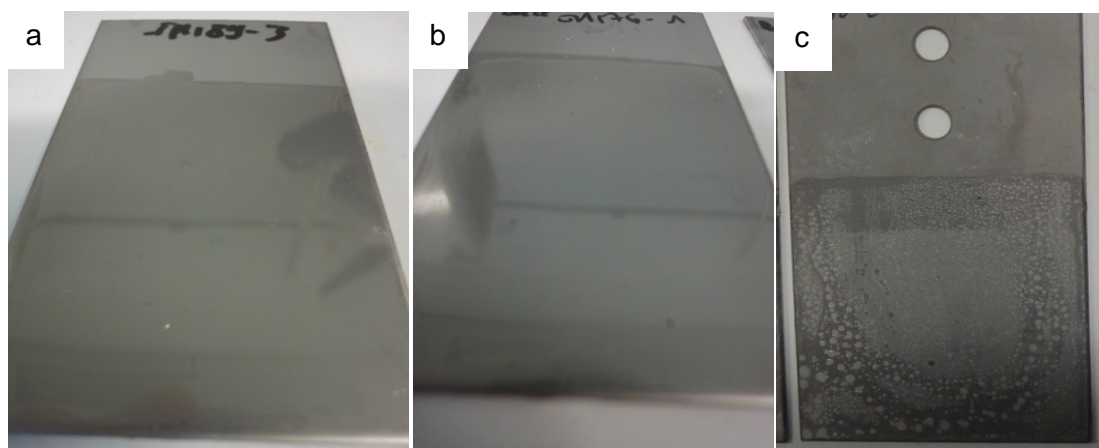


Figure V-4. Picture of a cleaned stainless steel plate coated with the RenLam CY 219 / Ren HY 5161 system: a. before immersion, b. after immersion in BuCl (75 °C), c. after immersion in water (80 °C).

Again, the aspect of the coatings obtained before immersion is very good. By removing the laminating oils layer, a greater number of polar interactions will be produced leading to a stronger adhesion. However, this is not sufficient as the immersion of the epoxy-coated stainless steel plate into water still leads to the formation of blisters. This is due to the fact that the adhesion of the epoxy / stainless steel system is only due to polar interactions. The interactions are sensitive to water whatever their amount and this leads, again, to the penetration of water at the polymer / substrate interface.

III.4. Conclusion

Cleaning of the stainless steel plates was achieved by using consecutively acetone and a dichloromethane ultrasonic bath. Complete removing of the laminating oils was confirmed by both contact angle measurements and XPS.

However, cleaning did not allow a sufficient increase of the adhesion of the epoxy coating on the substrate as the formation of blisters is again observed after immersion in hot water. This means that the optimization of the epoxy / stainless steel interface has to be continued and this can go through the use of a mechanical treatment before application of the coating.

IV. Mechanical treatment

A mechanical treatment is a way to both complete the surface cleaning of stainless steel but also to increase the surface roughness. As it has been shown previously, the studied epoxy system seems to provide a good wetting of the stainless steel's surface meaning that increasing the roughness must lead to a large enhancement of the mechanical adhesion of the coating.

During this study, a shot-blasting process was selected as a mechanical treatment.

IV.1. Presentation of the shot-blasting process

The shot-blasting treatment was performed by Mäder. During this process, the stainless steel plates were submitted to a high-pressure flow of brown corundum particles. Three particles sizes were tested to obtain a large range of surface roughnesses. For this purpose, some 40, 120 and 220 mesh corundum particles were used. The plates were stored in xylene after treatment in order to avoid important oxidation of the material. The treated stainless steel was cleaned by using the method validated previously (acetone and dichloromethane ultrasonic bath).

The resulting stainless steel surfaces were first analyzed before the application of the epoxy coating.

IV.2. Characterization of the shot-blasted stainless steel surface

The different roughnesses were measured using a Mitutoyo SJ-301 roughness tester. The results obtained after shot blasting are listed in table V-3 and the corresponding scanning electron microscopy (SEM) snapshots are presented on figure V-5.

Table V-3. Roughness values of stainless steel for different shot blastings

Particle size (mesh / μm)	Roughness R_a (μm) Arithmetic mean value	Roughness R_q (μm) Quadratic mean value	Roughness R_z (μm) Ten-point mean
No shot-blasting	0.19 ± 0.05	0.27 ± 0.01	1.60 ± 0.06
220 / 68	0.81 ± 0.11	1.33 ± 0.25	6.70 ± 0.93
120 / 125	1.16 ± 0.10	1.74 ± 0.10	12.80 ± 1.30
40 / 375	4.86 ± 0.18	5.95 ± 0.15	27.00 ± 0.85

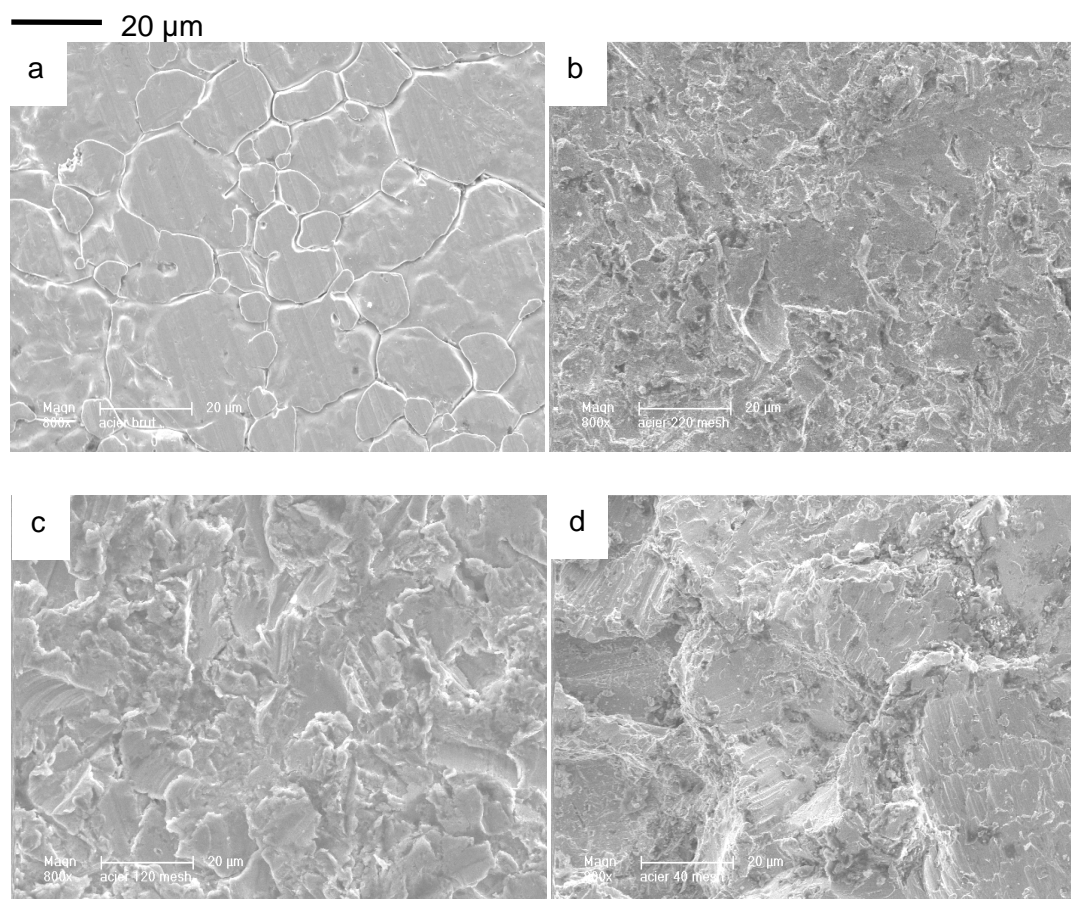


Figure V-5. SEM snapshots of stainless steel after a corundum shot-blasting: a. without shot-blasting, b. with 220-mesh particles, c. with 120-mesh particles, d. with 40-mesh particles.

First, this technique allows the observation of the crude stainless steel surface where its heterogeneity is again observed. Its slight roughness and the presence of various micro-

domains can provide mechanical adhesion of the epoxy coating which is, however, not sufficient for this application.

These results show that, as expected, the higher the corundum size (40 mesh), the higher the stainless steel roughness. These are simple observations but some other tests were made by coupling the SEM technique with the Energy Dispersive X-Ray (EDX) analysis which allows the obtaining of chemical information by characterizing the atoms composing a sample surface. The EDX spectra for each stainless steel samples are presented on figure V-6.

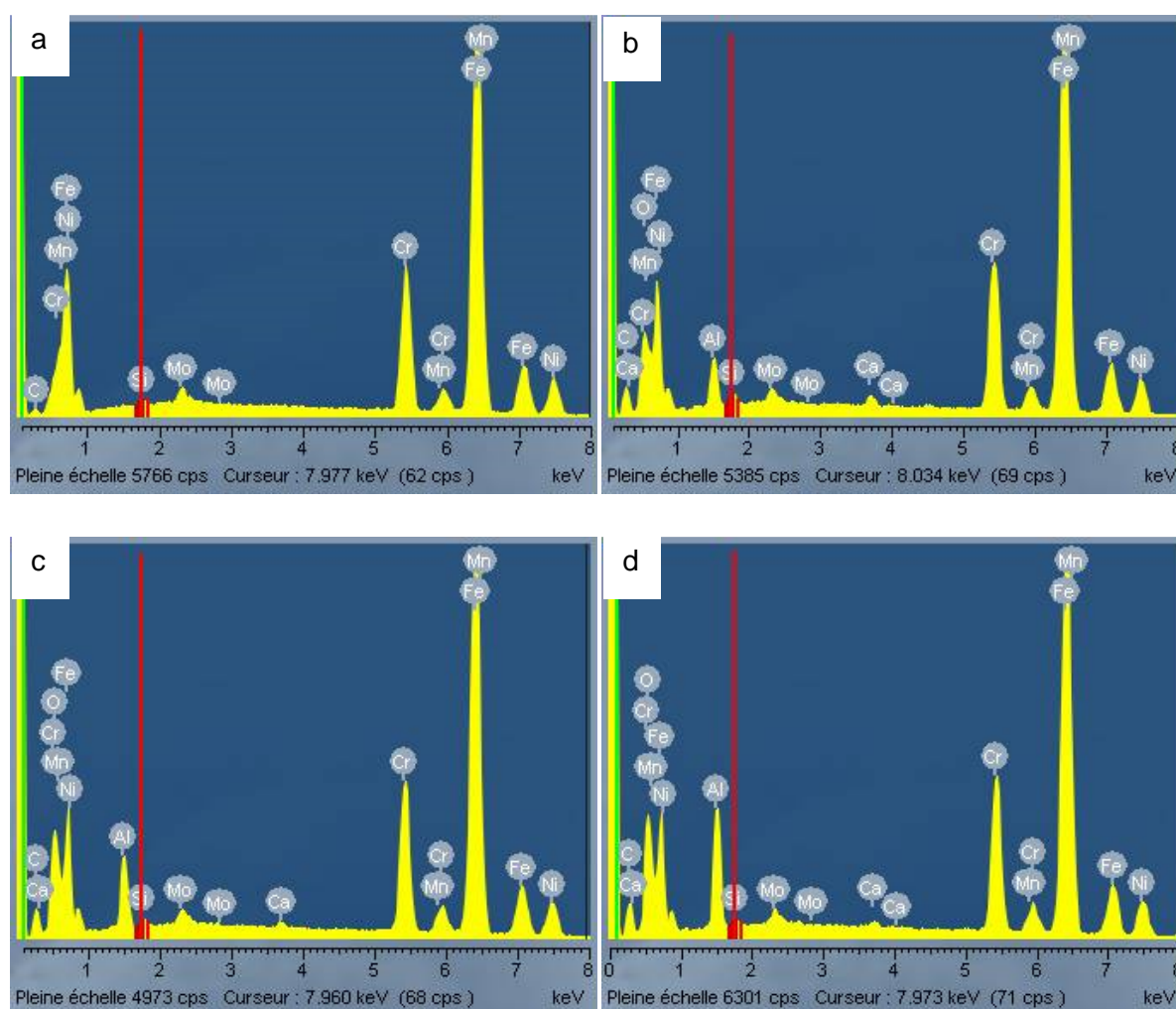


Figure V-6. EDX spectra of stainless steel before and after a corundum shot-blasting: a. without shot-blasting, b. with 220-mesh particles, c. with 120-mesh particles, d. with 40-mesh particles.

For the non-shot-blasted sample, peaks of typical stainless steel elements are observed with mainly iron, chromium and nickel. After the mechanical treatment, the appearance of new peaks has been noted. These new elements at the stainless steel surface are calcium (with two bands of very weak intensities) and mainly aluminum. These peaks are probably due to

the presence of interlocked corundum into stainless steel after the shot-blasting process ¹⁴. The fact that these peaks are still visible after cleaning of the plates with acetone and dichloromethane (ultrasonic bath) shows that these aluminum particles are strongly included in the stainless steel matrix. From that point, one can guess that the shot-blasting process might not only improve the mechanical adhesion of the coating by increasing the surface roughness but the presence of aluminum oxide might also improve the chemical adhesion of the coating. In fact, the aluminum particles surface reactivity is supposed to be quite higher than the one of stainless steel (mainly due to a higher specific surface area). The epoxy coating could be able to establish more interactions with an alumina-containing stainless steel surface. Moreover, a mapping of the aluminum element for the 40 mesh-shot-blasted stainless steel plate is presented on figure V-7. The white dots on the picture correspond to the detected presence of the aluminum element (corresponding to alumina) while the black part stands for the stainless steel matrix.

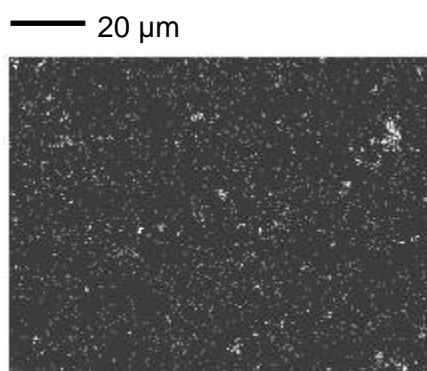


Figure V-7. EDX mapping of the Al element (white dots) on a stainless steel surface (in black) after a 40-mesh corundum shot-blasting.

This result shows a quite homogeneous distribution of the alumina particles on the mechanically treated surface meaning providing an adhesion improvement.

The benefit of this surface treatment on the epoxy / stainless steel adhesion was evaluated during immersion tests.

IV.3. Immersion test in model solvents

The RenLam CY 219 / Ren HY 5161 system was coated onto shot blasted stainless steel plates. These plates were then immersed in water (80 °C) during seven days. The results are listed in table V-4 and showed on figure V-8.

Table V-4. Aspect of the RenLam CY 219 / Ren HY 5161 coated onto shot blasted stainless steel plates after 7 days of immersion in water (80 °C).

Corundum size (mesh / μm)	Roughness R_a (μ)	Aspect of the coating after 7 days in water (80 °C)
No shot blasting	0.19 ± 0.05	Blisters
220 / 68	0.81 ± 0.11	Blisters
120 / 125	1.16 ± 0.10	Blisters
40 / 375	4.86 ± 0.18	Good

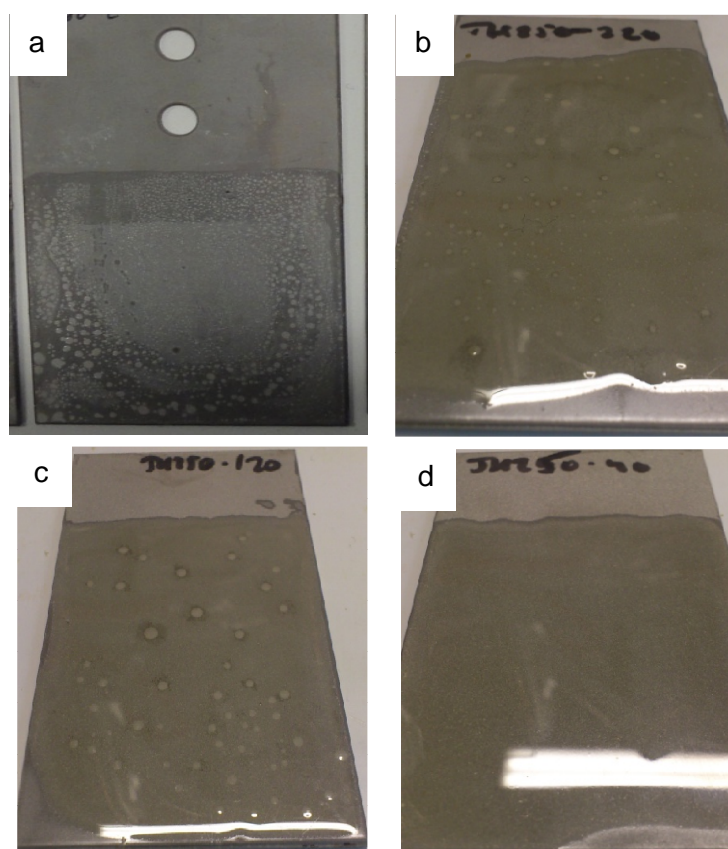


Figure V-8. Visual aspect of the coating applied with a painting brush and after immersion in water (80°C) of the RenLam CY 219 / Ren HY 5161 system on stainless steel: a. no shot blasting, b. 220 mesh shot blasting, c. 120 mesh shot blasting, d. 40 mesh shot blasting.

A significant improvement of the epoxy / stainless steel interface adhesion is observed for the coatings applied on the plate having the greater roughness. The mechanical anchorage of the polymer chains inside the substrate's roughness is really helpful to improve the epoxy / stainless steel interface. Moreover, shot blasting allows to eliminate the contaminant layer at the surface of stainless steel.

However, a shot-blasting with high-diameter particles is necessary in order to obtain a significant improvement. An improvement is visible for the 220-mesh and 120-mesh samples as the number of blisters formed after immersion in water is decreasing but the 40-mesh sample allows the obtaining of a seven-day immersion in hot water with no blisters formation. This result shows the significant role played by the mechanical adhesion mechanism on the stability of the epoxy / stainless steel interface.

IV.4. Conclusion

The benefits of using a corundum shot-blasting as a mechanical treatment for stainless steel have been proven during the last paragraph. This process allows to increase the roughness of the substrate and the SEM-EDX analyses showed that some Al_2O_3 particles are still interlocked in the stainless steel matrix.

Finally, the 40-mesh-shot-blasted stainless steel plates coated with the RenLam CY 219 / Ren HY 5161 system showed a satisfactory behavior during immersion tests in hot water as no blisters were formed.

V. Grafting of adhesion promoters onto stainless steel

Adhesion promoters were used in order to establish a covalent bonding between the epoxy coating and stainless steel. These molecules must have an affinity with both the polymer and the substrate to be efficient.

First, a sulfonate, a phosphonate and a bisphosphonate were tested in terms of grafting and of efficiency as adhesion promoters.

Then, alkoxy silanes were chosen as ideal candidates too. However, there is a large variety of such compounds that is available. First, the non-hydrolyzable functional group has to be chosen as a reactive group able to chemically react with the components of the epoxy / curing agent system. Another changing parameter for alkoxy silanes is the number of hydrolyzable alkoxy groups. The efficiency of trialkoxy silanes, bearing three hydrolyzable alkoxy groups, was compared to the one of monoalkoxy silanes, bearing only one alkoxy group.

The aim of the following part is to check the effect of both the functional group and the number of alkoxy functions on the behavior of these molecules in an aqueous solution but also on their grafting onto stainless steel.

V.1. Grafting of phosphonates, bisphosphonates and sulfonates onto stainless steel

Three molecules were tested as coupling agents on stainless steel: a sulfonate, a phosphonic acid and a bisphosphonic acid (figure V-9).

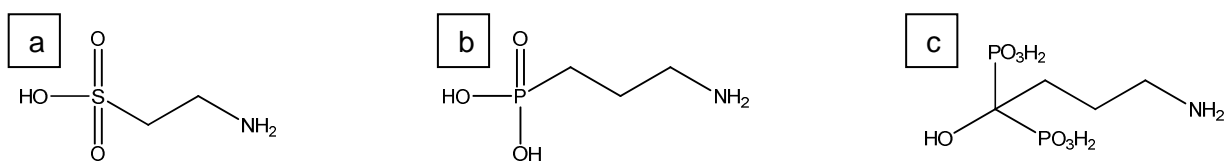


Figure V-9. Chemical formulas of a. taurine; b. 3-aminopropylphosphonic acid; c. 3-aminopropylbisphosphonic acid.

These molecules were chosen as they contain an amine group which will be able to react with the epoxy functions of the coating.

V.1.a. Functionalization of stainless steel plates

Aqueous solutions (at pH = 7) at a concentration of 10^{-3} M of these molecules were prepared and were then deposited onto cleaned stainless steel by dip coating¹⁵. An immersion in a water ultrasonic bath during 10 minutes and a drying step at 80 °C during 30 minutes are finally used. The dip coating and drying steps are repeated twice.

Polarized-Modulated Absorption Reflection InfraRed Spectroscopy (PM-IRRAS), Diffuse Reflectivity InfraRed (DRIFT) and Atomic Force Microscopy (AFM) were used to characterize the functionalized stainless steel surfaces.

No grafting was observed with these techniques for all of these molecules onto cleaned stainless steel plates. Different parameters of the application methods were varied (pH, concentration of the molecules, immersion time, drying method, type of rinsing and solvent used). Still, no grafting was observed onto stainless steel.

V.1.b. Use of these molecules as coupling agents

These molecules were however tested as coupling agents onto cleaned non-shot-blasted stainless steel and then covered of epoxy coating (RenLam CY 219 and curing agent Ren HY 5161). No improvement of the adhesion was observed as blisters were rapidly visible after immersion in hot water (80 °C). This definitely proves that no grafting of the coupling agents has been obtained. The utilization of these molecules was stopped as no significant results have been achieved and alkoxy silanes were then tested.

V.2. Grafting of alkoxy silanes onto stainless steel: Influence of the non-hydrolyzable functional group of an alkoxy silane on its grafting onto stainless steel

This first part of the study was made by comparing the behaviors of trialkoxysilanes with different functional groups. These latter were chosen as able to react with the epoxy resin or with the amine groups of the curing agents. For this purpose, trialkoxysilanes bearing amine, epoxy or succinic anhydride functions were chosen (figure V-10).

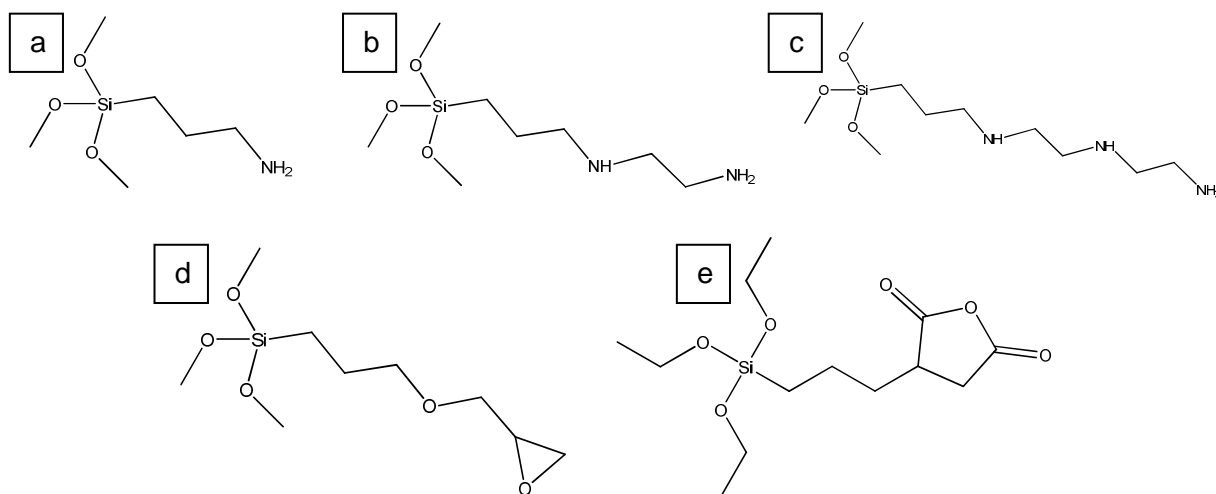


Figure V-10. Chemical formula of: a. 3-aminopropyl(trimethoxysilane) (APTS), b. N-[3-(Trimethoxysilyl)propyl]ethylenediamine (AAPS), c. N-(3-Trimethoxysilylpropyl) diethylenetriamine (TPDTA), d. (3-glycidyloxypropyl)trimethoxysilane (GPTMS), e. 3-(triethoxysilyl)propylsuccinic anhydride (TPSA).

It is interesting to note that four of these compounds exhibit methoxy functions (APTS, AAPS, TPDTA and GPTMS) compared to TPSA which has hydrolyzable ethoxy functions. This fact has an impact on the hydrolysis step of these molecules as this reaction is slower

with ethoxy functions than with methoxy ones ¹⁶. The prehydrolysis duration of TPSA may have to be adjusted in order to be sure to reach a reasonable amount of silanols formed.

Two key parameters for a trialkoxysilane prehydrolysis and grafting are the pH and the prehydrolysis duration.

V.2.a. Influence of the pH

The pH plays a major role during the deposition of trialkoxysilanes onto stainless steel. Its influence is mainly felt during the prehydrolysis step as the hydrolysis (formation of reactive silanols) / condensation (formation of a siloxane network) balance of trialkoxysilanes is totally controlled by the pH. There are also some consequences on the grafting onto a substrate as silanols are necessary to obtain the formation of a stable alkoxy silane bridge providing water-barrier properties.

However, it seems that the non-hydrolyzable functional group on the trialkoxysilane molecules plays a role on the hydrolysis / condensation balance by influencing the reactivity of the silicon atom.

V.2.a.i. Hydrolysis step

This step is crucial to obtain an efficient grafting of trialkoxysilanes onto a substrate as silanols are formed during this reaction. However, these species are highly reactive and can react between each other to form a siloxane network. This latter is less mobile and less reactive and does not provide efficient bond formation with a substrate.

An effective way to stabilize the formed silanols is to play on the solution's pH. As a matter of fact an acid medium is known as a stabilizing factor for silanols while a basic medium favors the condensation reaction ¹⁷.

An alkoxy silane (2% w / w) prehydrolysis takes place in a 95 / 5 (w / w) ethanol / water mixture at a controlled pH (use of acetic acid for an acid medium and caustic soda for a basic medium). The alkoxy silane is then poured into this solution during one hour to allow the hydrolysis to progress. The studied trialkoxysilanes were hydrolyzed during 1 h and a droplet of the solution was deposited on a silver bromide pellet and dried at 60 °C during 1 h. The resulting AgBr pellets were then analyzed by Transmission InfraRed spectroscopy (T-IR).

- *Aminosilanes*

A comparison of the T-IR spectra of TPDTA before and after prehydrolysis at pH = 2 is shown on figure V-11. Normalization and scaling were performed relative to the $\nu_{\text{as}}(\text{CH}_2)$ vibration mode at 2939 cm^{-1} because this one is not modified by the prehydrolysis process.

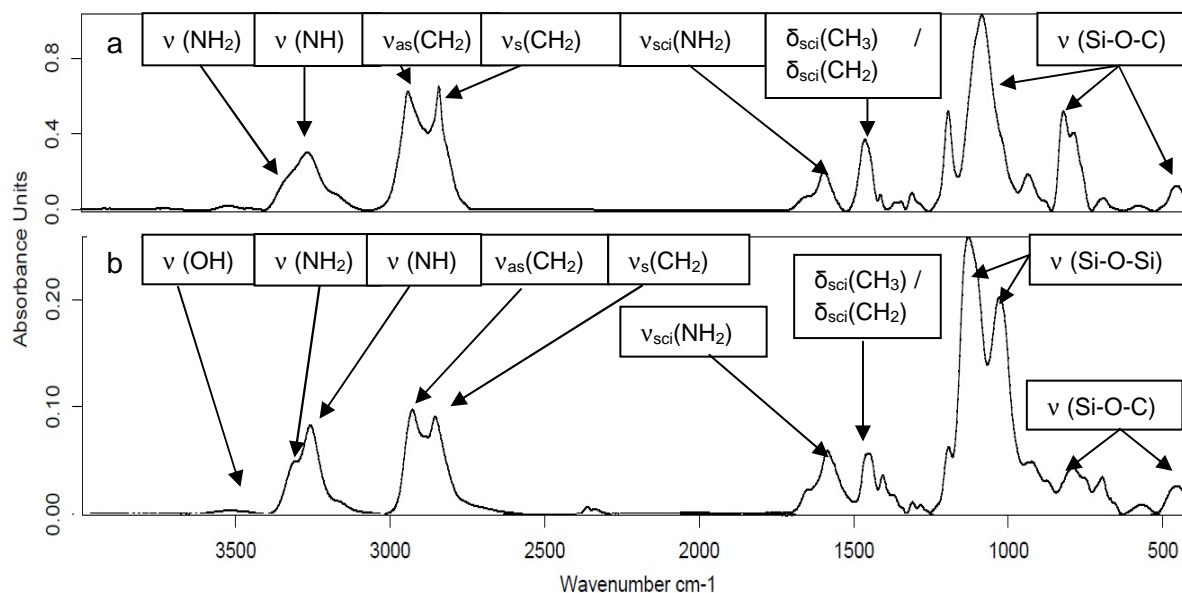


Figure V-11. T-IR spectra of TPDTA before (a) and after (b) prehydrolysis (at pH 2).

The hydrolysis of an aminosilane leads to the appearance of two strong and wide Si-O absorption bands (1128 and 1037 cm^{-1}) characteristic of the formation of siloxane (Si-O-Si) bonds. Moreover, some specific vibration modes of silanol functions are visible at 3500 cm^{-1} and 942 cm^{-1} . That means that the methoxy groups of the aminosilane are partially hydrolyzed into silanol groups (presence of Si-O-C vibration modes at 815 and 470 cm^{-1}). These functions are not highly stable in an aqueous solution and will lead to the formation of siloxane bonds. The presence of silanol groups is also needed because they will be useful regarding to the formation of covalent bonds between the aminosilane and the surface. It is also important to see that the primary and secondary amine characteristic absorption modes are still visible and available to form an aminated stainless steel surface when adsorbed. Moreover, the relative intensity of the amine stretching mode region (3200 - 3400 cm^{-1}) compared to the methylene and methyl groups stretching (2800 - 3000 cm^{-1}) and deformation (1460 cm^{-1}) regions increases as prehydrolysis occurs. This confirms the elimination of the methyl groups of the trimethoxy functions while hydrolysis reaction progresses. A slight shift of the $\delta_{\text{si}}(\text{CH}_3) / \delta_{\text{si}}(\text{CH}_2)$ vibration mode is observed after prehydrolysis leading to a decrease of their absorption wavenumber (from 1457 to 1452 cm^{-1}). This peak is also

composed of the $\delta_{\text{sci}}(\text{CH}_3)$ at 1482 cm^{-1} and the $\delta_{\text{sci}}(\text{CH}_2)$ at 1460 cm^{-1} . The shift observed is due to the decrease of the $\delta_{\text{sci}}(\text{CH}_3)$ contribution compared to the $\delta_{\text{sci}}(\text{CH}_2)$ which is another sign of the transformation of the methoxy groups into silanols.

The FTIR spectra obtained after prehydrolysis of TPDTA at different pH are presented on figure V-12. Normalization and scaling were also made relative to the $\nu_{\text{as}}(\text{CH}_2)$ vibration mode at 2939 cm^{-1} .

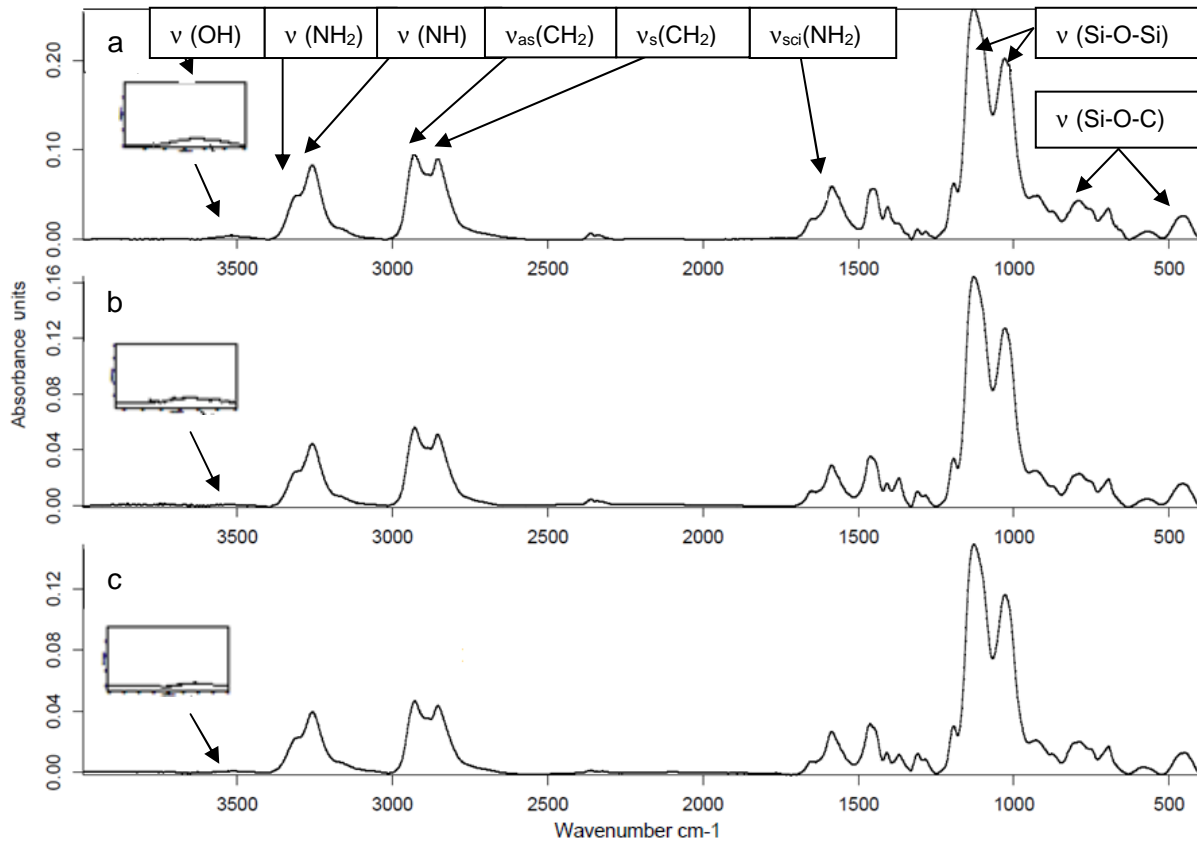


Figure V-12. T-IR spectra of prehydrolyzed TPDTA at: a. pH=2; b. pH=7; c. pH=12.

The formation of siloxane (Si-O-Si) bonds is observed whatever the pH. The formation of such a network is happening because of the heating period which is necessary to remove the solvent (ethanol and water) ¹⁶. This fact can explain the formation of a siloxane network regardless to the pH and the spectra obtained are not totally representative of the alkoxy silane solution. However, as the samples are all analyzed after the same drying conditions, it is possible to compare the intensities of the silanol characteristic vibration modes as a function of the prehydrolysis pH.

There are few differences between the vibration modes obtained whatever the pH. A slight difference in the intensities (normalization made on the CH_2 asym str vibration at 2939 cm^{-1})

of the Si-OH peak (-OH stretching vibration mode at 3500 cm^{-1}) is observed as this integrated intensity decreases with the increase of the pH as presented on figure V-13.

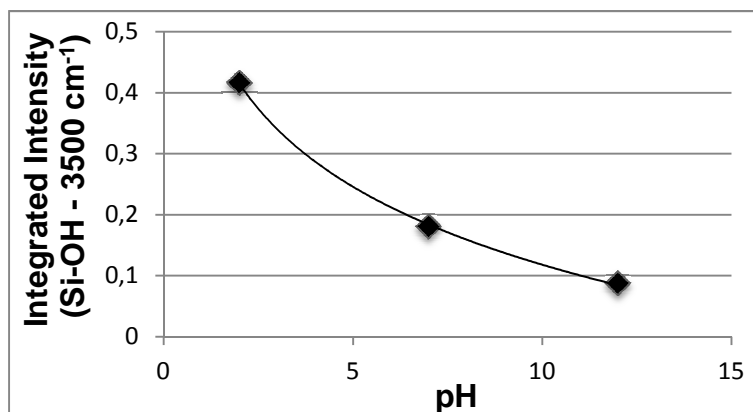


Figure V-13. Evolution of the relative intensity of the -OH stretching vibration mode (3500 cm^{-1}) of prehydrolyzed TPDTA as a function of the pH.

The decrease of the Si-OH peak area with the increase of the pH confirms that an acidic catalyzed hydrolysis will favor the formation of stable silanol groups whereas a basic catalyzed reaction will favor the condensation of the alkoxysilanes. This second process leads to a rapid gelation (which means opacification of the prehydrolysis solution) due to the formation of the Si-O-Si network. The peaks visible in the spectral range of $1180\text{-}950\text{ cm}^{-1}$ are related to the Si-O-Si vibration modes. There are also three components which are included in this spectral region: two Si-O-Si vibration modes at 1140 and 1020 cm^{-1} and one Si-O-C vibration mode at 1080 cm^{-1} . Deconvolution of the $1180\text{-}950\text{ cm}^{-1}$ spectral range was performed in order to estimate the exact contribution of the ν (Si-O-Si) vibration modes at 1140 and 1020 cm^{-1} relative to the ν (Si-O-C) vibration mode at 1080 cm^{-1} which is still present as polycondensation of the alkoxysilanes is not complete. The values presented on figure V-14 are the contributions of the Si-O-Si bands and the Si-O-C band divided by the integrated intensity of the whole spectral range (950 to 1180 cm^{-1}).

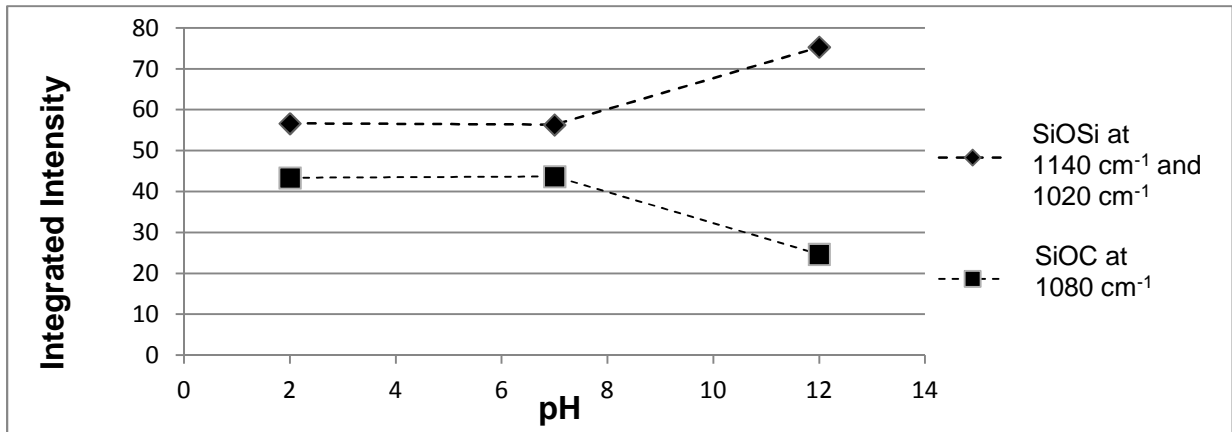


Figure V-14. Evolution of the relative intensity of the Si-O-Si deformation ($1180-950\text{ cm}^{-1}$) as a function of the prehydrolysis pH.

The evolution of the ν (Si-O-Si) peaks is the opposite of the one of the Si-OH peak. As a matter of fact, quantitative analysis through spectral decomposition shows that the integrated intensity of the ν (Si-O-Si) vibration modes increases with the pH of the prehydrolysis solution. This can also be related to the decrease of the integrated intensity of the ν (Si-O-C) vibration mode when the pH increases.

- *Epoxy silane*

It is now interesting to focus on the behavior of GPTMS which possesses an epoxy group instead of an amine function. A comparison of the T-IR spectra of GPTMS before and after prehydrolysis at pH = 2 is shown on figure V-15. Normalization and scaling were performed relative to the $\nu_{\text{as}}(\text{CH}_2)$ vibration mode at 2939 cm^{-1} because this one is not modified by the prehydrolysis.

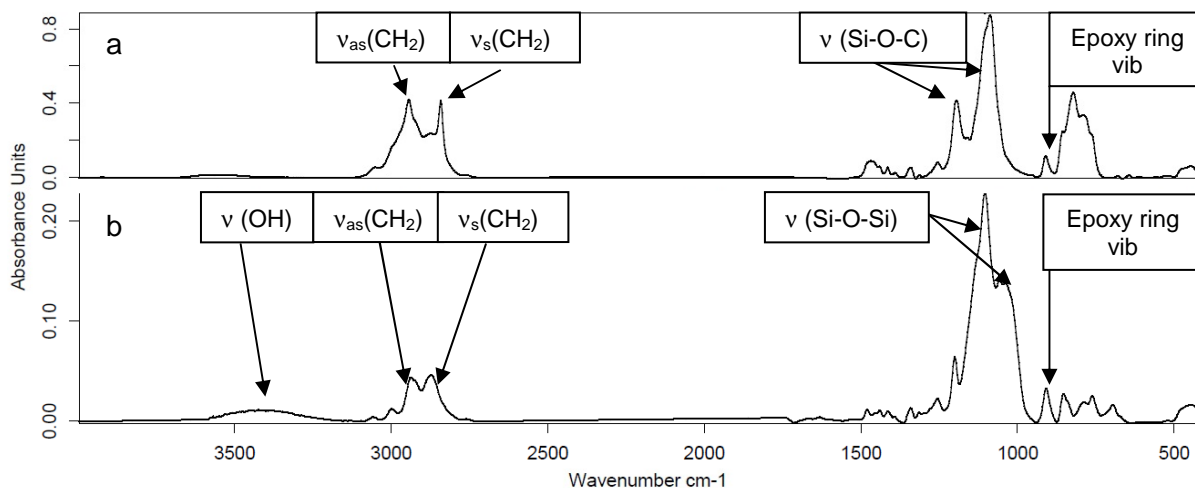


Figure V-15. T-IR spectra of GPTMS before (a) and after (b) prehydrolysis (at pH 2).

Again, specific stretching vibration modes of silanol functions are visible at 3500 cm^{-1} and 914 cm^{-1} . This fact, related to the formation of the two strong and wide Si-O absorption bands (1128 and 1037 cm^{-1}) characteristic of the formation of siloxane (Si-O-Si) bonds, indicates that the prehydrolysis and condensation of GPTMS has been obtained at pH 2. As explained, the obtaining of the siloxane network is due to the heating period necessary to remove the prehydrolysis solvents (ethanol and water).

It is now interesting to check if the behavior of GPTMS is similar to the one of aminosilanes (formation of silanols regardless to the pH of the prehydrolysis solution). The spectra obtained for prehydrolysis of GPTMS at different pH are reported on figure V-16.

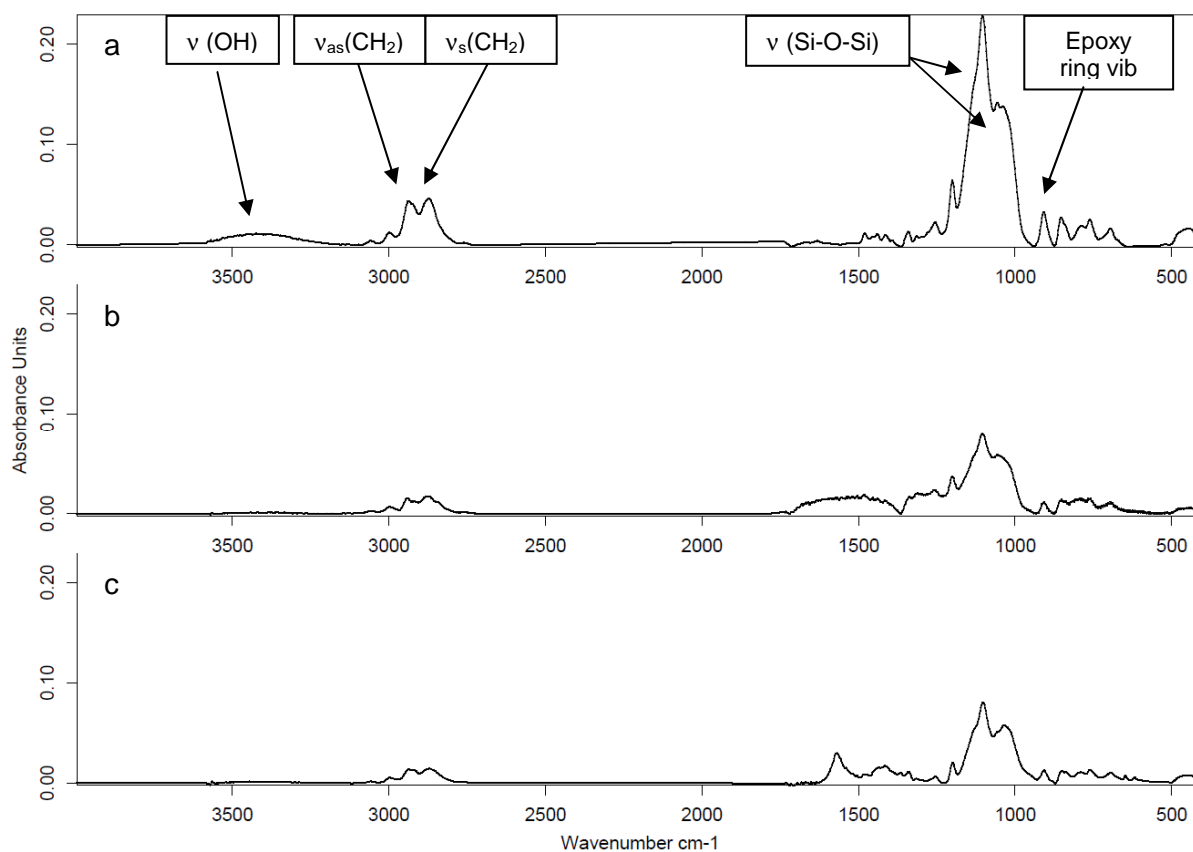


Figure V-16. T-IR spectra of prehydrolyzed GPTMS at a. pH=2, b. pH=7, c. pH=12.

The hydrolysis and polycondensation of this alkoxy silane is pH-dependent. On one hand, the Si-O-Si network is formed regardless to the pH of the prehydrolysis solution which means that the condensation reaction is happening. On the other hand, the ν (OH) absorption band at 3500 cm^{-1} is only visible for pH 2 meaning that silanols are only formed at this pH. For a pH in the range 7-12, the hydrolyzed species are fully consumed in the polycondensation reaction. The integrated intensity of the Si-OH vibration mode (-OH stretching vibration mode at 3500 cm^{-1}) was observed as a function of the pH (figure V-17).

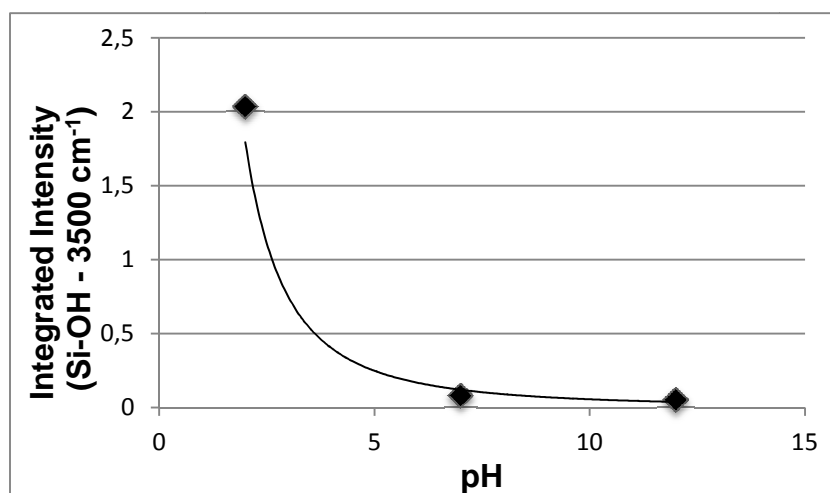
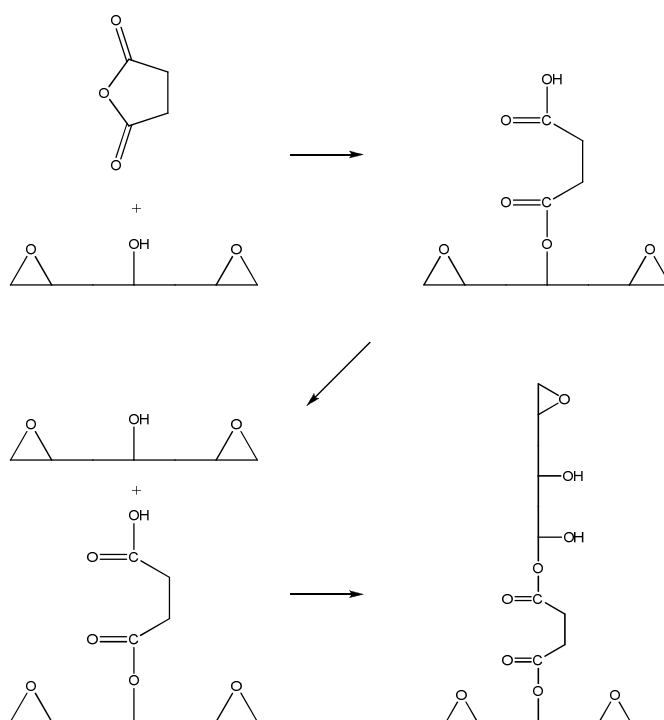


Figure V-17. Evolution of the relative intensity of the -OH stretching vibration mode (3500 cm^{-1}) of prehydrolyzed GPTMS as a function of the pH.

It is clear that the optimal prehydrolysis conditions for GPTMS are obtained at pH 2 as this pH allows the formation of a maximum of silanols compared to the other pH tested. It is known that the balance between hydrolysis and condensation, in the specific case of alkoxy silanes, is pH-dependant ¹⁹. In fact, the optimum pH for the hydrolysis reaction is not the same as for condensation. This means that the best balance between these two reactions must be found in order to use these compounds successfully. This balance has been determined for GPTMS and the best compromise is found for pH ranging between 3.5 and 5 ¹⁹.

- *Succinic anhydride silane*

This trialkoxysilane was studied as the succinic anhydride function is able to react with the epoxy prepolymer. This reaction goes through the formation of an ester bridge between the anhydride function and the hydroxyl of the BADGE prepolymer. The resulting carboxylic acid will form another ester function by opening one epoxy ring of the BADGE (scheme V-1).



Scheme V-1. Reaction of a succinic anhydride function with an epoxy prepolymer.

TPSA was prehydrolyzed during 1 h in solution at pH = 2, 7 and 12 and was then analyzed by T-IR (figure V-18).

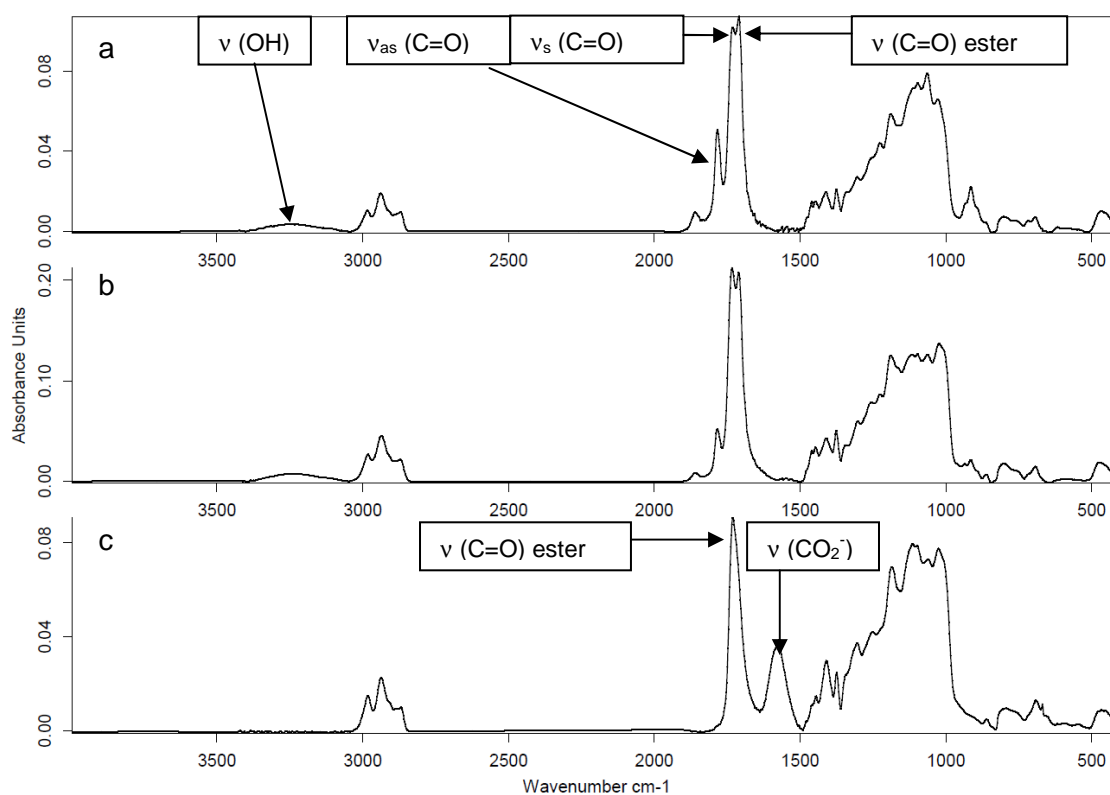


Figure V-18. T-IR spectra of prehydrolyzed TPSA at a. pH=2, b. pH=7, c. pH=12.

Normalization and scaling were performed relative to the $\nu_{\text{as}}(\text{CH}_2)$ vibration mode at 2939 cm^{-1} . This choice is debatable as TPSA possesses ethoxy functions ($-\text{OCH}_2\text{CH}_3$) meaning that the $\nu_{\text{as}}(\text{CH}_2)$ vibration mode will evolve during the hydrolysis reaction but, in the case of this molecule, the main focus was made on the evolution of the $1500 - 2000\text{ cm}^{-1}$ region. The vibration modes standing in this zone are directly related to the evolution of the carbonyl peaks composing the anhydride function. For the spectra performed at $\text{pH} = 2$ and 7 , three main $\text{C}=\text{O}$ vibration modes are observed. The highest one at 1865 cm^{-1} corresponds to the asymmetric stretching of $\text{C}=\text{O}$ of the succinic anhydride function while the next one, at 1790 cm^{-1} stands for the symmetric one. These two bands separated by 75 cm^{-1} are typical of an anhydride function. Thus, another very strong $\text{C}=\text{O}$ band is observed at 1730 cm^{-1} which is consistent with the presence of a carboxylic acid or an ester in the medium. This result, coupled with the presence of an (OH) vibration mode between 3050 and 3350 cm^{-1} , confirms the sensitivity of the anhydride function²⁰ as the addition of this compound in ethanol would lead to the formation of the resulting ester and carboxylic acid by opening of the anhydride ring.

For the $\text{pH} = 12$ sample, the $1500 - 2000\text{ cm}^{-1}$ zone exhibits different vibration modes. As a matter of fact, the anhydride double band has totally disappeared to leave a strong vibration mode at 1730 cm^{-1} and a weakest one at 1570 cm^{-1} . Both vibration modes can respectively correspond to the presence of the ester described earlier and to the presence of a carboxylate ion. This latter would come from the saponification²¹ undergone by the ester under strongly basic conditions as this slow reaction finally leads to the formation of a carboxylate ion and the corresponding alcohol, probably evaporated during the drying of the AgBr pellet.

Nevertheless, it is clear that there are some issues regarding to the stability of the succinic anhydride function in an aqueous medium. The use of TPSA was cancelled to this point and its grafting onto stainless steel was not studied.

V.2.a.ii. Grafting onto stainless steel

After a prehydrolysis step, silanes were deposited onto stainless steel. Different prehydrolysis pH were tested for each silane and the coated stainless steel plates were characterized by PM-IRRAS (after rinsing the stainless steel plates with ethanol to remove the physisorbed molecules and drying).

- *Aminosilanes*

Prehydrolyzed TPDTA (pH = 2) and stainless steel functionalized with TPDTA at pH = 2 were compared and the resulting spectra are presented on figure V-19.

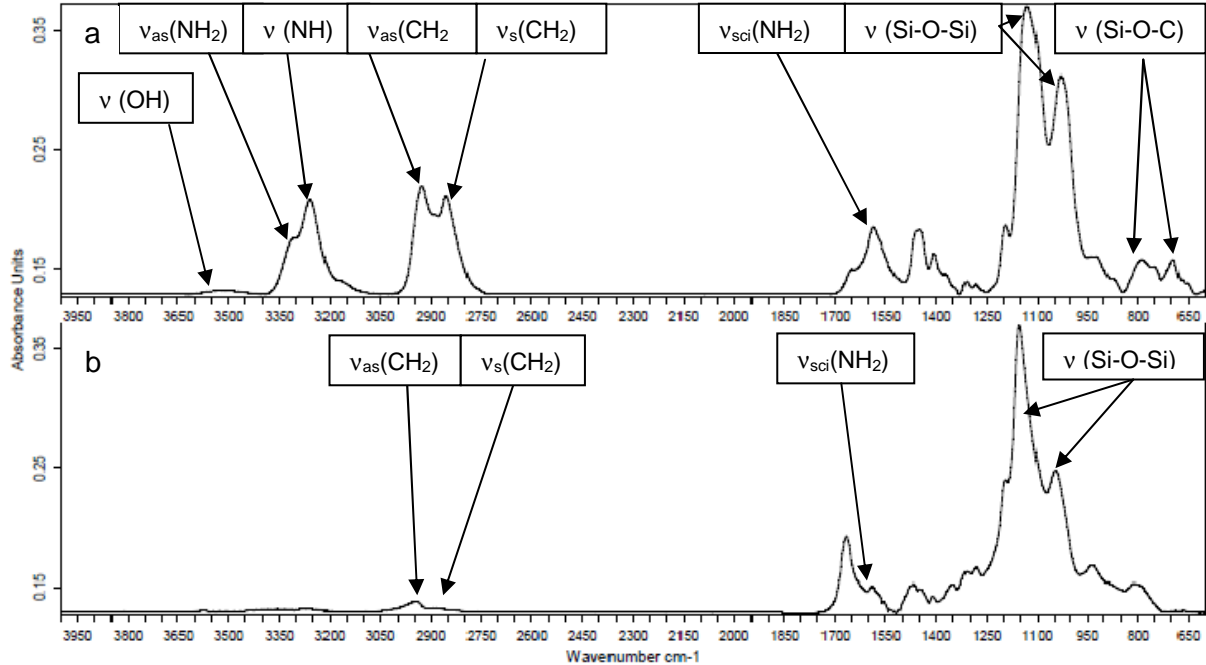


Figure V-19. a. T-IR spectrum of prehydrolyzed TPDTA (pH 2); b. PM-IRRAS spectrum of TPDTA grafted onto stainless steel (pH 2).

First, we can see that molecules are detected on the stainless steel surface (figure V-19.b) even after rinsing with ethanol (good solvent of the alkoxy silane). This evidences a chemical grafting of the alkoxy silane onto the stainless steel surface. Grafting is probably happening with the hydroxides (mainly iron and chromium ones) at the extreme surface of the substrate^{1,5}. The formation of a siloxane network is clearly visible as it was expected. The disappearance of the v(OH) absorption band of the silanol groups at 3500 cm⁻¹ indicates that the Si-OH function is responsible of grafting of alkoxy silanes onto stainless steel. Moreover, the presence of the v_{sci}(NH₂) (1598 cm⁻¹) indicates that this function is still available in order to react with an epoxy resin.

The PM-IRRAS analyses of the grafted stainless steel surface were made for the other aminosilanes (figure V-20).

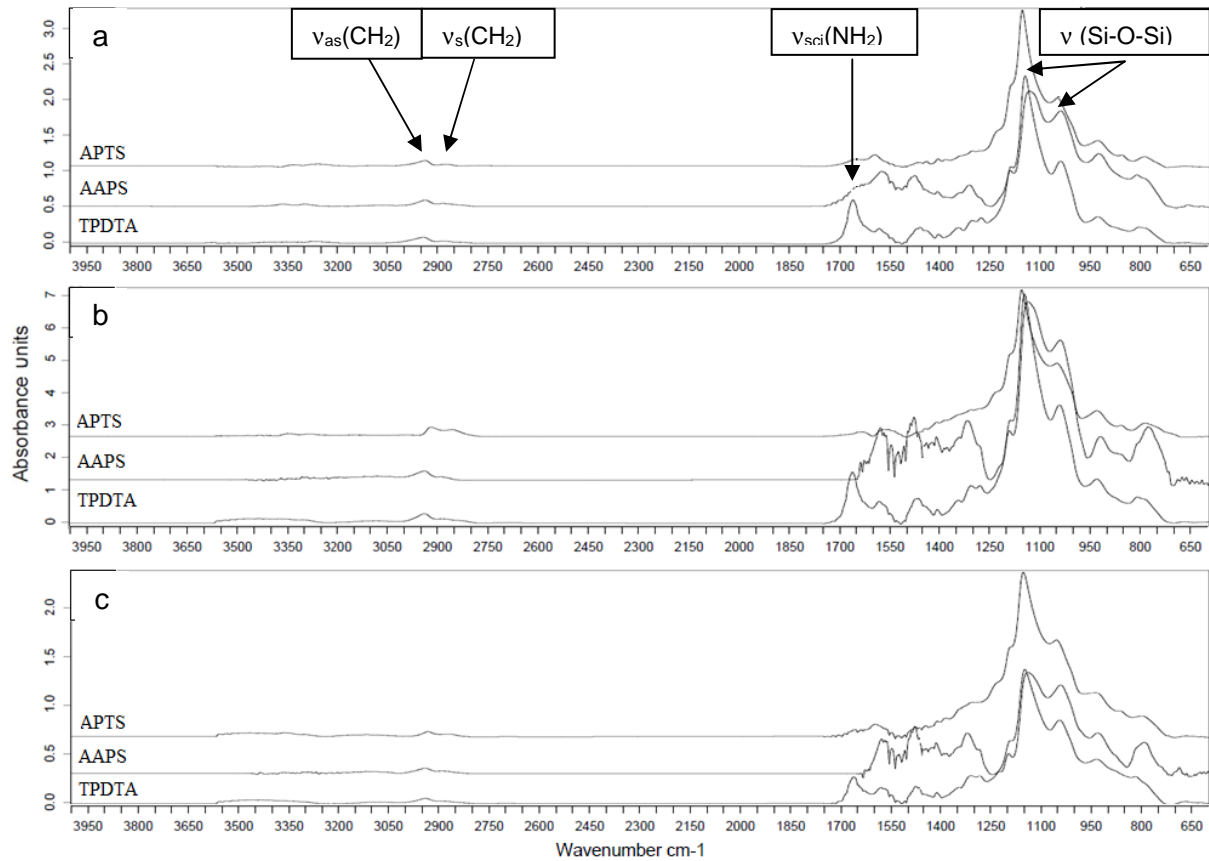
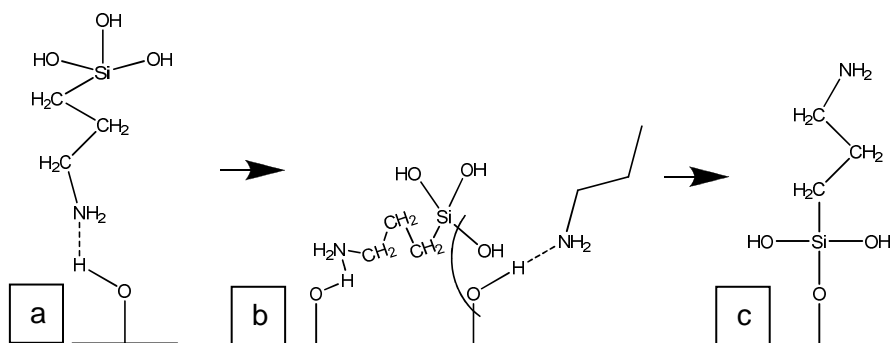


Figure V-20. PM-IRRAS spectra of APTS, AAPS and TPDTA deposited on stainless steel after a prehydrolysis step at a. pH=2, b. pH=7, c. pH=12.

PM-IRRAS spectra are showing that the three vibration modes of the aminosilanes are visible at the stainless steel surface even after rinsing with ethanol. This means that these aminosilanes are chemically bonded (or at least strongly adsorbed) to the metal surface regardless to the pH of the prehydrolysis. The fact that aminosilanes are grafted whatever the pH shows that this mechanism is catalyzed by the amine functions ²⁰.

Two hypotheses can be proposed to describe the fact that the grafting of aminosilanes is not pH-dependant. First, aminosilanes are the rare trialkoxysilanes that can efficiently be grafted using a base-catalyzed deposition ¹⁷. It has been proven that primary, secondary or tertiary amines can catalyze base-medium hydrolysis likely due to the basic character of the amine function which increases the nucleophilic character of the silicon atom ^{18,24} Si-OH can so be obtained whatever the hydrolysis pH.

Another hypothesis is the occurrence of a grafting process already described in the literature ²⁵. This phenomenon is known as “flip mechanism” as described for APTS on scheme V-2.



Scheme V-2. Flip mechanism between an aminosilane and a hydroxylated surface.

According to our study, the mechanism, already demonstrated in anhydrous solvents (DMF, toluene)^{23,24,26}, seems to take place in an aqueous medium. This mechanism can be divided into three steps: first, the formation of hydrogen bonds (a) between the amine function of the alkoxy silane and the hydroxyl groups of the stainless steel surface. Second, a coordination / condensation reaction (b) will happen with another aminosilane molecule which, third, will lead to the formation of a covalent bond (c) between the silanol group of the aminosilane and a hydroxyl group (with loss of water) of the stainless steel surface.

Atomic Force Microscopy was then used in order to observe the grafted alkoxy silane layer on stainless steel. This analysis was performed for all alkoxy silanes deposited on stainless steel. The case of TPDTA was first studied as a function of the pH. The resulting AFM snapshots are presented on figure V-21.

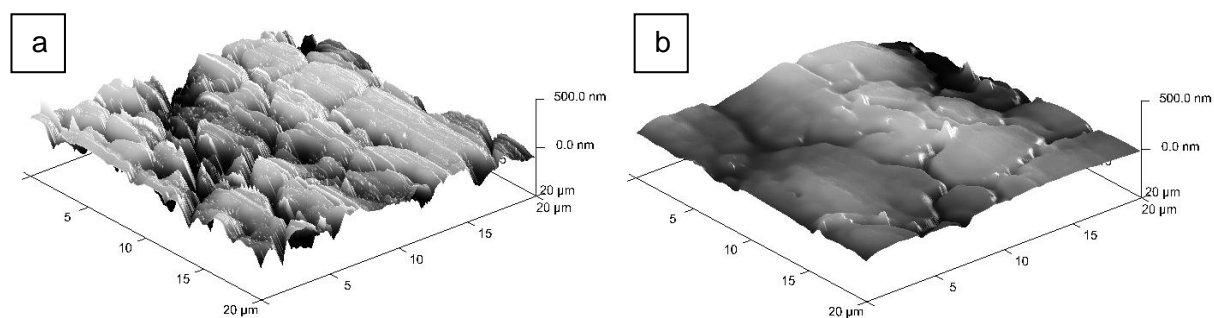


Figure V-21. AFM snapshots of: a. pure stainless steel and b. TPDTA grafted onto stainless steel after a prehydrolysis step at pH=2.

Crude stainless steel is a very rough surface at a nanoscale composed of numerous micro-domains of different shapes and sizes. The roughness of stainless steel surface (medium roughness determined with a Mitutoyo SJ-301 roughness tester $R_A = 190$ nm and medium roughness determined by AFM $R_A = 172$ nm) can explain the possible difficulties of analyzing

thin grafted layers by PM-IRRAS. After application of a TPDTA solution, a grafted layer of molecules is clearly visible regardless to the pH. The height of this adsorbed layer has not been measured but the evolution of the medium roughness has been determined (table V-5).

Table V-5. Evolution of the roughness of stainless steel plates coated by TPDTA as a function of its prehydrolysis solution pH.

TPDTA's prehydrolysis solution pH	Roughness (measured by AFM, in nm)
Crude stainless steel - no TPDTA grafted	172 ± 35
2	14 ± 7
7	39 ± 9
12	24 ± 4

The TPDTA grafted layer is able to cover the roughness of stainless steel and irreversible chemisorption of TPDTA leads to the formation of a multilayered network. The capacity of alkoxysilanes to form monolayers is relatively limited under the experimental conditions used during this study by the fact that condensation reactions occur very easily leading to the formation of a multilayered deposit ¹⁸.

- *Epoxy silane*

The same analyses were performed on GPTMS after prehydrolysis and after deposition onto stainless steel. The PM-IRRAS analyses of the grafted stainless steel surface are presented on figure V-22.

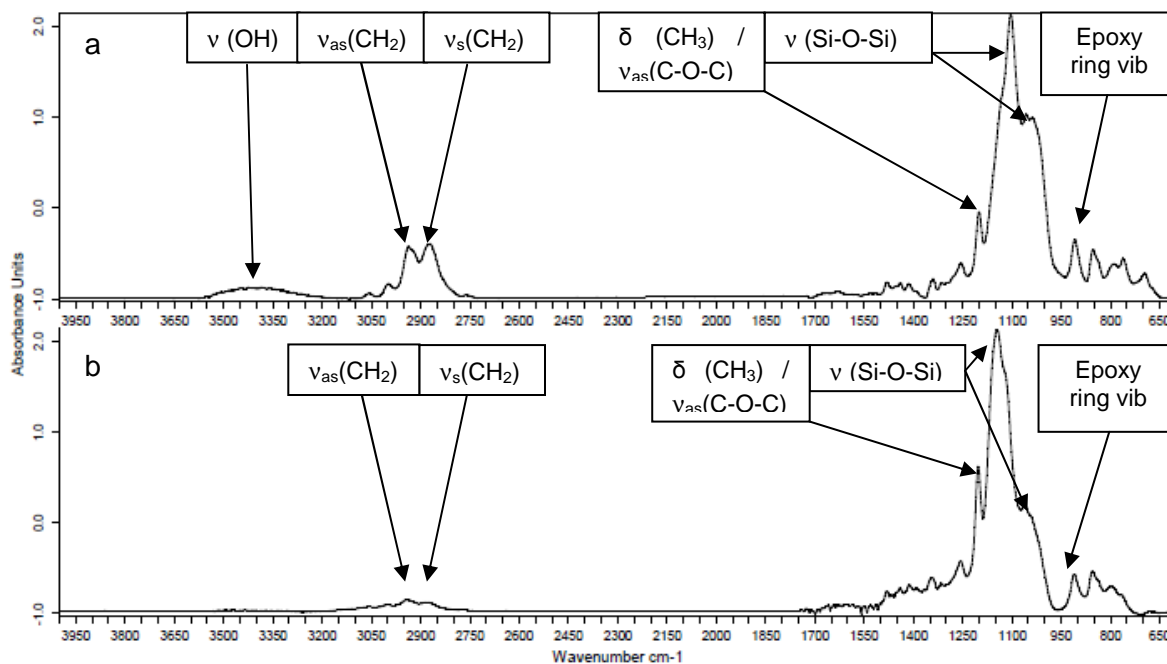


Figure V-22. a. T-IR spectrum of prehydrolyzed GPTMS (pH 2); b. PM-IRRAS spectrum of GPTMS grafted onto stainless steel (pH 2).

Again, the disappearance of the silanol absorption bands is due to bonding of this functional group with the substrate.

The PM-IRRAS analyses, performed after prehydrolysis at different pH, will give more information on the anchoring of GPTMS onto stainless steel (figure V-23).

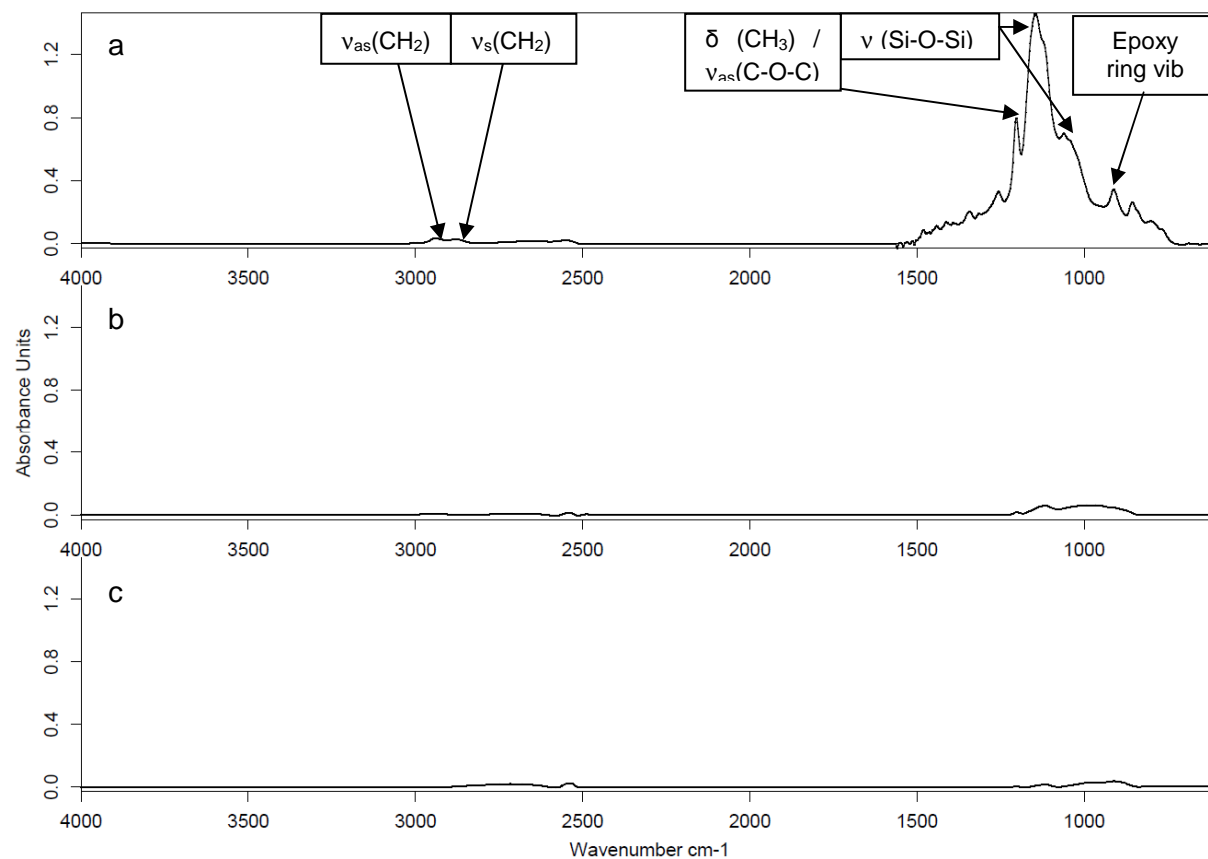


Figure V-23. PM-IRRAS spectra of GPTMS deposited on stainless steel after a prehydrolysis step at a. pH=2, b. pH=7, c. pH=12.

It is clear that the grafting of GPTMS onto the stainless steel plate is pH-dependant as GPTMS vibration modes are only visible on the stainless steel surface for a prehydrolysis at pH 2. Actually, the critical pH value for GPTMS grafting is 5. The epoxy function of this alkoxy silane does not catalyze the chemisorption of the alkoxy silane on steel contrary to the amine function. These results confirm the ones obtained during the hydrolysis study and show that a pH value inferior to 5 is the best way to achieve efficient grafting of GPTMS.

The grafting of GPTMS was studied by AFM as well (figure V-24).

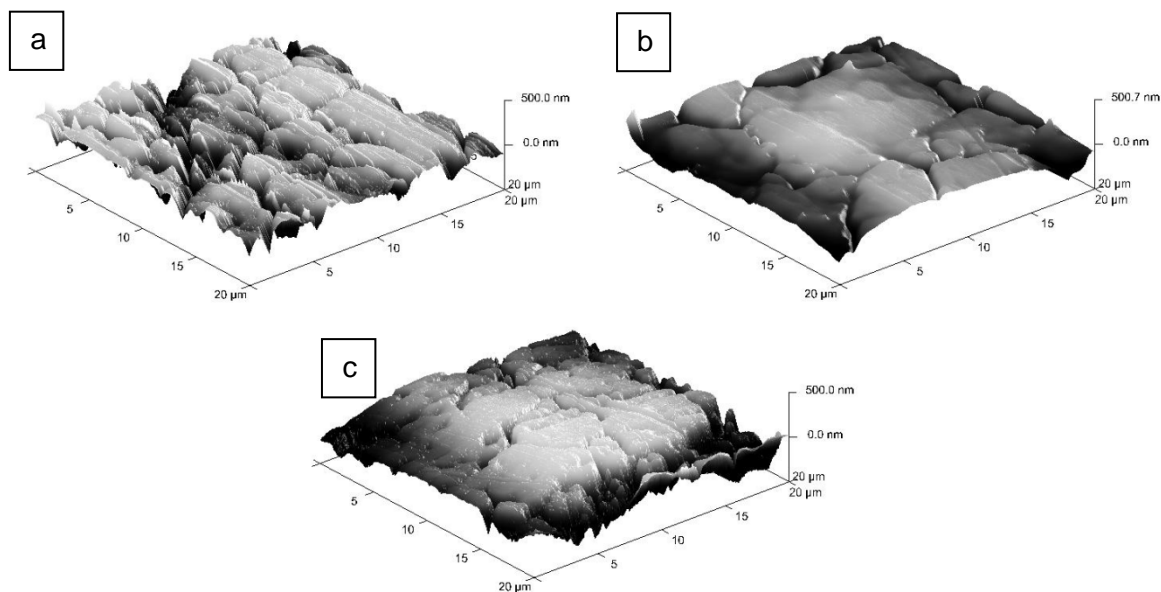


Figure V-24. AFM snapshots of: a. pure stainless steel and GPTMS adsorbed on stainless steel after a prehydrolysis step at b. pH=2, c. pH=7.

Again, the observation of the adsorbed molecules is possible for GPTMS at pH = 2 and as previously, a decrease of roughness is observed (R_A (pH = 2) = 39 nm). Covering of the surface has been reached too and GPTMS is most likely adsorbed in a multilayer way. On the other hand, the AFM snapshots taken for GPTMS prehydrolyzed at pH = 7 clearly show that adsorption of this alkoxy silane is not happening at this pH. Surface roughness is quite close to the one of crude stainless steel (R_A = 172 nm) and this confirms that adsorption of GPTMS has not been obtained under these conditions.

- *Conclusion*

The results obtained above prove both the influence of the pH and of the functional group on the grafting of these molecules. In fact, the behavior of a trialkoxysilane as a function of the pH is completely dependent on the nature of the non-hydrolyzable group.

For GPTMS (with an epoxy function) and TPSA (with a succinic anhydride function), an acid medium is needed to achieve efficient grafting onto stainless steel. Nevertheless, TPSA was cancelled due to the instability of the succinic anhydride function in an aqueous medium.

The case of aminosilanes is special as efficient hydrolysis and grafting is obtained whatever the solution's pH. However, an acid medium still favors the formation and stability of reactive

silanols. A pH value of 5 was also chosen as the best solution to have the higher hydrolysis / condensation balance.

The deposition method used during this part was adapted for the observation of alkoxy silanes by PM-IRRAS as it allows the obtaining of a thick alkoxy silane grafted layer. However, it seems that having a too large deposit at the stainless steel surface is not optimal in terms of adhesion improvement as it would cause a covering of the stainless steel surface roughness. In this case, a part of the mechanical adhesion, which is induced in the adhesion mechanism for epoxy / stainless steel system, would be lost. The idea was here to reduce the prehydrolysis duration (to form less silanols) and to perform rinsing of the plates before the drying step (to avoid the formation of a siloxane network thanks to heating). Starting from now, the alkoxy silanes were deposited thanks to a 15 minutes - dip coating, rinsed in an ethanol bath and finally dried at 110 °C during 30 minutes.

V.2.b. Prehydrolysis duration

V.2.b.i. Introduction

The prehydrolysis duration is a key factor as well. As a matter of fact, silanols are formed very rapidly when an alkoxy silane is added in an aqueous solution¹⁶⁻¹⁸. The formed silanols are important as they are responsible of the grafting on a substrate. However, these species, during the prehydrolysis, are consumed in the condensation reaction. A dense siloxane network is formed during this process. This network is less mobile and less reactive regarding to a substrate as it contains less reactive species. Moreover, the grafting of a thick siloxane layer induces a covering of the stainless steel surface roughness which is crucial for the adhesion of the epoxy coating. The aim of reducing the prehydrolysis time is to combine the effect of the natural stainless steel surface roughness with the formation of stable covalent bonds thanks to the alkoxy silanes.

Tests were made on APTS at pH = 5 as the grafting of these molecules has been characterized.

V.2.b.ii. Grafting onto stainless steel

The grafting of APTS was observed after 90 s and 1 h of prehydrolysis. As described earlier, the alkoxy silanes grafting onto stainless steel was already observed by PM-IRRAS after a 1 h prehydrolysis whatever the pH (figure V-20).

However, the grafting of APTS after a 90 s prehydrolysis was not observed by PM-IRRAS. Two hypotheses were made to explain the absence of signal during the InfraRed analysis.

First, the absence of the APTS characteristic vibration modes at the stainless steel surface might come from the fact that the prehydrolysis time was too short. During this period, not enough silanols are formed and these do not allow to reach grafting at the stainless steel surface.

Secondly, it can come from the fact that the grafted alkoxy silane layer is too thin to be identified by PM-IRRAS. This spectroscopy technique is able to detect species at the nanometric scale but the problem is that stainless steel is very rough (R_A (AFM) = 172 nm) and this fact bothers the observation of thin grafted species. Two possibilities were available at this point: using a polished stainless steel substrate with a very smooth surface or using another surface analysis technique. The second solution was chosen and some XPS analyses were performed on functionalized stainless steel plates.

An APTS-functionalized stainless steel plate after a 90 s prehydrolysis was analyzed by XPS (figure V-25).

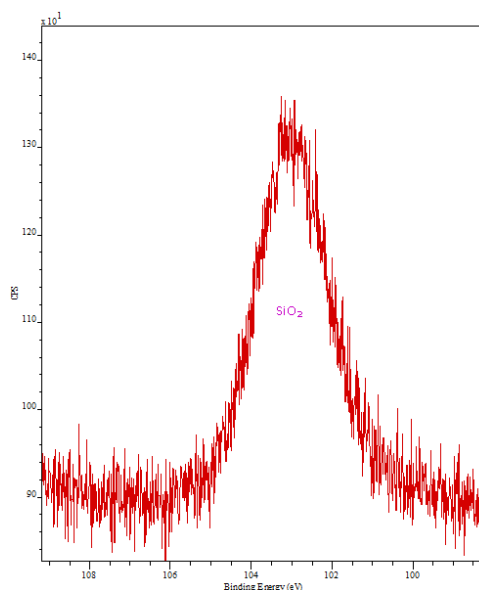


Figure V-25. XPS spectrum of an APTS-functionalized stainless steel (90 s prehydrolysis): zoom of the Si 2p peak.

A single peak is observed at 103.3 eV which is consistent with the formation of SiO₂ bonds²⁷. This result corresponds to the formation of an alkoxy silane layer at the surface of stainless steel and proves that some species are grafted at the surface.

Besides, some spectra were taken from APTS-functionalized samples that underwent 1 h of prehydrolysis. XPS proved again the grafting of the alkoxy silane molecules but it was more interesting to compare the intensities of the Si 2p peak obtained for each samples as the value obtained for the 1h sample was three times higher than the one obtained for the 90 s sample. This result proves that decreasing the prehydrolysis time leads to the formation of a thinner grafted layer that might be more efficient as an adhesion promoter as it would provide the formation of stable covalent bonds without covering the surface roughness of the substrate.

Finally, some immersion tests (water at 80 °C during 10 h) were performed on both samples to check the stability of the APTS-grafted layer. The spectra made after immersion exhibited exactly the same Si 2p peak than the one observed before immersion. This result confirms the fact that the bonds established between the trialkoxy silane and the substrate are stable in an aqueous medium and can provide an improvement of the adhesion of the epoxy coating onto stainless steel.

V.3. Influence of the number of hydrolyzable groups of the alkoxy silane on its grafting onto stainless steel

As described earlier, the aim of this study is to enhance the adhesion of an epoxy coating on stainless steel by combining the effect of surface mechanical treatment and chemical functionalization. Another way to obtain a thin-alkoxy silane grafted layer is to use monoalkoxy silanes. A monoalkoxy silane, thanks to its only alkoxy function, does not lead to the formation of a siloxane network. Self-condensation of the monoalkoxy silane causes the formation of a dimer which is not able to graft at the steel surface. This type of molecule leads to an ordered grafted monolayer with almost no covering of the substrate's roughness.

However, these molecules are not as common as trialkoxy silanes. Their prehydrolysis and grafting on metallic substrates has not extensively been described and the examples found in the literature mainly deal with biological uses or grafting onto silica²⁸⁻³¹. Again, these molecules were chosen to have a functional group able to react with the epoxy / curing agent system (figure V-26).

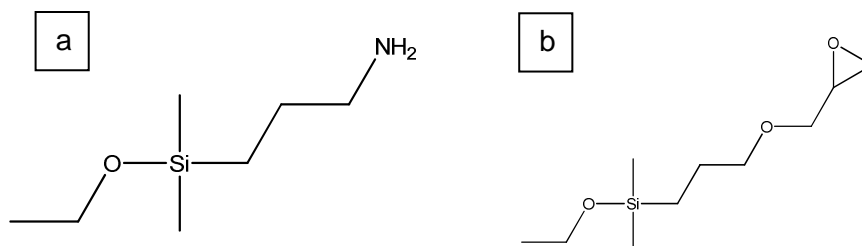


Figure V-26. Chemical formula of: a. 3-aminopropyldimethylethoxysilane (APDES) and b. 3-glycidoxypropyldimethylethoxysilane (GPDES).

It is interesting to note that the hydrolyzable functions are ethoxy ones compared to the trialkoxysilanes which bore methoxy functions. Some tests were performed to check again the effect of the pH on the prehydrolysis of these molecules. The optimal prehydrolysis pH and duration were chosen thanks to this study. Finally, the grafting of these molecules onto stainless steel was checked by XPS.

V.3.a. Hydrolysis study

The monoalkoxysilane solutions were prepared by adding 2% w / w of alkoxysilane in a non-deuterated 95 / 5 (w / w) ethanol / water mixture at a controlled pH (use of acetic acid for an acid medium and caustic soda for a basic medium). These solutions were homogenized and directly analyzed by ¹H NMR. The formation of silanols is performed by following the evolution of the methyl groups at 0.67 ppm. As a matter of fact, the transformation of the ethoxy functions into silanols leads to a shift of this peak to a lower value at 0.65 ppm (figure V-27).

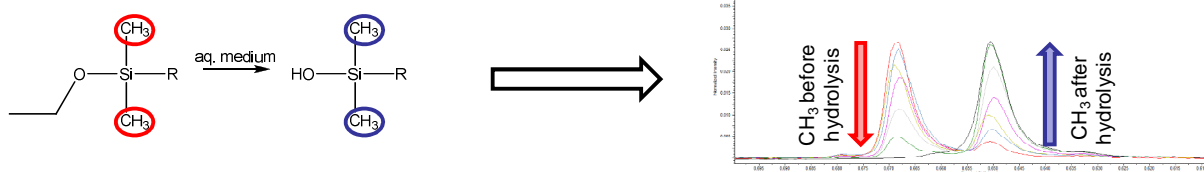


Figure V-27. Evolution of the methyl peak of monoalkoxysilanes before and after hydrolysis observed by ¹H NMR.

The amount of silanols formed during the prehydrolysis is calculated following equation V-1.

$$\%(SiOH) = \frac{I(CH_3 \text{ after hydrolysis at } 0.65 \text{ ppm})}{I(CH_3 \text{ after hydrolysis at } 0.65 \text{ ppm}) + I(CH_3 \text{ before hydrolysis at } 0.67 \text{ ppm})} * 100$$

Equation V-1. Calculation of the amount of silanols formed during the hydrolysis by ¹H NMR.

The other parts of the NMR spectrum did not give other information, as they mainly contain ethanol - water peaks and were not studied.

The results (amount of silanols formed as a function of time) obtained at pH 5, 7 and 12 for the APDES hydrolysis are presented on figure V-28.

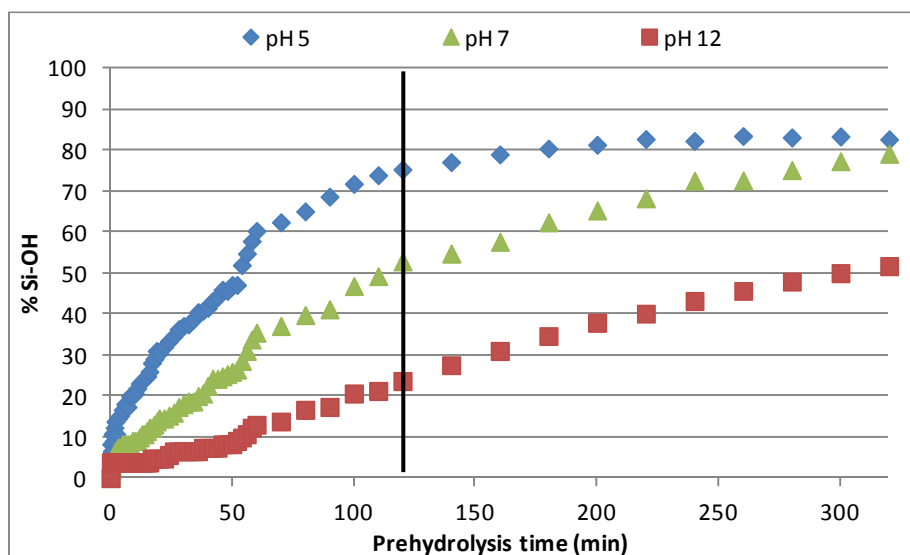


Figure V-28. Kinetic of APDES hydrolysis as a function of the pH followed by ^1H NMR.

The results obtained for prehydrolysis at pH = 2 are not presented because the hydrolysis was too fast. As a matter of fact, an amount of 83 % (mol) of silanols formed has been reached even before the first measurement (around 30 seconds after addition of APDES). This pH value was not considered as usable as it involves a too fast kinetic and as working at pH = 5 is more comfortable.

For the pH values presented on figure V-28, it is clear that the optimal prehydrolysis pH for APDES is 5 as it allows to reach a high silanol conversion rate (82 % mol) after around 120 minutes of reaction. Another interesting fact is that the formation of silanols is reached regardless to the prehydrolysis pH. This means that the behavior of APDES in an aqueous solution is comparable to the one of trialkoxy-amino-silanes with a hydrolysis catalyzed by the basic property of the nitrogen atom. Kinetics are slower for pH 7 and 12 as respectively 52 % (mol) and 23 % (mol) of silanols are formed after 120 minutes of reaction. It is also interesting to note that a final conversion of 79 % (mol) is obtained after 5 hours with the pH 7 sample and 51 % (mol) with the pH 12 sample. The conditions retained for APDES are a prehydrolysis at pH = 5 during 120 minutes.

It is interesting to note that these results have been obtained with ethoxysilanes. The length of the alkoxy function would also play a major role as it is known for trialkoxysilanes that a longer alkoxy chain would lead to a decrease of the hydrolysis speed ¹⁶.

The same study was performed with GPDES and the corresponding results are presented on figure V-29.

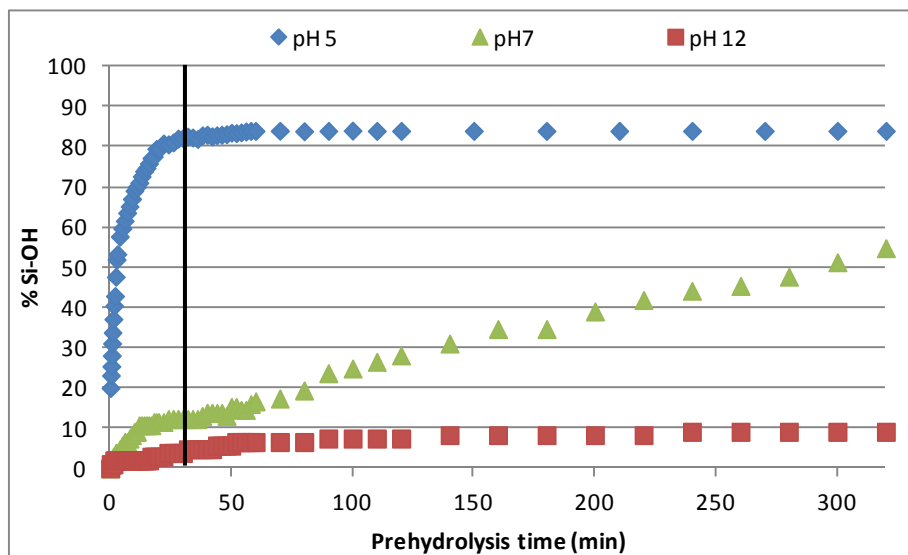


Figure V-29. Kinetic of GPDES hydrolysis as a function of the pH followed by ¹H NMR.

As for APDES, the prehydrolysis kinetic of GPDES was not measurable at pH 2. An amount of 85 % (mol) of silanols is formed even before the first spectrum was recorded. This value is again cancelled as it does not allow to follow the evolution of the hydrolysis reaction.

Again, it is interesting to note that the optimal pH value is 5. Under these conditions, an amount of 81 % (mol) of silanols is formed after only 30 minutes. Meanwhile, the amounts reached at pH 7 and 12 are respectively 12 % (mol) and 5 % (mol). The final conversions reached after 5 hours of reaction are around 50 % (mol) at pH = 7 and 9 % (mol) at pH = 12. It is here clear that the epoxy function at the chain-end of GPDES does not play any catalysis role in the prehydrolysis reaction. The conditions retained for GPDES are a prehydrolysis at pH = 5 during 30 minutes.

As the formation of reactive silanols has been achieved in the classical prehydrolysis conditions, it was interesting to then study the grafting of these molecules onto stainless steel.

V.3.b. Grafting of monoalkoxysilanes onto stainless steel

The tests presented in this paragraph were only made on APDES and extrapolations were made for the case of GPDES. APDES was deposited onto stainless steel by dip coating after a prehydrolysis of 120 minutes at pH 5. The functionalized plates were rinsed in an ethanol bath and then dried at 110 °C during 30 minutes.

PM-IRRAS analyses were performed on APDES-functionalized stainless steel plates. As obtained for APTS with a short prehydrolysis time, no signal was obtained by using this method. Again, it can be due to the absence of grafted species at the stainless steel, to a low grafting density or to the fact that the thickness of the APDES-layer is too thin compared to the stainless steel roughness to be detected by PM-IRRAS.

XPS analysis was performed on the same sample in order to obtain chemical information on the grafted species without taking into account the substrate's roughness. A zoom on the Si 2p peak is presented on figure V-30.

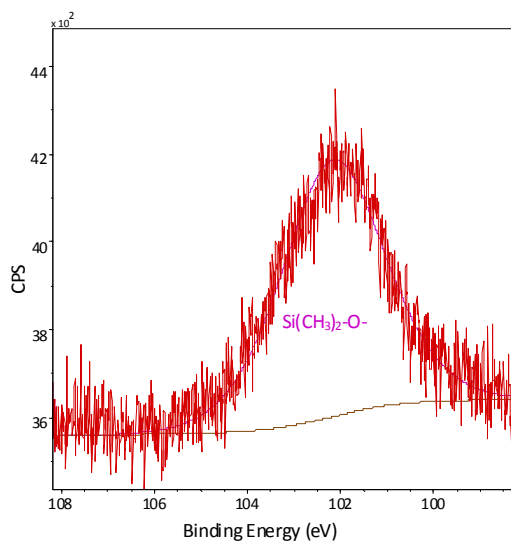


Figure V-30. XPS spectrum of an APDES-functionalized stainless steel: zoom of the Si 2p peak.

This spectrum can be fitted with only one component at 102.4 eV corresponding to a Si(CH₃)₂-O- bond³². This signal is consistent with the formation of a covalent bond between APDES and the stainless steel surface. Moreover, an XPS analysis was performed on the same sample after immersion in hot water (80 °C) during 10 h. The spectrum made after immersion exhibited exactly the same Si 2p peak than the one observed before immersion. This result confirms the fact that the bonds established between the monoalkoxysilane and

the substrate are stable in an aqueous medium and can provide an improvement of the adhesion of the epoxy coating onto stainless steel.

V.4. Conclusion

Grafting of alkoxy silanes has been achieved under controlled conditions.

Concerning the trialkoxysilanes, TPSA has been cancelled due to the instability of its reactive anhydride group in an aqueous medium. For the aminosilanes, a particular behavior has been observed as both hydrolysis and grafting are obtained whatever the solution's pH. For GPTMS, acid conditions seem to be more adapted for the grafting of this molecule. It has also been shown that grafting of these molecules can still be obtained by decreasing the prehydrolysis time to a very short value (90 s). In fact, decreasing the duration of this first step leads to a thinner alkoxy silane deposition at the surface.

Monoalkoxy silanes were studied as well and the analyses proved that the behavior of these molecules is quite similar to the one of trialkoxysilanes. The optimal prehydrolysis durations of 120 min and 30 min were set respectively for APDES and GPDES.

For the following of this study, the deposition pH used for mono- and trialkoxy silanes was set to 5. After studying the effect of each pre-treatment on the stainless steel surface, it was important to check the effect of each surface treatment on the adhesion of the epoxy coating.

VI. Impact of the surface pre-treatments on the adhesion of the epoxy coating onto stainless steel

Some pull-off tests were performed to better compare the systems with each other. At the moment, the adhesion and the stability of the epoxy / stainless steel interface was only based on visual observation by watching the formation of blisters. The pull-off test was a simple and rapid way to evaluate the adhesion strength of the coating on the substrate. For this purpose, this test was performed on coated stainless steel plates before immersion and after 1 and 5 days of immersion in the model liquids (at 75 °C for BuCl and 80 °C for water). The samples, after removal from the solutions, were dried under ambient conditions during 1 day.

This measurement was made by sticking a small steel disc-plate on the coating. The plate was then pulled off from the surface and the torque (in N) needed to take the stuck plate off is measured. The adhesion strength (in MPa) is then obtained by dividing the torque by the surface of the steel disc-plate according to equation V-2.

$$F(MPa) = \frac{F(N)}{r_{disc}^2 * \pi}$$

Equation V-2. Calculation of the adhesion force as a function of the disc surface.

Where $F(N)$ is the torque measured by the pull-off tester and r is the radius of the disc plate (here $r = 7 \text{ mm}$).

Two cases can be observed as the rupture can happen in the epoxy coating (cohesive rupture), at the substrate / epoxy coating interface (interfacial rupture) or at the disc-plate / adhesive interface (“glue” rupture). This latter case happens when the adhesion between the epoxy coating and the substrate is too high to be measured. In this case, the values obtained can not be compared with each other and the resulting adhesion force (for the results in the grey zone) is considered to be superior to 1.5 MPa. For each plate, 4 measurements were made and the result retained is an average of these 4 values.

VI.1. Non-optimized epoxy / stainless steel interface

The first test was made on the non-optimized system without cleaning of the stainless steel plate. To do so, the RenLam CY 219 / Ren HY 5161 system was coated on crude stainless steel plates. The resulting coating was immersed in water and in BuCl during 1 and 5 days (figure V-31).

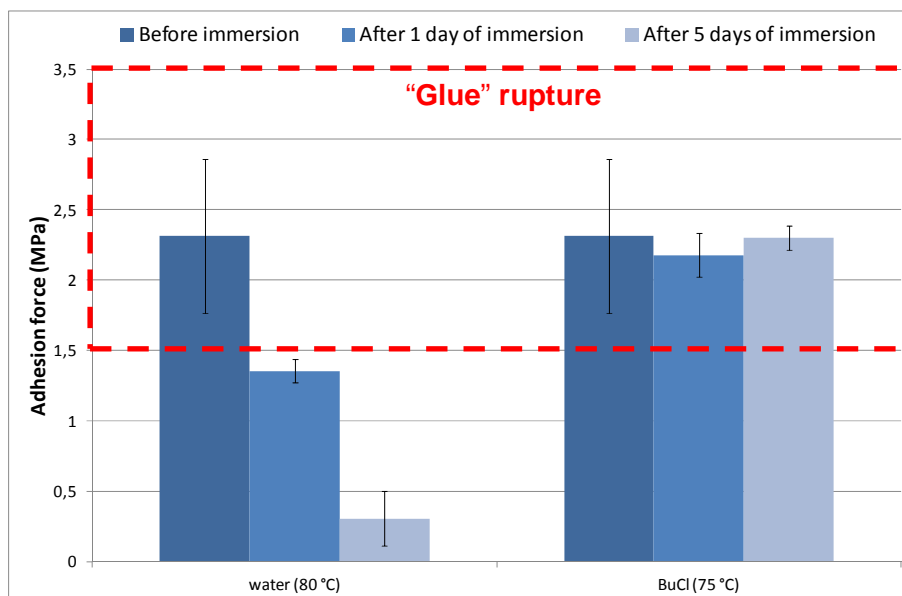


Figure V-31. Adhesion force of the RenLam CY 219 / Ren HY 5161 system coated onto stainless steel before and after immersion in water (80 °C) and BuCl (75 °C) during 1 and 5 days.

The results obtained here are consistent with the visual observations made in Chapter V., II. 2. The immersion in hot BuCl does not induce any loss of adhesion as a “glue” rupture happened before and after immersion. This means that BuCl does not induce any weakness at the epoxy / stainless steel interface. The epoxy coating is swollen by this solvent but it does not lead to a loss of adhesion. At this point, the immersion of the plates in BuCl has been cancelled for the pull-off tests.

The decrease of the adhesion force after immersion in water is consistent with the observations made earlier as well. In fact, some blisters are formed at the epoxy / stainless steel interface leading to a huge loss of adhesion. This means that, even if the epoxy network is less swollen by water, this solvent is more critical for the coating / substrate interface and this proves that the chemical adhesion of an epoxy coating onto stainless steel is mainly due to weak interactions (polar interactions, hydrogen bonds...) and that the covalent bonds formed are not stable regarding to hydrolysis..

The results obtained, in water, for the same system after cleaning of stainless steel with acetone and dichloromethane are not more convincing. Even if the contamination layer is removed and if the surface functional groups are more available, the same loss of adhesion is rapidly observed. The sensitivity of the bonds established between the epoxy coating and stainless steel regarding to water is confirmed and it is clear that this interface has to be strengthened.

The effect of the mechanical treatment of the stainless steel plates on the adhesion of the coating was then studied.

VI.2. Impact of the mechanical treatment

These tests were performed on the shot-blasted stainless steel plates. The plates were cleaned (following the classical cleaning method described in Chapter V., III.) before application of the RenLam CY 219 / Ren HY 5161 system. The adhesion force was measured before and after immersion for these samples (figure V-32).

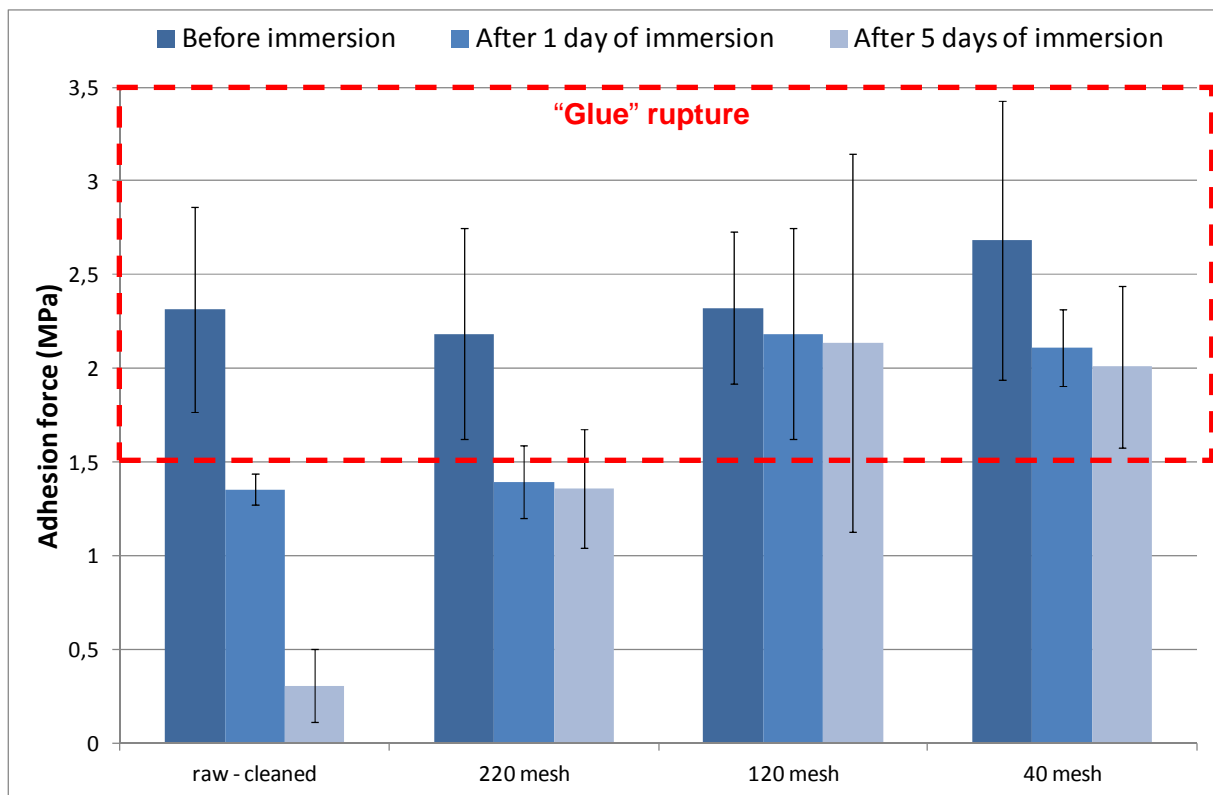


Figure V-32. Adhesion force of the RenLam CY 219 / Ren HY 5161 system coated onto shot-blasted stainless steel before and after immersion in water (80 °C) during 1 and 5 days.

It is visible here that the shot-blasting process has a positive effect on the wet adhesion of the epoxy coating as a great improvement is observed for each corundum particle size. This result proves the importance of the mechanical adhesion for the epoxy / stainless steel interface.

However, a shot-blasting with 220-mesh corundum particles does not provide sufficient adhesion improvement as an interfacial rupture is observed after immersion in hot water. The

increase of the surface roughness (R_A from 0.19 μm to 0.81 μm) is probably not sufficient to increase the resistance in water.

A greater improvement is observed for the samples pretreated with the 120- and 40-mesh particles as a “glue” rupture is observed even after 5 days of immersion in hot water even if the dispersion of results is high. This is due to the great increase of the surface roughness (R_A (120-mesh) = 1.16 μm and R_A (40-mesh) = 4.86 μm). Moreover, the presence of interlocked alumina particles in the stainless steel matrix may increase the surface reactivity as Al_2O_3 has more reactive sites at its surface. Anyway, these results proved that shot-blasting might be sufficient to reach a satisfactory adhesion improvement but this has to be proven by immersion tests in the pilot reactor.

VI.3. Effect of adhesion promoters

The effect of the use of adhesion promoters were evaluated by performing some adhesion tests as well. The aim here was to compare different parameters like the structure of the non-hydrolyzable functional group (R), the duration of the prehydrolysis and the number of hydrolyzable groups (OR').

VI.3.a. Influence of the non-hydrolyzable functional group

These first tests were performed on crude stainless steel plates which were previously cleaned and then functionalized with numerous trialkoxysilanes. These adhesion promoters were applied after a 90 s prehydrolysis (at pH = 5) and a dip coating during 15 minutes. The aminosilanes (APTS, AAPS and TPDTA) and the epoxysilane GPTMS were studied to evaluate the effect of the pendant R group on the wet adhesion of the coating (figure V-33).

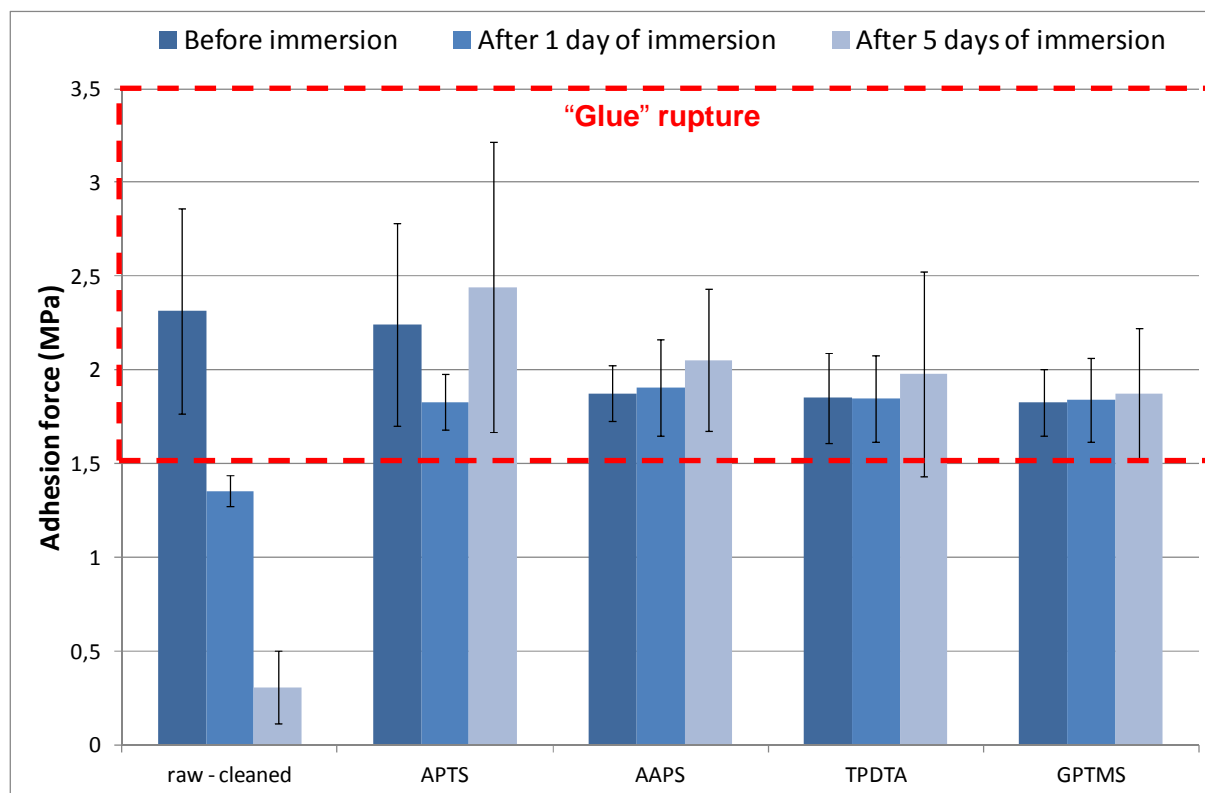


Figure V-33. Adhesion force of the RenLam CY 219 / Ren HY 5161 system coated onto trialkoxysilane-functionalized stainless steel before and after immersion in water (80 °C) during 1 and 5 days: comparison between the trialkoxysilanes.

The use of trialkoxysilanes is very beneficial as it provides a huge improvement of the adhesion after immersion in hot water as a “glue” rupture is observed even after 5 days of immersion. This result is obtained whatever the structure of the trialkoxysilane structure.

Concerning the structure of the non-hydrolyzable group, no major differences can be seen between a trialkoxysilane bearing an epoxy group (GPTMS) and one amine group (APTS). It first confirms that grafting has been obtained for each system. Then, it proves that the reaction between the aminosilane and the epoxy resin and the reaction between the epoxysilane and the curing agent might be equally efficient and lead to the formation of stable covalent bonds.

When comparing the aminosilanes, it is clear that the number of amine functions (1 primary amine for APTS, 1 primary and 1 secondary for AAPS and 1 primary and 2 secondary for TPDTA) does not play a major role in the stability of the epoxy / stainless steel interface in an aqueous medium. As a matter of fact, APTS, with only 1 amine function, provides a sufficient adhesion improvement.

These results prove the beneficial effects from the use of alkoxy silanes and more precisely from the formation of covalent bonds between the substrate and the alkoxy silane (Metal-O-

Si). These bonds are stable regarding to hydrolysis compared to the links normally formed between the substrate and the epoxy coating: secondary bonds (Van der Waals interactions, hydrogen bonds, polar interactions and Metal-O-C covalent bonds).

These results were reached by using a short prehydrolysis duration but some tests were made to check the influence of the prehydrolysis time on the adhesion performances.

VI.3.b. Influence of the prehydrolysis duration

Some tests were performed on APTS and GPTMS by extending the prehydrolysis duration from 90 s to 1 h. The trialkoxysilanes were deposited onto cleaned stainless steel by dip coating during 15 minutes. The results are presented on figure V-34.

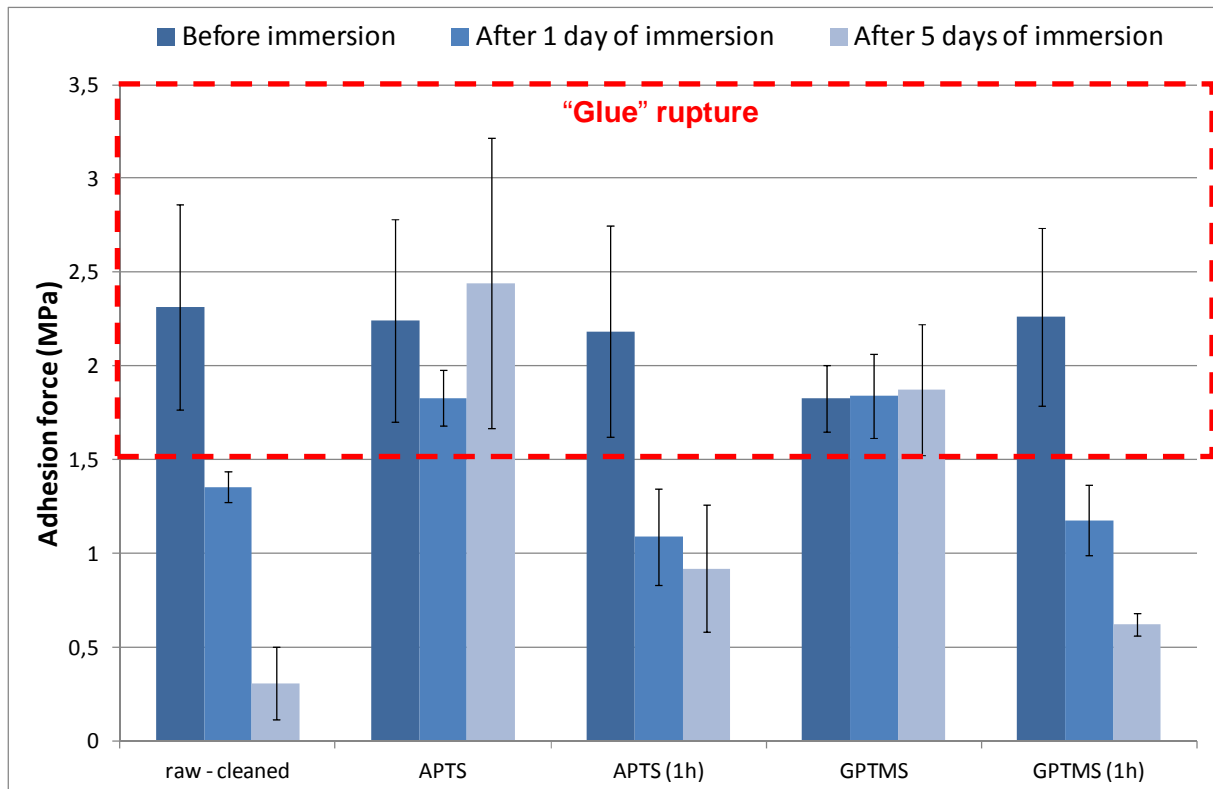


Figure V-34. Adhesion force of the RenLam CY 219 / Ren HY 5161 system coated onto trialkoxysilane-functionalized stainless steel before and after immersion in water (80 °C) during 1 and 5 days: evaluation of the effect of the prehydrolysis time.

The trend observed here is the same regardless to the structure of the aminosilane. Shorter prehydrolysis times lead to a better adhesion in hot water for both GPTMS and APTS. This comes probably from the fact that using a longer prehydrolysis time leads to the formation of a thicker trialkoxysilane deposit at the stainless steel surface. As a matter of fact, during a

long prehydrolysis, the silanols formed are weakly stable and consumed by the condensation reaction. The Si-O-Si network is then grafted onto stainless steel after deposition. The presence of this thick siloxane network causes a covering of the substrate's surface roughness and also a loss of the mechanical adhesion mechanism.

Another way to explain the increase of the adhesion force with the decrease of the prehydrolysis time is the structure of the grafted alkoxy silane layer. In fact, increasing the prehydrolysis duration leads to the formation of a higher amount of siloxanes causing the grafting of a larger alkoxy silane layer which is more disordered³³. The thinner layer grafted after a shorter prehydrolysis is more ordered and its ability to react with the coating will be greater.

A short prehydrolysis time is preferred but another parameter to watch is the number of hydrolyzable groups on the alkoxy silanes.

VI.3.c. Influence of the number of hydrolyzable groups

The aim here is to compare the performances of trialkoxy silanes (with 3 hydrolyzable methoxy groups) with the ones of monoalkoxy silanes (bearing 1 hydrolyzable ethoxy group and 2 non-hydrolyzable methyl groups). To do so, tri- and monoalkoxy silanes bearing the same non-hydrolyzable function were compared with each other (APTS and APDES with a primary amine function and GPTMS and GPDES with the epoxy ring). The prehydrolysis time for the trialkoxy silanes was 90 s, the one for APDES was 120 min and 30 min for GPDES. The results are presented on figure V-35.

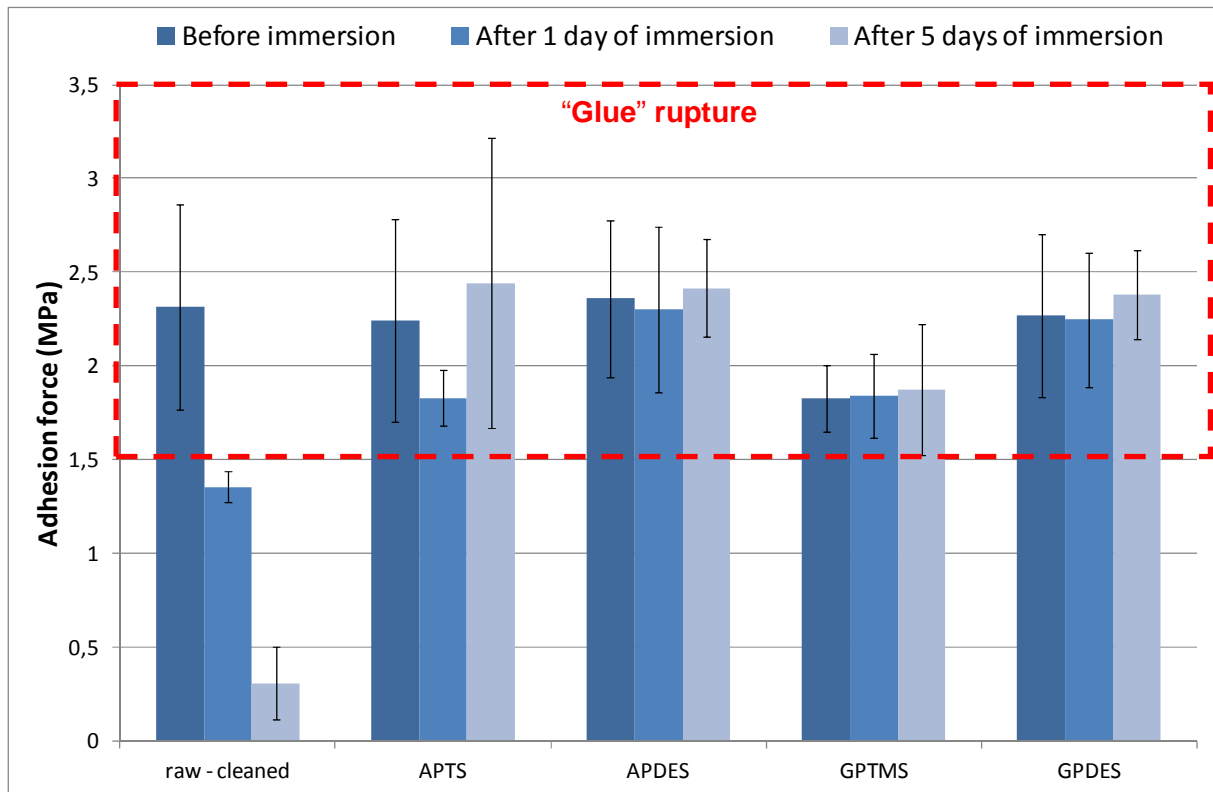


Figure V-35. Adhesion force of the RenLam CY 219 / Ren HY 5161 system coated onto functionalized stainless steel before and after immersion in water (80 °C) during 1 and 5 days: comparison between mono- and tri-alkoxysilanes.

The results obtained here are consistent with the ones observed in the previous paragraph. As a matter of fact, monalkoxysilanes are not able to undergo a condensation reaction. This means that the silanols formed (except from the ones that formed dimers) are used for grafting onto stainless steel and this leads to the formation of a very thin alkoxy silane layer. This latter is close to the structure obtained for the grafting of trialkoxysilanes after a short prehydrolysis time. There are still few differences as monoalkoxysilanes allow to obtain the formation of a monolayer while trialkoxysilanes, with short hydrolysis times, lead to a thin multilayer layer. The structures of both grafted molecules are so quite similar even if the trialkoxysilane leads to a thicker deposit.

These results confirm the fact that grafting a thin alkoxy silane layer provides a better improvement of the adhesion after immersion in hot water as it does not cause any covering of the surface roughness.

The final step is to check if the use of a mechanical treatment can be combined with the use of adhesion promoters to reach the best adhesion in the pilot reactor.

VI.4. Combination of mechanical treatments and adhesion promoters

These adhesion tests were made by comparing crude and 40-mesh shot-blasted stainless steel plates functionalized by either APTS or APDES. The results are presented on figure V-36.

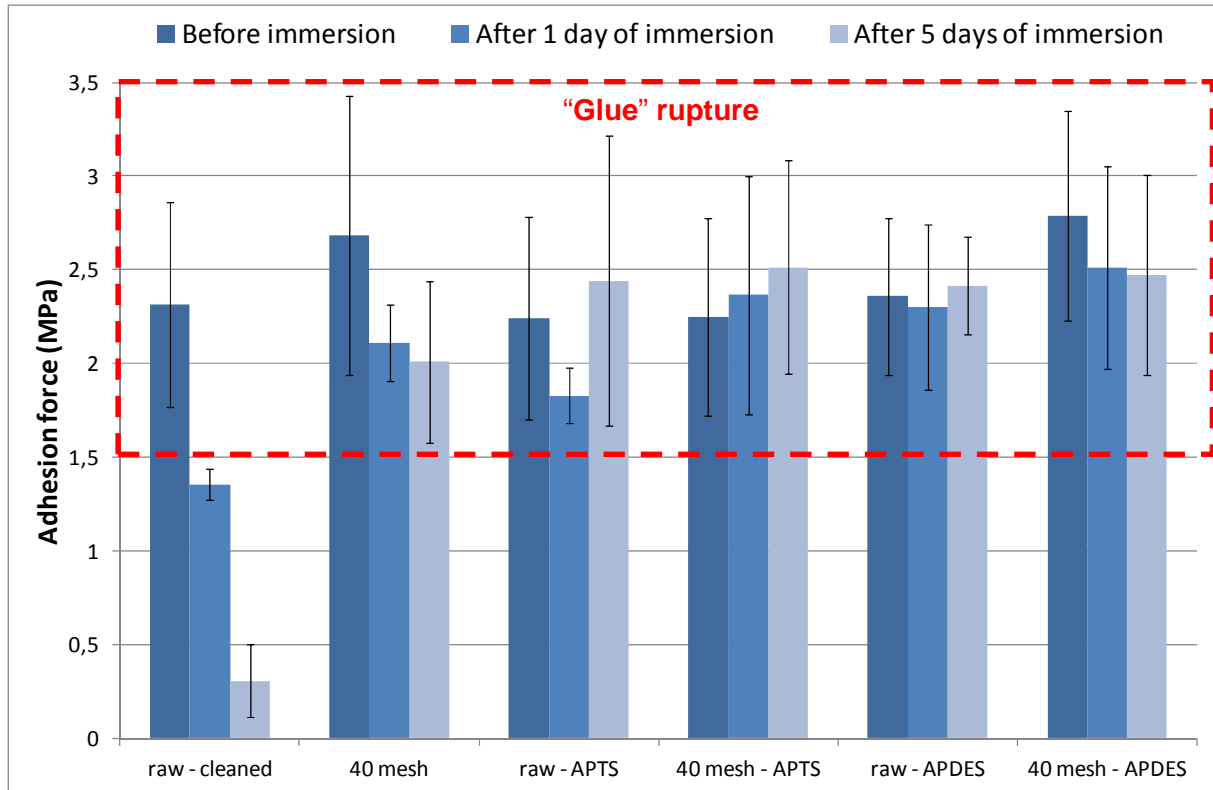


Figure V-36. Adhesion force of the RenLam CY 219 / Ren HY 5161 system coated onto shot-blasted and functionalized stainless steel before and after immersion in water (80 °C) during 1 and 5 days.

The adhesion tests do not allow to conclude if there is a beneficial effect from using both mechanical treatment and adhesion promoters because a “glue” rupture is observed for all cases. However, as mechanical treatment provides an increase of the surface roughness (in other terms the specific surface area) and a chemical modification (by the interlocking of alumina particles), it can be assumed that the grafting efficiency of alkoxy silanes at the shot-blasted stainless steel surface is higher because of the increase of the substrate’s surface reactivity.

VI.5. Conclusion

First, it is interesting to note that no cohesive rupture (inside the epoxy coating) was observed showing a high mechanical resistance of the epoxy network. The adhesion tests performed here proved again that water is critical for the epoxy / stainless steel interface compared to BuCl which do not disturb the adhesion of the coating.

Some of the strategies used for the improvement of the coating / substrate interface allowed to reach a satisfactory adhesion for the pull-off tests. Cleaning did not provide any adhesion improvement but the use of shot-blasting with high-diameter particles (120- and 40-mesh) and / or the use of alkoxysilanes permitted to drastically improve the wet adhesion of the coating.

For the alkoxysilane, the main issue is the thickness of the grafted layer as the use of short prehydrolysis times for the trialkoxysilanes and the use of monoalkoxysilanes allowed to obtain an important adhesion improvement without shot-blasting.

Pilot tests were finally performed to determine the system which is the most adapted for S-PVC reactors.

VII. Validation - pilot tests

Pilot tests were finally performed to evaluate the performances of the coatings and the benefits from each surface treatment. After these tests, an ideal system was proposed to coat the S-PVC reactors. These tests were more discriminating as the immersed samples underwent the real polymerization conditions with aggressive chemical compounds, temperature and pressure changes during 7 h per batch.

VII.1. Non-optimized epoxy / stainless steel interface

The RenLam CY 219 / Ren HY 5161 system was coated onto crude (without cleaning) stainless steel. These samples were immersed in the pilot reactor in order to check the resistance of the coating in the reactive medium without previous surface preparation. One polymerization was made on these samples. Pictures of the samples before and after 1 batch are shown on figure V-37.

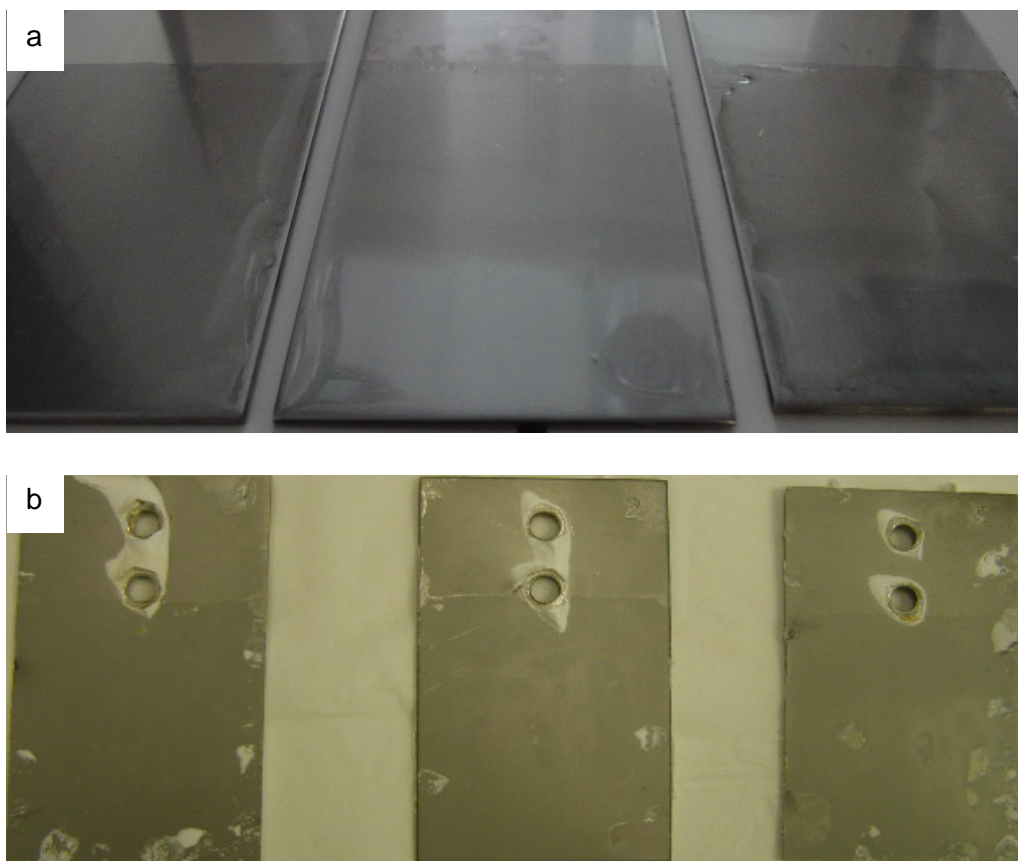


Figure V-37. Pictures of RenLam CY 219 / Ren HY 5161 system coated stainless steel plates before (a) and after (b) one polymerization.

The samples before immersion were well coated and the aspects of the coatings were satisfactory. After polymerization, the coating is totally delaminated. This is due to the weakness of the epoxy / stainless steel interface regarding to hydrolysis. Moreover, the effects of the temperature, the pressure, the abrasion of the growing PVC pellets and the agitation of the reactive medium can be major factors too.

The same results were obtained when stainless steel was cleaned before application of the coating. The adhesion of the epoxy / stainless steel interface must be strengthened.

VII.2. Effect of the mechanical treatment

These plates were prepared by applying the RenLam CY 219 / Ren HY 5161 onto shot blasted (by 40 mesh corundum) stainless steel plates with a painting brush without any silane treatment. These plates were immersed in the pilot reactor in order to check their resistance in the reactive medium. Ten polymerizations were made on these samples. Pictures of the samples are shown on figure V-38.

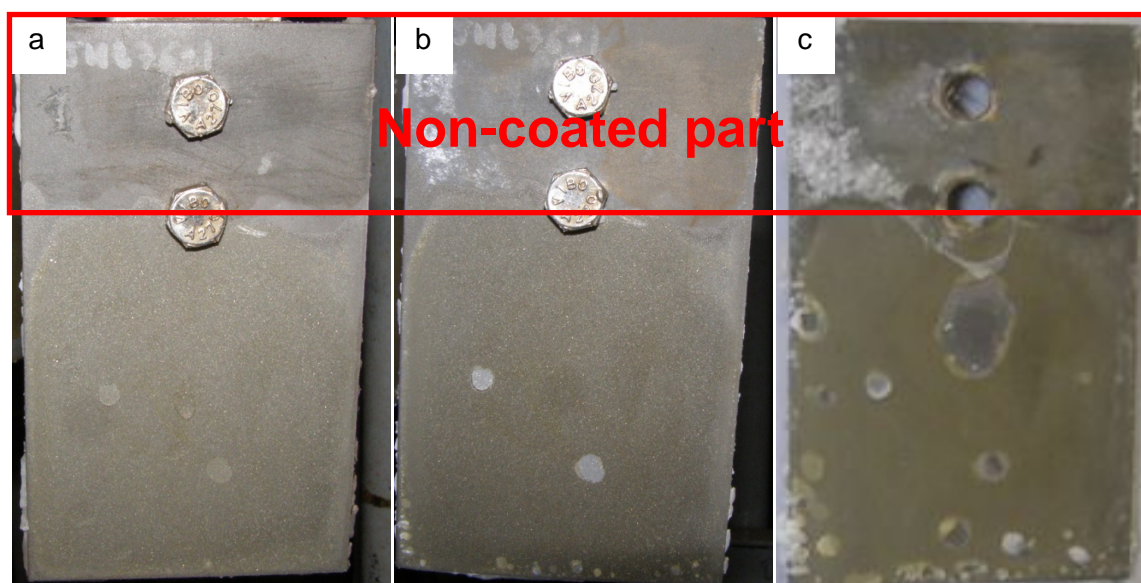


Figure V-38. Pictures of a RenLam CY 219 / Ren HY 5161 system coating applied on 40-mesh corundum-shot blasted stainless steel plates after: a. 5 batches, b. 7 batches, c. 10 batches.

The behavior of this coating after 10 polymerizations is really impressive. As a matter of fact, partial unsticking of the coating is observed after 10 batches but no significant formation of scale is noted. Partial unsticking can be due to the application process of the coating which is not optimal in the laboratory as the two sides of the plates must be covered simultaneously. This kind of problem can be overcome by using an industrial application to obtain a great covering of the surface while having a smooth surface. Nevertheless, the epoxy coating confirms its anti-encrusting properties as no traces of crust are observed on the plates and the mechanical treatment allows to reach a satisfactory adhesion of the coating.

VII.3. Effect of adhesion promoters

The following challenge was to achieve a durable adhesion on stainless steel plates without previous shot-blasting treatment. For this purpose, tests were made by using alkoxy silanes. Some parameters like the influence of the pendant functional group or the number of hydrolyzable groups were again regarded. The prehydrolysis duration was set at 90 s for the trialkoxy silanes, 120 min for APDES and 30 min for GPDES.

VII.3.a. Influence of the non-hydrolyzable functional group

These tests were made on 2 aminosilanes (APTS and TPDTA) and on the epoxysilane GPTMS grafted on cleaned stainless steel. The epoxy coating was then applied and the coated plates were immersed in the pilot reactor. The results obtained for APTS are presented on figure V-39.

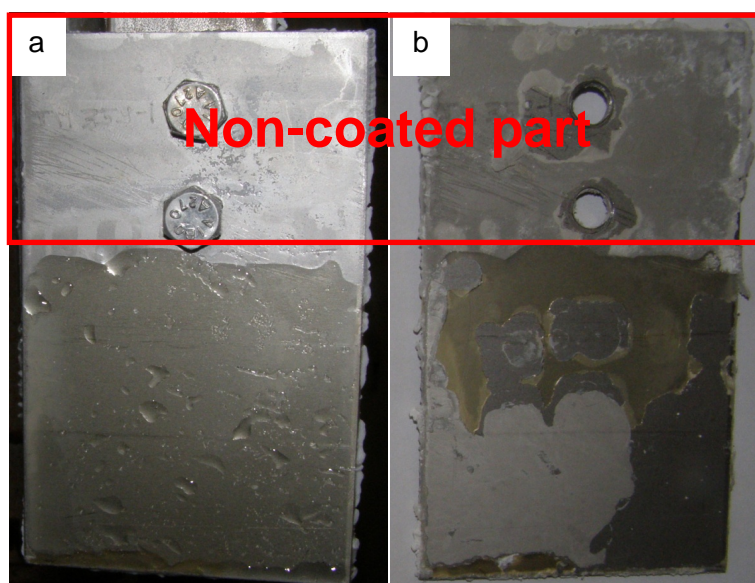


Figure V-39. Pictures of a RenLam CY 219 / Ren HY 5161 system coating applied on APTS-functionalized stainless steel plates after: a. 3 batches and b. 5 batches.

The best results on non-shot-blasted stainless steel were achieved with APTS. This formulation was able to sustain 3 straight batches without delamination of the coating and without formation of scale. However, a loss of adhesion started from the 4th batch and led to the delamination of the coating after the 5th batch. Still, it is interesting to note that no scale was observed after these tests.

The results obtained with TPDTA and GPTMS were poorer as degradation of the coating occurred after only 1 batch. For GPTMS, the difference can come from the fact that the reaction between the aminosilane and the epoxy resin and the reaction between the epoxysilane and the curing agent are finally not equally efficient. It seems to be more effective to have the aminosilane reacting with the epoxy resin to form stable covalent bonds. For TPDTA, having too many amine functions or a too long functional pendant chain can lead to a disordering of the grafted alkoxy silane layer causing a loss of the reaction efficiency.

VII.3.b. Influence of the number of hydrolyzable groups

The results obtained previously with trialkoxysilanes APTS and GPTMS were compared with the ones of monoalkoxysilanes APDES and GPDES. The RenLam CY 219 / Ren HY 5161 was coated on cleaned and functionalized stainless steel plates which were then immersed in the pilot reactor (figure V-40).

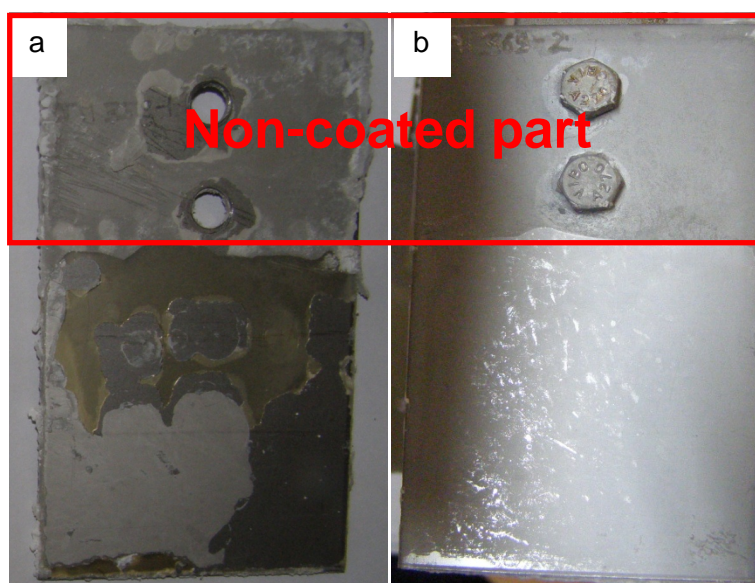


Figure V-40. Pictures of a RenLam CY 219 / Ren HY 5161 system coating applied on stainless steel after functionalization with: a. APTS (after 5 batches) and b. APDES (after 2 batches).

Again, the best results on non-shot-blasted stainless steel were obtained with APTS (delamination during the 4th batch). For APDES, degradation of the coating's adhesion happened during the 2nd batch. APTS seems to be more efficient. Using this molecule at a short prehydrolysis time allows to form an alkoxy silane multilayer which is even though thin. The monolayer formed by using APDES does not provide enough adhesion improvement and having a thin multilayer is the solution offering the best adhesion on non-shot-blasted stainless steel probably due to the combination of a thin grafted layer and of a better covering of the surface.

The samples with GPTMS and GPDES as adhesion promoters did not exhibit a suitable behavior as delamination of the coating happened after only 1 batch confirming the observation made earlier.

The final step is to check the efficiency of the combination of mechanical treatment with the use of adhesion promoters.

VII.4. Combination of mechanical treatments and adhesion promoters

The tests performed previously showed that a 40-mesh shot-blasting of stainless steel provides a sufficient adhesion improvement to obtain a durable adhesion in the pilot reactor. However, the goal here is to check if applying an adhesion promoter on previously cleaned and shot-blasted plates would lead to an even better stability of the coating during the VCM polymerization. Tests were also made on shot-blasted (40-mesh corundum) stainless steel plates functionalized with APTS, APDES, GPTMS and GPDES (figure V-41).

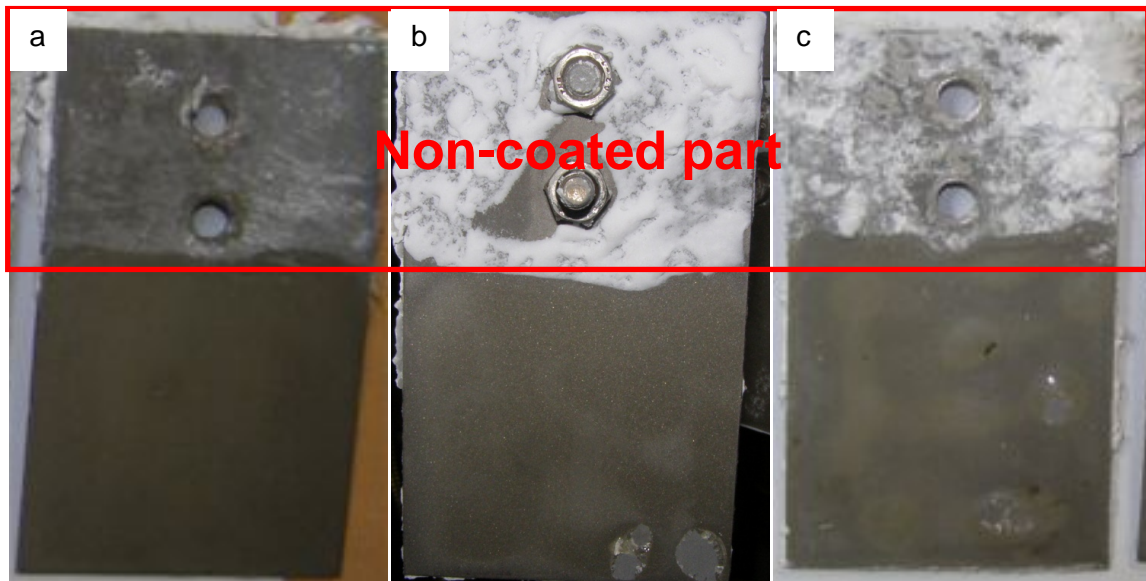


Figure V-41. Pictures of a RenLam CY 219 / Ren HY 5161 system coating applied on 40-mesh shot-blasted stainless steel functionalized with: a. APTS (after 6 batches), b. APDES (after 3 batches), c. GPTMS (after 8 batches).

The combination of mechanical treatment with the use of adhesion promoters allows to obtain a durable adhesion of the coating on stainless steel. Again, some samples with APTS and GPTMS were able to reach 10 consecutive batches without delamination of the coating. APDES and GPDES were reliable too as these alkoxy silanes allowed to reach both 7 batches at the moment (the tests were stopped after 7 batches but the coating was still performing well). The aspect of the samples after these batches clearly shows that these formulations are able to attain 10 batches.

The addition of adhesion promoters seems to be beneficial as the aspect of the coatings after numerous batches is still satisfactory. As a matter of fact, less partial unsticking is observed except for some located points where partial delamination appeared (lower right corner on figure V-41, b). Again, this is mainly due to application issues and it can be corrected by using an industrial application method (spray gun for example).

The strong adhesion achieved here is due to the presence of a thin alkoxy silane layer allowing to establish stable covalent bonds between the coating and the substrate while profiting from the increase of the surface roughness (enhancement of the mechanical adhesion).

VII.5. Conclusion – Selection of a system

The optimization of the epoxy / stainless steel interface was efficient enough to reach a durable adhesion in the S-PVC reactors.

Before optimization, a complete delamination was observed after only one polymerization. Using adhesion promoters on non-shot-blasted stainless steel permitted to perform 3 straight batches without delamination of the coating for the most efficient one (APTS).

Using a mechanical treatment of stainless steel was necessary to achieve an adhesion force which allows the coating to be durable in the reactor. In fact, the goal of 10 batches has been reached without delaminating of the coating and formation of scale.

Moreover, the use of adhesion promoters seems to strengthen even more the epoxy / stainless steel interface and might help reaching a longer durability.

- *Presentation of the coating corresponding to the given specifications*

The anti-scale coating developed during this study can be obtained by applying the following operational mode.

- Mechanical treatment:

Use of a 40-mesh corundum shot-blasting of stainless steel.

- Cleaning of stainless steel:

Cleaning with an acetone wet tissue followed by a dichloromethane ultrasonic bath during 5 min. Drying of the cleaned plate during 5 min at 110 °C.

- Application of APTS:

Preparation of an ethanol / water solution (weight ratio = 95 / 5) with the pH stabilized at 5 with acetic acid. Addition of 2 % w / w of APTS and prehydrolysis during 90 s under ambient

conditions. Application of the solution onto stainless steel by dip coating during 150 min. Rinsing of the plate in ethanol and drying at 110 °C during 30 min.

- Application of the epoxy coating:

Preparation of the RenLam CY 219 / Ren HY 5161 mix and manual homogenization during 5 min. Application of the coating and curing at 150 °C during 1 h.

VIII. Conclusion

The last part of this study was dedicated to the optimization of the epoxy / stainless steel interface to obtain a durable coating for S-PVC reactors.

A three-step strategy was chosen for this purpose. Contact angle measurements and XPS proved that cleaning was essential to reach the surface reactive functions of stainless steel. SEM-EDX analyses showed that a corundum shot-blasting of stainless steel led to an increase of the substrate's surface roughness while causing a chemical modification of the surface by strongly interlocking some alumina particles on the stainless steel matrix.

A large part of the study was made on the grafting of tri- and monoalkoxysilanes onto stainless steel as a function of the pH and also of the prehydrolysis duration. A combination of PM-IRRAS, AFM and XPS proved that grafting of these molecules was achieved under controlled conditions.

Pull-off tests showed that the adhesion of an epoxy coating on stainless steel in hot water can be highly enhanced by using either a mechanical treatment or an alkoxy silane onto cleaned stainless steel or a combination of both techniques. However, the pilot tests proved that the shot-blasting is necessary to achieve a durable adhesion in a S-PVC reactor. Samples pre-treated with 40-mesh corundum (with or without alkoxy silanes) were able to sustain a strong adhesion after 10 consecutive batches. Finally, it is clear that combining the use of mechanical treatment and adhesion promoters is the better way to obtain a long-term adhesion of the coating.

References

- (1) Legghe, E.; Aragon, E.; Bélec, L.; Margailan, A.; Melot, D. *Prog. Org. Coat.* **2009**, *66*, 276–280.
- (2) Rouw, A. . *Prog. Org. Coat.* **1997**, *34*, 181–192.
- (3) Galliano, F.; Landolt, D. *Prog. Org. Coat.* **2002**, *44*, 217–225.
- (4) Calvez, P.; Bistac, S.; Brogly, M.; Richard, J.; Verchère, D. *J. Adhes.* **2012**, *88*, 145–170.
- (5) Al-Harhi, M.; Loughlin, K.; Kahraman, R. *Adsorption* **2007**, *13*, 115–120.
- (6) Raman, A.; Dubey, M.; Gouzman, I.; Gawalt, E. S. *Langmuir* **2006**, *22*, 6469–6472.
- (7) Haïdopoulos, M.; Turgeon, S.; Laroche, G.; Mantovani, D. *Surf. Coat. Technol.* **2005**, *197*, 278–287.
- (8) He, W.; Knudsen, O. Ø.; Diplas, S. *Corros. Sci.* **2009**, *51*, 2811–2819.
- (9) Clayton, C. R. *J. Electrochem. Soc.* **1986**, *133*, 2465.
- (10) Brion, D. *Appl. Surf. Sci.* **1980**, *5*, 133–152.
- (11) Nemoshalenko, V. V.; Didyk, V. V.; Krivitskii, V. P.; Senekevich, A. I. *Zh. Neorg. Khimii* **1983**, *28*, 2182.
- (12) McIntyre, N. S.; Zetaruk, D. G. *Anal. Chem.* **1977**, *49*, 1521–1529.
- (13) Fredriksson, W.; Malmgren, S.; Gustafsson, T.; Gorgoi, M.; Edström, K. *Appl. Surf. Sci.* **2012**, *258*, 5790–5797.
- (14) Gettings, M.; Kinloch, A. J. *J. Mater. Sci.* **1977**, *12*, 2511–2518.
- (15) Lecollinet, G.; Delorme, N.; Edely, M.; Gibaud, A.; Bardeau, J.-F.; Hindré, F.; Boury, F.; Portet, D. *Langmuir* **2009**, *25*, 7828–7835.
- (16) Plueddemann, E. P. *Silane coupling agents*; Plenum Press: New York, 1982.
- (17) Arkles, B.; Steinmetz, J. R.; Zazyczny, J.; Mehta, P. *J Adhes Sci Technol* **1992**, *6*, 193–206.
- (18) Osterholtz, F. D.; Pohl, E. R. *J. Adhes. Sci. Technol.* **1992**, *6*, 127–149.
- (19) Materne, T.; de Buyl, F.; Witucki, G. L. *Dow Corning Rev.* **2006**.
- (20) Johnson, A. W. *Invitation à la chimie organique*; De Boeck Supérieur: Bruxelles, 2002.
- (21) Claverie, I.; Panet, M.; Barbeau, S. *Biochimie*; Wolters Kluwer France: Rueil-Malmaison, 2008.
- (22) Quinton, J. S.; Dastoor, P. C. *Surf. Interface Anal.* **2000**, *30*, 21–24.
- (23) Flesch, C.; Joubert, M.; Bourgeat-Lami, E.; Mornet, S.; Duguet, E.; Delaite, C.; Dumas, P. *Colloids Surf.* **2005**, *262*, 150–157.
- (24) Blitz, J. .; Shreedhara Murthy, R. .; Leyden, D. *J. Colloid Interface Sci.* **1988**, *126*, 387–392.

- (25) Vrancken, K. .; Possemiers, K.; Van Der Voort, P.; Vansant, E. *Colloids Surf* **1995**, *98*, 235–241.
- (26) Trens, P.; Denoyel, R. *Langmuir* **1996**, *12*, 2781–2784.
- (27) Fujita, K.; Oya, A.; Benoit, R.; Beguin, F. *J. Mater. Sci.* **1996**, *31*, 4609–4615.
- (28) Daehler, A.; Boskovic, S.; Gee, M. L.; Separovic, F.; Stevens, G. W.; O'Connor, A. J. *J. Phys. Chem. B* **2005**, *109*, 16263–16271.
- (29) Dorvel, B.; Reddy, B.; Block, I.; Mathias, P.; Clare, S. E.; Cunningham, B.; Bergstrom, D. E.; Bashir, R. *Adv. Funct. Mater.* **2010**, *20*, 87–95.
- (30) White, L. D.; Tripp, C. P. *J. Colloid Interface Sci.* **2000**, *232*, 400–407.
- (31) Kanan, S. M.; Tze, W. T. Y.; Tripp, C. P. *Langmuir* **2002**, *18*, 6623–6627.
- (32) Pertsin, A. J.; Gorelova, M. M.; Levin, V. Y.; Makarova, L. I. *J. Appl. Polym. Sci.* **1992**, *45*, 1195–1202.
- (33) Dorval, F. *Etude des propriétés d'adhérence et de durabilité du système acier inoxydable : adhésif époxyde, influence d'un primaire d'adhésion*, Thesis n°2003INPG0053, **2003**, Institut National Polytechnique de Grenoble, France.

General Conclusion

The Ph.D. work presented here was part of the FUI Ecoating project which aimed at developing a durable polymer coating able to prevent the formation of a PVC-scale during the suspension polymerization of VCM. This study was divided into two parts as the first goal was to establish a complete scenario allowing to explain the phenomenon from a chemical point of view. Having a better comprehension was helpful for the second part of this project which was the development of a polymer coating with an emphasis on the relationship between its network structure and its anti-scaling properties but also on its adhesion onto stainless steel.

The study of the formation of scale allowed, by the help of immersion tests of stainless steel plates in model solvents and in the pilot reactor, to establish a complete scenario explaining this phenomenon. These tests proved that the surfactants used for the stabilization of the VCM droplets, PVA, are highly incriminated as a PVA deposit is observed after only 15 minutes of reaction. This “crust” will then evolve as a PCV-rich phase is formed 30 minutes after the beginning of the batch. These results show that a good way to prevent the formation of scale on the reactors' walls would be to have a coating having a good adhesion onto stainless steel while having low interactions with the components of the reactive medium (mainly PVA).

In this way, some epoxy / curing agents systems were tested by varying the chemical nature of the curing agent. Experiments made on free films allowed to select the best BADGE / curing agent system. This latter allowed the obtaining of a suitable T_g value while exhibiting low swelling values in water, a correct mechanical resistance and most importantly a great stability in the pilot reactor with no formation of scale after 2 batches.

The last issue was the reinforcement of the epoxy coating / stainless steel interface which is very sensitive to water leading to a complete delamination of the coating after only 1 batch in the pilot reactor. Three parameters were tested and their influence on the adhesion of the coating were experimented by measuring the adhesion force (pull-off tests) before and after immersion in hot water (80 °C) and also by performing immersion tests in the pilot reactor. A combination of surface cleaning, mechanical pre-treatment (which seemed to be the most efficient) and functionalization by adhesion promoters provided a great lift of the adhesion. As a matter of fact, the most performing systems were able to sustain 10 straight batches without delamination and without formation of scale.

All this study finally led to the proposal to the other members of the consortium of an optimized coating and of the deposition process giving the best results. This system consists in a shot-blasting and cleaning pre-treatment of stainless steel followed by the application of

the epoxy coating. The use of adhesion promoters was not essential during 10 batches but can be helpful to keep a high adhesion of the coating on longer terms.

There are also some outlooks on this project and a lot of work that has still to be done.

First of all, there are some optimizations that can be performed concerning the alkoxy silanes deposition and mainly the ones bearing three alkoxy functions. Some work has been done on the pH and on the prehydrolysis duration. Another parameter that can be varied is the concentration of alkoxy silanes in the deposition solution. As a matter of fact, it is known that the amount of these molecules dispersed in an aqueous medium can have an effect on the hydrolysis / condensation balance. In fact, having a higher concentration will favor the occurrence of the condensation reaction. A 2 % w/w concentration was used during this study and this value is already quite low. As a matter of fact, it would have been interesting to check if the concentration would have an effect on the resulting adhesion force.

Still about the alkoxy silanes, another non-hydrolyzable functional group that could have been tested to react with the epoxy / curing agent couple is acrylate. These latter can react with the amines contained in the curing through a Michael addition in order to lead to the formation of a stable chemical bond.

The final outlooks of the project consist in the up-scaling of the developed coating. It will first go through an optimization of the coating in order to make its industrial application easier. This work, done by Mäder, mainly consists in formulation (addition of reactive diluents, thixotropic agents...). A large part of the work will be to check the effect of the formulation process on the properties of the cured network, on the stability of the film in the pilot reactor and of course on the anti-scaling properties. This will finally lead to a test performed on a real-size reactor blade to check the feasibility and the effectiveness of the coating at a higher scale.